The University of Sheffield

Department of Mechanical Engineering

DEVELOPMENT OF CVD COATED CERAMIC MILLING INSERTS FOR MILLING INCONEL 718

A Thesis submitted for the degree of

Doctor of Engineering

In Machining Science

By

Luke Osmond

Supervisors:

Professor Tom Slatter

Dr Ian Cook

2023

Dedication

To my family and friends to whom

I am greatly indebted

Acknowledgements

The author wishes to thank:

Abstract

Composite ceramic cutting tools such silicon aluminium oxynitride or 'SiAlONs' have often been utilised for machining heat resistant super-alloys such as Inconel 718. SiAlON ceramic cutting tools possess a very useful set of mechanical properties, which range from high hot hardness to high wear resistance, to thermochemical inertness, and have very high thermal shock resistance. However, when SiAlON milling tools are used to machine nickel based super-alloys such as Inconel 718, SiAlON milling inserts experience rapid tool wear and very short tool life compared to carbide tooling.

The work presented in this thesis attempts to understand the benefit of applying protective chemical vapor deposition (CVD) coatings to both positive (RPGN) and negative (RNGN) CTIS710 SiAlON milling inserts. The research addresses a hypothesis that a hard protective wear resistant coating will dilute the effects of thermomechanical and diffusion wear on the flank and rake faces of the inserts. Therefore, there has been focus on determining if these dilution effects will improve the wear resistance and prolong the tool life of SiAlON ceramic milling inserts.

The thesis is split into four main studies, the first of which has focused on preliminary research that concentrates on developing knowledge and understanding of machining Inconel 718 with ceramic turning inserts and chip morphology. The flank results of the turning machine trials concluded that CTIS710 SiAlON ceramic should be selected for the later machining trials and tribological testing.

The second and third parts of this thesis are focused on understanding the wear mechanisms of CVD coated SiAlON ceramics. A series of three axis machining trials were undertaken with CVD coated SiAlON (Coating A and Coating B) inserts. In addition to the machining trials, tribological tests were undertaken. The machining trials and tribological tests extracted valuable information that would influence the process development route for developing Coating C. The main output from this part of the thesis concluded that an interrupted tool path exacerbated the primary wear mechanisms, and textured amorphous aluminium oxide (α-Al_2O_3) displayed very high thermomechanical wear resistance and adhesion characteristics. The results of the tribological tests concluded that amorphous aluminium oxide (α-Al_2O_3) had superior adhesion wear resistant characteristics and was selected for Coating C.

There has been a particular focus on using readily available coating materials and coating techniques that are currently adopted by Ceratizit UK & Ireland. The final part of this thesis has focused on conducting three and five axis machining trials with Coating C inserts and comparing the flank wear to uncoated SiAlON milling inserts.

The main conclusion from the research is that uncoated CTIS710 SiAlON milling inserts exhibited better wear resistance than the Coating C SiAlON milling inserts. The results from the five axis machining trials managed to prove a sub-hypothesis for this thesis, in that, if SiAlON ceramic inserts are used in a continuous/near continuous cutting environment the flank wear would decrease and consequently, the tool life would increase.

List of Publications

L. Osmond, D. Curtis, and T. Slatter, 'Chip formation and wear mechanisms of SiAlON and whisker-reinforced ceramics when turning Inconel 718', Wear, vol. 486–487, p. 204128, Dec. 2021, doi: 10.1016/j.wear.2021.204128.

L. Osmond, I. Cook, and T. Slatter, 'Tribological Properties of Multilayer CVD Coatings Deposited on SiAlON Ceramic Milling Inserts', J. Manuf. Mater. Process., vol. 7, no. 2, p. 67, Mar. 2023, doi: 10.3390/jmmp7020067.

L. Osmond, I. Cook, D. Curtis, and T. Slatter, 'Tool life and wear mechanisms of CVD coated and uncoated SiAlON ceramic milling inserts when machining aged Inconel 718', Proc. Inst. Mech. Eng. Part B J. Eng. Manuf., p. 09544054231180653, Jun. 2023, doi: 10.1177/09544054231180653.

Table of Contents

Nomenclature

		Units
α	Alpha or Amorphous	
ae	Radial Engagement	mm
Ap	Depth of Cut	mm
φ_{seg}	Shear Angle at the Chip Segment	(°)
β	Beta	
δ	Delta Phase Platelet	
d	Pin or Ball Diameter	mm
DoC	Depth of Cut	mm
D	Disk Diameter	mm
D	Diameter of Milling Cutting Tool	mm
D_{eff}	Effective Cutting Diameter of Milling Cutting Tool	mm
Ds	Segmentation rate	
δ_{sb}	Shear Band Thickness	
fz	Table Feed Rate	mm/min
F	Normal Force on The Pin	N
F_c	Cutting Force	N
FPT	Feed Per Tooth	mm/rev
F_r	Resultant Cutting Force	N
F_t	Tangential Cutting Force	N
F_y	Table Feed Thrust Force	N
h	Undeformed Chip Thickness	mm
h_c	Average Thickness of the Segmented Chips	mm
IC	Insert Diameter	mm
IR	Insert Radius	mm
L_c	Critical Load (Newtons)	
L_{c1}	Lower Critical Load	N
L_{c2}	Higher Critical Load	N
l_N	The Distance in mm Between the Start of the Scratch Track	mm
L_{rate}	The Rate of Force Application in specific test	N/min
L_{start}	The Preload Stylus Force in Newtons Established at The Start of The Scratch Test	N
h_{c_min}	Minimum Experimental Chip Thickness	mm
h_{c_max}	Maximum Experimental Chip Thickness	mm
mN	Milli-newton	N
nm	Nanometre	m
ρ_{seg}	Chip Segment Angle	(°)
P_{ch}	Pitch Between Chips	
P_{sb}	Depth of Segmentation	
r_c	Chip Ratio	
R	Wear Track Radius	mm
Φ	Shear Angle	(°)
S	Spindle Speed	Revs/min

T_f	Table Feed Rate	mm/min
V_{bb}	Flank Wear	mm
$VB_{B, minor}$	Flank Wear Minor Cutting Edge	mm
$VB_{B, major}$	Flank Wear Major Cutting Edge	mm
V_c	Cutting Speed	m/min
V_{chip}	Average Sliding Velocity of Chip	
V_s	Average Sliding Velocity Along Shear Plane	
V_{seg}	Average Sliding Velocity of Segmented Chip	
w	Rotation Velocity of the Disk (m/s)	m/s
X_{rate}	The Rate of Horizontal Displacement in The Specific Scratch Test	mm/min
γ_1	Rake Angle	(°)
γ	Primary Shear Zone	
γ	Nickel Solid-Solution Austenite Matrix	
γ'	Gamma Prime	
γ''	Gamma Double Prime	
γ_{seg}	Average Shear Strain in Segmented Chip	
γ_{sb}	Average Shear Strain in the Shear Bands	
Z	Number of Inserts	

Table of Abbreviations

ALD	Atomic layer deposition
Al_2O_3	Aluminium oxide
$AlCl_3$	Aluminium trichloride
AMRC	Advanced manufacturing research centre
ASBs	Adiabatic shear bands
NH3	Ammonia
BCT	Body centred tetragonal
BUE	Built up edge
CO	Carbon monoxide
CBN	Cubic boron nitride
CrN	Chromium nitride
Cr_2O_3	Chromium oxide
EngD	Engineering doctorate
FCC	Face centered cubic
FoF	Factory of the future
GPa	Gigapascal
GBs	Grain boundaries
HFCVD	Hot filament chemical vapour deposition
HSS	High speed steel
HSM	High speed machining
H2	Hydrogen
HCl	Hydrogen chloride
MN-MCD	Monolayer-micrometric
MN-SMCD	Monolayer–sub-micrometric
KTC	Knowledge transfer centre
MPa	Megapascal
MRR	Metal removal rate
MRV	Metal removal volume
MT-MCD	Multilayer-micrometric
N2	Nitrogen gas (N2)
SEM	Scanning electron microscope
SiAlON	Silicon aluminium oxynitride
SiC	Silicon carbide
TiAlN	Titanium aluminium nitride
TiC	Titanium carbide
TiCrAlN	Titanium chromium aluminium nitride
TiN	Titanium nitride
TiSiN	Titanium silicon nitride
TiCl4	Titanium tetrachloride
TiZrN	Titanium zirconium nitride
WC	Tungsten carbide
WRA	Whisker-reinforced alumina
Y_2O_3	Yttrium oxide

Chapter 1 Introduction and Motivation

Heat-resistant super-alloys such as Inconel 718 and Waspaloy exhibit excellent mechanical strength and structural stability at elevated temperatures, therefore super-alloys create a very challenging machining environment for cutting tools. One such cutting tool material which display promising results when machining the likes of Inconel 718 are SiAlONs. This particular cutting tool material is a substitutional solid substitution of silicon nitride (Si_3N_4) and aluminium oxide (Al_2O_3) microstructure with additions of yttrium. Substitutional solid solutioning of these three elements creates a silicon aluminium oxynitride milling composite ceramic microstructure with a chemical composition of ($Si_3N_4+Al_2O_3+Y_2O_3$). This chemical composition is also known by the trade abbreviation "SiAlON". However, SiAlON milling tools experience rapid tool wear as a result of the intense machining environment. One of the main motivations for this research is to find a cost-effective improvement, which will improve the machining performance and overall tool life of SiAlON milling tools when machining nickel-based alloys.

Therefore, the present doctoral thesis attempts to understand the benefit of applying protective CVD coatings to both positive (RPGN) and negative geometry (RNGN) CTIS710 SiAlON milling inserts. The application of a protective coating to the surface of a SiAlON milling insert, works around the research hypothesis that a hard protective coating will dilute the effects of mechanical, thermochemical and diffusion wear on the flank and rake faces of the inserts during high-speed machining trials. Tribological experiments were also conducted to ascertain the stability of the applied coating systems. The successful application of a suitable protective coating system to SiAlON milling insert, will undoubtedly increase productivity in high value industries such as aerospace and the oil and gas sectors.

During the research, worn CVD coated RNGN and RPGN SiAlON inserts were analysed and compared to uncoated RNGN and RPGN inserts to clarify the benefits of applying hard protective coatings. Three studies were conducted using the mentioned experiments to develop greater understanding of what coating system were effective. These studies are described in each thesis chapter, and they are comprised of wear assessments of SiAlON ceramic milling inserts and chip morphology analysis, an analysis of the tribological wear characteristics of the coating systems, and finally, a wear assessment of SiAlON ceramic milling inserts when operating in a 5-axis machining environment. The aerospace sector is currently experiencing a significant downturn due to the global impact of CoVid-19. The worldwide travel ban has had big

financial impacts on airlines, which has been equally felt by aerospace companies around the world [1]. Both Boeing and Airbus have very large aircraft order books at present, but even they have felt the impact of CoVid-19, which has impacted the output from aero-engine manufacturers such as General Electric's aircraft engines division, Pratt and Whitney, and Rolls Royce.

As a result, air travel will require a steady return to its original passenger volumes over the coming years. Airbus claims that the global market forecast report for air traffic is set to increase by 4.9 % annually between the years 2007-2026 [2]. With regards to commercial market outlook report for global airline aircraft during the years 2018-2038, global airline aircraft fleet numbers are set to rise as more fuel-efficient airliners replace less fuel-efficient aircraft in a bid to reduce emissions [3]. As a result of Covid-19, airlines are applying more pressure to aircraft manufacturers such as Boeing and Airbus to achieve evermore demanding emission levels, fuel-burn targets and now, more cost-effective aircraft.

In order to meet these continually stringent emission and fuel burn targets, the percentage of super-alloy content in gas turbines will be required to increase. Since the 1950s, super-alloy weight percentage in aero-gas turbines was 10%, whilst in today's modern turbofan gas turbines, super-alloy weight percentage has increased to 50% [4]. The reason for the increase usage of superalloys is down to the greater requirement of airlines to reduce greenhouse gas emissions and improving fuel efficiency. The improvements in fuel efficiency are attained when modern turbofan gas turbines run at higher operating temperatures which necessitates the increased use of nickel-based superalloys.

One of the most versatile and widely used super-alloys that is utilised in aero-gas turbine construction, oil and gas components, and spacecraft components is the nickel-based alloy, Inconel 718. This particular nickel-based alloy is used in the manufacture of aerospace components, such as bladed disks (blisks), turbine/compressor discs, compressor aerofoils and structural engine components. Together with the aerospace industry, another industry sector which also saw the weight percentage of nickel-based alloys increase was the oil and gas industry. As the oil and gas industry moved more towards coastal regions, and the wells that were being drilled were experiencing higher pressures and temperatures, which together with highly corrosive liquids, resulted in acidic drilling environments [5]. Inconel 718 is defined as a difficult material to machine due to the high work-hardening rates of the tool, rapid tool wear and high cutting temperatures that are experienced by the machine tool during the machining process.

This means low cutting speeds and feed rates are required, with long expensive cycle times and low manufacturing productivity being the end result. One current high speed machining technique, which can help with reducing the prospective manufacturing lead times and cost of producing complex nickel-based alloy components, is milling with ceramic cutting tools.

Milling super-alloys such as Inconel 718 with ceramic inserts can provide metal removal rates four times higher than when using carbide milling tools. The typical cutting speed for carbide tools is 100 m/min when compared to 600 m/min, typically used for ceramics. Wear rates for ceramic cutting tools are highly prolific on the flank and rake face [6]. The extreme cutting environment, which is generated during the ceramic machining process, causes rapid tool wear.

However, when SiAlON ceramic cutting tools are operated at cutting speeds in the region of 700-1000 m/min the level of cutting force reduces as the temperature increases in the chip tool interface. The rise in temperature in the chip/tool interface causes the Inconel 718 microstructure to lose a substantial amount of its yield strength and therefore induces rapid plastic deformation during the machining process [7].

The sequence which influences the deformational behaviour of Inconel 718 is heavily related to the high temperature characteristics of the fine dispersion of gamma prime (γ') and gamma double prime (γ''). The submicron age hardening effects for Inconel 718 is a result of the fine dispersal of Ni_3Nb body centred tetragonal (BCT) gamma double prime (γ'') precipitates together with the gamma prime (γ') to assist Inconel 718 in attaining a high strength microstructure [8], [9] and [10]. The BCT Ni_3Nb (γ'') phase also contributes to rapid reductions in strength above temperatures of 650°C, which is a result of the (γ'') phase having a lower solvus temperature than the (γ') phase.

That said, when SiAlON ceramics are operated at high cutting temperatures in the present of elements such as iron, the SiAlON microstructure become vulnerable to thermochemical wear mechanisms such as diffusion wear. Tribo-chemical interactions are initiated between the rake face of the SiAlON insert and the hot Inconel 718 chips [11], [12]. The silicon in the SiAlON microstructure has a high affinity for the iron In the Inconel 718 microstructure which results in diffusion between the SiAlON and Inconel 718 via solid solution. This in turn causes crater wear to form on the rake face, which is vulnerable to notch wear and potential catastrophic insert failure. Therefore, the present doctoral thesis aims to examine the main hypothesis of determining the benefit of adding a protective wear resistant coating to dilute the effects of the wear mechanisms.

1.1 Aim and Objectives

Given the research hypothesis, the main aim of this work was: To determine what coating system provides the best cutting performance and tool life and see how the cutting performance compares to uncoated SiAlON ceramic inserts when high-speed milling of Inconel 718.

Where the main research objectives were:

1. To review existing literature on (a) workpiece material and machining characteristics of nickel based super-alloys (b) cutting processes and chip formation (c) tool and coating wear and failure mechanisms; (d) ceramic cutting insert materials; (e) coating techniques; (f) coating selection for coated ceramic cutting insert materials, in order to understand the gap in knowledge in this area of cutting tool development.

2. To plan and carry out experimental testing to collect coating cutting performance, cutting force signal data and tool wear data. To establish what is the most effective coating system for protecting SiAlON milling inserts when machining nickel based super-alloys.

3. To establish what coating technique would be suitable and would be able to deposit a coating with high adhesion properties suitable high temperature wear properties. A series of insert wear machining trials and tribological testing will be conducted. The tribological tests will involve pin-on-disc and scratch testing and in-depth analysis via SEM techniques. Other in-depth wear analysis will be conducted via non-contact 3D profilometer (focus - variation type) scans.

4. To assess the wear of SiAlON ceramic milling inserts and clarify the optimum cutting parameter for machining nickel based super-alloys.

5. To evaluate and select the coating system which delivers the desired cutting performance and tool life.

1.2 Outline of Thesis

1. The thesis has been submitted in the University of Sheffield \Publication format thesis style. As such, it is written and structured with four sequential chapters, with three of the

four chapters having been published at the time of submission, which forms a coherent body of work.

2. **Chapter 2** reviews the literature that focuses on the history of cutting tools, chip formation, wear mechanisms, ceramic cutting tool materials, coating techniques, coating material selection and the metallurgy of nickel based super alloys. The chapter gives a broad understanding of these subject area and process of how they are applied to this type of high-performance tooling application.

3. **Chapter 3** presents the experimental techniques and analysis methods that were utilised throughout this research study.

4. **Chapter 4** presents published work titled "Chip formation and wear mechanisms of SiAlON and whisker-reinforced ceramics when turning Inconel 718. The paper defines the optimum cutting conditions and wear characteristics of SiAlON and whisker-reinforced ceramics when turning solution annealed Inconel 718. The research characterises the level of tool wear of SiAlON and whisker-reinforced ceramics and the type of chip formation when machining solution annealed Inconel 718. The research provided an early insight into machining Inconel 718 with ceramic inserts. The results of a literature review highlighted the lack of research which had focused on coated SiAlON milling inserts. Determining the benefits of adding a protective CVD coating to a SiAlON insert became the focus of the remaining chapters.

5. **Chapter 5** presents published work titled 'Tool life and wear mechanisms of CVD coated and uncoated SiAlON ceramic milling inserts when machining aged Inconel 718'. The paper presents the tool life and the associated wear mechanisms of CVD coated and Uncoated SiAlON inserts when face milling Inconel 718. The research characterises the levels of cutting force, wear mechanisms and tribological interaction of coated and uncoated SiAlON inserts with the Inconel 718 samples. The research also establishes the failure mechanisms for the coated SiAlON milling inserts, and what should be utilised in future protective coating systems.

6. **Chapter 6** presents published work titled 'Structure and Tribological Properties of Multilayer CVD Coatings Deposited on to the SiAlON Ceramic Milling Inserts'. The paper presents the failure mechanisms of two Coating A and Coating B when subjected to pin-on-disc and scratch testing. The research in this chapter looks to combine the conclusions of Chapter 5 and Chapter 6, to provide further substantiation of what CVD coating materials should be utilised in future protective coatings.

7. **Chapter 7** presents research which has utilised conclusions from Chapter 5 and Chapter 6, and has focused on comparing the wear characteristics of uncoated SiAlON milling inserts and SiAlON milling inserts that have been CVD coated with Coating C. The chapter is split into two parts, part A and part B. Part A focuses on the machining trial that utilised interrupted non-continuous 3-axis toolpaths to machine precipitation hardened Inconel 718 samples with Coating C inserts. Part B focuses on the machining trial that utilised a combination of continuous and near-continuous 5-axis toolpaths to machine two bar blades from precipitation hardened Inconel 718. The wear characteristics and attained tool life of the Coating C inserts were compared with that of the uncoated inserts. The machining trials have provided some interesting results in terms of wear characteristics and tool life, some important conclusions will be found in this chapter.

8. **The final chapter, Chapter 8** will present the general conclusions, which will include a summary of all of the discussions that are written in this thesis, followed by two sections: contributions and novelty, further future work. The second section will refer to the future work and the implications of continuing the research.

Chapter 2 Literature Review

This chapter provides a critical review of the relevant literature along with justification as to why these have been selected by the author during the experimental work. However, although the majority of the relevant literature is discussed in this chapter, other relevant literature will be discussed in later chapters.

2.1 Historical Background of Cutting Tools

The development of suitable cutting tool materials is process that has taken place over the last 120 years. The development of high-speed steels took place in the early part of the 1900's. English metallurgist Robert Forester Mushet began to experiment with different alloying elements such as manganese and tungsten that ultimately lead to creation of high-speed steels which were utilised during the industrial revolution. The development of high-speed steels ran in parallel to rise of consumer products, demand for high productivity also came from industry sectors such as the automotive and defence sectors. The rise in demand called for harder more durable high-speed steels and early development of cemented tungsten carbide cutting tool materials [13]. During years of 1923 – 1925 a series of patents and developments for tungsten carbide were attained by Spriggs et al. [14]. Spriggs et al also concludes that Friedrich Krupp Aktiengesellschaft of Essen, were the first manufacturers of hard metals. By 1929 the grain size of tungsten carbide had been further refined by Krupp researchers.

2.2 Terminology Used in Metal Cutting

The Cutting speed of the milling cutting tool (V_c), is the rate at which the workpiece moves across the cutting edge of the tool and is measured in metres per minute (m/min). Table Feed rate (fz) is defined as the distance travelled by the machine table for each revolution of the cutting tool and is calculated in millimetres per revolution (mm/rev). Depth of cut (Ap) is the thickness of the material that needs to be removed from the stock material or near net shape in the z-axis direction and is expressed in millimetres (mm).

Metal removal rate (MRR) is a parameter which is often used to determine the efficiency of a machining operation i.e., turning, milling, and grinding; it is the product of cutting speed of the cutting tool, feed rate and the depth of cut. The rake face is the cutting tool surface which the chip flows during the machining processes. The flank face is the cutting tool surface of the tool over which the freshly cut surface of the workpiece passes. The primary cutting edge is the

intersection of the flank with the rake face and forms the cutting edge; Secondary cutting edge, is the remainder of the cutting edge which may not actually be engaged in the cutting process.

Shear zones there are two major zones of shear when a chip forms. One is the primary shear zone which is the boundary between the unsheared work material and the chip. And the other is the secondary shear zone, also known as flow zone which, is the interface between the tool and the chip on the rake face.

2.3. Workpiece Materials – Super-alloys

Objective 1a focuses on looking at workpiece materials and the machining characteristics of nickel-based alloys. Super-alloys are a branch of high-performance alloy which have predominantly a nickel, cobalt, or iron matrix, strengthened with a series of intermetallic compounds like chromium, aluminium, titanium, tungsten, niobium, tantalum, and molybdenum, as seen in Figure 2.1. In Figure 2.2, a list of some of the super-alloys which have either a nickel, iron or cobalt matrix can be seen. A lot of the super-alloys that can be seen in Figure 2.2 were developed over 75 years ago. The likes of nickel-based alloy Nimonic 75 were the very first turbine blade alloys used in the jet engine designed by Sir Frank Whittle. Some of the most thorough research into super-alloy development has been conducted by Reed et al.[15]. The research that has been completed by Reed et al, looks at the full cycle of nickel based super-alloy development from the early wrought nickel-based alloys to the most advanced single crystal nickel-based alloys.

This image has been removed by the author of this thesis for copyright reasons
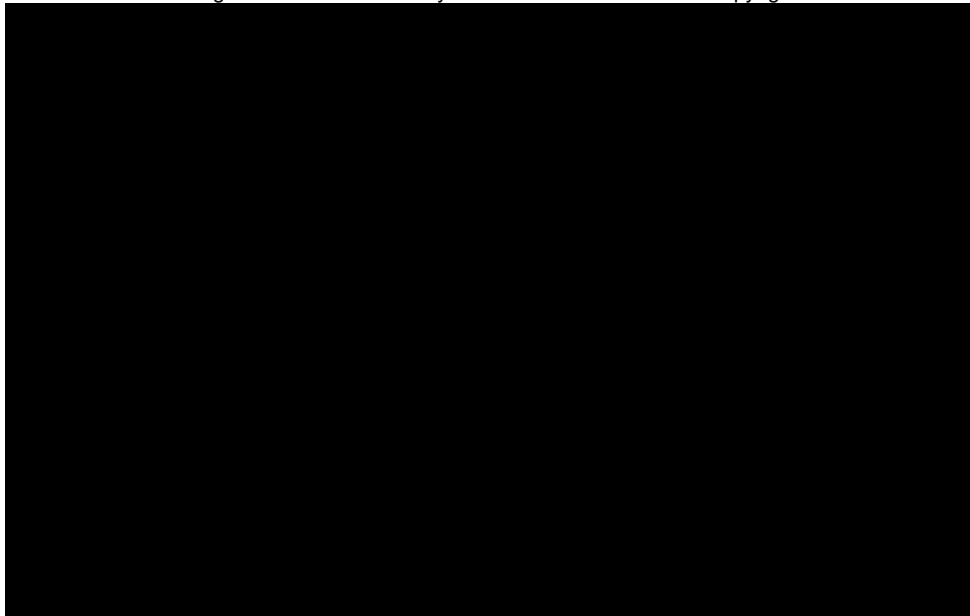
Figure 2.1.Categories of important alloying elements in constitution of nickel alloys and their relative positions in the periodic table. [15]

The latest single crystal alloys are now alloyed with the likes of rhenium, ruthenium and hafnium which has improved their high temperature performance and allowed significant improvements in turbine inlet temperature and specific fuel consumption. Figure 2.3 shows the improvements which have been attained with the adoption of single crystal casting technology and the inclusion of alloying additions such as rhenium.

This image has been removed by the author of this thesis for copyright reasons
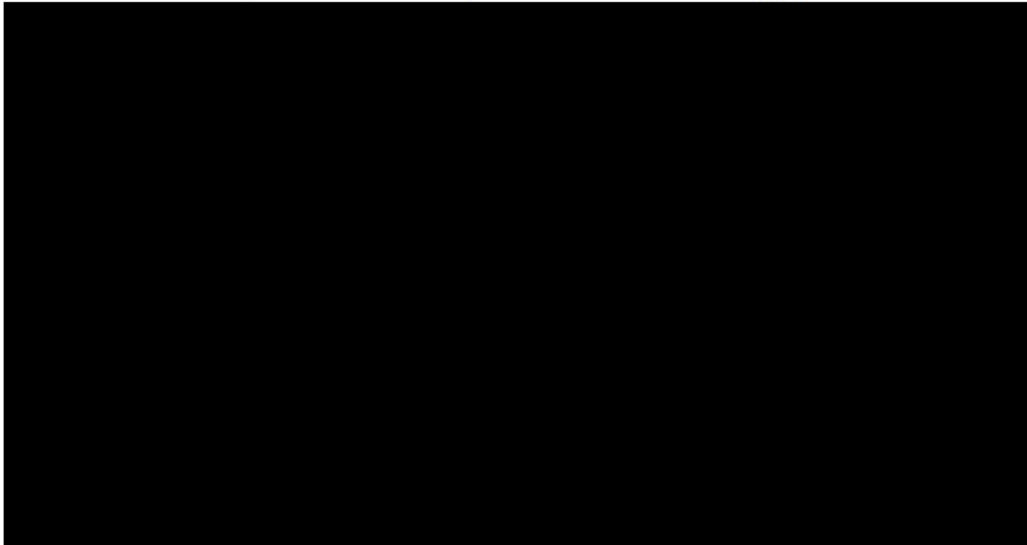
Figure 2.2. Classification of different super-alloys. [16]

Nickel-based alloys have always been considered hard to machine, both in terms of machine efficiency and cost effectiveness, the favourable high temperature property and resistance to creep being the predominant reasons as to why.

This image has been removed by the author of this thesis for copyright reasons
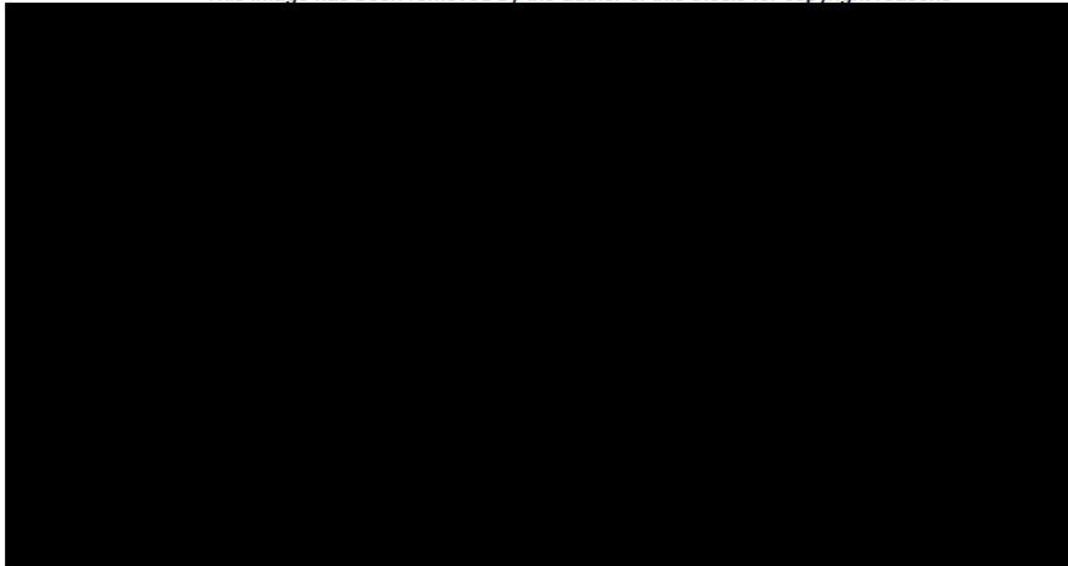
Figure 2.3. Evolution of the high-temperature capability of the super-alloys over a 60-year period since their emergence in the 1940s. [15]

2.3.1 Nickel Based Super-alloys

Nickel-based alloys are a special group of alloys which have a complex microstructure. The special characteristics allow nickel-based alloys to retain their high temperature strength, up to 70% of the melting point. All nickel-based alloys have a face-centre cubic crystal structure; this crystal structure is visible in Figure 2.4. The use of nickel-based alloys has predominantly been high in the aerospace sector but in recent decades, other industries, such as the oil and gas industry, have looked to exploit the enhanced corrosion and high temperature strength capabilities for deep-hole oil exploration.

This image has been removed by the author of this thesis for copyright reasons
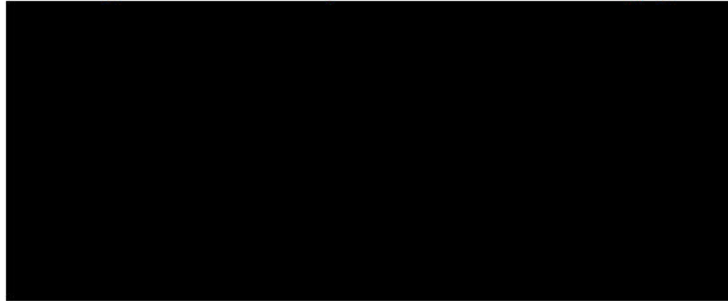
Figure 2.4. The unit cell of the face-centered cubic (FCC) crystal structure, which is displayed by nickel. [15]

2.3.2 Inconel 718

Inconel 718 is one of the most widely used nickel-based alloys currently available to engineers in the aerospace sector and other high-performance sectors like the oil and gas sector. Inconel 718 has found widespread use due to its exceptional thermal resistance and the ability to retain its mechanical properties at elevated temperatures over 700°C. Inconel 718 attains very high strength from a nickel austenitic face-centre cubic crystal structure which is reinforced with intermetallic compounds such as chromium, iron, molybdenum, and niobium (formerly columbium). Inconel 718 contains a rather large percentage of iron, which allows for good forming characteristics i.e., superplastic forming and forging. Iron creates a problem because of diffusion wear, which is a contributing factor to ceramic tool failure [17]. Table 2.1 and Table 2.2 outline the chemical composition and key mechanical properties of Inconel 718.

Table 2.1. Typical chemical composition of Inconel 718 (wt %). [17]
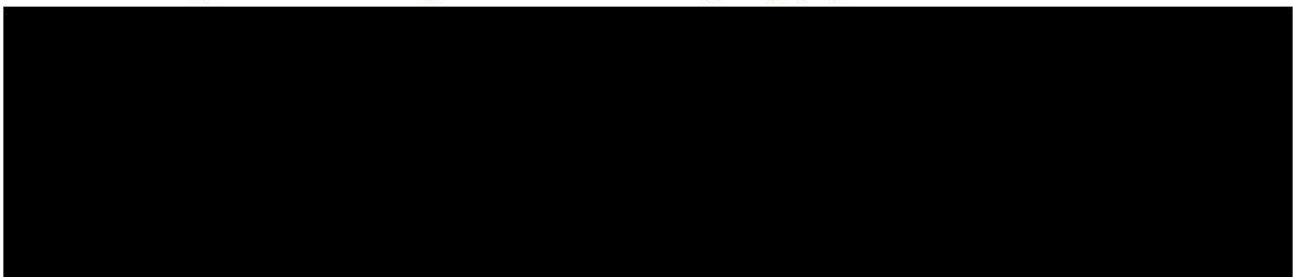
This image has been removed by the author of this thesis for copyright reasons

Table 2.2. Mechanical properties of Inconel 718 (AMS5663). [17]
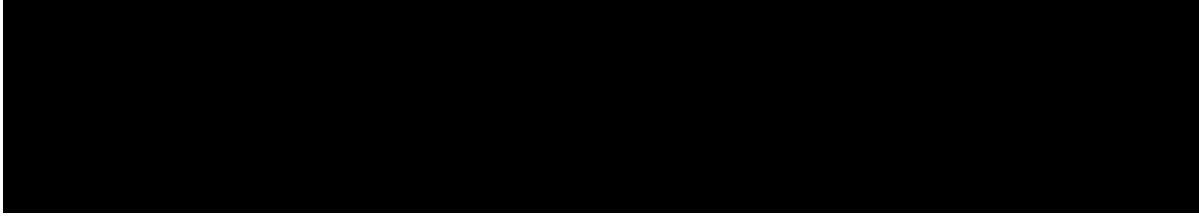
This image has been removed by the author of this thesis for copyright reasons

2.3.3 Machining Characteristics of Nickel Based Super-Alloys

Machining nickel-based alloys results in rapid wear of the cutting tool due to the highly abrasive austenitic microstructures which is exhibited by all nickel based super-alloys. The austenitic microstructure creates an intense environment for all types of cutting tool be it a tungsten carbide insert; ceramic insert or cubic boron nitride insert. High cutting forces, high cutting temperatures and localised heating of the cutting edge are the end result of the machining process.

2.3.4 Machining Induced Changes to Microstructure

When machining difficult to machine materials such as nickel based super-alloy Inconel 718, the machining process can induce surface changes in the form of white layer and a swept grain microstructure on the near surface. When ceramic cutting tools are used to machine Inconel 718, the chip/tool interface generates high cutting temperatures and high levels of insert wear. This particular machining environment and insert wear rate has a profound influence on the depth of surface transformation and white layer generation. Machining induced white layer is generated during phase transformation and plastic deformation of the immediate surface layer of the workpiece material. The level of white layer is driven by insert wear which can vary from 0.024 mm up to 0.060 mm in depth [18]. Assessing the level of machining induced white layer is of key importance as it determines the level of material that may need to be removed to prevent reduction in the fatigue life of industry components. One such area of machining induced white layer non-destructive assessment, has focused on establishing the size of machining induced white layers and plastic deformation with x-ray diffraction peak breath measurements [19].

2.4 High Speed Machining

In the last two decades, high speed machining (HSM) has gained a lot of interest and attention with regards to improving productivity in high value manufacturing sectors such as automotive and aerospace [20]. Machining nickel based super-alloys such as Inconel 718 at high cutting speeds, results in high metal removal rates and low cutting forces. High speed milling of Inconel 718 results in a high-quality surface finish and high manufacturing productivity [21]. Machining nickel-based alloys at high cutting speeds requires specialist spindle setups, high machine bed

stability, high machine power capability, specialist CAD/CAM packages and cutting tools (endmill or inserts) that withstand high temperature machining environments. Spindle speeds used for high-speed machining for creating curved surfaces in Inconel 718 can range from 3000-17000 rev/min. However, when spindle speeds are too high the tool wear is excessive due to the poor thermal conductivity and work hardening characteristics of Inconel 718 [22]. Machining nickel-based alloys with ceramic cutting tools comes under the high-speed machining category. Machining Inconel 718 with ceramic endmills can require spindle speeds of up to 18000 rev/min, to achieve a cutting velocity of 300-400 m/min. High cutting speeds (above 315 m/min) are required with ceramic cutting tools to induce a reduction in resultant cutting forces as a result of thermal softening of the Inconel 718 microstructure [23]. Cutting speeds for ceramic inserts are lower with respect to cutting speeds required by endmills. Typically, spindle speeds for ceramic inserts can be in the range of 10000 rev/min, which can attain a cutting velocity of 800 m/min. These cutting speeds are required for effective thermal softening of the Inconel 718 microstructure which reduces tool wear and improves tool life.

2.5 Cutting Processes and Chip Formation

2.5.1 Segmented Chips

Objective 1b focuses on looking at the cutting processes and chip formation. Segmented chips are predominantly formed when machining high strength materials such nickel-based superalloys. Inconel 718 exhibits poor thermal conductivity properties, which are highly influential when it comes to the formation of segmented chips [24]. The heat which is generated in the chip tool interface causes the severe plastic deformation of the cut chip material as can be seen in Figure 2.5.

This image has been removed by the author of this thesis for copyright reasons
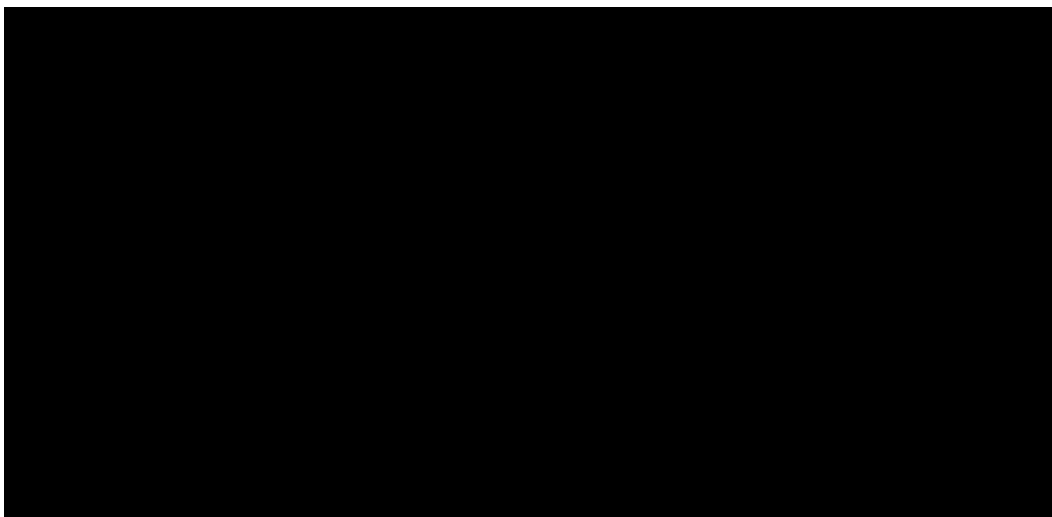
Figure 2.5. SEM images of the segmented Inconel chip cross-section at: (a) V_C = 900 m/min; (b) V_C = 500 m/min. [25]

Inconel 718 retains its high tensile strength to temperatures of 650°C, and this causes fluctuations of the specific cutting forces and shear strain energies. These fluctuations in specific cutting forces and shear strain energies during the chip formation deformation process, tend to focus along localized intense shear bands [26]. Segmented chips are produced due to the tendency of thermal softening and localized shear band deformation; Hao et al states that shear band deformation in the Inconel 718 chip strain harden to the point of fracture. The localized shear bands and deformation twinning are identified in Figure 2.5(a) and (b).

The feathering effect that is represented in Figure 2.6, highlights the evenly spaced localised shear band that take place during high-speed machining of materials such as Inconel 718.

This image has been removed by the author of this thesis for copyright reasons
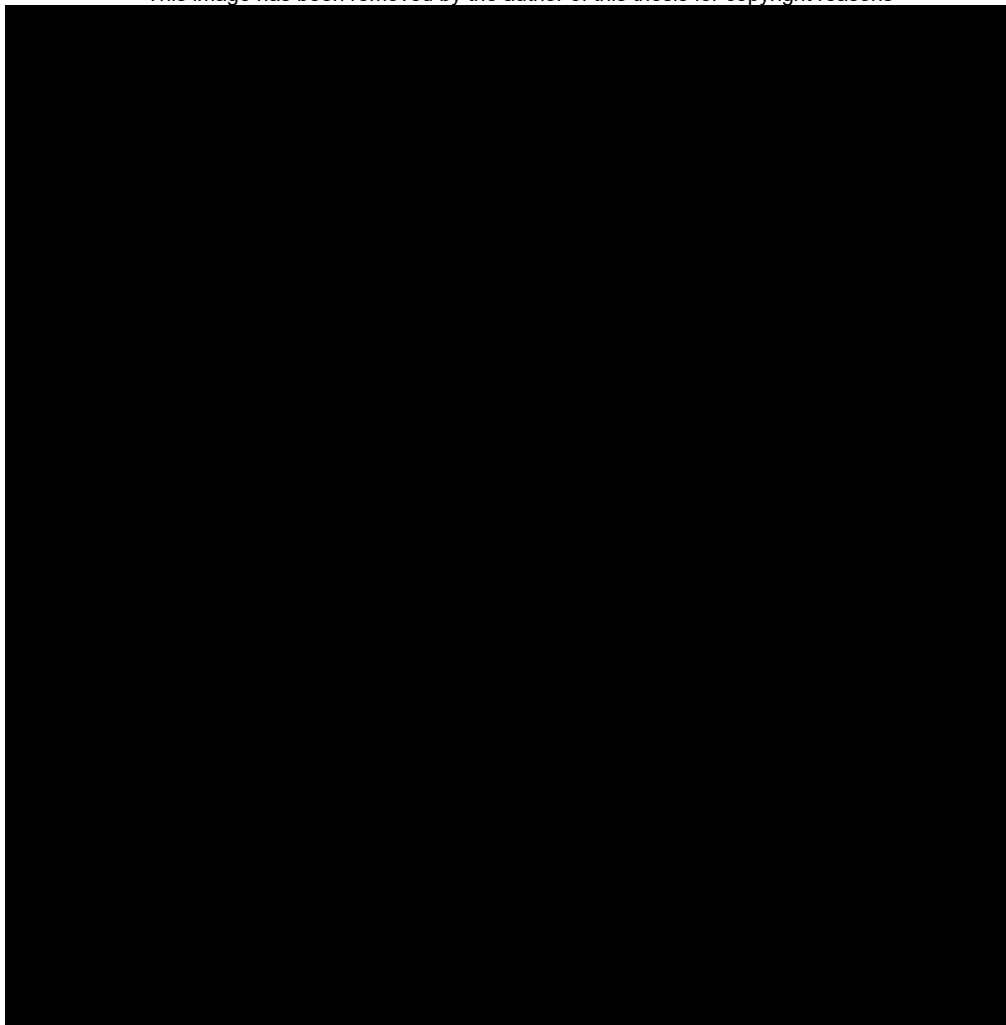
Figure 2.6. (a) Patterns of the serrated chips at fz =0.07mm=tooth, Ap=1.5 mm, and ae=19.0 mm.(b) SEM images of serrated chips. [24]

In Figure 2.7 a serrated chip formation model is depicted, Ulutan et al [27] states the model analytically describes serration process of a chip, which ultimately creates a saw- tooth shape.
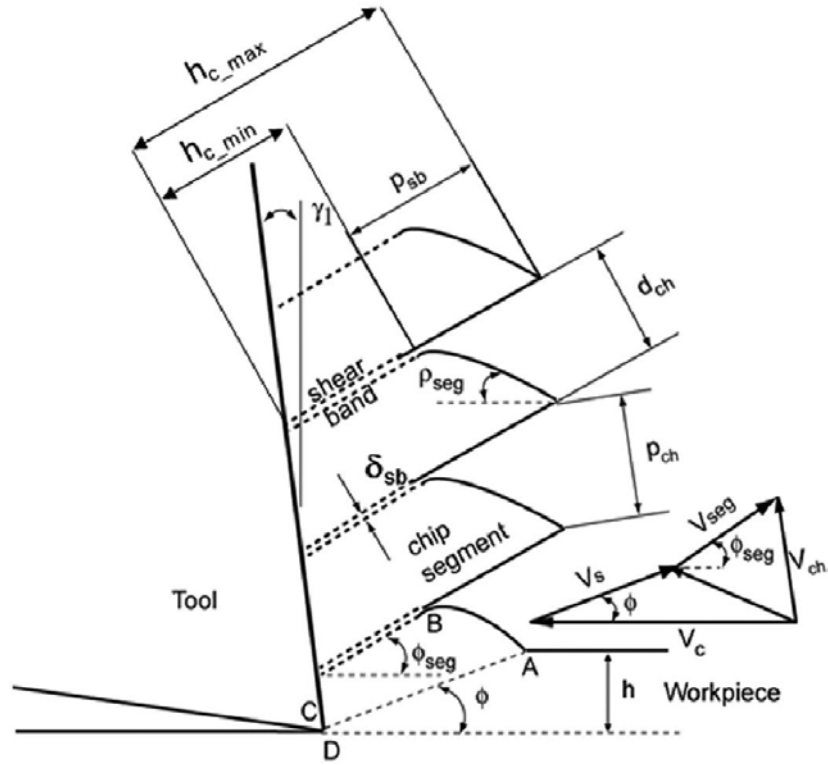
Figure 2.7. Serrated chip formation model and its hodograph. [27]

The shear band thickness (δ_{sb}) and the pitch of these chips (P_{ch}) become important factors when determining the shear strain at the adiabatic shear band. Ulutan et al concludes that in order to ascertain the experimental chip thickness, an arithmetic average can be utilised to attain this chip thickness. In order to calculate the average shear strain the model in Figure 2.7 can be adopted. Nickel based alloys chip formation undergoes adiabatic shearing and crack formation. The segmentation rate (Ds) is calculated using the minimum (h_{c_min}) and maximum (h_{c_max}) experimental chip thicknesses along the serrated chips where their locations are indicated in Figure 2.7.

$$Ds = \frac{h_{c\_max} - h_{c\_min}}{h_{c\_max}} \qquad \text{Equation 2.1}$$

The chip ratio (r_c) is defined by the ratio of undeformed chip thickness (h) (or feed in orthogonal cutting) to the average thickness of the segmented chips (h_c).

$$r_c = \frac{h}{h_c} \qquad \text{Equation 2.2}$$

The shear angle (ϕ) can now be calculated by utilizing the measured chip ratios using the following formula, which is then derived by using the ratio (r_c) of undeformed chip thickness (h) to the average chip thickness (h_c) and rake angle (γ_1).

$$\phi = atan\left(\frac{r_c cos(\gamma_1)}{1 - r_c sin(\gamma_1)}\right)$$

<div align="right">Equation 2.3</div>

Following this formulation, the shear strain in the primary shear zone (γ) can be found and the calculation based on continuous chip formation assumption becomes.

$$\gamma = \frac{cos(\gamma_1)}{sinsin(\phi)\ cos(\phi - \gamma_1)}$$ Equation 2.4

In addition, the average shear strain in segmented chip (γ_{seg}), average shear strain in the shear bands (γ_{sb}) and average strain rate based on segmented chip calculations.

$$\gamma_{seg} = \frac{sinsin(\rho_{seg})}{sinsin(\phi_{seg})\ sin(\phi_{seg} + \rho_{seg})}$$ Equation 2.5

$$\gamma_{sb} = \gamma_{seg} + \frac{P_{sb}}{\delta_{sb}}$$ Equation 2.6

where (ρ_{seg}) is the chip segment angle, (ϕ_{seg}) is shear angle at the chip segment, (P_{sb}) is depth of segmentation, and (d_{sb}) is shear band thickness.

2.6 Heat Generated During Milling

The heat generated at the chip/tool interface-rake surface can vary in temperature based on the cutting speed (V_c), table feed rate (T_f) and the depth of cut (DoC). The heat which is generated during a milling process is highly influence by the cutting speed which is utilised. Figure 2.8 represents what happens to the cutting tool edge temperature when machining Inconel 718 at different cutting speeds [28].

This image has been removed by the author of this thesis for copyright reasons
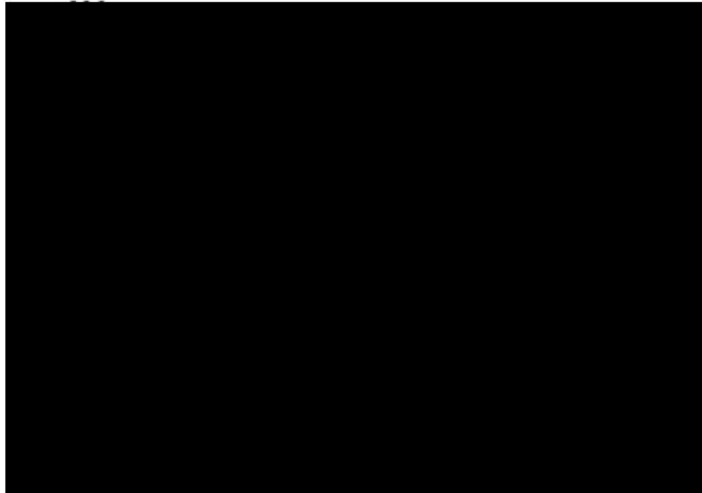
Figure 2.8. Variation in tool edge temperature (Al_2O_3-TiC ceramic cutting tool) with cutting speed during turning operation on Inconel 718. [28]

The cutting edge will drop in temperature up to cutting up to a cutting speed of 600 m/min and then will increase beyond this cutting speed. In Chapter 7, the importance of cutting temperature becomes very evident on tool life and tool wear. Controlling the fluctuation in cutting temperature with well refined toolpaths, has proven in later chapters to be highly influential and had a positive effect on flank wear versus material removal volume.

The primary increase in cutting temperature is generated in the chip/tool interface, the cutting temperature increases further still as the tool begins to wear. The link between tool wear and cutting temperature is shown graphically in Figure 2.9.

This image has been removed by the author of this thesis for copyright reasons
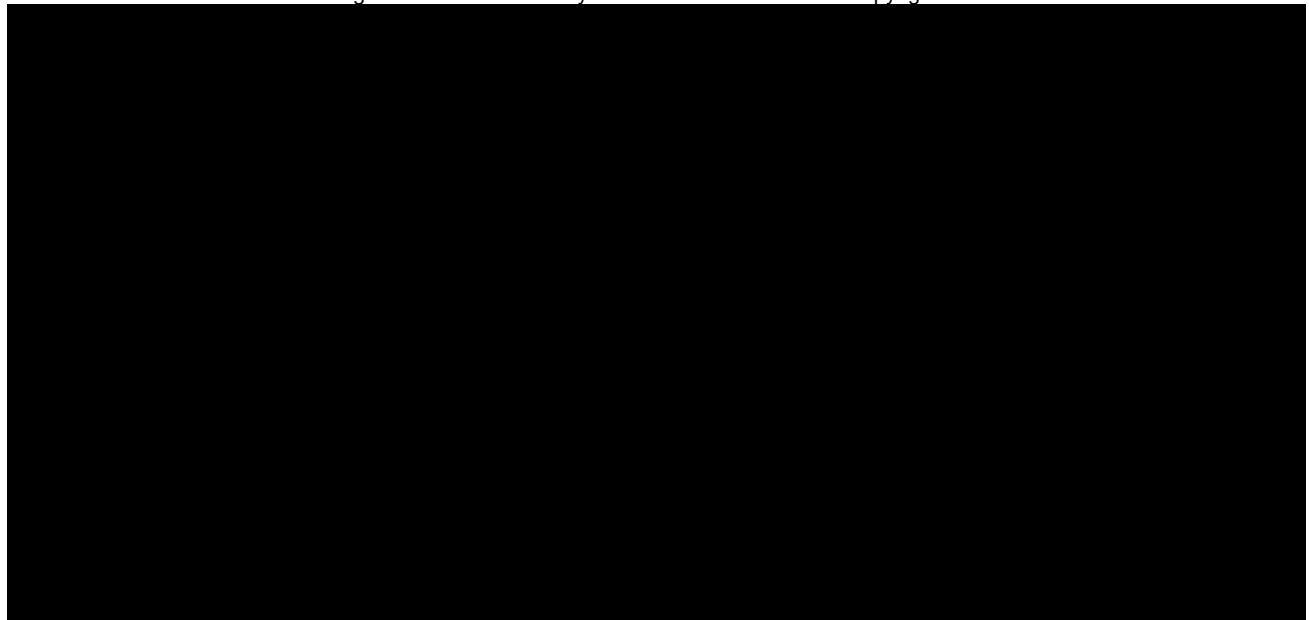
Figure 2.9. Orthogonal cutting process (schematic) at distinct conditions of the tool(a) standard tool; (b) worn-out tool. [29]

2.6 Cutting Force

Determining the cutting forces in a machining process is an important parameter to clarify. The magnitude of the cutting force necessary to cause a shearing action on the metal workpiece can vary somewhat depending on the mechanical properties of metal being cut. Understanding the behaviour of certain metals when being cut has had direct impact on design and manufacture of machine tools, so they have sufficient rigidity, mechanical properties and eliminate vibration during the machining process. The design of suitable tool geometries is further enhanced with the accurate measurement of the forces present in metal cutting process. The forces present during the cutting process can be resolved into three components which are shown in Figure 2.10.

The first component is the cutting force (F_c) which is usually the largest force acting on the rake face in the direction of the cutting velocity. (F_t) is the tangential cutting force and (F_r) is the resultant cutting force.
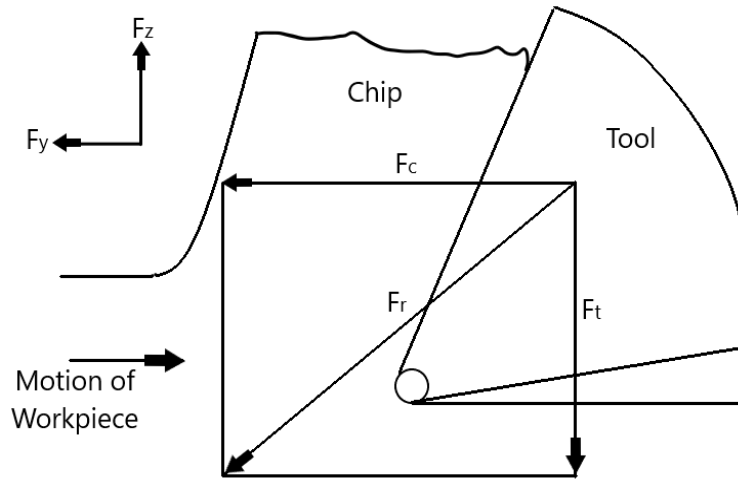
Figure 2.10. Schematic of cutting force in metal cutting.

The table feed thrust force in (F_y) direction is directly linked with the cutting force, which cutting tools will experience during the machining process. Finally, the resultant force (F_r) is the true cutting force which is shearing the material.

2.7 Types of Wear Mechanisms for Ceramic Cutting Tools

Objective 1c looks to focus on the types of wear mechanisms experienced by ceramic cutting tools. The machining of nickel-based super-alloys inherently causes rapid tool wear and degradation of ceramic cutting tools; as a result, ceramic inserts experience a range of different wear mechanisms when cutting nickel-based alloys. Figure 2.11 shows a typical SiAlON milling insert.
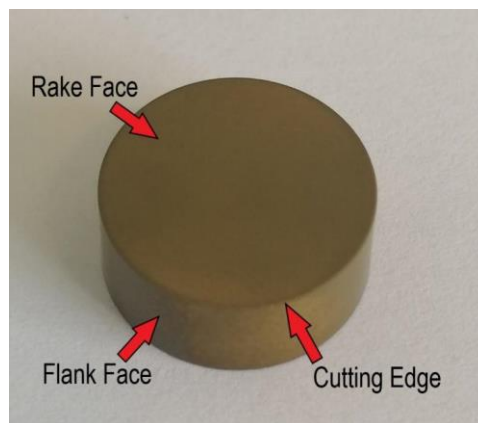
Figure 2.11. CVD coated SiAlON ceramic RNGN milling insert.

17

In the forthcoming sections some of primary and secondary wear mechanisms experienced by ceramic inserts are discussed. One focus for this project is understanding the wear and failure characteristics of ceramic cutting tool materials, which is important for improving the tool life and making ceramic cutting tools more reliable in the workplace.

Another area of interest is predicting the fracture characteristics of SiAlONs. A typical SiAlON ceramic cutting tool matrix mainly constitutes a mixture of α-SiAlON grains and β-SiAlON whiskers with the remaining matrix volume being filled with yttrium oxide (Y_2O_3), which influences densification and reinforcement of the SiAlON microstructure with glassy phases. When SiAlON microstructures are subjected to sufficient levels of stress, β-SiAlON whiskers separate from the SiAlON matrix, leading to crack nucleation [30]. Hao et al also state that preventing this separation characteristic would lead to better fracture resistance and more resistance to cyclic impact loads. In the next section, the types of wear mechanisms that are experienced by ceramic cutting tool materials are discussed.

2.7.1 Flank Wear

Milling insert flank wear can be attributed to the amount of frictional heat and flank forces, caused because of chip sliding along the rake face. The sliding process generates abrasive wear and causes a series of deleterious effects on the rake face. During up-milling and down-milling operations have a direct impact on the life of the SiAlON cutting tool, which has been explored in detail by author like Tian et al. [31]. In the relevant research conducted by Tian et al, SiAlON milling inserts were operated at cutting speeds of 600, 1000, 1800 and 3000 m/min when machining Inconel 718.

The research conducted by Tian et al developed a thorough understanding of the effects of up and down-milling on the flank face wear of SiAlON milling inserts. Tian et al. [31] determined that a cutting speed of more than 1000 m/min must be used to get optimal tool life. However, in Chapter 5 and Chapter 7, it is concluded that the optimal cutting speed for machining precipitation hardened Inconel 718 is between cutting speeds of 800-900 m/min. SiAlON ceramics have excellent high temperature capabilities and resistance to thermal shock, which means that SiAlON ceramic have been used at high cutting speeds. The high thermal shock resistance allows SiAlON ceramics to have high resistance to fracture. Later studies have determined that SiAlON milling inserts have higher flank wear-resistance compared to whisker-reinforced alumina milling inserts [32], [33], as can be seen in Figure 2.12.
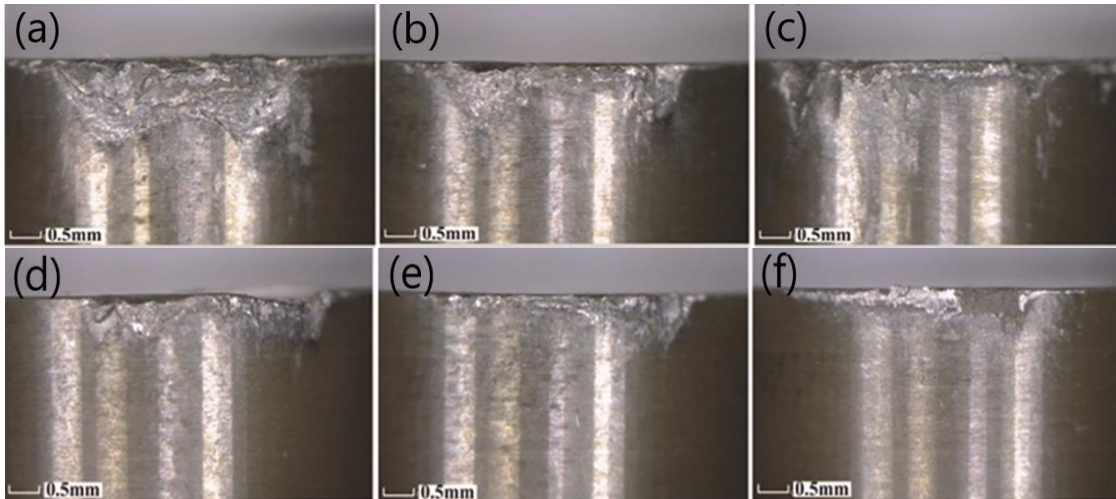
Figure 2.12. Flank face wear patterns of SiAlON ceramic grade KY1540 under different cutting speeds (metal removal volume of 1500 mm^3): (a) Vc = 900 m/min, (b) Vc = 1100 m/min, (c) Vc = 1300 m/min, (d) Vc = 1800 m/min, (e) Vc = 2500 m/min and (f) Vc = 3000 m/min. [32]

They also note that flank wear reduces with an increase in cutting speed from 900 m/min to 1400 m/min but ultimately leads to higher rates of adhesion wear when increased to 3000 m/min.

2.7.2 Rake Face or Crater Wear

Rake face wear is due in part to the frictional forces and cutting temperatures which are being generated in the shear zone. As the chips slide over the rake face, abrasive particles that are found in the nickel-based alloy metallic microstructure, such as titanium carbides, niobium carbides and aluminium oxides begin to wear away the ceramic cutting tool. The rake face wear is attributed to high contact pressures and high temperatures due to the high frictional forces that are generated in the shear zone between the swarf chip and cutting tool [24]. At high cutting temperatures, crater wear is also caused by diffusion of the SiAlON cutting tool into tool piece. This is due to the affinity between iron in the Inconel 718 material and the silicon in the SIAlON cutting tool. Race face wear is of particular interest to this research and has been analysed at length in Chapter 4, 5, 6 and 7.

2.7.3 Depth of Cut Notch Wear

One of the main failure modes when machining nickel-based alloys with ceramic cutting tools is depth of cut notch wear. Authors like Xiao et al. [34] and Shalaby et al. [35] investigated and determined that one of the primary failure mechanisms for ceramic cutting tools is notching and determining the amount of wear and time a ceramic cutting tool can endure is important. Depth of cut notch wear is highly dependent on understanding the wear characteristics of the cutting tool material. Shalaby et al suggest that notch wear appears on primary cutting edges and

trailing edges of the cutting inserts. They state that steep stresses, work-hardened surfaces, adhesion, and temperature gradients are potential causes for notching. Improving the resistance to notching is paramount for improving the life of ceramic cutting tools.

2.7.4 Adhesion Wear

Adhesion wear is very evident during the high-speed machining of nickel-based alloys such as Inconel 718, as can be seen in Figure 2.13a and Figure 2.13b. To reduce the effects of adhesion wear, it is necessary to reduce the amount of friction that is generated in the chip/tool interface. The investigation that was conducted by Liu et al. [36], achieved promising results by applying a hard titanium carbo-nitride (TiCN) coating onto the surface of the SiAlON turning insert.

Another investigation that was found to be of relevance in the present research was conducted by Çelik et al. [37]. Çelik et al achieved success in improving adhesion wear-resistance by adding titanium nitride (TiN) particulates into the SiAlON matrix. These relevant studies conducted by Lui et al and Çelik et al highly influenced a critical review of literature to see whether coated SiAlON milling inserts should be pursued. Adhesion wear is of high interest to this research and is highly prevalent in Chapter 5.

This image has been removed by the author of this thesis for copyright reasons
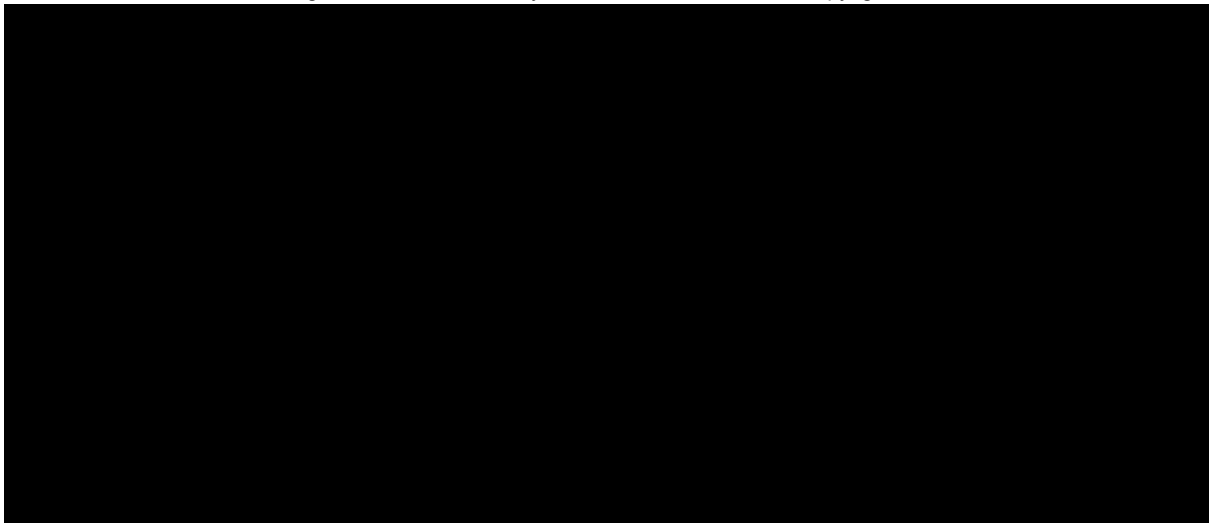
Figure 2.13. (a) Shows the flank face abrasion and adhesion of an uncoated SiAlON insert, (b) shows the flank face abrasion and adhesion of a coated SiAlON insert. [36]

2.7.5 Edge Cracks (Micro-cracks), Chipping, Flaking

Ceramic cutting tools (due to their brittle microstructure) are inherently more at risk of catastrophic tool failure. One of the failure mechanisms that contributes to this catastrophic tool failures is via edge cracks or micro-cracks which is captured in Figure 2.14.
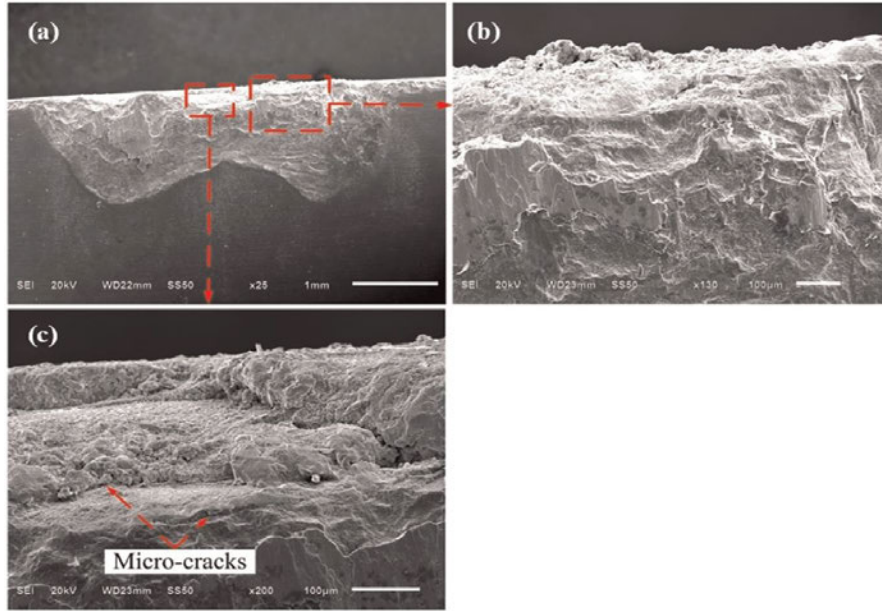
Figure 2.14. (a) SEM image of chipping, (b) and (c) are magnified SEM images of micro cracks on the flank face of KY1540 SiAlON milling insert at a cutting speed of Vc = 900 m/min. [32]

Authors including Molaiekiya et al. [38] and Shalaby et al. [39] have investigated that micro-cracks are generated via a combination of factors, such as high temperatures and mechanical contact pressures in the chip/tool interface, together with interrupted cuts. These factors can ultimately lead to thermal fatigue of the ceramic cutting tool material, this is more apparent in SiAlON cutting tools. Reducing the creation of micro-cracks where feasible will improve the longevity and tool life of SiAlON cutting tools [23]. Figure 2.14a, 2.14b and 2.14c show typical chipping that takes place on the flank face. Tian et al notes that using the correct cutting parameter will help prevent edge cracks that consequently result in chipping and flaking of the flank face. Figure 2.15 images (a) and (b) show typical flaking that takes place on the rake race of the cutting tool.
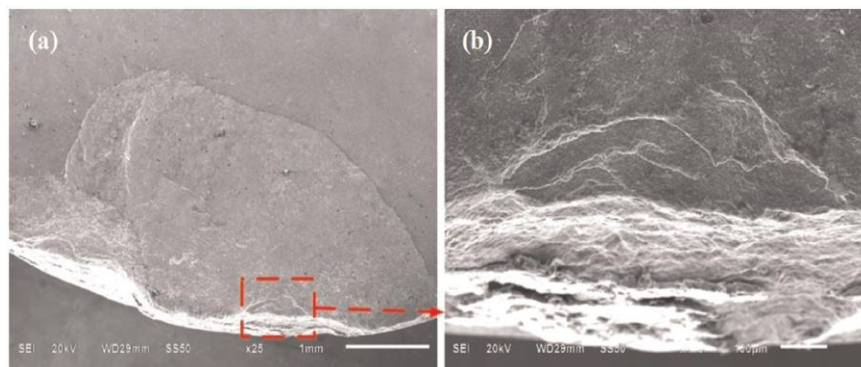
Figure 2.15. (a) SEM image of flaking (b) magnified SEM image of rake face of KY4300 WFA milling insert at a cutting speed of Vc = 500 m/min. [32]

Fine tuning the cutting parameters so that flaking and chipping is prevented where possible is of obvious importance, and must be implemented for all machining strategies [31].

2.7.6 Diffusion Wear (Solid Solution Wear)

One of the principal reasons for studying the benefits of applying a protective coating to SiAlON milling inserts, has been to dilute the effects of diffusion wear mechanisms. When silicon nitride-based ceramic and silicon aluminium oxynitride ceramic cutting tools are used to machine materials with high iron content, especially at high temperatures above 1000°C. Nickel based alloys such as Inconel 718 typically contain, 17-18% iron. Therefore, when silicon nitride-based ceramic and silicon aluminium oxynitride ceramic cutting tools are used to machine Inconel 718, diffusion wear will take place.

Diffusion wear is believed to be one of the secondary wear mechanisms contributing to a reduction in tool life when machining nickel-based super-alloys. Diffusion wear will take place when the temperature of the chip/tool interface causes mass transfer between the nickel-based alloy and the ceramic cutting tool. In diffusion or solid solution wear, the cutting tool material diffuses into or forms a solid solution with the evacuated nickel alloy chip material as seen in Figure 2.16. Figure 2.16 shows the structure of the diffusion interface, which takes place between the SiAlON substrate and Inconel 718. Therefore, the flank and rake face of the cutting tool edge is broken down and craters begin to form.

So, finding ways of reducing diffusion wear is of key importance for this research. The investigation by Diniz et al. [40], was focused on milling gray cast iron at high cutting speeds with both SiAlON ceramic and carbide tools. And the investigation by Diniz et al established that the probable cause of the tool wear for the SiAlON inserts to be diffusion wear.

Çelik et al. [37] and Sun et al. [41] also present studies that suggest diffusion wear is one of the dominant wear mechanisms contributing to flank and rake face wear when SiAlON milling inserts are used to machine Inconel 718.

Addhoum et al. [42] present a closer more in depth study, which explores the diffusion reactions which take place between silicon nitride-based ceramics and nickel-based alloys take place at 1100°C   with the formation of liquid phases. Addhoum et al also conclude that silicides, carbides, and potentially nitrides, are created due to the complex interaction mechanism and chemical reactions that take place between the silicon nitride-based ceramic cutting tool and the nickel-based alloy chip.
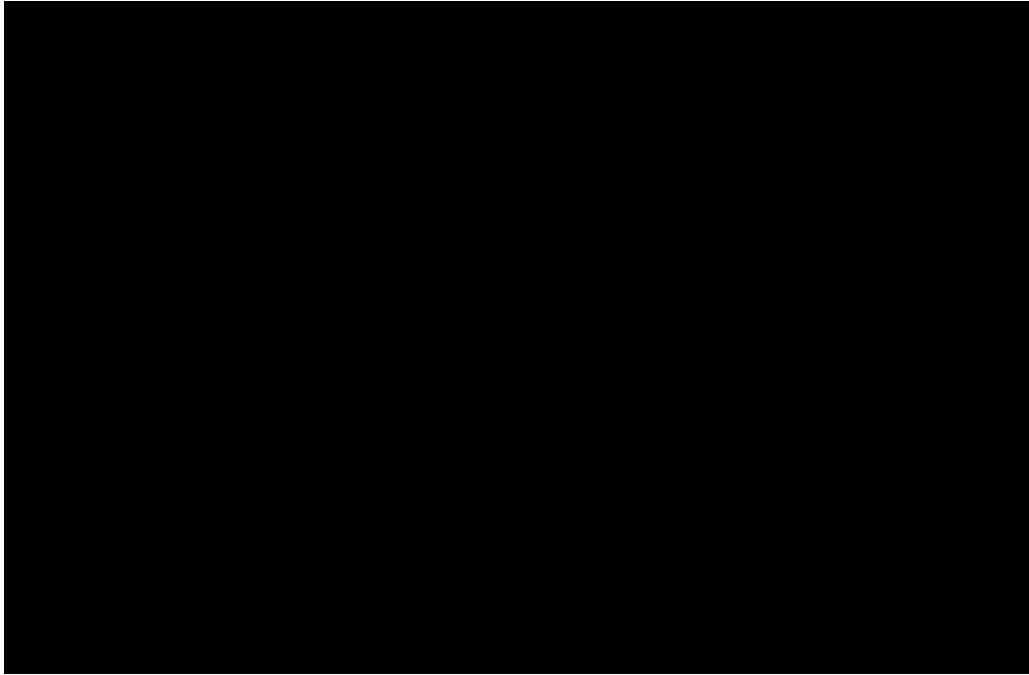
Figure 2.16. Schematic illustration of the structure of diffusion interface between SiAlON and Inconel 718 alloy. [43]

Further to the investigation that was conducted Addhoum et al, is the relevant study that was conducted by Çelik et al. [43], who state high-speed machining of nickel-based alloy Inconel 718 produces a chip-to-tool interface which is continuous/ near-continuous sliding movement on the rake face of the cutting tool. Çelik et al also noted that the chemical wear-resistance of α/β – SiAlON ceramics when machining Inconel 718 at high cutting speeds is dependent on the ease of diffusion product formation and the structural integrity of the SiAlON substrate when subjected to thermal and mechanical stresses.

2.7.7 Thermo-mechanical Wear – (Oxidation, Chemical Reaction)

Stephenson et al. [44] claim that oxidation occurs when constituents of the tool (especially the binder used in the tungsten carbide (WC) tools) react with atmospheric oxygen, while Vleugels et al. [45] concludes in their research that the primary wear mechanism for machining steel is chemical wear, and that the inter-diffusion of silicon, iron and yttrium between the ceramic cutting tool material and the steel workpiece was a lot less apparent than when machining solely iron. Vleugels et al also claim that the degradation of the cutting tool is due chemical disassociation of the SiAlON grains that ultimately leads to creation of craters on the rake face of the SiAlON cutting tool. Sun et al suggest that chemical wear contributes heavily to flank and rake face wear and also contributes to notch wear. Thermomechanical wear such as oxidation and thermal cracks can be seen in Figure 2.17.
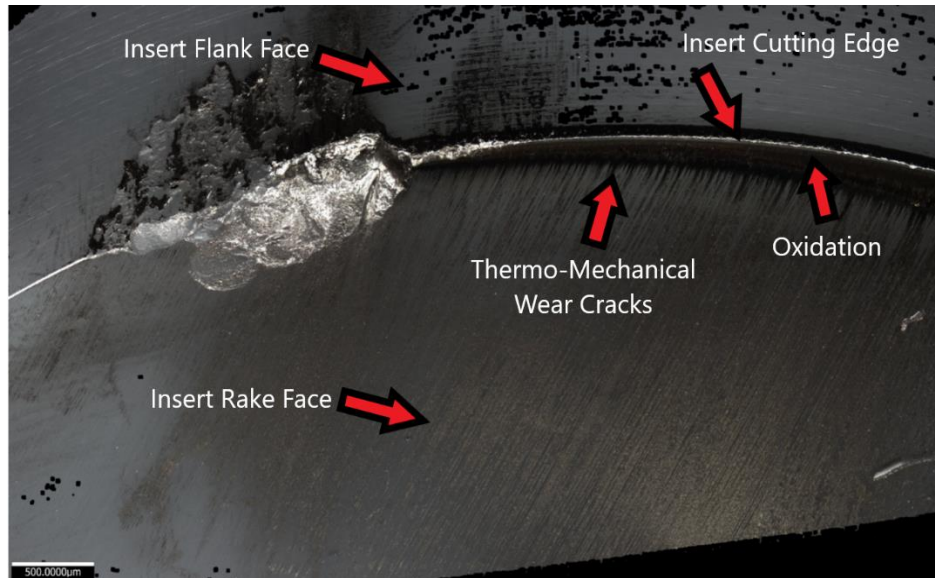
Figure 2.17. SiAlON insert showing thermo-mechanical wear on the rake face. Figure taken from publication arising from this thesis. [46]

2.7.8 Plastic Deformation

Plastic deformation of SiAlON cutting inserts is an indirect wear process, which results in the degradation of the cutting-edge geometry by the application of heat and pressure. Plastic deformation occurs when cutting materials with poor machinability characteristics like super-alloys and certain high alloyed steels. Due to high stresses involved during machining of materials with high yield strength, plastic deformation of the tool materials, even at low speeds takes place.

2.8 Tool Materials (Excluding Ceramics)

Cutting tool materials requirements differ greatly and depend not only on the machining process but also on the material that needs to cut. Several different toughen to super hard materials have been created to tackle the problems that are associated when machining certain metals, alloys, plastics and even ceramics. Essentially the cutting tool selection is based in accordance with material to be cut and the cutting conditions. Typical cutting tool material characteristics are as follows:

1. High hardness and strength at elevated temperatures.
2. Good resistance to thermal shock.
3. High resistance to thermal oxidation and impact loads.
4. High compressive, shear and tensile strength.
5. High resistance to deformation.
6. High chemical inertness.

24

2.8.1 High Speed Steels

At the beginning of the 19th century a new tool material was invented by Taylor and White, they had invented what would be classed today as high-speed steel (HSS). However, Rizzo et al. [47] states that the first alloy to be formally called high speed steel, was patented by the Crucible Steel Co in the beginning of the 20th century. The AISI T1 steel designation contains weight percentage 0.7% carbon, 18.0% tungsten, 4.0% chromium 1.0% vanadium and Iron being the remaining element to make up the AISI T1 steel grade.

Rizzo et al maintain that the alloy design for high-speed steel remained unchanged for the first 40 years; until additions of 12% cobalt were substituted for tungsten. The improved heat treatment technique of high-speed steel allowed for significant increases in metal removal rates. During World War two, metallic raw material such as tungsten and vanadium were in short supply and new leaner alloy content high speed steels needed to be developed. The necessity for leaner alloy high speed steels brought about the creation of the M-series of high-speed steel. The vanadium and tungsten were substituted for molybdenum and the AISI M2 HSS steel was established in the 1950's.

The molybdenum (Mo) grades or M series contain 3.5-10% molybdenum (Mo) with chromium (Cr), vanadium (V), tungsten (W) and cobalt (Co) as the other alloying elements. Rizzo et al. [38] concludes that M-series high speed steels can be manufactured either by casting or via powder metallurgy techniques. Incorrect processing of cast HSS will result in undesirable microstructural features and non-even distribution of the carbides. Rizzo et al states that refinement of the eutectic carbide dimensions and homogenous distribution of carbides throughout the matrix is highly important in achieving high cutting performance and hot hardness.

2.8.2 Cemented Tungsten Carbide

Ever since their creation in the early twentieth century in Germany, cemented tungsten carbide cutting tools have been in utilised for their superior hot hardness, chemical stability and substantially higher cutting performance when compared to high-speed steels. Rizzo et al explains that tungsten carbide is manufactured as a mixture of tungsten carbide powder and cobalt which acts as binder and holds the tungsten carbide together. This cobalt binder is the primary limiting factor when it comes to cutting temperature. As this binder is heated to above 600-700°C the thermal stability of the tungsten carbide microstructure begins to wane. Powder metallurgy techniques have been the preferred way of producing complex cutting tool

geometries and features. The fine tungsten carbide powder, which is bonded with cobalt, has helped to raise the production rate several fold when machining cast iron.

It was later discovered that this type of cutting tool material would not deliver the same improvements when machining high temperature alloy steels, nickel-based alloys, and stainless steels. This short tool life was due to severe crater wear on the rake face of the tool. Subsequently it was discovered that high temperature chemical interactions between the tool and the chip were responsible for this wear pattern. Improvements were made by coating the cemented tungsten carbide tools with titanium carbide and later with aluminium oxide via chemical vapour deposition and plasma vapour deposition techniques. Mohammad et al. [48] and Krishnan et al. [49] states tool failure modes are related to attrition and lead to exposure and result in built up edge.

CVD and PVD coated carbide cutting tools have allowed for higher cutting speeds (m/min), feed rates (mm/rev) and depths (mm), which is has resulted in significant gains in productivity. Textured carbide cutting tools are also gaining interest in regard to machining nickel-based alloys and 316 stainless steel. Khan et al. [50] and Soni et al. [51] concludes that the tool wear resistance is substantially increased, this is due to the reduction in friction and heat that is generated using a textured surface.

2.8.3 Poly-crystalline Cubic Boron Nitride (Ultra Hard Cutting tools)
Poly-crystalline cubic boron nitride (PCBN) is an ultra-hard refractory compound of nitrogen and boron. Vel et al. [52] states the high hardness comes from the intralayer B-N bonds are highly covalent and the interlayer bonds are weak van der waal bonds. The weak van der waal bonds are one of the reasons why PCBN tooling have the tendency to chip.

2.9 Ceramic Cutting Tool Materials
2.9.1 Development of Ceramic Cutting Tool Materials
Objective 1d consists of understanding ceramic cutting tool development and the materials that have been developed for the past forty years. Whitney et al. [53] state in early 1970s ceramic research that aluminium and oxygen could be substituted for silicon and nitrogen in the β-phase Si_3N_4 crystal structure. The solid substitution process would ultimately form silicon-aluminium-oxygen-nitrogen solid solutions, commonly known as β-phase SiAlONs.

Ceramic cutting tool development continued further as processes for producing ceramic cutting tool materials suitable for machining nickel-based super-alloys were refined early on in the 1980's and 1990's by Vigneau, J. et al. [54], Aucote et al. [55], Brandt et al. [56] and Richards at

al. [57]. Aucote et al and Vigneau, J. et al conducted comparison studies of the cutting performance between whisker-reinforced alumina (WRA), SiAlON ceramics and tungsten carbide cutting tools.

The early comparison research that was conducted by Vigneau, J. et al. [54], Aucote et al. [55], Brandt et al. [56] and Richards at al. [57] helped to clarify the machining capabilities, wear mechanisms and the manufacturing challenges of producing these new ceramic cutting tools. Research conducted by Choudhury at al. [16] in the late 1990s continued the development process with a machinability study, which compared tungsten carbide, ceramic and cubic boron nitride (CBN) cutting tools when machining nickel-based alloys. Choudhury et al concluded that whisker-reinforced alumina and SiAlON cutting tool flank wear resulted from diffusion wear.

Another comparative study related to ceramic tooling was conducted by Grigoriev et al. [58], comparing in detail the characteristics of the four main families of ceramic cutting tool but also comparing these characteristics with competing cermet and tungsten carbide cutting tools. The four families of ceramic cutting tool assessed in the study were Al_2O_3-based ceramics, Si_3N_4-based ceramics, SiAlON-based ceramics, and cermet tool materials.

2.9.2 Manufacturing Processes for Ceramic Cutting Tools

The most tried and tested manufacturing approach for manufacturing ceramic cutting tools, relies upon the hot isostatic pressing of finely ground ceramic powders at a high temperatures and pressures. Jack et al. [59] state that sufficiently dense cutting tool inserts can be produced from α-silicon nitride powder at a isostatic pressures of 30 MPa in graphite dies at 1700-1800°C, which results in a β-silicon aluminium oxynitride cutting tool.

2.9.3 Silicon Nitride Based Ceramics

At present there is large variety of non-oxide ceramic cutting tools, which are based on silicon nitride that are widely available. Current silicon nitride cutting tool materials can be arranged into two groups, the first group is silicon nitride and other group is SiAlON tool materials. Silicon nitrides cutting tools have high strength, high fracture toughness and very high resistance to thermal shock, which is due to low expansion properties of SiAlON materials. Silicon nitride ceramic tools at present can be manufactured with different quantities of elements that can used for different machining applications. Jack et al. [59] goes onto state that additives such as yttrium oxides are added to reduce the porosity of silicon nitride cutting tools via the promotion and of glasses phases.

2.9.4 Silicon - Aluminium - Oxy - Nitrides (SiAlONs)

When silicon nitride (Si_3N_4) is subjected to a substitution process where aluminium and oxygen can be substituted for silicon and nitrogen, a group of tough, highly abrasion-resistant ceramics are created. Table 2.3 compares the properties of other ceramic cutting tool materials and the standard K10 tungsten carbide grade with SiAlON.

Table 2.3. Comparison of different cutting tool material properties. [58]
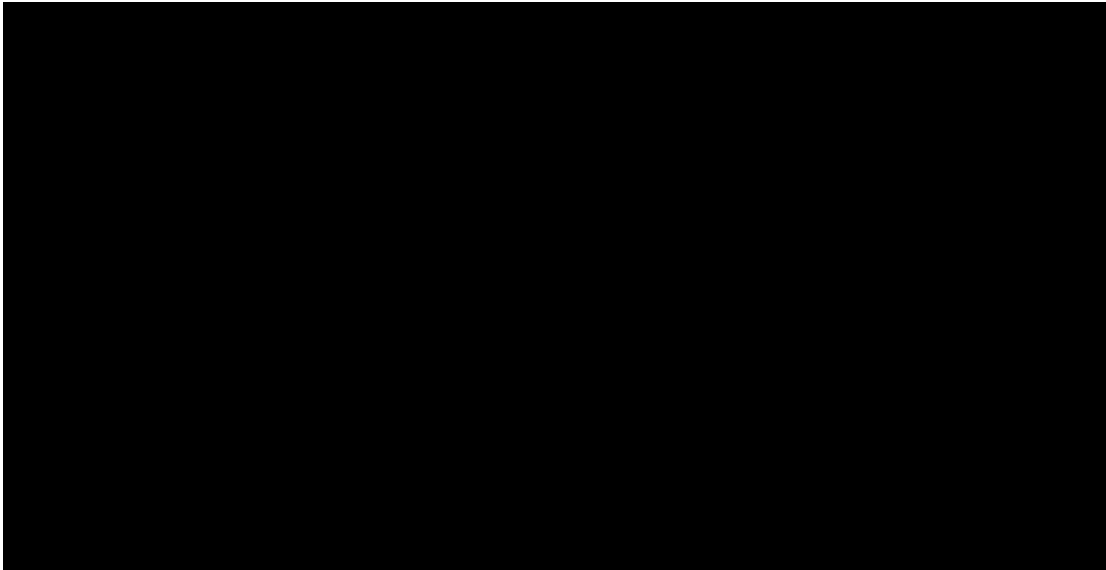
This image has been removed by the author of this thesis for copyright reasons

Silicon nitride powder compacts are sintered to full density using combinations of rare-earth oxides such yttrium oxide (Y_2O_3) and alumina sintering aids, which helps take a porous matrix of silicon aluminium oxynitride powder and form a dense ceramic material. The high hot hardness, thermal shock resistance and excellent wear-resistance characteristics of SiAlONs allow for improved machining capability when machining materials, such as nickel-based alloys.

2.10 Coating Techniques for Ceramic Materials

Objective 1e focuses on looking at the coating techniques for ceramic materials. One of the fundamental challenges with the application of ceramic cutting tools has been the unpredictable nature of brittle fracture. The other challenge relates to the amount of tool life that can be attained from a ceramic cutting tool, be it an insert or solid end-mill. Improving the fracture resistance and wear-resistance of SiAlON ceramics requires the right amount of β-Si_3N_4 (β-SiAlON) and α-Si_3N_4 (α-SiAlON) to be sintered with yttrium oxide (Y_2O_3) to strengthen the overall microstructure of the SiAlON ceramic. Rosenflanz et al. [60] noted that adding the correct amount of β-Si_3N_4 (β-SiAlON) will improve the fracture resistance. The wear-resistance of SiAlON-based ceramics is usually acquired through the correct additions of α-Si_3N_4 (α-SiAlON), due to its higher hardness.

One way of cost-effectively improving the wear and temperature resistance of a cutting tool is to apply a hard protective coating. The process of applying a hard ceramic coating to ceramic cutting tools has been around since the early 1980s. Gatto et al. [61] managed to conduct some of the earlier attempts at coating a ceramic cutting tool and understand the effects that a hard protective coating has on the tool life. **One of the main reasons for applying a hard protective coating is to reduce diffusion wear (solid solution wear)**, a secondary wear mechanism, which contributes to primary wear mechanisms such as flank, rake, and crater wear.

At temperatures of 1100 – 1150°C silicon chemically reacts with iron and creates diffusion couples [62]. This is particularly relevant for nickel-based alloys such as Inconel 718, as Inconel 718 also contains as much as 17% weight iron; this means when SiAlON cutting tools are used to machine nickel-based alloys such as Inconel 718, they are more susceptible to tool failure because of diffusion wear.

2.10.1 Physical Vapour Deposition Techniques

One of the principal ways of applying hard coating onto the surface of cutting tool material has been to adopt physical vapour deposition (PVD) techniques. In 1993 Hofmann et al. [63] began to discuss their research on the early adoption of PVD techniques when applying a multi-layered titanium aluminium nitride (TiAlN) coating to drill bits and hobbing tools to extend the life of the tool. PVD coating techniques work by having two opposing magnetron cathodes that are combined with magnetic coils and two opposing hollow anodes in an inert high vacuum atmosphere. A typical PVD chamber is shown in Figure 2.18.

This image has been removed by the author of this thesis for copyright reasons
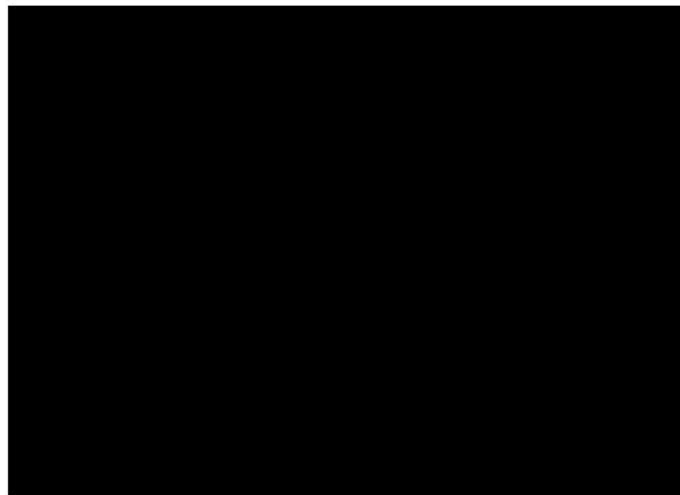
Figure 2.18. Cross-sectional view of the process chamber of a typical Physical Vapour Deposition machine. [63]

The tooling substrate is heated by radiative heaters, a plasma is generated and then the substrate is cleaned via ion-etching. The deposition of the coating is controlled via reactive sputter ion-plating and then allowed to cool. Some of the earliest PVD-coated ceramic insert research was conducted by Gatto et al. [61] in 1997, which assessed the benefit of applying a chromium nitride (CrN) and TiAlN coating to a silicon carbide whisker-reinforced aluminium oxide cutting insert via PVD techniques.

The next comprehensive study was conducted by Peng et al. [64] in 2003: the research focused on applying titanium nitride (TiN) films with pulsed high energy density plasma techniques. The research conducted by Peng et al concluded that the adhesive strength of the TiN film coating onto the silicon nitride ceramic cutting tool substrate provided satisfactory results. The pulsed plasma coating technique also allowed the TiN film coating to attain a very high critical load up to 80 milli-Newton mN, measured by a nano-scratch tester.

Another comprehensive study focused on applying a multi-layered coating via PVD techniques was conducted by Dobrzański et al. [65] in 2004. It focused on understanding the structure and properties of applying PVD titanium-aluminium-silicon nitride (TiAlSiN) coatings to silicon nitride (Si_3N_4) ceramic cutting tool substrates.

The principle aims of the research looked to establish which coating had the best adhesive properties and wear-resistance characteristics. Applying protective wear resistant coatings via PVD techniques, produces very hard, wear resistant coatings that have prolonged the longevity of ceramic cutting tools. However, very hard PVD coatings are more susceptible to chipping and flaking due to their hard coating microstructure, especially if the tool/coating interfacial layer suffers from poor interfacial bonding between the ceramic substrate and interfacial layer [65].

Similar research conducted by Soković et al. [66] in 2005 and Dobrzański et al. [67] in 2006, focused on discussing the tribological characteristics of coatings that have been applied with PVD and CVD techniques, conclusions from which stated that CVD coatings attained higher adhesion characteristics when applied to the ceramic cutting tool substrates, when compared with to PVD coatings.

The multi-layered CVD coatings that were applied to the aluminium oxide + silicon carbide whisker (Al_2O_3 + $SiC_{(w)}$) and silicon nitride ($Si_3N_{4)}$ increased the tool life of the insert when compared to PVD coatings which had been applied to the same ceramic tool substrate. The PVD coatings suffered from poor adhesion characteristics and as a result, attained critical load values far lower than the CVD coatings. Dobrzański et al concluded that one of the main

reasons for the CVD coating having higher adhesion strength was down to the high temperature heat activated processes that create the coating-forming elements.

Recent research has highlighted that applying a coating to a ceramic insert can improve its strength. The research conducted by Staszuk et al. [68] in 2017 and Volosova et al. [69] in 2018 state that adding the following PVD coatings, titanium nitride (TiN), aluminium nitride (AlN), diamond like coating (DLC), titanium zirconium nitride (TiZrN), titanium chromium aluminium nitride (TiCrAlN), to the surface of SiAlON, Al_2O_3 + TiC and Al_2O_3 + SiC ceramic cutting tool inserts can improve the tool life by as much as 50%. Staszuk et al noted that covalent interatomic bonds of the isomorphic AlN coating, exhibited much better adhesion to SiAlON inserts than the isomorphic TiN coating.

Something that has also taken place in parallel to the improved coatings is the PVD coating techniques themselves. Baptista et al. [70] claim that PVD techniques have continued to be in a constant state of evolution from improved energy consumption to better reactor designs. As a result of these improvements, better coating adhesion characteristics are more easily attained, leading to improved capability of the coatings. Figure 2.19 shows a schematic of two conventional PVD techniques that are utilised to coat ceramic cutting tools.
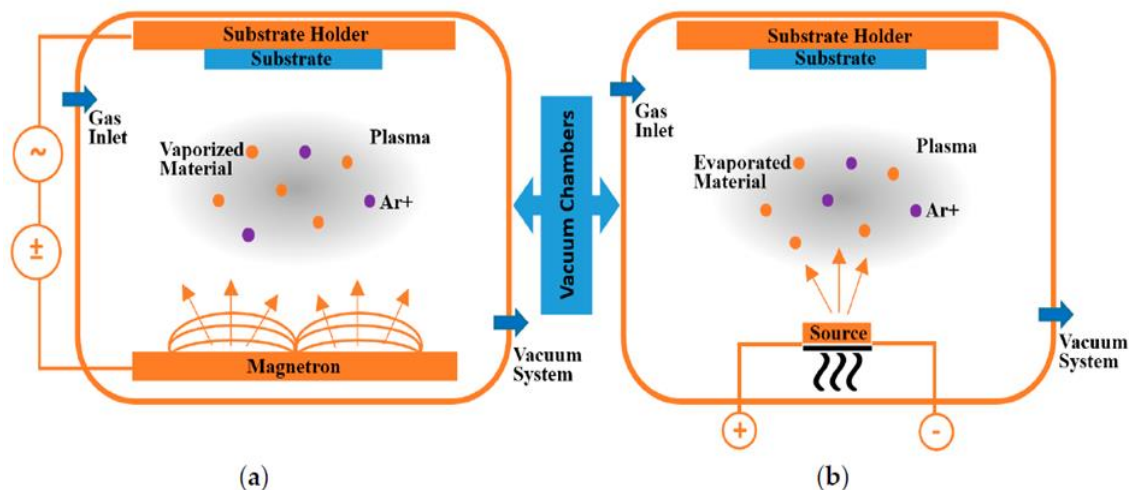
Figure 2.19. Schematic of two conventional PVD processes (a) Sputtering PVD technique and (b) evaporating PVD technique using ionized Argon (Ar+) gas. [70]

In the last five years, nano-scale coatings have found precedence as they deliver even greater control, reliability, and tool life. Grigoriev et al. [71] mention that the application of PVD multi-layered composite coating to mixed ceramic (Al_2O_3) cutting tools can deliver increased wear-resistance and better tool reliability, which is important when companies consider using ceramic cutting tools.

2.10.2 Chemical Vapour Deposition Techniques

Another way of applying a coating to a cutting insert involves using chemical vapour deposition (CVD) techniques. Fukui et al. [72] claim the application of thin ceramic film coatings to protect cutting inserts began in 1969, when West German company, Krupp, began using CVD techniques to deposit titanium carbide (TiC) film coatings onto tungsten carbide cutting tools. The commercialization of CVD in the 1970s, when the titanium nitride (TiN) and titanium carbo-nitride (TiCN) coatings were first applied to tungsten carbide cutting tools. Fukui et al clarify that CVD techniques form coatings whereby chemical reactions take place at temperatures close to 1000°C inside a chamber.

Such high temperature chemical reactions produce residual stresses in the thin film coating due to the difference in thermal expansion coefficient between the cutting tool substrate and the thin ceramic film coating. Fukui et al further state the CVD coating process produces uniform coatings with excellent adhesion characteristics. CVD coatings have high purity and high crystallinity, and multi-layer coating can be achieved with ease. Table 2.4 highlights some of the benefits that CVD coatings have compared to PVD coatings.

Table 2.4. Comparison between CVD and PVD method. [72]
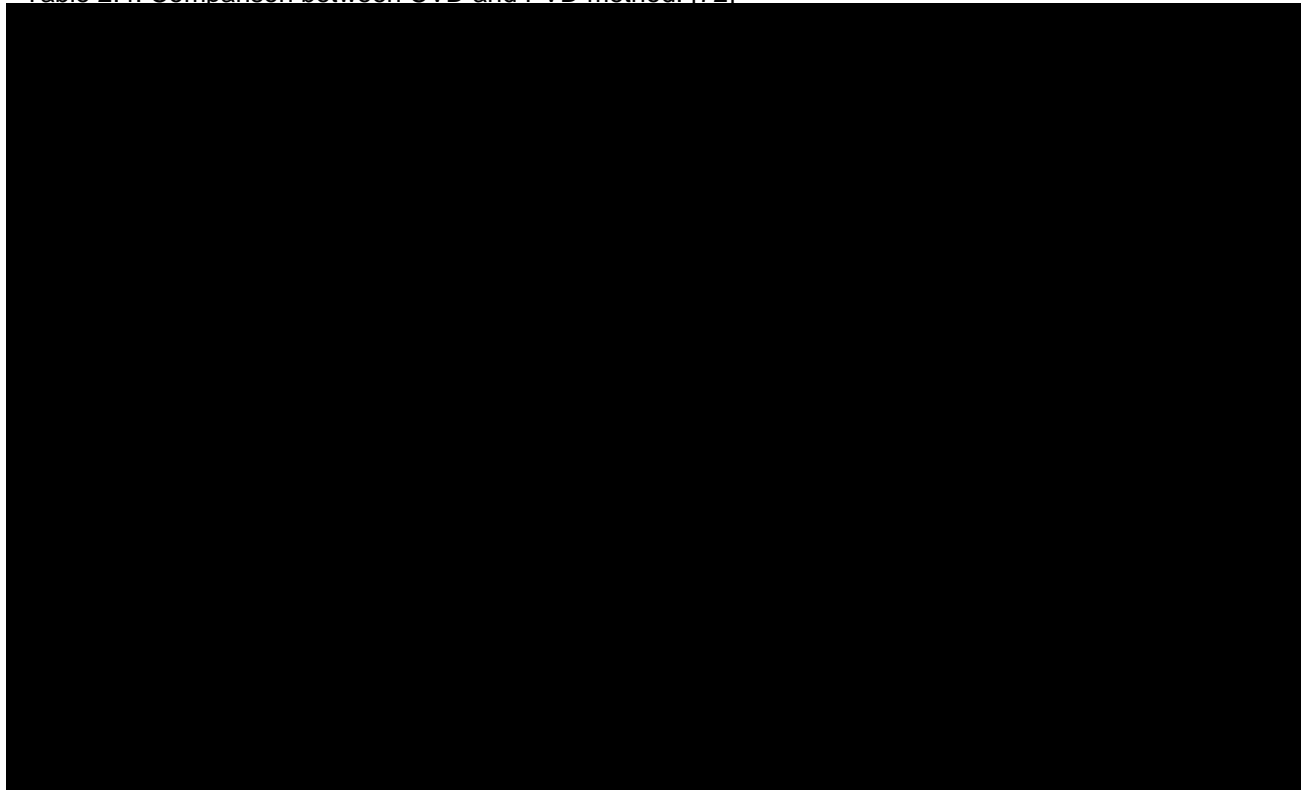
This image has been removed by the author of this thesis for copyright reasons

The coating of ceramic cutting tools began in the early 1980s: Sarin et al. [73] and Sarin et al. [74] obtained patents for coating silicon nitride-based and composite oxynitride cutting tools with nitride and carbo-nitride coating via CVD techniques. The research focused on understanding the benefits of coating a ceramic cutting tool and was continued by Gatto et al [61], who looked to clarify whether a PVD ceramic coating would improve the overall tool life of the ceramic insert.

Further comparative research was conducted by Dobrzański et al. [67] and Soković et al. [66], looking to compare the tribological properties of CVD and PVD coatings that were applied to SiAlON cutting inserts. Dobrzański et al concluded that CVD techniques attained coatings with the best adhesion and critical load (L_c) characteristics. The tool flank wear (V_B) of CVD coated SiAlON was also measured as considerably better than PVD coated SiAlON inserts.

The comparative analysis continued, with research being conducted by Dobrza et al. [75] in 2010 and Staszuk et al. [76] in 2014, in regard to applying CVD and PVD coating to tungsten carbide (WC) and SiAlON inserts. They attempted to understand the impact of a coating on the durability of the inserts and to clarify whether it is cost-effective to coat WC and SiAlON inserts. Figure 2.20 shows a typical production CVD reactor used to coat cutting tools.

This image has been removed by the author of this thesis for copyright reasons
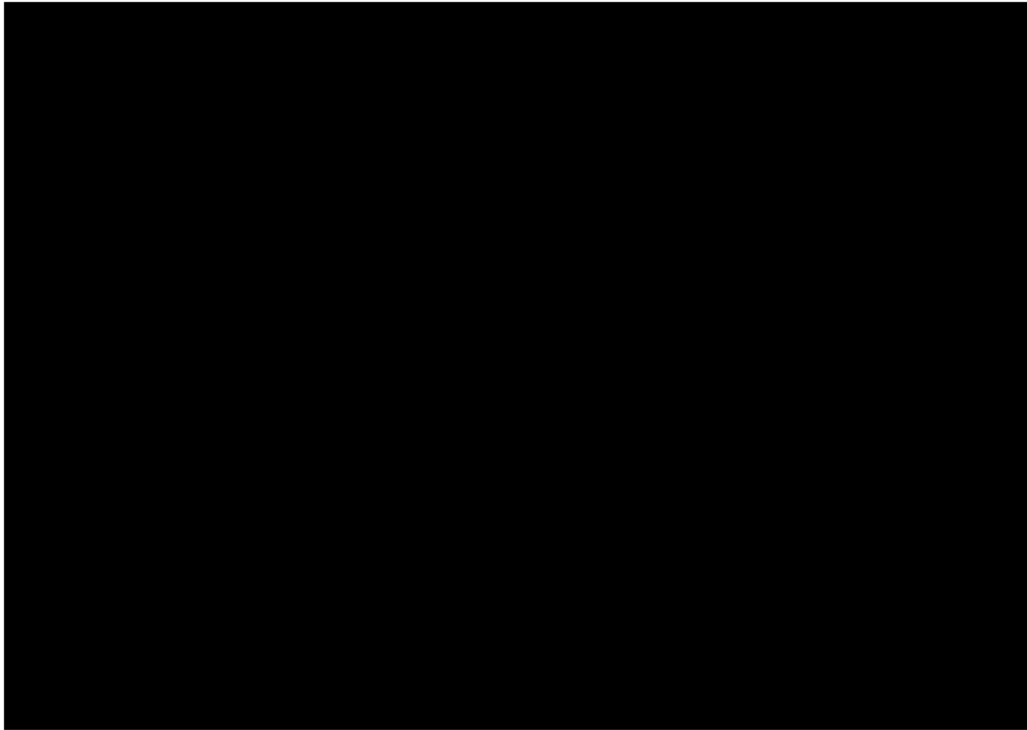
Figure 2.20. A schematic of a typical Production CVD reactor for the coating of cutting tools. Adapted version. [77]

The benefits of using ceramic cutting tools for machining cast iron, steels and super-alloys have been apparent for 30 years. Thus, researchers are continuing their pursuit of improving the wear capability and reliability of ceramic cutting inserts, as increased interest, and demand from industry for greater tool life continue to grow.

SiAlON ceramic cutting inserts have found great acceptance in the automotive sector for machining grey cast iron brake discs. Early research that is relevant to this research which had took place in the mid 1990's, suggest applying a CVD titanium oxy-carbide coatings to Al_2O_3 index-able inserts resulted in considerable improvements in tool life [78]. Some of the recent research has focused on applying CVD TiN-Al_2O_3 coatings to a SIAlON cutting tool delivered a three-to five-fold increase in tool life when machining grey cast iron with continuous and varied depth of cuts. The results demonstrated the CVD TiN-Al_2O_3 coating improved the wear and oxidation resistance of the SiAlON inserts and improved resistance to crack propagation. The SiAlON inserts' resistance to crack propagation was enhanced with a CVD TiN-Al_2O_3 coating, due to the elimination of grinding marks and potential stress concentration formed during the insert manufacturing process [79].

An interesting aspect of chemical vapour deposition coatings has been the application of monolayer-micrometric (MN-MCD), monolayer–sub-micrometric (MN-SMCD) and multilayer-micrometric (MT-MCD) diamond films. Chen et al [80] discuss applying MN-MCD, MN-SMCD and MT-MCD super hard diamond film coatings onto silicon nitride with hot filament chemical vapour deposition (HFCVD). The research concluded that MT-MCD diamond film coatings attained low friction coefficients and high wear-resistance.

Pierson et al. [77] state two common reactions for creating titanium nitride (TiN) which is highlighted in red in Equations 2.7 and 2.8. The CVD reactants are titanium tetrachloride (TiCl4), nitrogen gas (N2), ammonia (NH3), hydrogen (H2), hydrogen chloride (HCl).

$$Reaction\ (1)\ TiCl4\ +\ \tfrac{1}{2}N2\ +\ 2H2\ \rightarrow\ TiN\ +\ 4HCl \quad \text{Equation 2.7}$$

$$Reaction\ (2)\ TiCl4\ +\ NH3\ +\ 0.5H2\ \rightarrow\ TiN\ +\ 4HClE \quad \text{Equation 2.8}$$

Reaction 1 takes place at a temperature from 900°C to 1200°C , with the best results obtained at 1000 °C. Reaction 2 takes place at a temperature from 480°C to 700°C. Pierson et al. [77] state a common reaction for creating titanium carbo-nitride (TiCN) which is highlighted in red in Equation 2.9.

$$Reaction\ (3)\ TiCl4\ +\ xCH4\ +\ \tfrac{1}{2}(1-x)N2\ +\ 2(1-x)H2\ \rightarrow\ TiCxN1-x\ +\ 4HCl \quad \text{Equation 2.9}$$
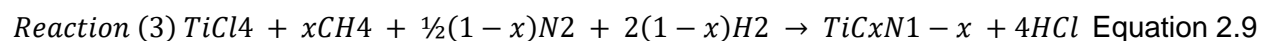
Reaction 3 takes place in a hydrogen (H_2) atmosphere at a temperature of approximately 1000°C. Pierson et al. [69] state a common reaction that takes place via the hydrolysis process of aluminium trichloride. This process is used for the deposition of aluminium oxide (alumina), highlighted in red in Equation 2.10.

$$Reaction\ (4)\ 2AlCl\_3\ +\ 3H\_2\ +\ 3CO\_2\ \rightarrow\ Al\_2\,O\_3\ +\ 3CO\ +\ 6HCl$$ Equation 2.10
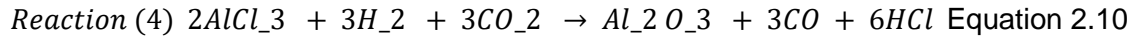
The CVD reactants are aluminium trichloride ($AlCl_3$), carbon monoxide (CO), hydrogen chloride (HCl). Reaction 4 is based on a classic water-gas reaction which takes place in an excess hydrogen atmosphere; the optimum temperature of the reaction takes place at 1050°C at low pressure.

The species transport and reaction sequence which takes place during chemical vapour deposition, is a complex process and is illustrated schematically in Figure 2.21. The reactant gases that are used to create α-Al_2O_3 CVD coatings involve the utilisation of aluminium trichloride ($AlCl_3$), carbon monoxide (CO), hydrogen chloride (HCl). The gas phase reaction will take place and species will diffuse to the surface of the substrate from the boundary layer.

Once the species have transported to the surface of the substrate there will be reactions with the substrate. If the activation energy is high enough the valence electrons will begin to exchange, and this starts the absorption of reactants into the surface of heated substrate. Further chemical reactions will take place and homogenous nucleation will take place and the island will start to grow in the interfacial layer. Then the desorption of the species take place and is removed with gaseous by-products.
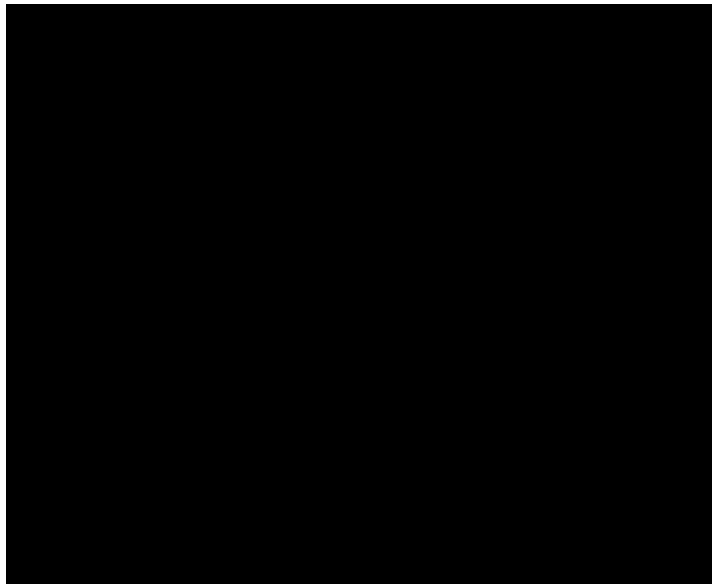
This image has been removed by the author of this thesis for copyright reasons

Figure 2.21. Transport and reaction sequence during CVD. [77]

2.11 Coating Selection for Ceramic Cutting Tools

Objective 1f focuses on looking at the coating selection process for protecting ceramic cutting inserts. Protective coatings have been adopted for improving the wear, oxidation, and chemical resistance of cutting tools since the 1970s. Bobzin et al. [81] discuss the historical development of CVD and PVD processes and the necessary process of improvement, allowing for continuous improvements in cutting tool performance. Coating selection is heavily influenced by the dominant failure mechanisms that the coating is likely to experience during the machining process. Figure 2.22 shows graphically types of tool failure mechanisms based on cutting speed temperatures. Figure 2.22 also influences what type of coating materials will be necessary to resist this mechanism of tool failure.
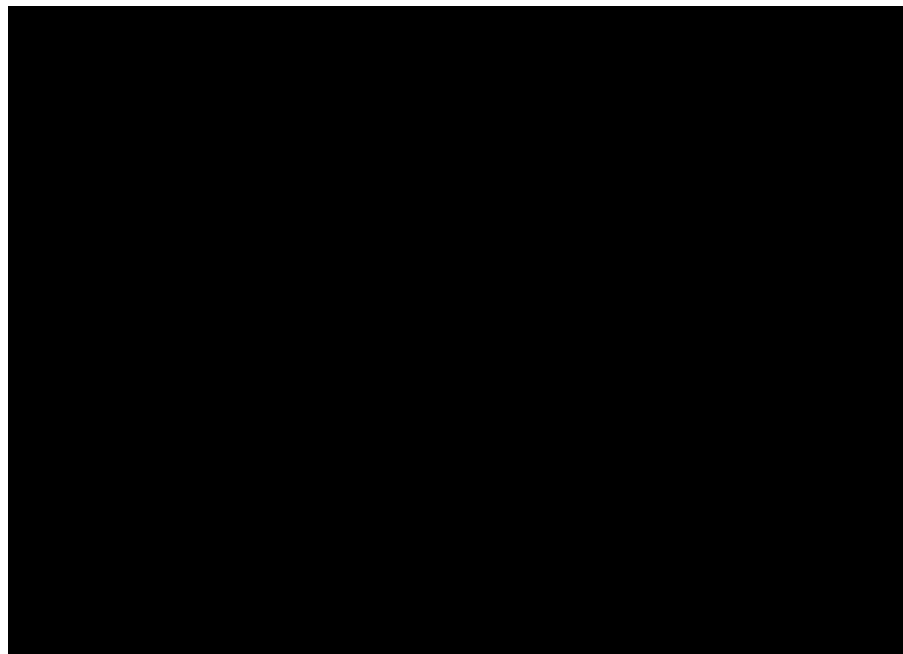
This image has been removed by the author of this thesis for copyright reasons

Figure 2.22. Dominant failure mechanisms influencing cutting tools depending on the cutting temperature. [81]

2.11.1 Material Selection for Protective Coatings

Material selection for hard wear-resistant protective coatings is of paramount importance. Materials selected for coatings should be suited to the final machining application. Coatings selected for the purpose of protecting SiAlON cutting tools need to include material elements, which adhere to the surface of the SiAlON cutting tool and provide increased resistance to abrasion, oxidation, and thermochemical wear, such as diffusion wear. As a result, the types of materials that are best suited to wear-resistant coatings and the chemical in bonding characteristics of such compounds [82]. Figure 2.23 shows the layer configuration that is typically used for coating tungsten carbide inserts.
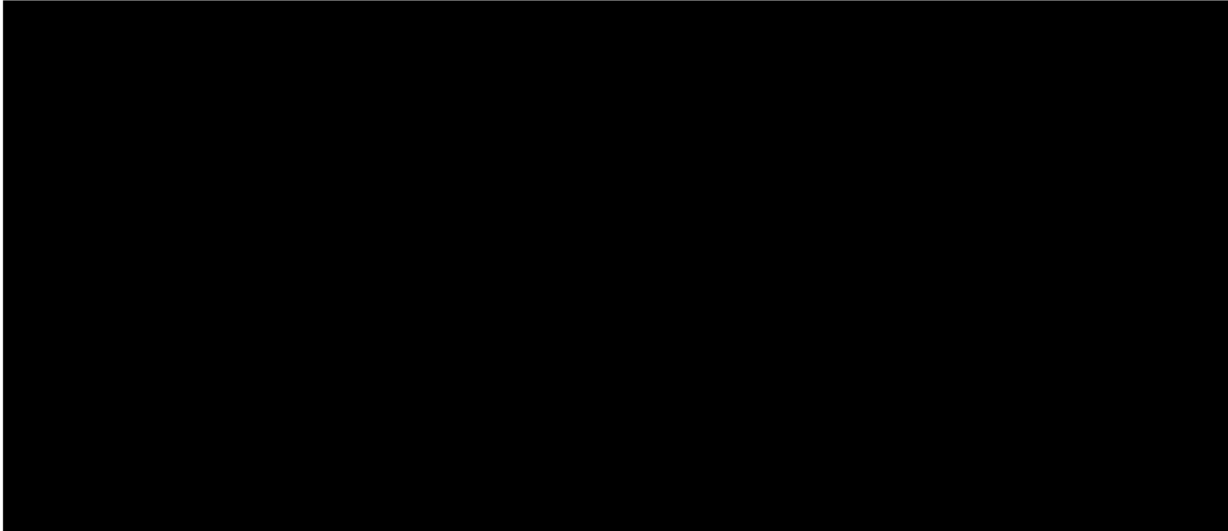
This image has been removed by the author of this thesis for copyright reasons

Figure 2.23. Cross-sections of the (a) CVD (nominal layer thickness: 2.0 mm Ti (C, N), 2.0 mm multilayer Al_2O_3, 0.5 mm TiN) and (b) PVD (nominal layer thickness: 2.0 mm (Ti, Al) N, 0.7 mm (Al, Cr)$_2$ O$_3$ coatings investigated. Note the presence of droplets in the arc evaporated PVD coating. [83]

Holleck et al conclude that ceramic materials such as titanium nitride (TiN), titanium carbonitride (TiCN) and aluminium oxide (Al_2O_3) are utilised in bi-layer and multi-layered coatings to provide the desired amount of resistance to wear, adhesion, oxidation, and thermochemical wear. Pierson et al state that TiN has a very low coefficient of friction and has high hardness, which provides high wear-resistance and lubrication to a coating. TiCN is a solid solution of both TiN and titanium carbide (TiC), which provides even higher wear-resistance and lubrication to a coating than TiN can provide. Al_2O_3 or alumina is utilised in protective coatings for its high hardness and oxidation resistance.

2.11.2 Mechanical Properties of Coatings

The mechanical properties of a coating are fundamental to the effectiveness of the coating and its ability to provide adequate protection of the cutting tool insert. the mechanical properties fundamentally important to a coating are roughness, micro-hardness, and critical load (L_c N). Ceramic cutting tools rely upon heat being generated in the shear zone. The frictional heat that is produced in cut shear zone reduces the yield, the strength of the material and hence the cutting forces [84].

However, it is micro-hardness and L_c N mechanical properties that are of particular importance. Table 2.5 shows highlighted values for CVD and PVD coated Si_3N_4 sintered cutting tools. The highlighted values in Table 2.5 indicate that CVD coated Si_3N_4 cutting tools attain better mechanical properties and high adhesive characteristics when compared to PVD coated Si_3N_4 cutting tools.

Table 2.5. Characteristics of the PVD and CVD coatings deposited on the sintered tool materials. [76]

1) Chemical composition (mass concentration. of elements, %): C 0,80; N 2,00; Ti 48,70; Ta 13,50; Ni 4,70; Co 8,60; W 21,65. This image has been removed by the author of this thesis for copyright reasons

2) Commercially available inserts from various manufacturers.

The critical load (L_c N) values captured in Table 2.5 clarify that CVD coating techniques create more robust coatings when applied to Si_3N_4 cutting tools. The L_c N values highlighted in Table 2.5 are the main way of testing the adhesion strength of the coating.

2.11.3 Adhesion Characteristics of Coatings

The adhesion strength of a protective coating is a key characteristic that determines how long a coating will essentially stay on the surface of the cutting tool substrate. **Determining key adhesion characteristics becomes a key part of this research and is discussed at length later in this Thesis**. The coating of ceramic cutting tools has been around since the 1980s however coating ceramics with good adhesive properties has been a challenge.

A series of methodologies have been developed to test the adhesive characteristics and toughness of a hard coating and thin films. Nano-indentation techniques are utilised to test the bond strength between the tooling substrate and the hard coating/film. Scratch testing is utilised to evaluate the adhesion of a coating to the tool substrate Increased acoustic emissions are used to determine when and to what degree the coating has failed [85]. As a result of in depth tribological testing for ascertaining adhesion, it is CVD coatings that clearly attain better adherence to Si_3N_4 cutting tool substrates due to the thermally activated chemical reactions that take place at high temperature of 1000°C [67].

The high adhesion characteristics of the CVD coating are down to intermix diffusion of elements in the Si_3N_4 cutting tool substrate in the inter-layer between the coating and cutting tool substrate [67], [68]. Figure 2.24 shows the configuration of the multi-layer coating system that is used to protect ceramic cutting tools. Creating a coherent interface between the interface layer and the substrate is hugely important for gaining good adherence to the ceramic cutting tool substrate.

Based on the results stipulated by Dobrzański et al, the thermodynamically stable polymorphic structure of aluminium oxide has been highlighted as one of the best materials to coat SiAlON cutting inserts as shown in Table 2.5. This is due to the stable adhesive bonds created at the interface between the substrate and the coating layer. The secondary phase particles such as titanium nitride and titanium carbo-nitride act as nucleation sites, where diffusion bonding can take place and generate good adhesion characteristics and have therefore also been highlighted for coating SiAlON cutting inserts [86].

Another important point, raised by Holleck et al. [82], and key for adhesion, is the focus on grain size, grain orientation and coating thickness. As a result, new coating technologies, such as hybrid PVD coating techniques, are now being investigated for creating nano-layer thick multi-layer coatings onto ceramic cutting tools.
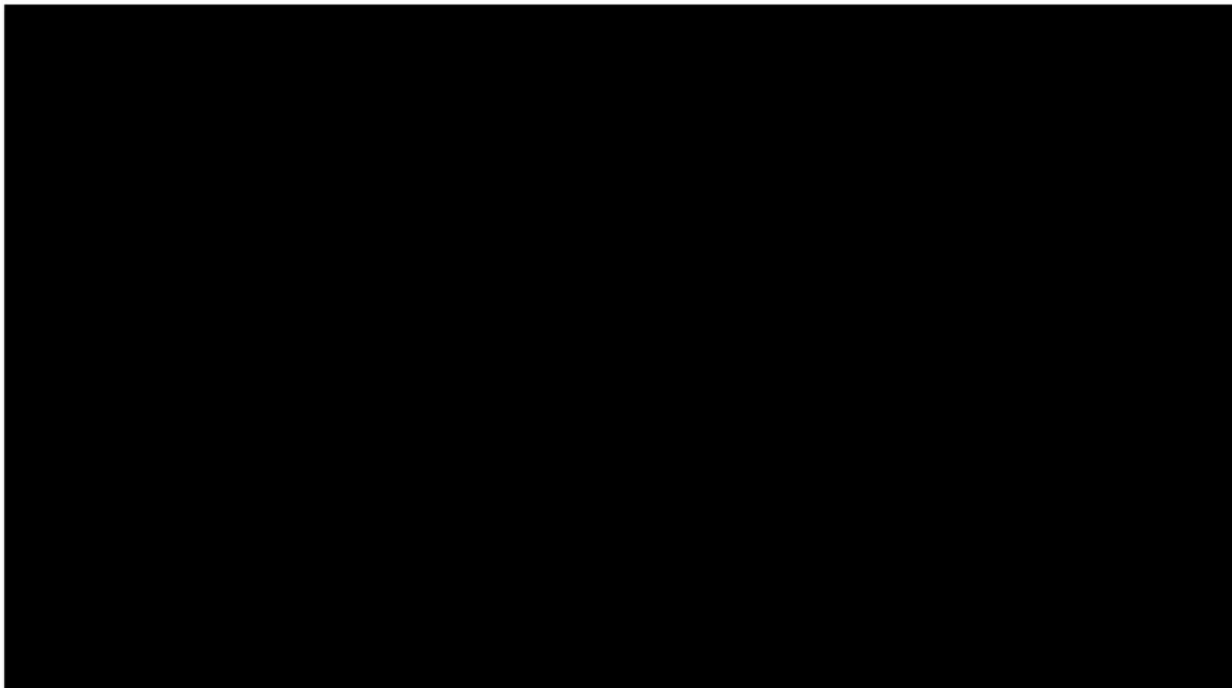
This image has been removed by the author of this thesis for copyright reasons

Figure 2.24. Schematic drawing of the multi-layer CVD coating system for ceramic cutting inserts. [82]

Table 2.6 compares the coating capability of CVD, ALD and PVD coating techniques and highlights which technique has the potential for applying a reliable coating onto a ceramic insert.

Table 2.6. Attribute comparison of CVD, ALD, and PVD processes (M= molecular beam epitaxy, S= sputtering, E= evaporation, P = pulsed laser deposition). [87] This image has been removed by the author of this thesis for copyright reasons
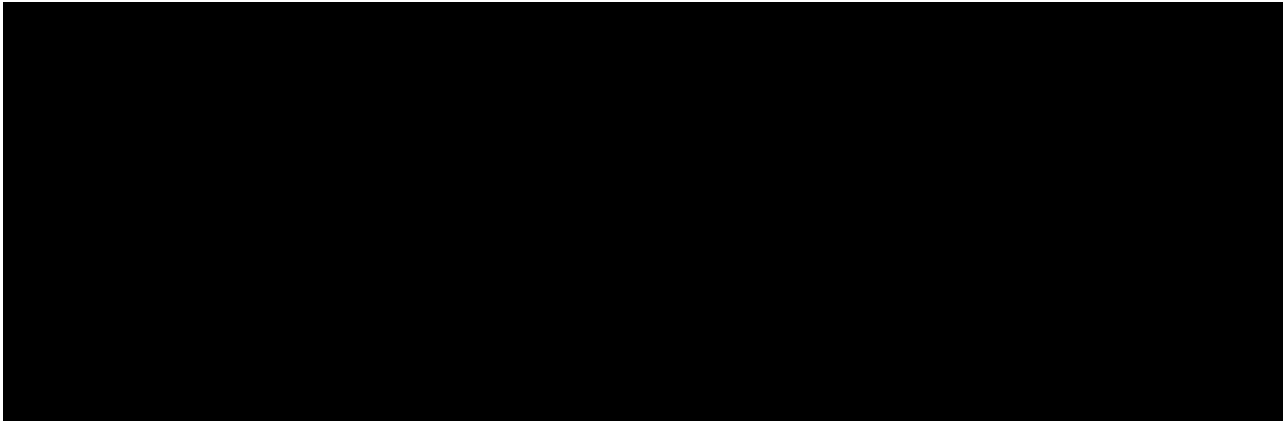
The benefits of using atomic layer deposition (ALD) techniques for creating improved grain structure of CVD and PVD coatings, which correlates in greater control of the mechanical properties of the coating can be attained [87], [88].

2.11.4 Evolution of CVD Coating Microstructure

The refinement of the microstructure of a protective wear resistant coatings has gained a lot of prevalence in the last 15 years. Figure 2.25 shows the improvement in the textured α-Al_2O_3 CVD coating microstructure from a crystallographic point of view [89].

This image has been removed by the author of this thesis for copyright reasons
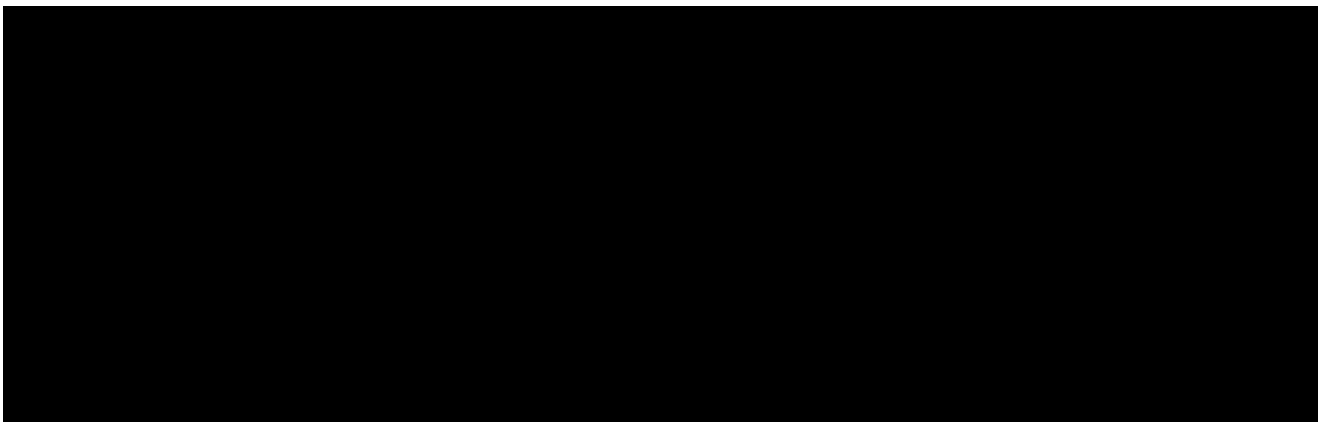
Figure 2.25. Cross-sections of CVD Al_2O_3 coatings investigated; α-Al_2O_3 $\langle 0001 \rangle$ texture (a), α-Al_2O_3 $\langle 10\bar{1}2 \rangle$ texture (b), α-Al_2O_3 $\langle 10\bar{1}2 \rangle$ stronger texture (c), α-Al_2O_3 $\langle 10\bar{1}4 \rangle$ texture (d) and κ-Al_2O_3 (e). [89]

Early research concluded that controlling the orientation and texture of the α-Al_2O_3 coating demonstrated lower rates of wear when compared to κ-Al_2O_3. The lower rates of wear for highly textured α-Al_2O_3 coating, are thought to be due to the controlled microchipping and deformation rates of the texture microstructure in the 1014 basal plane [89]. Figure 2.26(a) shows a

transformed κ-Al$_2$O$_3$ microstructure, which has high amounts of dislocation and an abundance o of cracks.
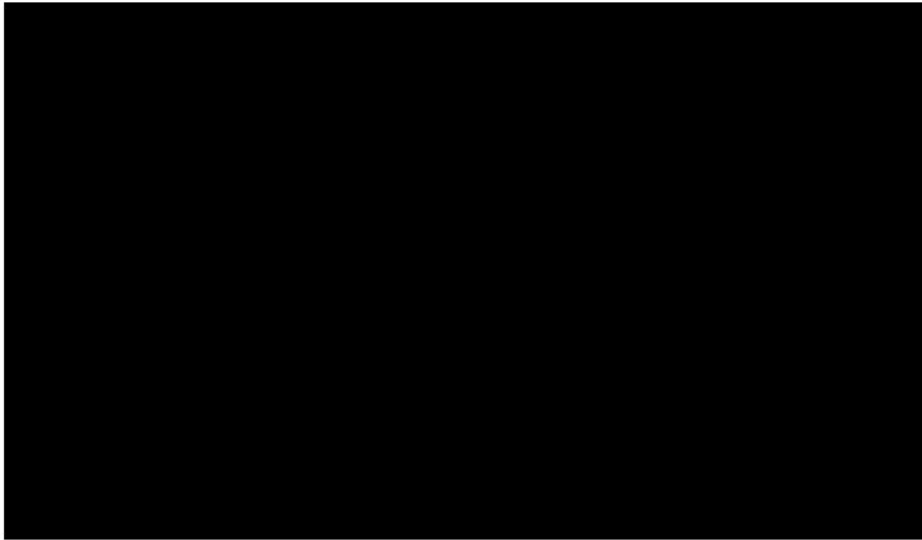
Figure 2.26. Cross-section TEM micrographs of a) coating A (transformed κ-Al$_2$O$_3$) with high dislocation density and abundance of cracks and b) coating B (as-grown, textured α-Al$_2$O$_3$) being composed of dislocation-free grains. [90]

In Figure 2.26(b), and Figure 2.27(a)(b) a textured α-Al$_2$O$_3$ coating microstructure is evident, which is composed of dislocation free grains. If the orientation of the textured microstructure can be controlled, the quantity of potential dislocation and failure sites are removed [90].
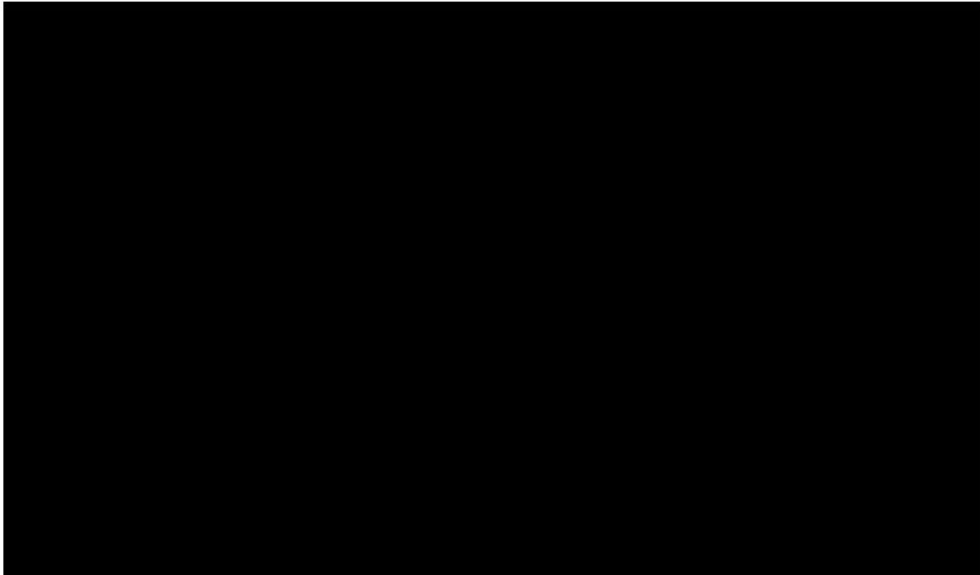
Figure 2.27. a) Surface and b) cross-section images of the (10$\bar{1}$0) textured α-Al$_2$O$_3$ coating. [90]

In Figure 2.28, the surface morphologies of textured α-Al$_2$O$_3$ are shown in the (0001) basal plane, which is parallel to the surface of the substrate.

Figure 2.28. SEM secondary electron micrographs showing the surface morphologies of the α-alumina coatings. (a) and (b) The basal plane (0001) is parallel to the surface. (c) The prismatic plane (011¯0) is parallel to the surface. [91]

When the textured α-Al_2O_3 coatings are grown parallel to the surface, the coating microstructure exhibits very high resistance to deformation. The high resistance to deformation will be an important tribological characteristic for future coating systems that are analysed in detail in Chapters 5, 6 and 7 of this thesis.

2.12 Summary

This chapter has endeavoured to give a comprehensive appreciation of the literature that have supported the decisions that have been taken throughout the course of research. This chapter has presented and reviewed previous work which is thought to be relevant to the application of this thesis. SiAlON's as a cutting tool material exhibit a series of impressive mechanical characteristics, which makes it highly effective at machining of nickel based superalloys at high cutting speed and attaining high material removal rates. The high potential material removal rates allow for high levels of productivity. However, the effective productivity which can be attained when using SlAlON milling inserts is inhibited by the rapid rates of tool wear.

While there has been significant previous research in the fields of ceramic cutting tool development, the wear mechanisms of associated ceramic cutting inserts and coating development. It is evident that a fundamental knowledge gap does exist in regard to the cutting performance of coated SiAlON milling inserts. Specifically, SiAlON milling inserts which are used to machine nickel-based alloys. Therefore, a significant proportion of this investigation will concentrate on understanding the benefits of depositing a series of protective wear resistant coatings on to the surface of the SiAlON milling inserts.

Chapter 3 Experimental Techniques and Methods

3.1 Introduction

After assessing previous studies that have been completed in this field, with a primary focus on the challenges that are discussed in the Chapter 1. It is evident that representative data needs to be collated, in order to define the benefit of applying specific coating systems for protecting SiAlON milling inserts, when machining nickel based super alloys. Therefore, this chapter focuses on the design and implementation of machining trials, coating characterization and development, which is intended to provide the datasets and in-depth analysis for subsequent chapters.

Prior to main EngD research being conducted, the first experiment involved a preliminary machining trial which was conducted on a CNC turning centre with same CTIS710 SiAlON grade that was utilized throughout the milling inserts wear trials. The preliminary machining trial provided valuable experience and understanding of how composite ceramic cutting tools degrade and wear when machining nickel-based alloys and the influence on chip formation and metallurgical expects, which are discussed in depth in later chapters of this thesis. Three top-level tables give an overall understanding of the experimental machining trials that have been completed during the course of this engineering doctorate is given in Table 3.1, Table 3.2 and Table 3.3.

Table 3.1. All completed turning EngD machining trial experiments.

Experiment No	Test No	Machining Operation	Tool Material	Bar Sections Machined	Cutting Speed (m/min)	Feed rate fz (mm/tooth)	Depth of Cut (Ap) mm	Radial Engagement (ae) (mm)
One	T1.1, T1.2	Turning	SiALON Grade 1481	1-1 to 1-2	250	0.20	2.0	N/A
One	T2.1, T2.2	Turning	SiALON Grade 1481, chamfered	2-1 to 2-2	250	0.20	2.0	N/A
One	T3.1, T3.2	Turning	CTIS710 SiAlON Uncoated	3-1 to 3-2	250	0.20	2.0	N/A
One	T4.1, T4.2	Turning	WRA Alumina	4-1 to 4-2	250	0.20	2.0	N/A
One	T5.1, T5.2	Turning	SiALON Grade 1481	5-1 to 5-2	300	0.20	2.0	N/A
One	T6.1, T6.2	Turning	SiALON Grade 1481, chamfered	6-1 to 6-2	300	0.20	2.0	N/A
One	T7.1, T7.2	Turning	CTIS710 SiAlON Uncoated	7-1 to 7-2	300	0.20	2.0	N/A
One	T8.1, T8.2	Turning	WRA Alumina	8-1 to 8-2	300	0.20	2.0	N/A

Table 3.2. All completed 3-axis milling EngD machining trial experiments.

Experiment No	Test No	Machining Operation	Tool Material	Bar Sections Machined	Cutting Speed (m/min)	Feed rate fz (mm/tooth)	Depth of Cut (Ap) mm	Radial Engagement (ae) (mm)
Two	M1	3-axis Milling	CTIS710 SiAlON Uncoated	1-1 to 1-4	700	0.1	1.0	30
Two	M2	3-axis Milling	CTIS710 SiAlON +Type A Coating	1-1 to 1-2	700	0.1	1.0	30
Two	M3	3-axis Milling	CTIS710 SiAlON +Type B Coating	1-1 to 1-4	700	0.1	1.0	30
Two	M4	3-axis Milling	CTIS710 SiAlON Uncoated	2-1 to 2-5	800	0.1	1.0	30
Two	M5	3-axis Milling	CTIS710 SiAlON +Type A Coating	2-1 to 2-5	800	0.1	1.0	30
Two	M6	3-axis Milling	CTIS710 SiAlON +Type B Coating	2-1 to 2-4	800	0.1	1.0	30
Two	M7	3-axis Milling	CTIS710 SiAlON Uncoated	3-1 to 3-5	900	0.1	1.0	30
Two	M8	3-axis Milling	CTIS710 SiAlON +Type A Coating	3-1 to 3-4	900	0.1	1.0	30
Two	M9	3-axis Milling	CTIS710 SiAlON +Type B Coating	3-1 to 3-2	900	0.1	1.0	30
Two	M10	3-axis Milling	CTIS710 SiAlON Uncoated	4-1 to 4-4	1000	0.1	1.0	30
Two	M11	3-axis Milling	CTIS710 SiAlON +Type A Coating	4-1 to 4-4	1000	0.1	1.0	30
Two	M12	3-axis Milling	CTIS710 SiAlON +Type B Coating	4-1 to 4-2	1000	0.1	1.0	30
Two	M13	3-axis Milling	CTIS710 SiAlON +Type B Coating 'Retest'	2-1 to 2-3	800	0.1	1.0	30
Four	M14	3-axis Milling	CTIS710 SiAlON +Type C Coating	2-1 to 2-3	800	0.1	1.0	30
Four	M15	3-axis Milling	CTIS710 SiAlON +Type C Coating	3-1	900	0.1	1.0	30

Table 3.3. All completed 5-axis milling EngD machining trial experiments.

Experiment No	Test No	Machining Operation	Tool Material	Bar Sections Machined	Cutting Speed (m/min)	Feed rate fz (mm/tooth)	Depth of Cut (Ap) mm	Radial Engagement (ae) (mm)
Four	M16A	5-axis Milling	CTIS710 SiAlON Uncoated	1-4, 5-8	840	0.06	1.5	35.5-10.0
Four	M16B	5-axis Profile Milling	CTIS710 SiAlON Uncoated	9-11, 12	880	0.07	1.0	26.14-7.0
Four	M17A	5-axis Milling	CTIS710 SiAlON +Type C Coating	1-3, 4-6, 7-8	840	0.06	1.5	35.5-10.0
Four	M17B	5-axis Profile Milling	CTIS710 SiAlON +Type C Coating	9-10, 11-12	880	0.07	1.0	26.14-7.0

As introduced in Section 1.1 and 1.2, the main drive of the research is focused on developing an understanding of the benefits of applying a CVD coating onto the surface of silicon aluminium oxynitride ceramic cutting tools, when milling Inconel 718. Therefore, to understand these benefits, a thorough understanding of the wear and failure mechanism of certain ceramic materials is required. The wear mechanisms which are exhibited by the ceramic material, is matched in parallel with detailed understanding of what materials and microstructures can potentially improve wear resistance and tool life. The different experimental techniques that were utilised for each of the chapters are captured in Table 3.4.

Table 3.4. Experimental Techniques for each chapter.

Chapter No	Experiment No	Round Insert Wear Technique	Tool Life Characterisation Technique	Scratch Testing Technique	Pin-on-Disc Technique	Non-contact 3D Profilometer Imaging	Digital Imaging Technique
Four	One	Yes	No	No	No	Yes	Yes
Five	Two	Yes	Yes	No	No	Yes	No
Six	Three	No	No	Yes	Yes	Yes	No
Seven	Four	Yes	Yes	No	No	No	Yes

3.2 Tool Wear and Life Characterization

3.2.1 Round Insert Wear Technique

Machining nickel-based alloys such as Inconel 718 generates significant amounts of thermal energy in the chip/tool interface for round geometry button inserts. Round geometry button inserts will be utilised in Experiment One, Two and Four. Inconel 718 exhibits high temperature mechanical strength properties, high resistance to deformation and low coefficient of thermal conductivity, which in turn creates a very challenging environment for cutting tool materials. Tungsten carbide (WC-Co) cutting tools are regularly utilized to machine complex, expensive and safety critical components either via milling or turning operations.

The influence of this extreme machining environment is captured in the research conducted by Jadam et al. [92]. The machinability characteristics of PVD coated cermet's and PCBN (Polycrystalline Cubic Boron nitride) materials in comparison to uncoated WC-Co tools. The WC-Co, Cermet and PCBN all suffer from high amounts of notch wear and rake face wear. Ceramic cutting tools exhibit different mechanical characteristics to WC-Co, Cermet and PCBN cutting tools.

Ceramic cutting tools materials such as silicon aluminium oxynitride (SiAlON) have high hot hardness, chemical inertness, very high oxidation resistance and high resistance to thermal expansion and fracture. SiAlON ceramics can used to machine nickel-based alloys at cutting speeds of 1000 m/min in high milling operations. Machining nickel-based alloys at cutting speeds of up to 1000 m/min results in significant amounts of tool wear in a matter of minute as stated by the research conducted by Guo et al. [93]. But the very high cutting speeds are complimented with high feed rates, which culminates into high metal removal rates (MRR), which is the principal reason for using ceramic cutting tools.

Insert wear measurements with round inserts are principally focused on the flank face, although rake face wear is still important measurement to capture. The flank wear measurement value can determine the level of tool life that can be attained with round geometry button inserts. Round geometry button inserts will be utilised later experimental activities in Experiment One, Two and Four. The flank wear measurements can also signify where inherent insert failure initiates from and how much material can be removed before the insert must be replaced. The cutting edges which are involved in face milling operations are captured in Figure 3.1.
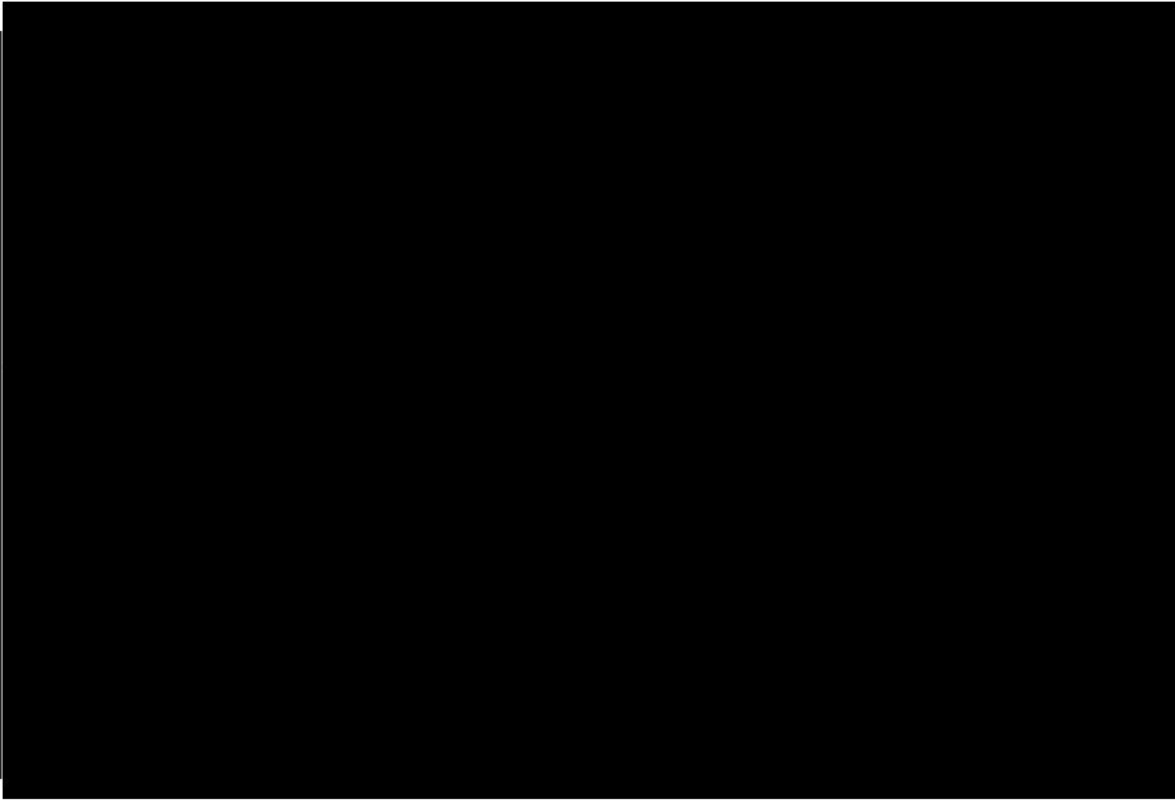
Figure 3.1. Schematic representation of the cutting edges involved in cut during face milling. [44]

The different levels of tool wear measurement for round geometry inserts are seen in Figure 3.2. The flank wear limit for different tool material such high speed steel (HSS) and tungsten carbide (Wc-Co) turning tools are stipulated by ISO 3685:1993, and for high-speed steel (HSS) and tungsten carbide (Wc-Co) milling tools the flank wear limit is typically stipulated by ISO 8688-1 and ISO 8688-2. The flank wear measurements are in relation to the turning and milling of iron and steel workpiece materials.
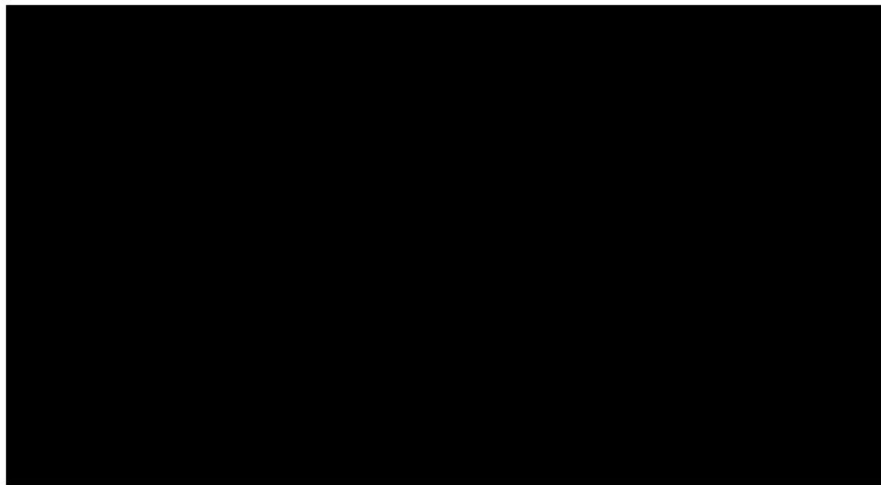
Figure 3.2. Tool wear measurement on a round insert. [94]

47

The three wear regions which are monitored throughout the life of the tool: flank wear (namely $VB_{B, minor}$ and $VB_{B, major}$). When machining nickel-based alloys such as Inconel 718, the progression of wear around the round insert takes a very short time period. Ceramic cutting tools such as SiAlON ceramic rapidly wear when machining Inconel 718. Therefore, the typical wear limits that have been utilised in previous research is not readily adopted in this research. The extreme machining environment which is encountered by ceramic cutting tool materials when machining nickel-based alloys causes multilayer levels of wear as seen in Figure 3.3.

This image has been removed by the author of this thesis for copyright reasons
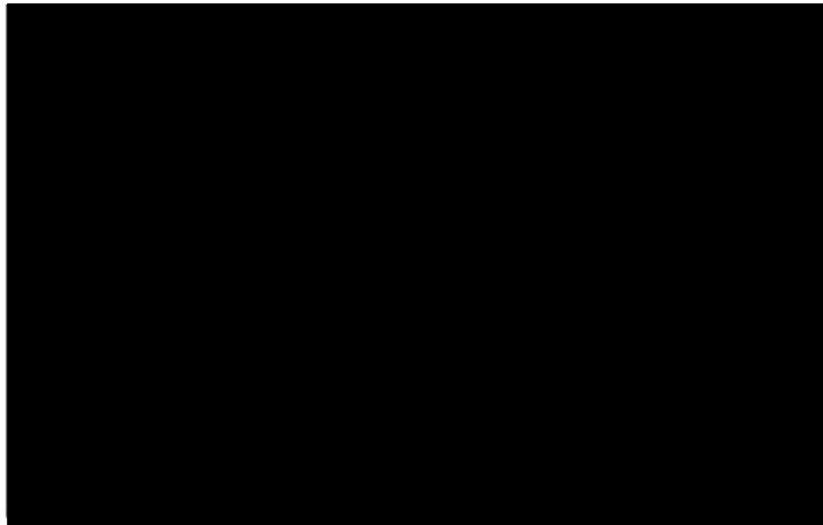
Figure 3.3. Progression of flank face wear on a round insert. [94]

3.2.2 Tool Life Characterization Technique

Tool life is very much directly related to the wear of the cutting tool. Wear of both the flank and rake face of the cutting tool is influence by different machining environments. The relief face or flank face is subjected to rubbing forces and interaction with the swarf chips which are formed during the machining process. The rake face is subjected to very high contact pressures in gigapascal (GPa) region. The high contact pressures generate high frictional forces between the workpiece Inconel 718 material and the cutting tool. Which creates very high temperatures in the primary and secondary shear regions in the chip/tool interface.

As mentioned in Section 2.7.6, thermochemical wear mechanisms such as diffusion wear, is defined as the interaction at high cutting temperatures between the workpiece/chip material and the cutting tool. The high temperatures initiate solid solution to take place between the silicon and iron. The silicon in the cutting tool diffuses and forms a solid solution with the iron in the evacuating Inconel 718 chip at 1000°C. This is where the cutting tool or insert begins to break down, which results in primary wear mechanisms such as notch and crater wear to commence.

The process of cutting tool degradation is depicted in Figure 3.4, whereby the cutting tool material wears in a three-stage process.

The initial wear region is usually small, the steady wear region is much larger and encapsulates the main flank wear measurements. The severe wear region is also small and will have the final flank wear measurement. **The three-stage wear process is particularly evident later on in the results Section 5.4 and Section 7.5.**

This image has been removed by the author of this thesis for copyright reasons
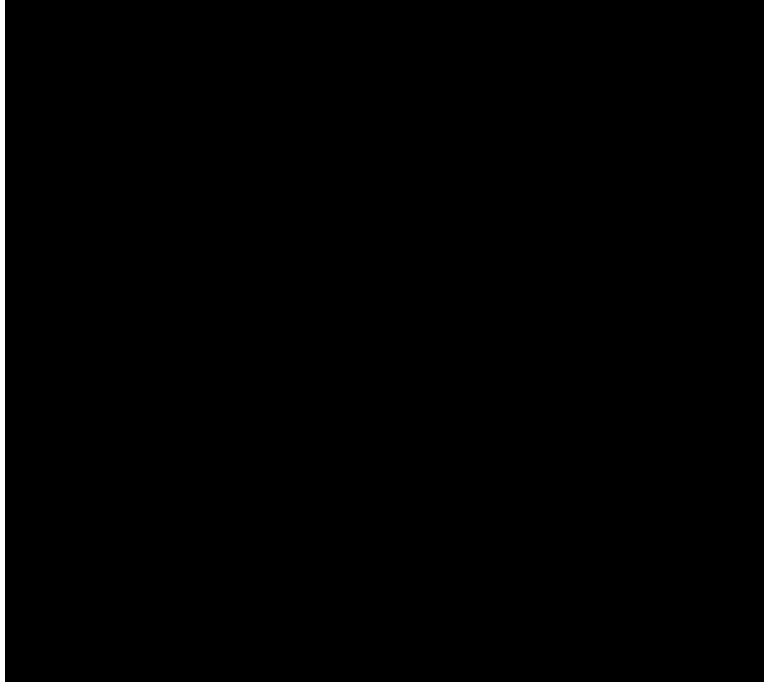
Figure 3.4. Variation of the flank wear rate with cutting time, showing the initial wear, steady wear, and severe wear periods. [44]

3.3 Coating Selection Process for Experiments

3.3.1 Coating Selection Process for Experiment Two

As discussed earlier in Section 2.11, the selection of protective wear resistant coatings for demanding cutting tool applications are influenced primarily by the cutting conditions. Coating A was a typical CVD coating system that was typically used by Ceratizit for coating tungsten carbide inserts. Therefore, Coating A was used for comparative needs. For the coating selection process for Coating B, results from an in-depth literature review were utilised. The research that has been completed previously that focused on the depositing wear resistant coatings onto the ceramic inserts [66], [67], [95], had a big influence on the what coating elements should be selected for Coating B. The research conducted by Dobrzanski et al concluded that CVD coating TiN + Al_2O_3 attained the best critical load (L_c) values and exhibited the least amount of flank wear (V_{BB}).

49

Based on the results from the literature review aluminium oxide and titanium nitride was selected for Coating B. Aluminium oxide (Al_2O_3) was selected as it has high thermodynamic stability, high hot hardness, high resistance to chemical wear and exhibits high adhesion to SiAlON ceramic. Titanium nitride (TiN) was selected based on the high wear resistance and resistance to deformation. Al_2O_3 and TiN are also readily used by Ceratizit on an industrial production level, which meant the costs associated with introducing these CVD coated SiAlON inserts into production would be small. Figure 3.5 highlights the multilayer and bilayer coating systems for Coating A and Coating B and mechanical characteristics of each coating element.
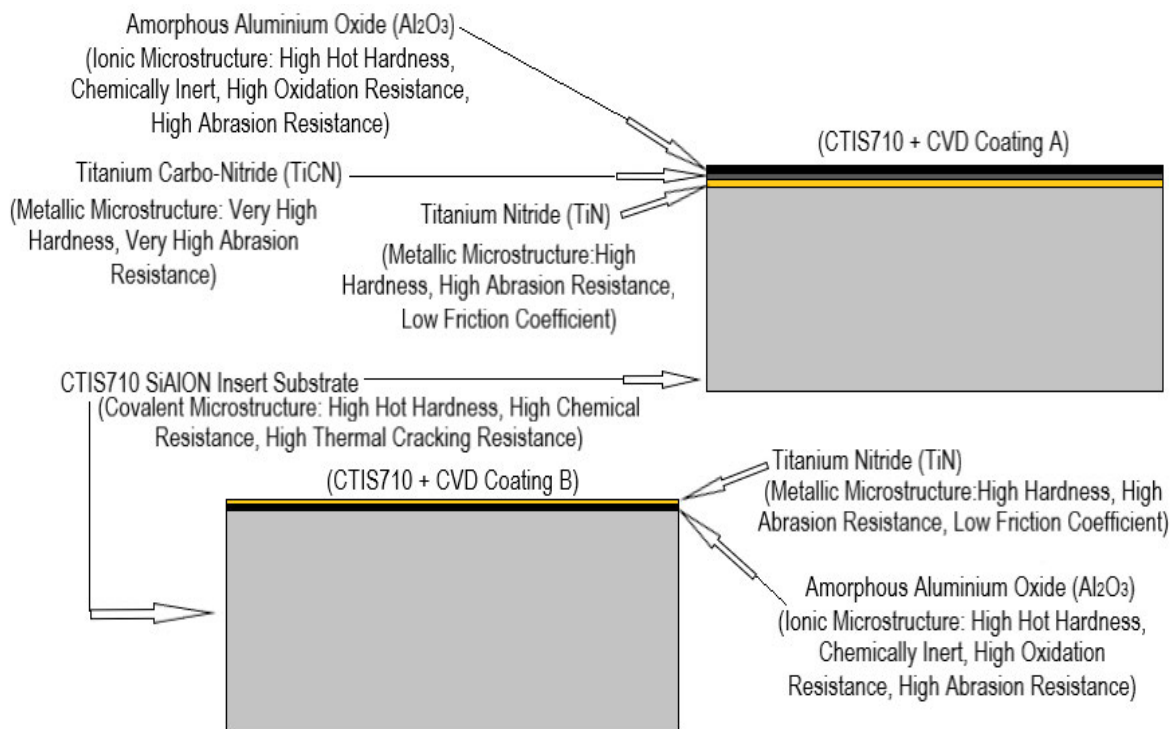
Figure 3.5. Experiment two coating microstructure and mechanical characteristics. [96]

3.3.2 Coating Selection Process for Experiment Four

The selection process for Coating C was influenced by the results that were attained in the machining trials in Chapter 5 and coating characterization in Chapter 6. Figure 3.6 highlights the single layer coating system that was selected for Coating C and the mechanical characteristics of a single layer of amorphous Al_2O_3.

A single layer system was selected for Coating C, as there was a desire to improve the wear deformation characteristics of the Coating C CVD coating. In the previous coating systems that were used for Coating A and B, the CVD layers that made up the coating system varied from 0.5 μm - 2 μm thick. The premise with Coating C, was to use a single 6.5 μm thick amorphous

Al$_2$O$_3$ CVD coating. It was hoped that a thicker CVD coating would have more structural stability and have better resistance to deformation at high cutting temperatures.

(CTIS710 + CVD Coating C)

Amorphous Aluminium Oxide (Al2O3) (Ionic Microstructure: High Hot Hardness, Chemically Inert, High Oxidation Resistance, High Abrasion Resistance)

CTIS710 SiAlON Insert Substrate (Covalent Microstructure: High Hot Hardness, High Chemical Resistance, High Thermal Cracking Resistance)
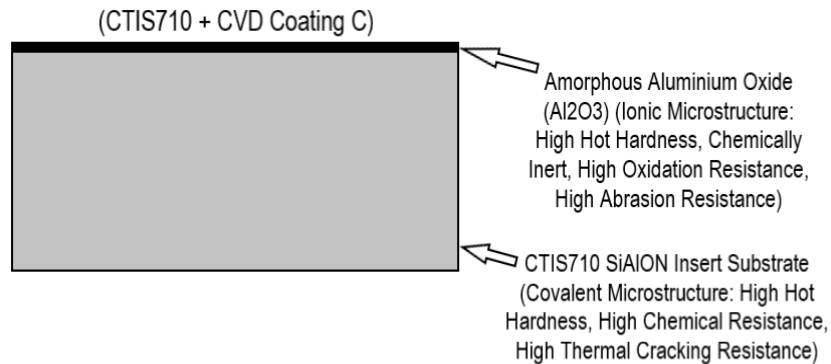
Figure 3.6. Experiment Four coating microstructure and mechanical characteristics.

3.4 Metallurgical Sample Preparation

3.4.1 Metallographic Polishing

Bakelite is an electrically conductive materials which is moulded around four swarf chip samples. The low electrical conductivity properties of Bakelite help to view electrically conductive samples with either a scanning electron microscope or transmission electron microscope.

In order for the Inconel 718 microstructure to be analysed, the Bakelite samples had to be mounted in Buehler simplimet 1000 automatic mounting press and prepared via grinding and polishing operations on the Buehler auto-met 250 machine. Carbi-met 320 [P400] 35-micron grit size pad, carbi-met 400 [P800] 22-micron grit size pad and carbi-met 600 [P1200] 15-micron grit size pads.The polishing sequence that was utilized to polish the mounted Bakelite chip samples are stated in Table 3.5.

Table 3.5. Metallographic Polishing Sequence for Inconel 718 Mounted Samples. [97]

51
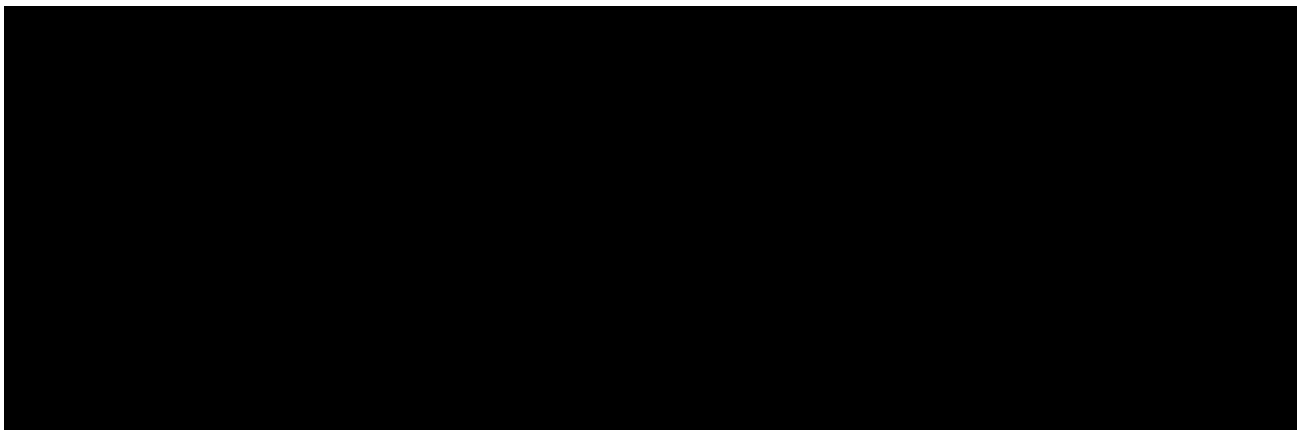
3.5 Imaging Techniques and Analysis

3.5.1 Non-contact 3D Profilometer (Focus-Variation Type)

To study the wear of SiAlON milling inserts during and after machining trials and after the scratch tests had been completed, an Alicona SL non-contact profilometer was used. The orientation of the worn SiAlON milling inserts was either kept on a flat surface to take top-down images of the wear regions or the SiAlON milling inserts.

3.5.2 Digital Imaging Techniques

To study the wear of SiAlON milling inserts and Inconel 718 chip morphology during and after the machining trials had been completed, a Keyence digital microscope and Leica digital microscope was used.

3.5.3 Scanning Electron Microscopy (SEM)

To study microstructures at higher magnifications, a Hitachi TM3030 Plus scanning electron microscope (SEM) was used to capture images of coated inserts that had been subjected to micro scratch testing. The Hitachi TM3030 SEM was also used to take images at different magnification to analyze the level of deformation that the swarf chip samples had sustained. The setup that was utilized for capturing the SEM images of the scratched SiAlON inserts is seen in Figure 3.7.
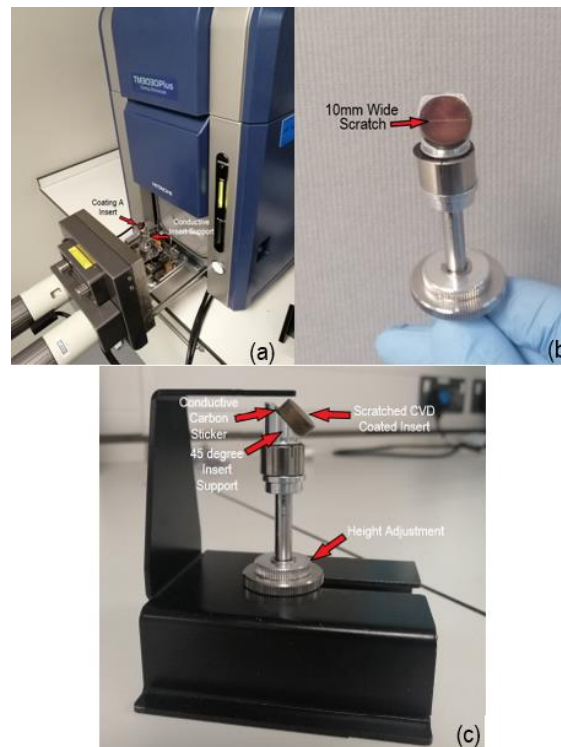
Figure 3.7. (a) SEM scratched SiAlON insert setup, (b) scratched insert on 45 degrees insert support, (c) z-axis sample setup.

3.6 Micro-scratch Testing Technique of Thin Film Coatings

Determining the minimum and maximum adhesion and mechanical failure characteristics of thin film coatings is paramount in determining useful life of the coating. The process of improving of improving the coating is based on the data that is extracted from micro-scratch testing techniques. These techniques for this tribological research were conducted to ASTM:C1624-22. This standard provides the framework to which the micro-scratch testing should be conducted to. Figure 3.8 graphically shows the micro scratch process where a diamond stylus is moved in a linear direction whilst an applied normal force is increased. As the applied normal force is increased the progressive damage increases.

This image has been removed by the author of this thesis for copyright reasons
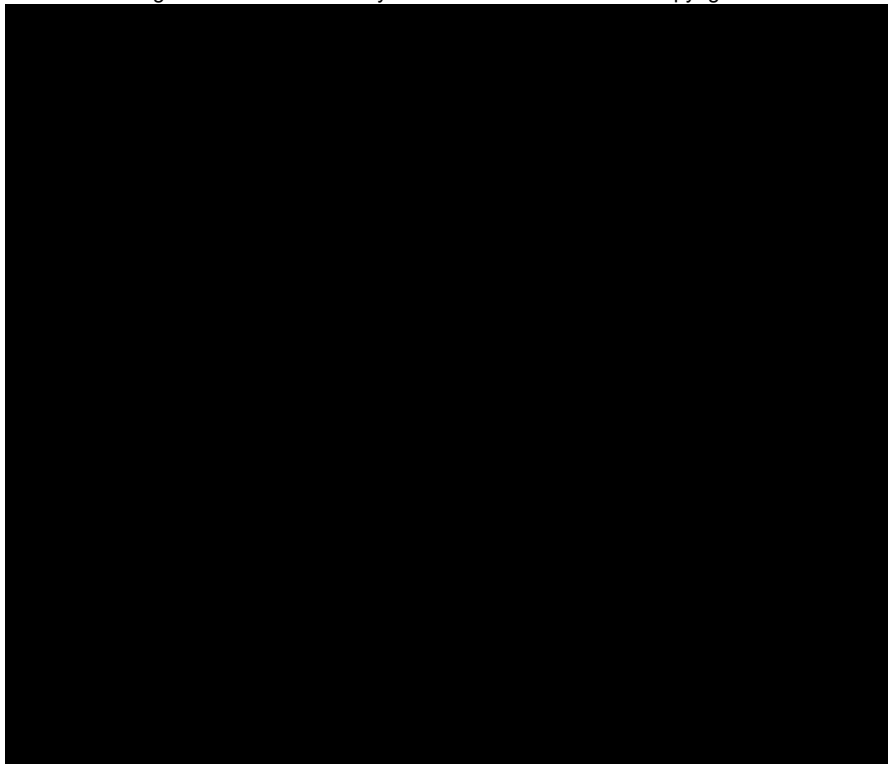
Figure 3.8. Micro Scratch Test Method Schematic. [98]

An example of the scratch test setup is shown in the schematic in Figure 3.9. This specific test standard is applicable to a wide range of hard ceramic coatings with a composition consisting of carbides, nitrides, oxides, diamond, and diamond-like carbon that have been deposited on ceramic and metal substrates. The test provides an engineering measurement of the practical adhesion strength of the coating. Evaluation of the adhesion characteristics of both coatings was investigated on each of the inserts using the scratch test on the Bruker UMT Tribo-lab device, by moving the diamond stylus along the examined specimen's surface with a gradually increasing load (0-100 N; 100 N/min).
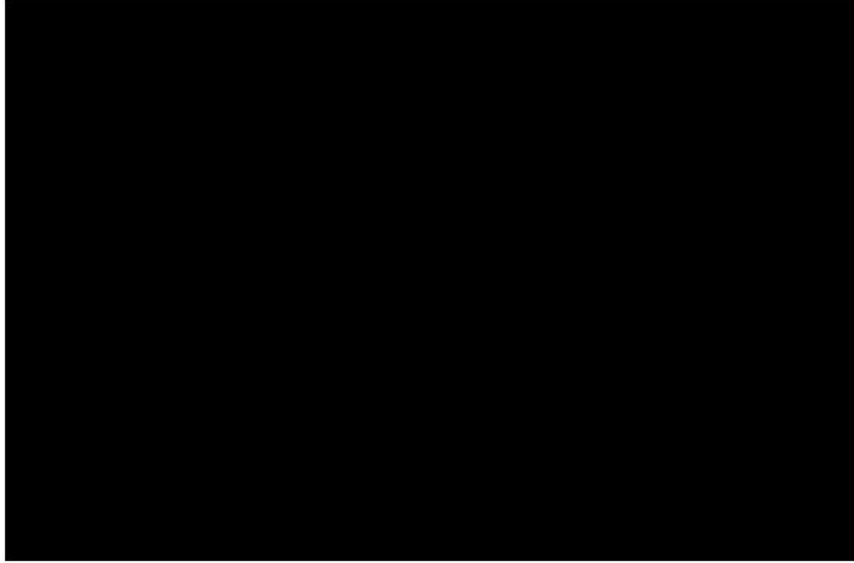
Figure 3.9. Scratch Adhesion Test System Schematic. [98]

The stylus's travel speed was 10 mm/min; and acoustic emission detector's sensitivity was AE 1 to record the elastic waves, the elastic waves are generated because of deformation and propagation of the fractured microstructure with an increasing normal force underneath the stylus.

3.7 Pin on Disc Testing Techniques

Determining the wear characteristics of different materials has required use of tribological techniques to determine these wear characteristics. One of the widely used tribological techniques is via pin on disc testing. Essentially a solid pin or ball has a normal force applied so that the solid pin or ball is pressed into the disc. The disc will be worn away in the form of a circular track and the solid pin or ball will also wear away.

The schematic seen in Figure 3.10 shows a set up for pin on disc testing. F is the normal force on the pin, d is the pin or ball diameter, D is the disk diameter, R is the wear track radius, and w is the rotation velocity of the disk.

Figure 3.10. Schematic of Pin-on-Disk Wear Test System. [99]

The level of wear that the disc and pin/ball sustain during the test will depend on the mechanical properties of the both the disc and pin/ball. For the tests that have been conducted for this research project, the standard ASTM G99-17: Standard test method for wear testing with a pin on disk apparatus was adopted to provide a framework to for testing the wear characteristics for the two CVD coated SiAlON inserts.

3.8 Experiment One Method

The aim of Experiment One has been to look at comparing the wear characteristics of four different ceramic turning inserts at cutting speeds of 250 m/min and 300 m/min, when machining solution annealed Inconel 718 (AMS5662). The focus of Experiment One has been to determine which ceramic tool material exhibits the highest wear resistance. The ceramic tool that exhibits the highest wear resistance was selected for the rest of the experimental trials.

3.8.1 Experiment One - Machining Operations (Test No T1.1-T8.2)

A machining trial was conducted on a high precision turning machining centre (a DMG MORI NLX2500/700), fitted with a high-pressure coolant delivery system, this was used throughout Experiment One. A refractometer was used throughout the machining trial experiments to take measurements of the cutting fluid (Blaser-Swisslube Vasco 7000 water-miscible, vegetable ester based, high performance cutting fluid). The cutting fluid concentration level was monitored and maintained at 10%. Flood cutting fluid supply was used in all the eight sets of test cuts and kept at 2 MPa pressure.

3.8.2 Experiment One - Tool Materials

Two different type of ceramic turning inserts SiAlON ceramic turning inserts tools were used during the machining trial and they were held in the machining centre by the supplier-recommended tool holder (a CRGNL 2525 M12-07) for external turning operations. The two grades of ceramic that were used in the machining trial have slightly different material characteristics. The typical properties of whisker-reinforced alumina (Al_2O_3+ SiC_w) ceramic inserts and silicon aluminium oxynitride (SiAlON) ceramic inserts can be viewed in Table 2.3. G. Brandt et al [56] discuss in their research the route of manufacture of whisker-reinforced alumina inserts. The hot-pressing process generates a high strength anisotropic whisker distribution of silicon carbide, which is preferably perpendicular to the face of the insert. The SiAlON inserts are a substitutional solid substitution of silicon nitride, aluminium oxides, and yttrium oxide. The cutting conditions for experiment one can be viewed in Table 3.6.

3.8.3 Experiment One Cutting Conditions (Test T1.1-T8.2)

Each combination of tool material and process parameters was tested twice, as can be seen in Table 3.6. Test cut numbers T1.1-T1.2, T2.1-T2.2, T3.1-T3.2 and T4.1-T4.2 were conducted at 250 m/min, with a feed rate of 0.20 mm/rev and constant depth of cut (Ap) of 2.0 mm. Test numbers T5.1-T5.2, T6.1-T6.2, T7.1-T7.2 and T8.1-T8.2 were conducted at 300 m/min, with a feed rate of 0.20mm/rev and constant (Ap) of 2.0 mm. For each of the test numbers, the (T) in front of the number represents turning test.

Table 3.6. Cutting conditions for Experiment One.

Test Cut number	Tool material	Insert Identification Letter	Cutting Speed (m/min)	Feed Rate (mm/rev)	Depth of Cut (mm)	Material Removal Rate (mm³/s)
T1.1, T1.2	SiAlON Grade 1	A	250	0.20	2	160
T2.1, T2.2	SiAlON Grade 1 (chamfered)	B	250	0.20	2	160
T3.1, T3.2	SiAlON Grade 2	C	250	0.20	2	160
T4.1, T4.2	Whisker - Reinforced Alumina	D	250	0.20	2	160
T5.1, T5.2	SiAlON Grade 1	A	300	0.20	2	200
T6.1, T6.2	SiAlON Grade 1 (chamfered)	B	300	0.20	2	200
T7.1, T7.2	SiAlON Grade 2	C	300	0.20	2	200
T8.1, T8.2	Whisker – Reinforced Alumina	D	300	0.20	2	200

3.8.4 Experiment One - Workpiece material

A single workpiece piece of solution-annealed (27HRC) Inconel 718 round bar, nominally 100.0 mm diameter and 350.0 mm in length, was used In Experiment One. The solution annealing heat treatment was conducted 1021 – 1038°C. The chemical composition and mechanical properties of Inconel 718 (AMS5662) are given in Table 2.1 and Table 3.7.

Table 3.7. Mechanical Properties of Inconel 718 (AMS5662).

Yield stress (MPa)	Tensile stress (MPa)	Strain (%)	Elastic modulus (GPa)	Thermal conductivity (W/m K)	Density (kg/m³)
751	939	23.3	206	11.6	8470

3.8.5 Experiment One - Tool Life Criteria (Test No T1.1-T8.2)

The default conditions for tool failure are when tool flank wear scar is measured at 1.0mm or more. This tool flank wear limit was stipulated by ISO 3685:1993.

3.9 Experiment Two Method

The aim of Experiment Two has been to look at comparing the machining performance of CVD coated and uncoated CTIS710 SiAlON milling inserts when machining aged hardened (AMS5663) Inconel 718 test samples. The focus of Experiment Two has been to determine the impact of hard protective coatings and their effectiveness on increasing the tool life and metal removal rates of SiAlON milling inserts. Four sets of milling insert wear test trials were conducted to ascertain the impact on tool life when applying a hard CVD coating to a CTIS710 SiAlON milling insert.

The milling insert wear tests consisted of using two CVD coated and uncoated milling inserts for each set. Each set of tests will adopt four different speeds and feed rates. A constant depth of cut of 1.0 mm was employed for each of the milling wear tests. The depth of cut was selected based on certain chip thickness (H_{ex}) values which is discussed further in Section 3.9.3. A Kistler dynamometer will be utilised to measure the cutting forces during the machining process to clarify any variance between the uncoated and coated milling inserts.

3.9.1 Experiment Two - Machining Operations (Test No M1-M13)

The machining operations for this experiment took place on DMG Mori NVX5080 three axis machining centre. The machine structure of NVX 5080 2nd Generation including guideways has been thoroughly optimized to achieve high accuracy and high rigidity. The NVX5080 has a maximum spindle speed of 15000 min^{-1} and has F_x-axis, F_y-axis, and F_z-axis travel speeds of 30000 mm^{-1}. The milling operations were conducted in dry conditions, the NVX5080 local exhaust ventilation system was employed to remove unwanted dust before opening the access door.

3.9.2 Experiment Two - Cutting Tool Path Selection and CAM Programming

One of the most important processes which has a direct effect on the tool life and the types of wear mechanisms that the cutting inserts encounter, whilst cutting difficult to machine materials such as Inconel 718, is tool path selection and CAM programming. The custom cutting tool path highlighted in Figure 3.11 were designed to minimise fluctuations in the specific cutting forces that the inserts experienced during the machining trial. Each of the sections involved machining 12-off 1.0 mm depth of cut (Ap).
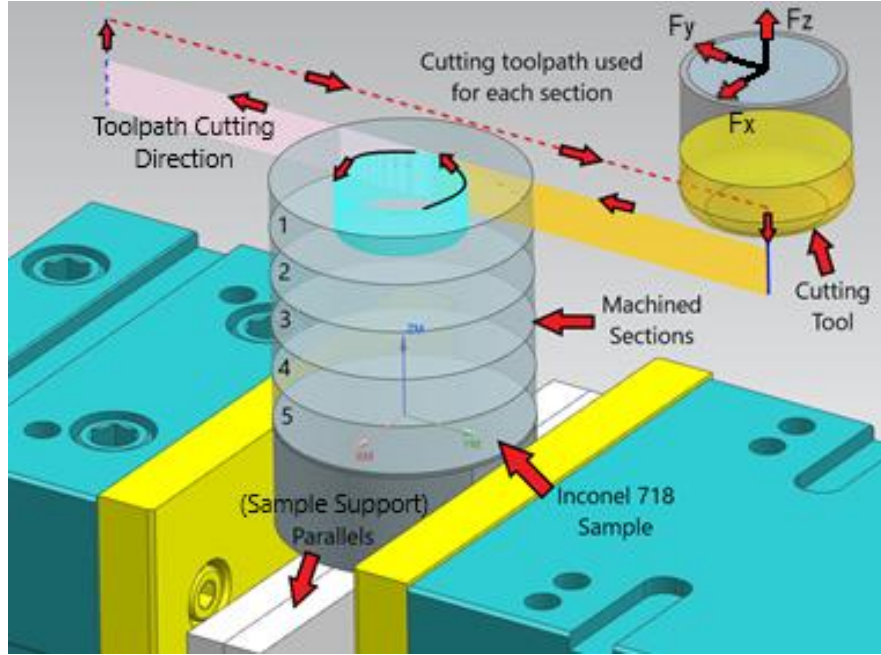
Figure 3.11. Siemens NX CAM model assembly 3D view of cutting tool path. [100]

3.9.3 Chip Thinning Effect

Throughout the machining process the maximum chip thickness (H_{ex}) must be maintained at a constant level to avoid fluctuations of specific cutting forces, which contribute to premature tool failure. Equation (3.1) was used to calculate a value that would prevent shocking the cutting tool during the machining process of each 1.0 mm Ap and insert diameter (IC) [101].

$$Hex = Fz \times \sqrt{\left(4 \times \frac{Ap}{IC} - \left(2 \times \frac{Ap}{IC}\right)^2\right)} \qquad \text{Equation 3.1}$$

Another important factor regarding the cutting forces is the spindle speed (S) (revs/min) and cutting speed (Vc) (m-min) this has a direct impact on the level of cutting force and quantity of heat that is being generated in the primary shear zone. The diameter (D) of the milling tool also has influential impact on the how quickly a milling tool can rotate governing the limitations of current spindle arrangement in the latest 5-axis milling machines and machining centres.

$$Vc = \frac{\pi * D * S}{1000} \qquad \text{Equation 3.2}$$

An important factor in attaining the true cutting speed of the milling insert holder is to define the effective diameter (D_{eff}) Insert radius (IR), depth of cut (DoC).

$$Deff = D - 2 * IR + 2 * \sqrt{(DoC * (2 * IR - DoC)} \qquad \text{Equation 3.3}$$

58

Another machining parameter which also has a direct impact on cutting force is the table feed rate (fz). Maintaining a constant feed per tooth (FPT) value of 0.1 mm/rev is heavily influenced by the number of inserts (Z) and spindle speed (Vc).

$$Fz = FPT * Z * Vc \hspace{4cm} \text{Equation 3.4}$$

Figure 3.12 highlights how the chip thickness can change and very much depends on which Ap is adopted. A 30.0 mm radial engagement (ae) was used for each cut as this would help to maintain the chip thickness during the Experiment Two. A 30.0 mm radial engagement meant a complete section of material could be removed in one cut. The radial engagement has a direct on the specific cutting force that the insert experience during the machining process. Therefore, the radial engagement needs to be maintained where possible.
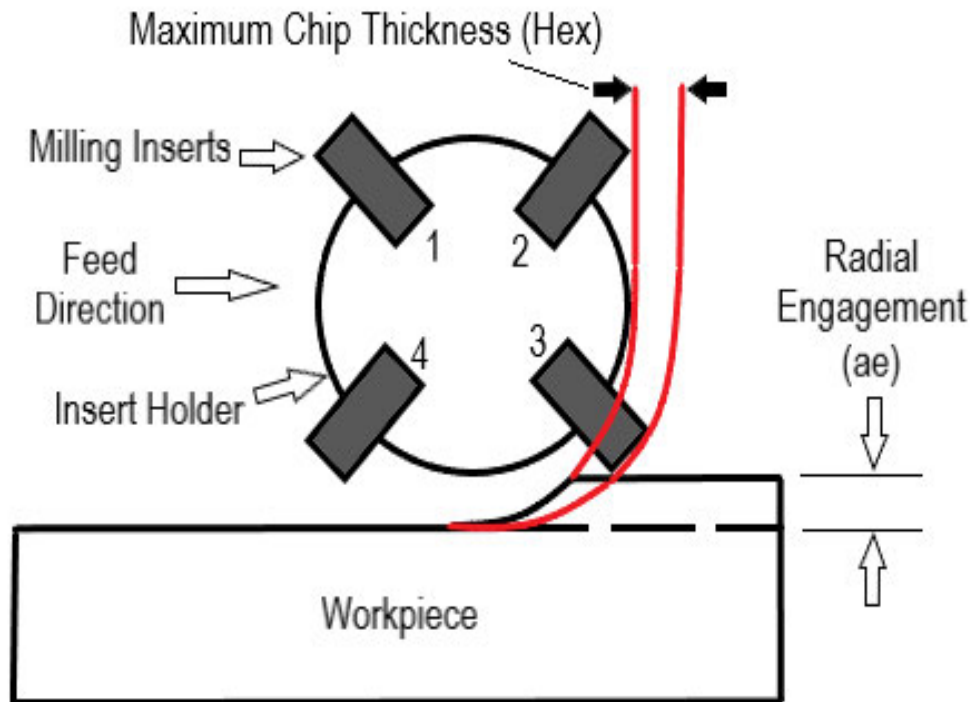
Figure 3.12. Schematic representation of the chip thinning effect. [24]

The selection of cutting speeds, feed rates, depth of cut, and radial engagement for Experiment Two, were influenced by the machining research which was conducted by AB Sandvik Coromant. Figure 3.13 displays a comparison between cutting speed (Vc) versus maximum chip thickness (H_{ex}) and the potential wear effects on the cutting inserts and the workpiece material. The potential optimum (H_{ex}) is captured in the grey 'application' box.

This image has been removed by the author of this thesis for copyright reasons

Figure 3.13. Cutting Speed (V_C) versus Maximum Chip Thickness (H_{ex}). [102] (Courtesy of AB Sandvik Coromant)

3.9.4 Experiment Two - Tool Materials and Coatings

The round SiAlON milling inserts will have a TiCN + Al_2O_3 multilayer coating (type A) and an optimised ceramic coating (Type B), both coatings were applied via chemical vapour deposition techniques at Ceratizit's Ruette facility in Austria can be viewed in Table 3.8. The oxide coatings were deposited at a temperature of 1000°C, the deposition rate was 1-2 µm per hour. A MaxiMill A262.40.R.04-1204 insert holder and BT40 spindle were utilised for all the machining tests, which had a maximum cutting diameter of 40.0 mm. Four inserts were used in each milling test.

Table 3.8. Round insert grades to be tested in Experiment Two.

Geometry	Insert Grade	Coating Grade	Manufacturer
Round (RNGN)	CTIS710 SiAlON	Uncoated	Ceratizit
Round (RNGN)	CTIS710 SiAlON +Type A coating	CVD 6 µm TiN-TiCN-Al_2O_3 coating with α-Al_2O_3 – black colour	Ceratizit
Round (RNGN)	CTIS710 SiAlON +Type B coating	CVD coating optimised for Silicon Nitride (SiN) ceramics: 3-4 µm α-Al_2O_3 – TiN coating – yellow colour	Ceratizit

The set of milling trials for Experiment Two used the following cutting parameters. For each of the test numbers, the (M) in front of the number represents milling test.:

1. At the start of each test the new and unused insert will be imaged for reference.

2. Tool wear life Test M1, M4, M7, M10 will be conducted with an uncoated CTIS710 milling insert.

3. Tool wear life Test M2, M5, M8, M11 will be conducted with a coated CTIS710 (Type A Coating) milling insert.

4. Tool wear life Test M3, M6, M9, M12 and M13 will be conducted with a coated CTIS710 (Type B Coating) milling insert.

For each test to be successful 169.64 cm^3 will need to be removed. The 169.64 cm^3 of material will be machined away in five 12.0 mm long sections. Once the section has been successfully machined away, the tool will be removed so that wear data for the inserts can be gathered on the Zeiss microscope (As shown in Section 3.9.8). The five sections of material to be removed will account to 33.929cm^3 each.

3.9.5 Experiment Two Cutting Conditions (Test No M1-M13) - Interrupted Cut Insert Wear Test Machining Trial

Tool wear life Tests M1, M2 and M3 were conducted at a cutting speed of 700 m/min, a feed rate of 0.10 mm/tooth, table feed rate of 2610 mm/min and a depth of cut of 1.0 mm.

Tool wear life Tests M4, M5, M6 and M13 were conducted with an uncoated CTIS710 milling insert at a cutting speed of 800 m/min, a feed rate of 0.10 mm/tooth, table feed rate of 2983 mm/min and a depth of cut of 1.0 mm. Successful tests have remove 169.64 cm^3 of material. Test 13 was a repeated test with Coating B inserts.

Tool wear life Tests M7, M8 and M9 were conducted at a cutting speed of 900 m/min, a feed rate of 0.10 mm/tooth, table feed rate of 3356 mm/min and a depth of cut of 1.0 mm. Successful tests will remove 169.64 cm^3 of material.

Tool wear life Tests M10, M11 and M12 were conducted at a cutting speed of 1000 m/min, a feed rate of 0.10 mm/tooth, table feed rate of 3729 mm/min and a depth of cut of 1.0 mm. Successful tests will remove 169.64 cm^3 of material. Tool condition will be checked, and images taken on the Zeiss microscope after each section has been machined, this information was used to create S/N curves. An additional sample will be machined so that comparable amount of cutting time is attained by each test.

3.9.6 Experiment Two - Workpiece material

Each machining trial utilised a single piece of precipitation hardened Inconel 718 round bar stock 60.0 mm diameter x 86.0 mm long were used for the trial. A portion of the material residual material from other machining research projects at Sheffield. The prior stock came in the form as solution annealed (AMS5662) round bar billet 101.60 mm diameter x 350.0 mm long was provided by a Maher Ltd via an in-kind contribution.

Maher Ltd also provided another in kind contribution in the form of two pieces of Inconel 718 60.0 mm diameter X totalling 1480.0 mm in length of alloy 718 to AMS 5662 specification. The precipitation hardening heat treatment (AMS5663) for the 60.0 mm diameter x 85.0 mm long specimens was conducted by Special Steels Group in Sheffield. As the material was supplied in the solution annealed (AMS5662) condition an aging heat treatment was conducted at Special Steels to age harden the Inconel 718.

The AMS5663 precipitation hardening heat treatment for the 60.0 mm diameter states the following: Aged at 726°C for 8:03 hours and then cool furnace to 621°C and hold for a further 8 hours and cool in air. This heat treatment process is typically used for attaining Inconel 718 at 43-45 Rockwell C hardness. The mechanical properties of the samples were verified on a Rockwell hardness testing machine. The average hardness of the sample was 44 Rockwell C, which means the samples have a max tensile strength of 1417 MPa.

3.9.7 Experiment Two - Tool Life Criteria (Test No M1-M13)

The tool life criteria for this machining trial were selected to gain a greater understanding of the true machining tool life limit with which these three SiAlON ceramic inserts can perform within. Traditionally in industry, SiAlON ceramic milling inserts are changed are quickly changed once typical flank wear (V_{bb}) has surpassed 1.0 mm. The basis for the selection of the wear criteria for this experimental work was influenced by previous experimental studies that were conducted by Tian et al [32], Yildirim et al [103] and Guo et al [93].

These three studies highlighted that ceramic milling inserts can still perform their function of removing material during a machining process, even if the inserts have sustained significant amounts of the flank and rake face wear. Therefore, based on the flank wear results which have been recorded in these three studies the following tool life criteria was selected. Once flank wear for any of the four inserts had surpassed 2.5 mm (V_{bb}) or the insert has sustained significant damage on the rake face the test was stopped. The distance travelled by the cutting

tool, volume of metal that has been removed and a flank wear measurement is captured after each bar section has been removed.

The following tool life criteria was used:

1. The maximum flank wear (V_{bb}) land reaches 2.5 mm, once this value is surpassed the test is stopped to prevent tool failure.

2. Chipping (flaking) or premature failure occurs after the first cut of Inconel 718 sample had been machined.

3.9.8 Experiment Two - Insert Wear Imaging and Wear Measurement

A Zeiss Discovery V8 microscope was used for examining the worn inserts throughout the machining trials. The Zeiss microscope allowed for quick and efficient image capture during the machining trial. Figure 3.14 and Figure 3.15 shows the setup that was utilised for capturing the multitude of wear on the rake face for each of the four SiAlON inserts.
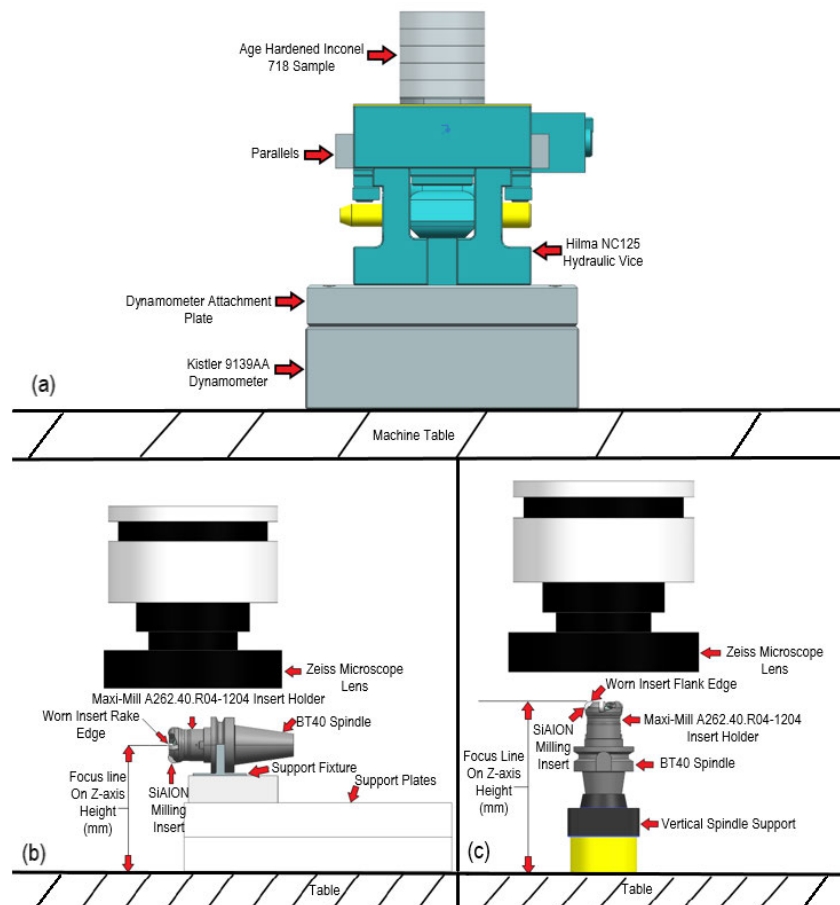
Figure 3.14. (Image a) Machine trial work-piece setup on the DMG Mori NVX5080 machining centre, (Image b-c) Zeiss set-up for rake and flank wear measurement. [100]

A USB microscope was also considered as an alternative means of capturing the level of wear that the inserts, however the Zeiss microscope was deemed to be a superior image capturing technique as its setup was more stable and the images were of higher quality.
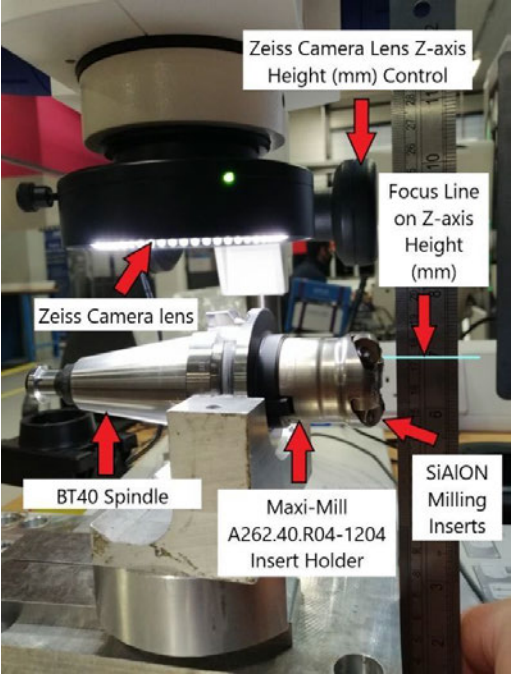
Figure 3.15. Rake face wear examination setup on the Zeiss discovery V8 digital microscope.

Figure 3.16 shows the setup that was utilised for capturing the magnitude of wear on the flank face for each of the four SiAlON inserts. This set-up helped with the timely and efficient image capture of all the flank wear images that will be analysed in this Thesis.

Figure 3.16. Flank face wear examination setup for the Zeiss discovery V8 digital microscope.

3.9.9 Experiment Two - Cutting Force Measurement

A Kistler 9139AA dynamometer was used to measure cutting forces during the machining process. Figure 3.17 shows the setup that was utilised for capturing the cutting force data that was generated at the four cutting speeds of 700, 800, 900 and 1000 m/min. This particular set-up was adopted due to it being very similar to what will be adopted in industry.
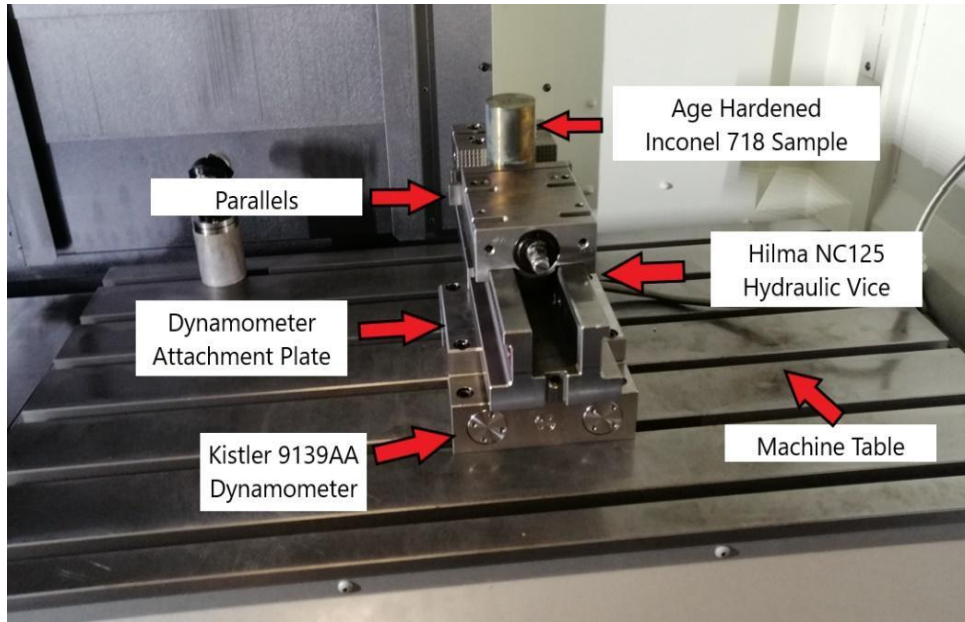
Figure 3.17. Machine trial work-piece setup on the DMG Mori NVX5080 machining centre.

This machine trial work-piece setup was selected to keep it as close to a real-world machining setup that is like to be used in industry. This set-up was designed to put the inserts under sufficient duress during the machining process to make sure that they would be experiencing realistic cutting forces during the machining trial.

3.9.10 Experiment Two - Data Analysis – Cutting Force and Insert Wear Data

Analysis of the cutting force data and insert wear data that was created during the machining trial has proven to be a challenging area of this project. The challenge has come in the form of manipulating very large comma separated value (.csv) files and extracting useful information. A cycle rate of 20000 Hz was utilised for each section and each section involved twelve 1.0 mm depths of cut. Each section required 120 seconds of force capture time, which ultimately caused the CSV files to be 2400000 data cells in length.

This resulted in CSV files which were too big to open completely in excel, as excel has a cell length limit of just over a 1 million cells. The CSV files can be opened but only a portion of CSV file will be displayed in excel. Therefore, it was determined that MATLAB 2020a be utilised for

opening the CSV by importing the CSV file into Matlab 2020a and then generating a MAT. File which is specific Matlab file for exporting data. Once the data is in a .mat file format reduced the overall size of the data and means it can be readily analysed in Matlab so that Matlab Figure and PNG files can be created for further analysis.

Figure 3.18 illustrates the process which was utilised for generating the cutting force data and also the process for extracting useful pieces of information.
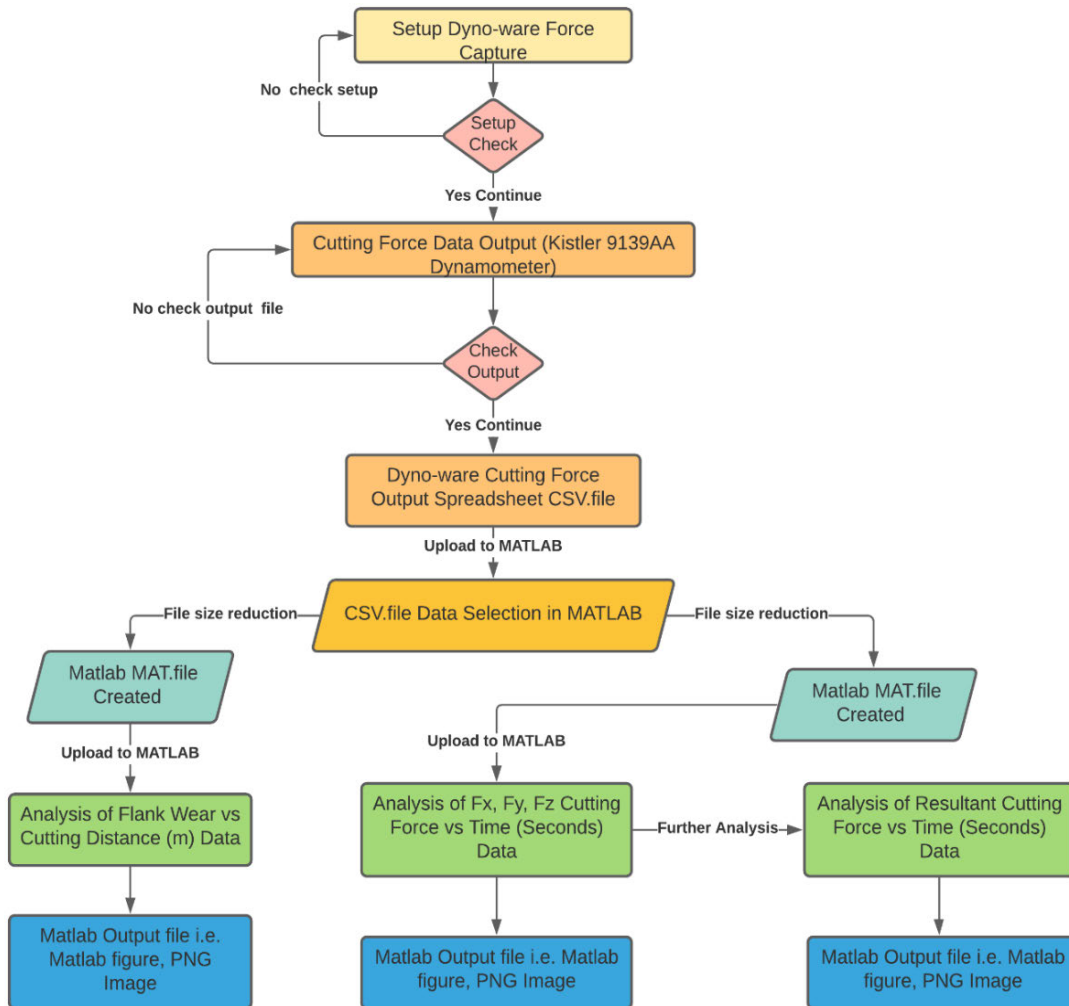
Figure 3.18. Cutting Force vs Time and Flank Wear vs Cutting Distance Data Collation Framework.

The cutting force signal data that was collated in Dyno-ware software, in the F_x-axis, F_y-axis and F_z-axis was used to calculate the resultant cutting force (F_r). The resultant cutting force was then calculated in Matlab 2020a using the Equation (3.5).

$$F_{xyz} = (Fx^2 + Fy^2 + Fz^2)^{0.5}$$

Equation 3.5

3.10 Experiment Three Method

The aim of Experiment Three has attempted to characterize the structure and mechanical properties such as adhesion and wear resistance of two different CVD coatings. These two CVD coatings have been deposited onto silicon aluminium oxynitride round (RNGN) milling inserts.

3.10.1 Experiment Three - Scratch Testing - Machine Setup

Evaluation of the adhesion characteristics of both coatings was investigated on each of the inserts using the scratch test on the Bruker UMT Tribo-lab device, by moving the diamond stylus along the examined specimen's surface with a gradually increasing load (0-100 N; 100 N/min). The stylus's travel speed was 10 mm/min; and acoustic emission detector's sensitivity was AE 1 to record the elastic waves, the elastic waves are generated because of deformation and propagation of the fractured microstructure with an increasing normal force underneath the stylus. Further Information on the scratch testing analysis is provided in Section 6.2.

3.10.2 Experiment Three - Machine Setup - Pin on Disc Testing

The pin-on-disc tests themselves were carried out on a Bruker UMT Tribolab machine as seen in Figure 3.19, in accordance with the ASTM standard for this method (ASTM G99-17). A sliding distance of 1000 metres equalling a time of 8 minutes and 19 seconds for a complete test was stipulated by ASTM G99-17.
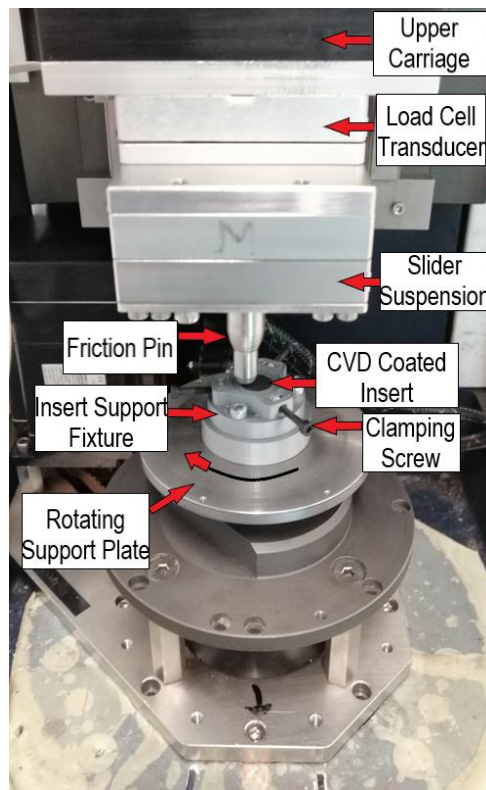
Figure 3.19. Pin-on-disc set up on the Bruker UMT Tribolab.

3.10.3 Experiment Three - Tool Materials and Coatings

Six inserts (Figure 3.20(a-b)) were used throughout the experimental tests, a single insert for each of the Coating A and Coating B inserts were used in the scratch testing. For the pin on disc testing two round SiAlON ceramic milling inserts with TiN + TiCN + Al_2O_3 multilayer coating (Coating A); and two round SiAlON ceramic milling inserts multilayer coated with Al_2O_3 + TiN (Coating B), which had been optimised for coating the SiAlON ceramic inserts. used in the pin-on-disc testing. A single insert for both coating A and coating B were used in the scratch testing. As mentioned earlier both coatings were applied via chemical vapour deposition (CVD) techniques at the manufacturer's 'Ruette' facility in Austria, on a Sucotec (SCT600TH) industrial-scale CVD machine. The oxide coatings were deposited at a temperature of 1000°C, the deposition rate was 1-2 μm per hour.
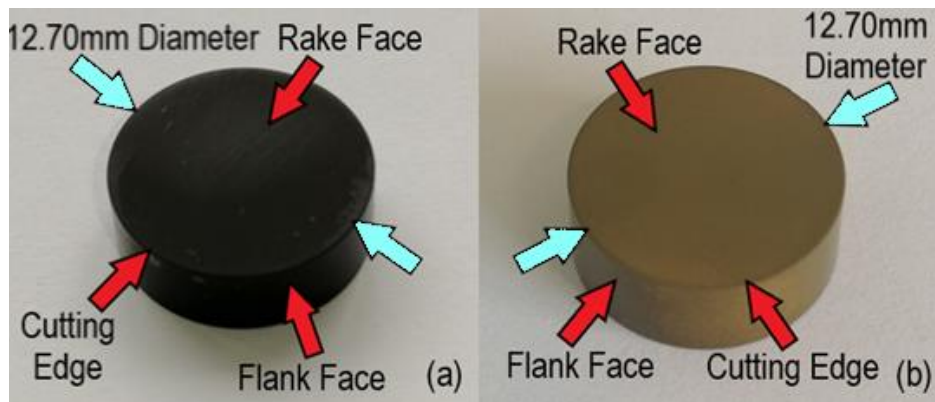
Figure 3.20. (a) CTIS710 SiAlON ceramic +Type A coating - CVD 6 μm thick TiN-TiCN-Al_2O_3 coating with α-Al_2O_3 (Corundum structure) – black colour, (b) CTIS710 SiAlON ceramic +Type B coating - CVD coating optimised for Silicon Nitride (SiN) ceramics: 3-4 μm thick α-Al_2O_3 – TiN coating – yellow colour.

The physical properties of the uncoated and CVD-coated SiAlON ceramic milling inserts, and the two CVD coating grades, are stipulated in Table 3.9.

Table 3.9. Physical properties of uncoated and CVD-coated SiAlON ceramic milling inserts.

Tool Material Grade	SiAlON Insert Composition	Insert Shape	SiAlON Insert Mechanical Properties			
			Fracture toughness ($MPa \cdot m^{1/2}$)	Density (g/cm^3)	Vickers Hardness (Hv)	Hardness (GPa)
CTIS710 SiAlON Uncoated	Si_3N_4 + Al_2O_3 + Y_2O_3	(RNGN) 120400	7	3.3	1800	17.65
CTIS710 SiAlON +Type A coating						
CTIS710 SiAlON +Type B coating						

3.10.4 Experiment Three Test Conditions – Pin on Disc Tests

A Hertzian analysis was conducted to ascertain the diameter of the ball counter specimens that could replicate average contact pressures of 3.6 GPa, experienced by the SiAlON ceramic insert rake face when machining materials such as Inconel 718 in high-speed face milling machining environments [104]. The pin-on-disc tests themselves were carried out on a Bruker UMT Tribolab machine as in Figure 3.19, in accordance with the ASTM standard for this method (ASTM G99-17) [99] with conditions presented in Table 3.10. To reach the designated 1000 m sliding distance as in Table 3.10, the tests would each need to last 496 seconds for a complete test was stipulated by ASTM G99-17.

Table 3.10. Pin-on-disc test parameters used in this study.

Test No	Tool Material	Friction Track Diameter (mm)	Ball Diameter (mm)	Ball Specimen Material	Ball Specimen Hardness (HRC)	Linear Velocity (m/s)	Load (N)	Sliding Distance (m)
1a	CTIS710 SiAlON + Type A Coating	8	4	AISI 52100-steel	60-67	2.0	78	1000
1b	CTIS710 SiAlON + Type B Coating	8	4	AISI 52100-steel	60-67	2.0	124	1000
2a	CTIS710 SiAlON + Type A Coating	8	4	AISI 52100-steel	60-67	1.0	78	1000
2b	CTIS710 SiAlON + Type B Coating	8	4	AISI 52100-steel	60-67	1.0	124	1000

The differing loads for the pin-on-disc tests which are stipulated in Table 3.10, were established by Hertzian analysis. The loads (N) in Table 3.10 are half of those calculated from Hertzian analysis due to stability issues which were encountered with the initial pin-on-disc test. The characterisation of the developed surface wear tracks and scratches was achieved with observations made on a Hitachi TM3030 scanning electron microscope. Ten nano-indentation hardness tests were conducted on each of the Coating A and Coating B inserts for each of which the indentation load was ramped up to 100 mN.

The resulting indentation depths (See Appendix B) ranged from 557 nm to 1132 nm for Coating A and 479 nm to 1857 nm for Coating B. The results of nano-indentation hardness tests had

significant scatter for both Coating A and Coating B (See Appendix B). This scatter means that the true hardness has proven to be very difficult to attain accurately, therefore value from the literature have been used in this analysis.

3.11 Experiment Four Method

The aim of experiment four has endeavoured to compare the machining performance of both CVD coated and uncoated CTIS710 SiAlON milling inserts, when machining age hardened (AMS5663) Inconel 718 test samples. Experiment four has been completed in two parts, Tests M14-M15 essentially repeated experiment two by reusing the same interrupted three axis CAM program to machine five sections away with twelve 1.0 mm cuts. Tests M16-M17 utilized continuous to near continuous cylindrical and elliptical tool paths to form a bar blade from age hardened Inconel 718. The principal focus of this two-part experiment is to clarify the difference between non-interrupted and interrupted toolpaths, and how these toolpaths have an effect on tool wear and subsequentially tool life. The other focus of Experiment Four has been to determine the impact of a hard protective single layer coating and the effectiveness on increasing the tool life and metal removal rates of SiAlON milling inserts.

3.11.1 Experiment Four (Test No M14-M15) - Machining Operations

The machining operations for this project took place on XYZ800HD three axis machining centre. The XYZ800HD has a max spindle speed of 12000 min^{-1} and has x-axis, y-axis and z-axis travel speeds of 24000 $mm^{-1.}$ The milling operations were conducted in dry conditions.

3.11.2 Experiment Four (Test No M16-M17) - Machining Operations

The machining operations for this experiment took place on DMG Mori MTX2500 Five axis mill turn machining centre. The machine structure of NTX2500 2nd Generation including guideways has been thoroughly optimized to achieve high accuracy and high rigidity. The milling operations were conducted in dry conditions.

3.11.3 Experiment Four (Test No M16-M17) - Cutting Tool Path Selection and CAM Programming

The process of creating the CNC programmes and custom toolpaths for experiment four Tests M16-M17 has involved a series of iterations which has taken place in consultation with senior engineers at the AMRC. After a few in-depth reviews of the tool paths had been completed in Vericut, It was concluded that the 3D CAD aerofoil model should be simplified. The simplification of the tool path has created a concise link between Test No M1-M15 and Test No M16 and M17.

The simplification process included simple cylindrical mill turning operations (Stages 1-8). The simple cylindrical mill turn operations involved utilising eight of the sixteen machining operations, which would account for 50 percent of the total NC programmes used to machine the bar blades. These continuous programmes would create a machining environment that was completely opposite to the machining environment that the milling inserts had experienced in Tests M14-M15. The continuous spiral (Streamline) toolpaths created a greater link from a physics point of view as the continuous tool paths had a completely non-interrupted machining environment in the chip/tool interface. Whereas the previous machining trials (Experiment two) for Tests M1-M15 had utilised interrupted cuts. The elliptical near/continuous tool paths (Stage 9-12) would account for the other 50 percent of the NC programmes would adopt positive geometry insert to machine a simple elliptical aerofoil profile.

The machining of the elliptical profile would satisfy the requirement of the EngD to produce an industrially focused geometry.

The custom cutting tool path shown in Figure 3.21 is a representation of the toolpath which has been created in Siemens NX. This toolpath represents the type of machining environment of the DMG Mori NTX2500 five-axis machining centre machine tool. The continuous/near continuous tool paths were designed to minimise fluctuations in maximum chip thickness (H_{ex}), cutting temperature and specific cutting forces by programming the cutting tool to tangentially engage and exit from cut. The tangential engagement into cut resulted in a gradual decrease in radial engagement (ae) in cut from 35.5 mm to 10.0 mm. The radial engagement was then kept at a
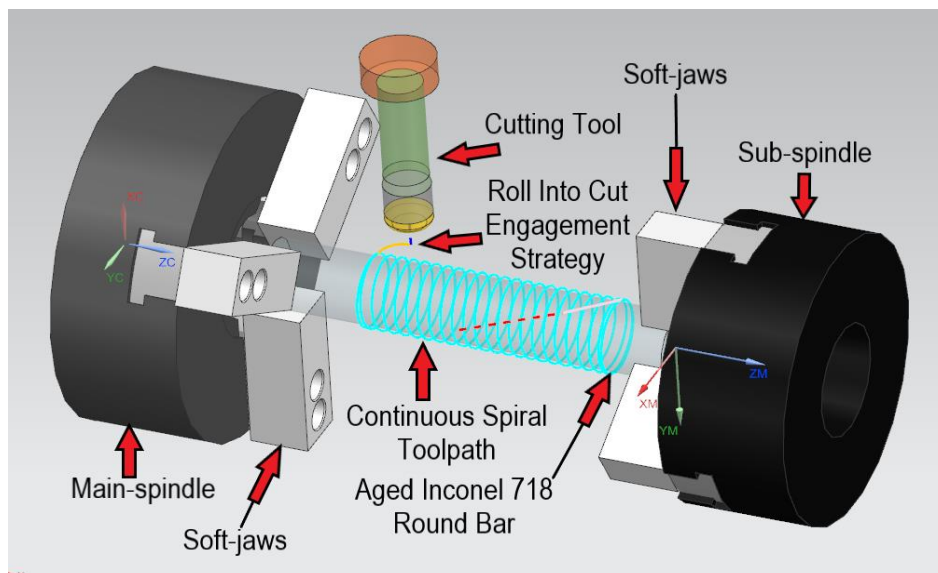
Figure 3.21. Siemens NX CAM model assembly 3D view of cutting tool path.

The cutting tool then radially travelled through a full 360° cut and tangentially exited the cut workpiece via the F_y-axis direction. The tangential engagement into and out of cut together with the radial change in toolpath direction is graphically shown in Figure 3.21.

The near-continuous elliptical tool paths that were used to machine the aerofoil were designed to minimise variations in specific cutting forces. The elliptical tool paths reduced the bar diameter in the F_x-axis direction, with a gradual increase and decrease in radial immersion to create the 2D aerofoil geometry as can be seen in Figure 3.22.

The gradual ramp into cut with elliptical near-continuous tool path worked favourably in reducing the fluctuations in specific cutting force and helped to prevent the SiAlON ceramic inserts from experiencing cutting forces that could cause premature tool failure.
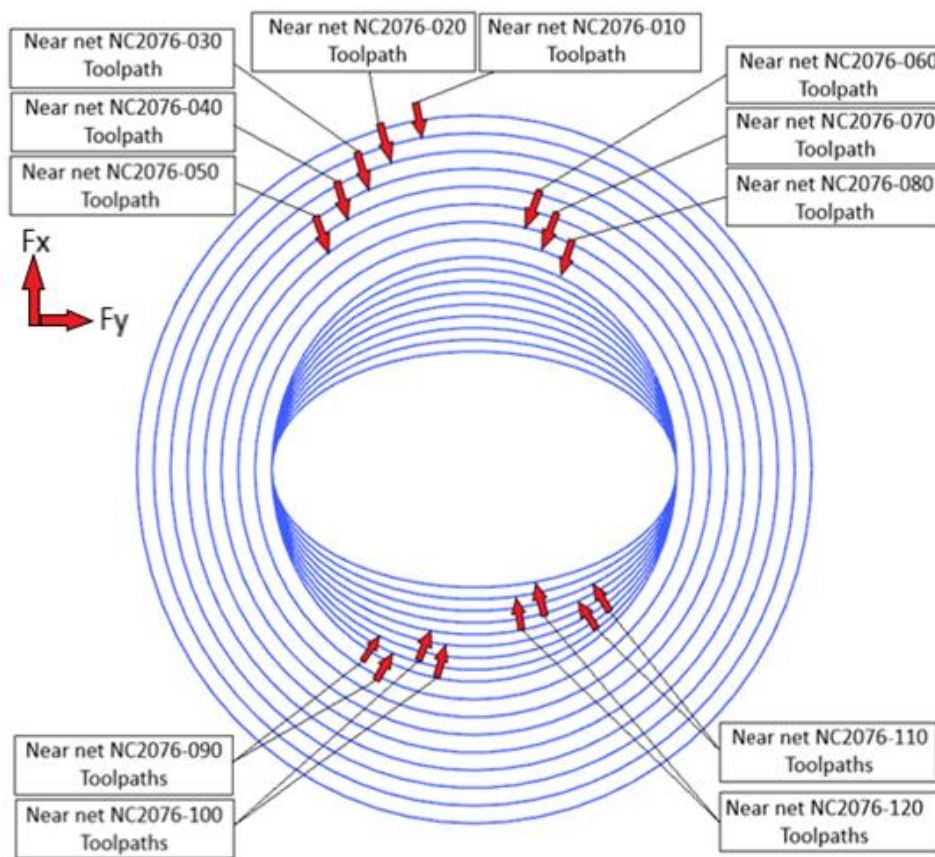
Figure 3.22. Cross section near net shape circular continuous and elliptical near-continuous toolpath.

Each of the near net shapes that can be seen in Figure 3.23 are offset from each other by 5.10 mm on each side. The distance of 5.10 mm was selected through a process of refinement in Vericut software. The refinement process focused on the engagement depth of cut in Vericut, which would fluctuate upon engagement if the near net shape offset distance was not correct.
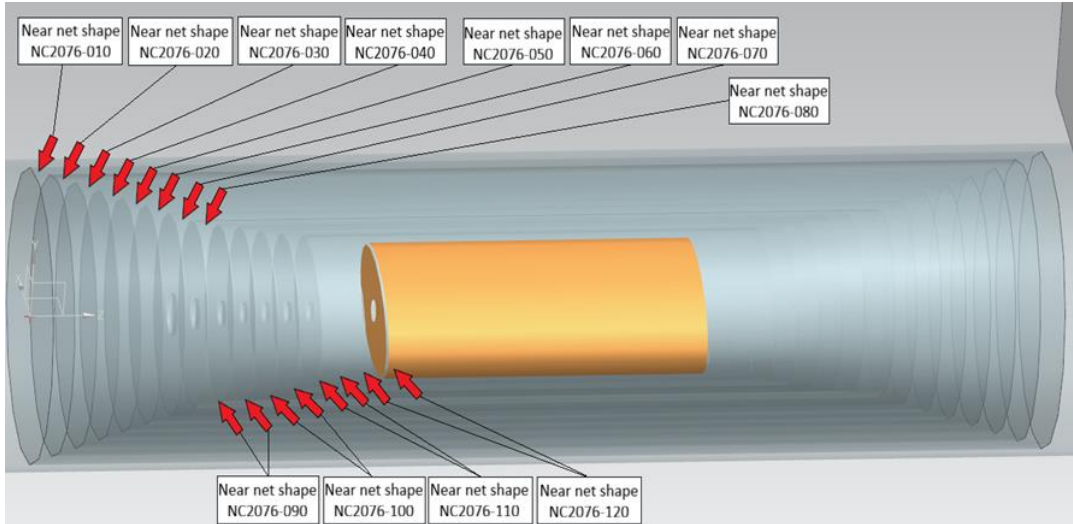
Figure 3.23. Siemens NX circular continuous and elliptical near-continuous near net shape.

The continuous and near continuous too paths that are shown in Figure 3.23 and Figure 3.24 represent the two different types of circular and elliptical spiral toolpaths that were utilised to machine bar blades. As can be seen in Figure 3.24 and Figure 3.25, both of the continuous and near-continuous toolpaths roll into cut. The rolling into cut means the tools experience a gradual increase in radial immersion, which results in full tool immersion initially and then reduces down to the specified radial engagement distance as stipulated in Table 3.3. Rolling into cut was adopted to reduce the shock on the inserts upon engaging with the workpiece material.
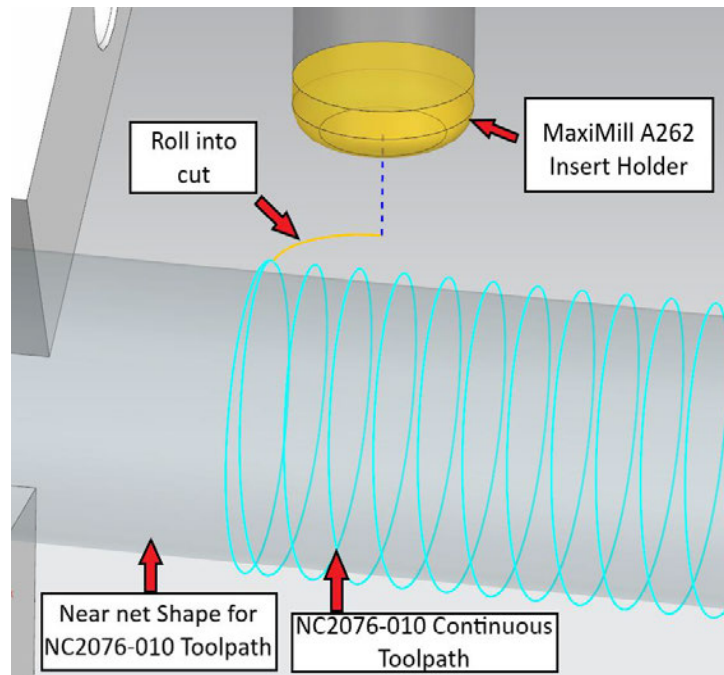
Figure 3.24. Continuous toolpath development.
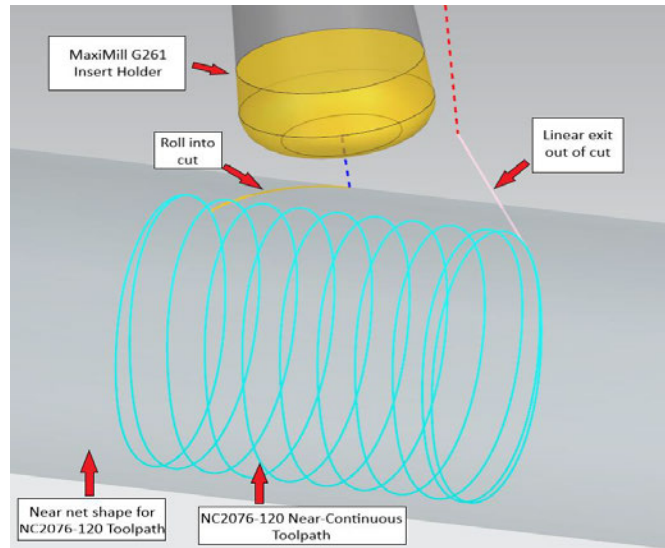
Figure 3.25. Near-Continuous toolpath development.

The circular spiral toolpaths allowed for minimal fluctuations in cutting temperature in the chip/tool interface, which meant cutting forces were kept as constant as possible. The elliptical spiral toolpaths allowed for near minimal fluctuations in cutting temperature in the chip/tool interface. However, in order to form the aerofoil geometry, the depth of cut increased from 0 mm to 1.0 mm and then ramped down from 1.0 mm to 0 mm in the F_y-axis on DMG Mori NTX2500 machine.

To avoid collisions between the two cutting tools and the tailstock in the machine. A generic motion positioning program was inserted before and after each NC program. This was so that the two cutting tools could enter into and out of machining area safely and under complete control by the machine operator. Figure 3.26(a-b) represents the generic motion positioning that was used throughout the machining trial.
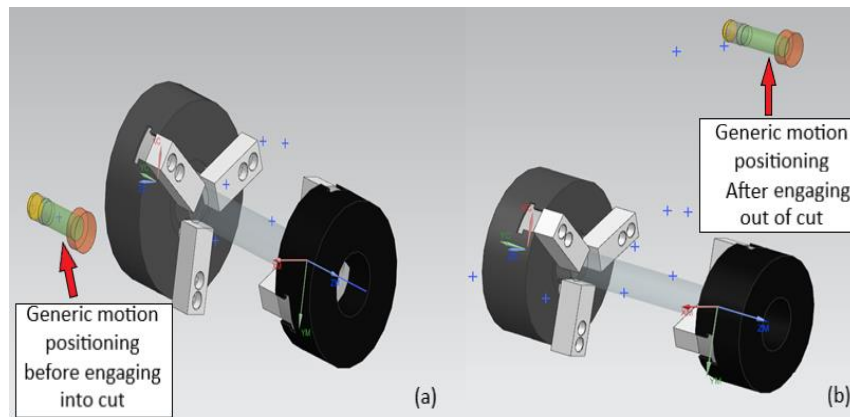
Figure 3.26. (a) Generic motion into cut, (b) Generic motion out of cut.

3.11.4 Experiment Four - Tool Materials and Coatings

The original composition of Coating C as seen in Table 3.11, is a 6.5 μm thick α-amorphous Al_2O_3 coating, which has been applied via chemical vapor deposition (CVD) techniques. However, due to a coating error a thin 0.5 μm thick layer of TiN was deposited onto the surface of the α-amorphous Al_2O_3 coating. A post processing operation was utilised to remove the 0.5 μm thick TiN coating on the rake face of the round button (RNGN) SiAlON milling inserts. The thin layer of TiN could not be removed on the flank face. The coating was applied via chemical vapour deposition techniques at Ceratizit's Ruette facility in Austria. The oxide coatings were deposited at a temperature of 1000°C, the deposition rate was 1-2 μm per hour.

Table 3.11. Round insert grades to be tested in PhD experiment Four.

Geometry	Grade	Coating Grade	Manufacturer
Round (RNGN)	CTIS710 SiAlON	Uncoated	Ceratizit
Round (RPGN)	CTIS710 SiAlON	Uncoated	Ceratizit
Round (RNGN)	CTIS710 SiAlON +Type C coating	CVD 6.5 μm Al_2O_3 coating with α-Al_2O_3 (Corundum structure) – black colour	Ceratizit
Round (RPGN)	CTIS710 SiAlON +Type C coating	CVD 6.5 μm Al_2O_3 coating with α-Al_2O_3 (Corundum structure) – black colour	Ceratizit

3.11.5 Experiment Four Cutting Conditions (Tests M14-M15)- Interrupted Non-continuous Toolpath Machining Trial

The cutting conditions for experiment four-part A looked to essentially recreate where possible the conditions that were experienced in experiment two on the DMG Mori NVX5080 with Tests M1-M13, but on the XYZ800HD three axis machining centre. A cutting speed of 800 and 900 m/min, a feed rate of 0.10 mm/tooth, table feed rate of 3356 mm/min and a depth of cut (Ap) of 1.0 mm. For each test to be successful 169.64 cm^3 needed to be removed.

3.11.6 Experiment Four Cutting Conditions (Tests M16-M17) - Continuous/Near-continuous Machining Trial

This section will analyse the method which have been used to collate the results during the latest set of milling insert wear machining trials. The trials were conducted at the AMRC factory

of the future. For a test to be successful, the bar blade needs to be completely machined. To establish a relationship with the previously completed machine trials, the bar blade machining trial was split into two parts (Test M16A-B and Test M17A-B).

Tests M16A and M17A of the machining trial was used as a direct comparative to the previously completed non-continuous machining trial, which used uncoated and CVD coated RNGN SiAlON milling inserts. Tests M16A and M17A utilised staggered continuous spiral tool paths which reduced the bar diameter with a constant radial Ap of 1.5 mm at a cutting speed of 840m/min and a feed rate of 1807.68 mm/min (0.06 mm/tooth). Inserts were changed based on flank and rake face wear. (Stages 1-8)

In Tests M16B and M17B of the machining trial the uncoated and CVD coated RPGN inserts were used to machine a simple 2-D aerofoil geometry via elliptical 5-axis spiral tool paths. Tests M16B and M17B utilised staggered near-continuous elliptical spiral tool paths which reduced the bar diameter with a maximum radial depth of cut (Ap) which ramped up from 0 to a maximum of 1.0 mm at a cutting speed of 880m/min and a feed rate of 2250.36 mm/min (0.07 mm/tooth). Insert were changed based on flank and rake face wear. (Stages 9-12)

The utilisation of both a main spindle and sub-spindle machine setup has provided high workpiece stability during the machining trial. The setup that is shown in Figure 3.27 has contributed favourably to the tool life that has been attained by both the uncoated and coated SiAlON inserts.
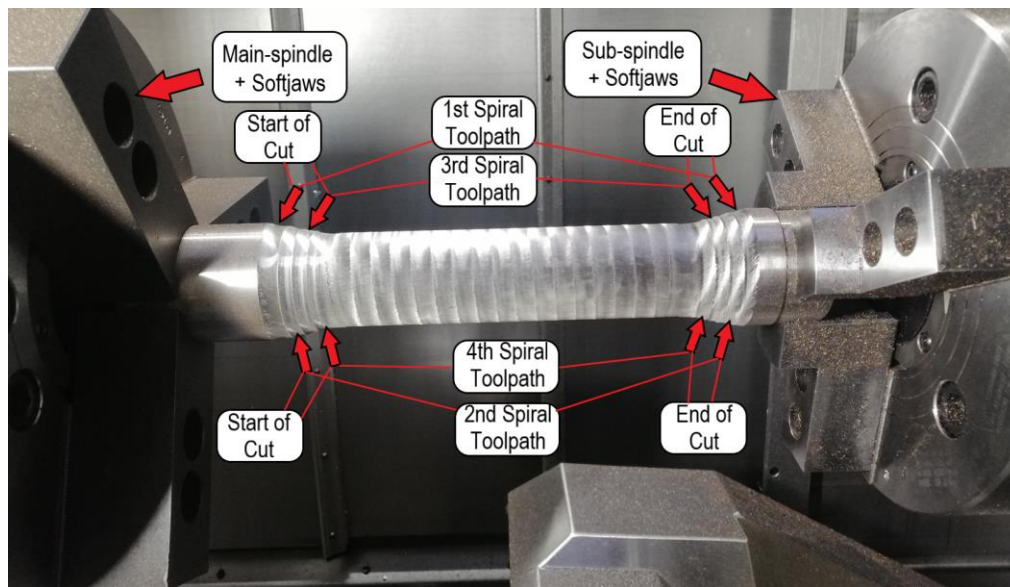
Figure 3.27. Partly machined Inconel 718 sample utilising spiral continuous toolpaths. (DMG Mori NTX2500 five-axis machining centre).

The spiral tool paths that have been adopted in the machining trial are seen in Figure 3.28. The selection of spiral toolpaths was determined principally for stability reasons.
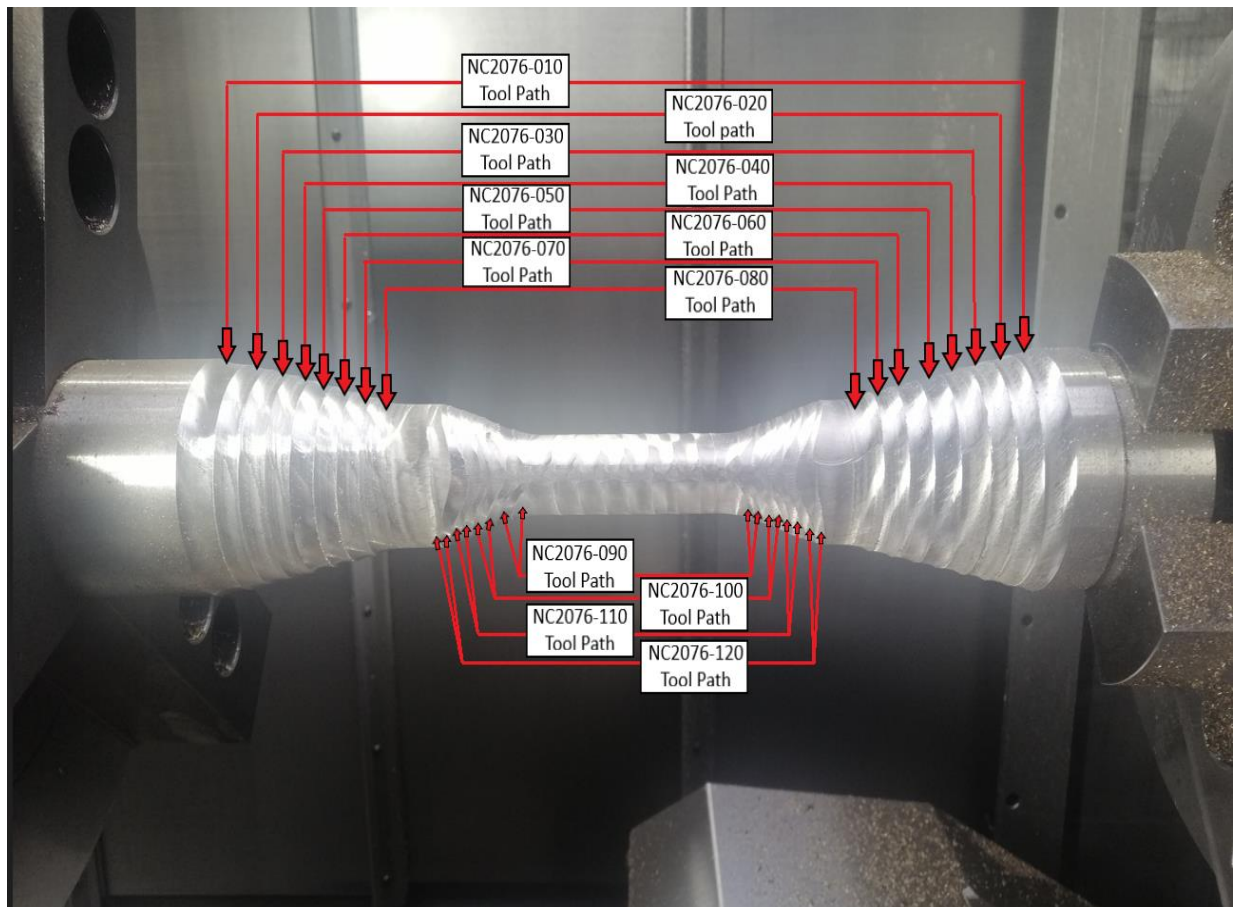
Figure 3.28. Spiral and elliptical spiral tool paths utilised for the bar blade machining trial.

The removal of the workpiece material with continuous spiral and near-continuous elliptical spiral tool paths, results in the workpiece material being removed uniformly. The adoption of continuous spiral to near-continuous elliptical spiral tool paths culminates in minimal fluctuation in cutting temperature in the chip/tool interface.

The NC programme which reduced the bar diameter utilised a radial engagement which varied from 35.10-10.0 mm with a constant radial depth of cut (Ap) of 1.5 mm. The radial immersion is at its highest upon engagement into cut and lowest upon exiting out of cut in the F_y-axis direction. The NC programme that formed the 2-d elliptical aerofoil utilised a radial engagement which varied from 27.5-7.0 mm with a depth of cut (Ap) of which varies from 0-1.0 mm. For the 2-d elliptical aerofoil, the radial immersion is at its highest upon engaging into cut and lowest upon exiting out of cut in the F_y-axis direction. The test number, machining parameters and test sequence which have been used in the machining trials are stipulated in Table 3.12.

Table 3.12. Test parameters machining trial. cutting conditions, used in this Test No 16A-B and 17A-B.

All the RNGN inserts had an axial rake angle - 7.1°, Radial rake angle -12.3° and 0.1 mm edge chamfer.

All the RPGN inserts had an axial rake angle 3°, Radial rake angle -1.8° and 0.1 mm edge chamfer.

Test No	Tool Material	Insert Edge Number	Completed NC Programmes	Stage No	Cutting Speed (m/min)	Table Feed rate fz (mm/tooth)	Depth of Cut (Ap) mm	Radial Engagement (ae) (mm)
M16-part A	CTIS710 RNGN SiAlON	1.1	NC2076-010 - NC2076-040	1-4	840	0.06	1.5	35.5-10.0
M16-part A	CTIS710 RNGN SiAlON	2.1	NC2076-050 - NC2076-080	5-8	840	0.06	1.5	35.5-10.0
M16-part B	CTIS710 RPGN SiAlON	1.1	NC2076-090 - NC2076-110	9-11	880	0.07	0-1	26.14-7.0
M16-part B	CTIS710 RPGN SiAlON	2.1	NC2076 -120	12	880	0.07	0-1	26.14-7.0
M17-part A	CTIS710 RNGN SiAlON + Type C Coating	1.1	NC2076-010 NC2076-030	1-3	840	0.06	1.5	35.5-10.0
M17-part A	CTIS710 RNGN SiAlON + Type C Coating	2.1	NC2076-040 NC2076-060	4-6	840	0.06	1.5	35.5-10.0
M17-part A	CTIS710 RNGN SiAlON + Type C Coating	3.1	NC2076-070 NC2076-080	7-8	840	0.06	1.5	35.5-10.0
M17-part B	CTIS710 RNGN SiAlON + Type C Coating	1.1	NC2076-090 NC2076-100	9-10	880	0.07	0-1	26.14-7.0
M17-part B	CTIS710 RNGN SiAlON + Type C Coating	2.1	NC2076-110 NC2076-120	11-12	880	0.07	0-1	26.14-7.0

3.11.7 Experiment Four (Tests M16-M17) - Workpiece material

Two round bar pieces of precipitation hardened Inconel 718 were supplied by Maher Ltd to (AMS5663) specification. These two round bars are from a different batch of material that was used in Experiment Two. Each machining trial utilised a single piece of precipitation hardened Inconel 718 (AMS5663) round bar stock 60.0 mm diameter x 350.0 mm long were used for the trial. The mechanical properties of the Inconel 718 workpieces were stipulated in Table 3.13 and the information is collated from the Certificate of Conformity cert no: 50063/1 and ASTM E18.

Table 3.13. Mechanical Properties of Inconel 718 (AMS5663).

Hardness (HRC)	Yield stress (MPa)	Ultimate Tensile Strength (MPa)	Strain (%)	Elastic modulus (GPa)	Thermal conductivity (W/m K)	Density (kg/m^3)
43	1112	1390	23.3	206	11.6	8470

3.11.8 Experiment Four - Tool Life Criteria (Tests M14-M15)

The tool life criteria for this machining trial are the same as Experiment Two, which is stated in Section 3.9.7. The sample workpiece material that was used in Section 3.9.6 was also used for Test no M14-M15.

3.11.9 Experiment Four - Tool Life Criteria (Tests M16-M17)

The default conditions for tool failure are when tool flank wear scar is measured at 2.0 mm or less. For this particular machining trial, the tool life was also influenced by on-machine sensors that measured vibration. The DMG Mori NTX2500 main spindle vibration sensor had to be adhered to, as once a vibration threshold is surpassed the main spindle would stop immediately. The level of vibration was heavily influenced by the level of wear the inserts had sustained. Regular monitoring of the insert wear was therefore required.

3.12 Summary

This chapter has detailed the experimental techniques that have been utilized to characterize the tribological mechanisms, tool wear and material interaction that are exhibited by uncoated and CVD coated SiAlON milling inserts.

This chapter covered the key aspects associated with tool wear and tool life characterization and looks at the coating selection process that has been used to select coating selection. This chapter has also considered the procedure of metallographic preparation and the imaging and analysis techniques which provide a key understanding, of how CVD coated SiAlON milling inserts compare to uncoated SiAlON milling inserts.

The simple machining trial that was discussed at the start of this chapter, was employed to develop a thorough understanding of the type of wear mechanisms that ceramic inserts undergo when machining Inconel 718. The first, second, third and fourth experiments which are discussed in this chapter all used the same grade of silicon aluminium oxynitride SiAlON CTIS710 grade. The first experiment was highly influential in the selection of this grade of SiAlON for the subsequent second, third and fourth experiment, principally because of the high wear resistance that was demonstrated in the first experiment.

This chapter however also discusses each of the experiments, the chosen device (machine tool, tribological equipment), parameters, and why these experiments have been adopted to achieve different objectives that were set out in Chapter one. Additionally, all the experiments were planned to deliver specific results and conclusion which could be used to compare the performance between coated and uncoated SiAlON inserts.

Chapter 4 Initial Machining Trials and Chip Morphology Analysis

Author's note: The work in this chapter in Sections 4.1, 4.2, 4.4.1 and 4.5 has been published in Wear Osmond et al. [46].

4.1 Introduction

This chapter will include the published preliminary research, which focused on comparing the wear results of different ceramic turning when turning solution annealed Inconel 718 at different cutting speeds.

4.2 Preliminary Research - Chip formation and wear mechanisms of SiAlON and whisker-reinforced ceramics when turning Inconel 718

The research which I undertook in this chapter was focused on turning solution-annealed Inconel 718 with different ceramic grades of button insert. This preliminary work helped me develop some basic experience of machining Inconel 718 with ceramic inserts, something which influenced my decision to focus on developing ceramic milling inserts in future experimental trials. The research focused on the chip formation and wear mechanisms of silicon aluminium oxynitride SiAlON ceramic and silicon carbide whiskers reinforced alumina (WRA) (Al_2O_3 + SiC_w) round (RNGN) inserts, when turning solution-annealed Inconel 718 (27<HRC<30) with a 10% concentration cutting fluid.

As discussed in Section 3.8, four sets of cutting trials were conducted at a cutting speed of 250 m/min and another four at 300 m/min, the machining conditions are captured in Table 4.2. The turning inserts that were used in Experiment One are captured in Table 4.1. The results showed that using SiAlON turning inserts at a cutting speed of 300 m/min delivered the best results in terms of tool flank wear, total tool life, and work-piece surface finish.

Table 4.1. Turning insert identification.

Test Cut number	Insert Identification Letter	Tool Material Classification	Tool Material	Edge Chamfer (mm)
T1.1, T1.2, T5.1, T5.2	A	SiAlON Grade 1	SiAlON Grade 1481	
T2.1, T2.2, T6.1, T6.2	B	SiAlON Grade 1 (chamfered)	SiAlON Grade 1481	0.10mm
T3.1, T3.2, T7.1, T7.2	C	SiAlON Grade 2	SiAlON Grade CTIS710	
T4.1, T4.2, T8.1, T8.2	D	Whisker Reinforced Alumina	Whisker Reinforced Alumina Grade CTKS710	

The morphology of the Inconel 718 chip, at cutting speeds above 250 m/min, presented an intense shear band localisation in the primary shear zone of the chip/tool interface, which led to chip segmentation.

Table 4.2. Cutting conditions for Experiment One.

Test Cut number	Tool material	Insert Identification Letter	Cutting Speed (m/min)	Feed Rate (mm/rev)	Depth of Cut (mm)	Material Removal Rate (mm³/s)
T1.1, T1.2	SiAlON Grade 1	A	250	0.20	2	160
T2.1, T2.2	SiAlON Grade 1 (chamfered)	B	250	0.20	2	160
T3.1, T3.2	SiAlON Grade 2	C	250	0.20	2	160
T4.1, T4.2	Whisker - Reinforced Alumina	D	250	0.20	2	160
T5.1, T5.2	SiAlON Grade 1	A	300	0.20	2	200
T6.1, T6.2	SiAlON Grade 1 (chamfered)	B	300	0.20	2	200
T7.1, T7.2	SiAlON Grade 2	C	300	0.20	2	200
T8.1, T8.2	Whisker – Reinforced Alumina	D	300	0.20	2	200

The results showed that using SiAlON turning inserts at a cutting speed of 300 m/min delivered the best results in terms of tool flank wear, total tool life, and work-piece surface finish. The morphology of the Inconel 718 chip, at cutting speeds above 250 m/min, presented an intense shear band localisation in the primary shear zone of the chip/tool interface, which led to chip segmentation.

4.2.1 Tool wear (Test No T1.1-T4.2)
The first set of test cuts involved using Insert A (SiAlON grade 1, 250 m/min, 0.20 mm/rev, 2.0 mm depth of cut (Ap). Large vibrations were encountered over 50 % of the first cut due to the faster than expected degradation of the cutting edge.

Figure 4.1 shows the wear scar of Insert A after the first ceramic cut that was conducted on the Inconel 718 round bar. The tool was subsequently deemed to have failed because the wear scar that was generated in the first cut exceeded the default wear scar limit of 1.0 mm.
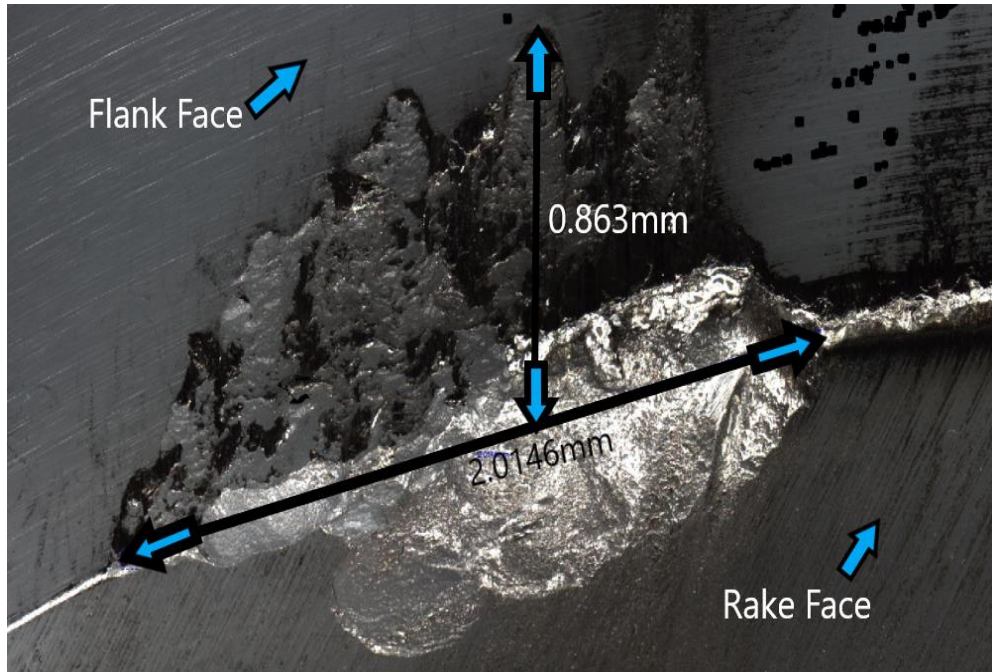
Figure 4.1. Image of the width and height of the wear scar on Insert A (SiAlON Grade 1). Image captured on Alicona infinite-focus SL microscope.

Figure 4.2 clearly shows the wear scar that was generated after the first cut. The images show the flank edge of the insert at the top part of image and rake face on the bottom part of the image. The large crater that is visible clearly shows signs of flank wear on the top part of the image and crater wear and notch wear.
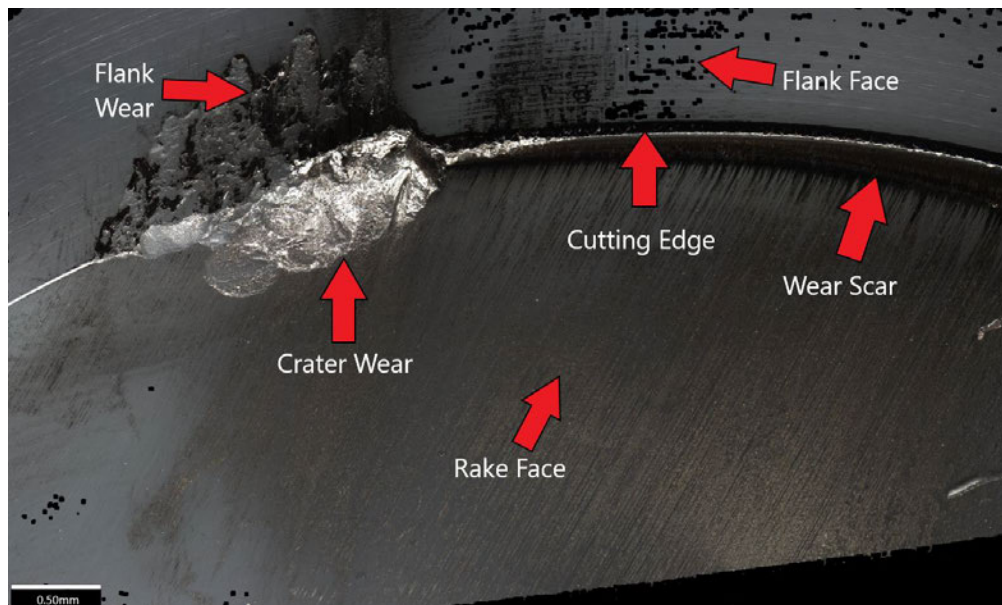
Figure 4.2. Wear scar on turning insert B (SiAlON Grade 1) after Test Cut T1.1. Test was classed as a failure.

A second test utilised Insert B (SiAlON Grade 1), but with a 0.1 mm chamfer on at the same cutting conditions. Vibrations were encountered again, over 25 % of the second cut, but at a reduced level, apparently due to the chamfer. Figure 4.3 has managed to capture the entire wear scar. The potential reason for large amounts of the wear is likely due to the high fluctuation of tensile and compressive stresses that were being generated in the shear zone between the workpiece and the insert [46].
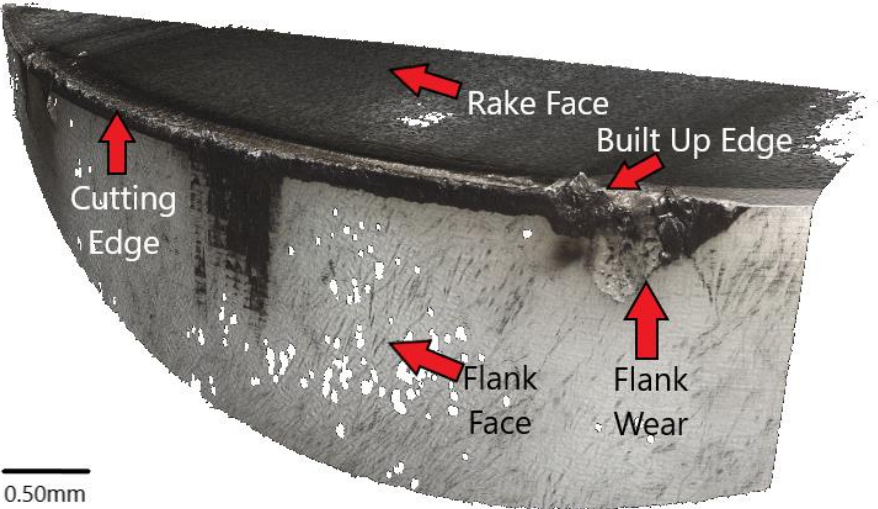
Figure 4.3. Wear scar on turning Insert B (SiAlON Grade 1) after Test Cut T2.2.

The third set of test cuts of the machining trial used Insert C (SiAlON Grade 2). Figure 4.4 shows a wear scar on turning Insert C (SiAlON Grade 2) after Test Cut T3.2.
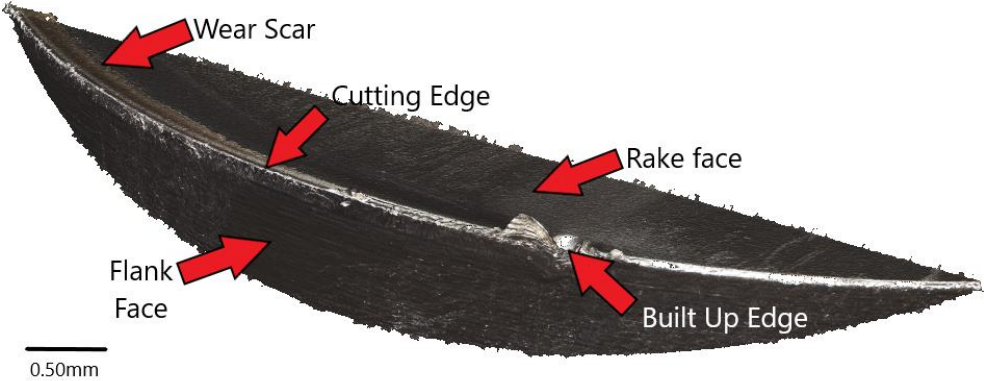
Figure 4.4. Wear scar on turning Insert C (SiAlON Grade 2) after Test Cut T3.2.

Tool 5 provided noticeable results when compared to first two sets of test cuts with the insert demonstrating excellent resistance to abrasion. Insert C showed no real signs of flank wear, crater wear or notch wear. The cutting edge was in very good shape after the first test cut.

There were slight signs of abrasion on the rake face but that was to be expected considering the cutting conditions. Insert C is a standard grade for machining nickel-based alloys, and it performed as expected.

The same flank wear and notch wear patterns that can be seen with Insert A and Insert B also affect Insert C, but visually show less abrasive wear of the rake and flank face of the insert. The reason for the improved resistance to abrasion, flank wear and notching are that that Insert C seems to demonstrate higher hot hardness and a tougher microstructure. The tougher microstructure will come from the inclusion of more β-SiAlON grains, and the abrasion resistance and hot hardness will come from the α-SiAlON. The β-SiAlON is a substitutional solid solution of aluminium and oxygen in beta Si_3N_4, and α-SiAlONs are a solid solution of yttrium, oxygen and nitrogen in alpha Yx (Si Al)12 (O N)16. From the visual information captured in Figure 4.4, the α- and β-SiAlONs in Insert C look to have been hot-pressed to form an insert with superior hot hardness, toughness and abrasion resistance when compared to Insert A and Insert B.

The fourth test of the machining trial used Insert D (whisker-reinforced alumina). The test consisted of two cuts at equal length and depth. In Figure 4.5, a wear scar on turning Insert D after Test Cut T4.2 is shown. During the fourth test, very few vibrations were encountered over of the course of the fourth cut. The reason for the little vibration is likely due to the high strength and abrasion resistance of the cutting edge. The mechanical properties of whisker-reinforced alumina inserts are shown in Table 2.3, indicating that whisker-reinforced alumina grades of insert have a higher modulus and fracture toughness when compared to Insert A and B, which aids the inserts' ability to resist the intense cutting conditions.
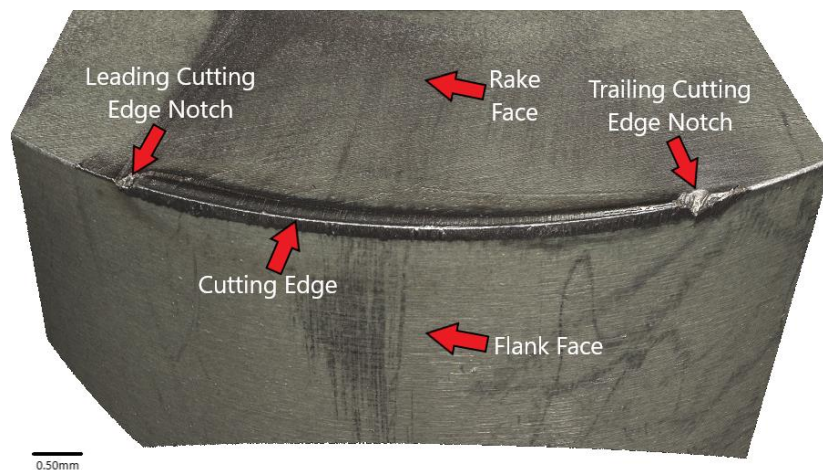
Figure 4.5. Wear scar on turning Insert D (whisker-reinforced alumina) after Test Cut T4.2.

The fourth set of test cuts provided noticeable results when compared to first two sets of test cuts. Insert D again showed no real signs of flank wear, crater wear or notch wear. The cutting edge was exhibited very little wear after Test Cut T4.1 There were signs of abrasion on the rake face, which are caused by high temperatures being generated in the tool/chip interface. The high temperatures are due to the low thermal conductivity of Inconel 718 and the abrasion of the cutting tool against hard Ni_3Nb particulates distributed within the Inconel 718 material. The lack of wear is visible in Figure 4.5 and the insert delivered as expected.

Insert D suffered from similar flank, rake and notch wear patterns that can be seen with Inserts A, B and C but were significantly less than Insert A and B. The reasons for the high abrasion resistance are due to the higher overall hardness of alumina than that of silicon nitride (Si_3N_4) based ceramics such as SiAlON. The rake face wear of Insert D is slightly worse than that of Insert C. From the information in Figure 4.6, it appears that whisker-reinforced alumina inserts have lower hot hardness than that of that SiAlON.
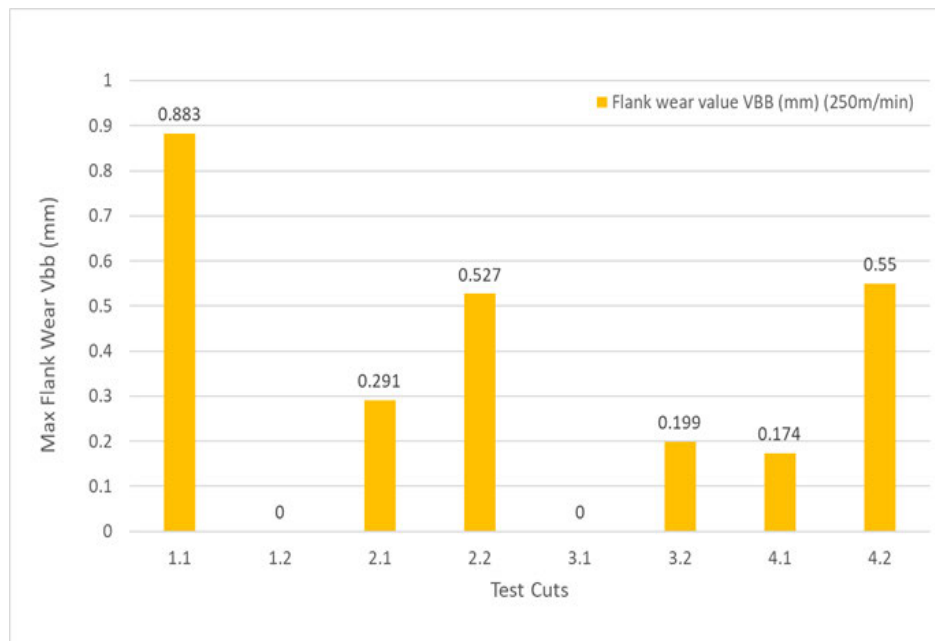
Figure 4.6. Measured flank wear (Vbb) experienced for each test cut at a cutting speed of 250 m/min.

However, the silicon carbide whiskers distributed throughout the alumina matrix provide increased fracture resistance and abrasion resistance. The abrasion resistance of Insert C was better than Insert A and B and highlights that Insert C has marginally better wear resistance than Insert D. Each test cut was repeated twice so that intended amount of material was removed. Figure 4.6 is raw data directly gathered from the machining trial, so no error bars have been included in the graph.

4.2.2 Tool Wear (Test No T5.1-T8.2)

During the fifth set of test cuts (SiAlON Insert A, 300 m/min, 0.20 mm/rev, 2.0 mm Ap, there were no signs of any large vibrations as encountered in the first test.

Figure 4.7. show the wear scar on turning Insert A after Test Cut T5.2. The reason for the reduction in vibration is likely due to the higher surface speed and the lack of degradation is clearly visible. The increase in surface speeds has generated higher cutting temperatures in the primary and secondary deformation zones, which in turn reduces cutting forces required to cut the material. The higher surface speed also reduces the ploughing effect that caused the earlier vibration with Insert A and Insert B in Test Cuts T1.1 and T2.1.
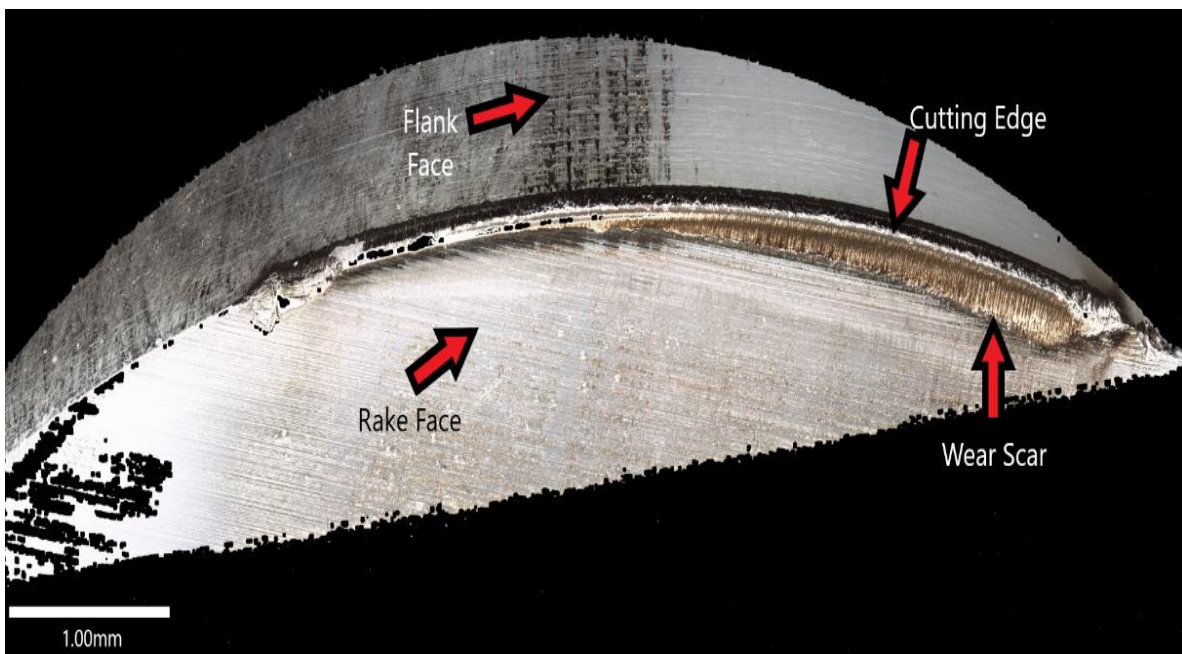
Figure 4.7. Wear scar on turning Insert A (SiAlON Grade 1) after Test Cut T5.2.

Figure 4.7. highlights the improvement in wear resistance. The improvements in wear resistance have come from an increase in surface speed from 250 m/min to 300 m/min, which has definitely had a positive effect and helped reduced the amount of wear that is generated whilst in cut. The higher surface speed has managed to stabilise the cutting process and helped to reduce the vibration that was experienced with Insert A in Test Cut T1.1. The increase in surface speed will have increased the cutting temperature between the Inconel 718 workpiece and the insert, hence this reduces the yield point of the Inconel 718 and the subsequent cutting forces that the Insert A experiences. The rake face wear that is visible in Figure 4.7. indicates better abrasion resistance, which is down to localised heating and softening of the Inconel 718, in turn reducing the amount of wear that the cutting insert experienced.

The sixth set of test cuts used Insert B (SiAlON Grade 1). Again, the test consisted of two cuts at equal length and depth. Figure 4.8 shows a wear scar on turning Insert B after completing Test Cut T6.2. The 0.10 mm chamfer on Insert B together with the increase in surface speed, delivered improved wear resistance and reduced notch and crater wear. The rake face wear that is visible in Figure 4.8 indicates better abrasion resistance.
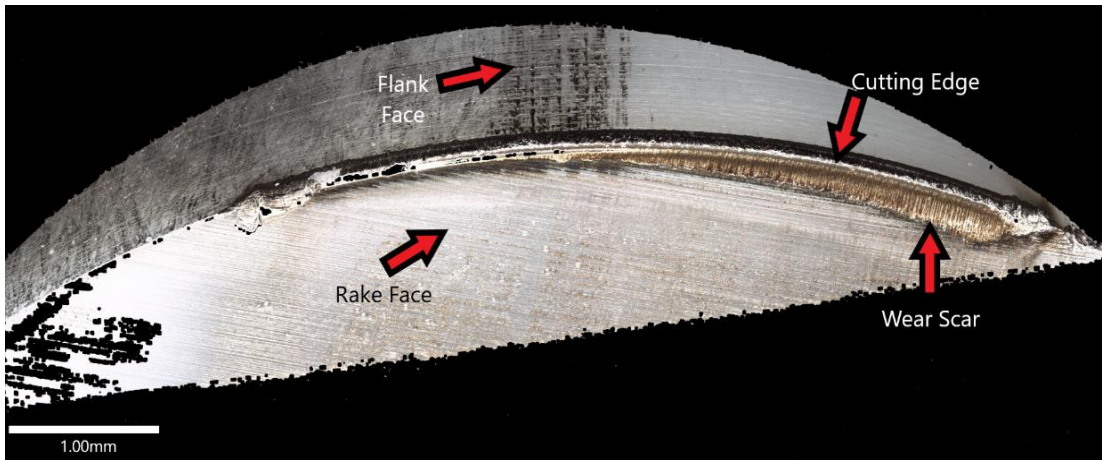
Figure 4.8. Wear scar on turning Insert B (SiAlON Grade 1) after Test Cut T6.2.

The seventh set of test cuts used Insert C (SiAlON Grade 2), consisting of two cuts at equal length and depth. In Figure 4.9, a wear scar on turning Insert C (SiAlON Grade 2) after Test Cut T7.2 is shown.
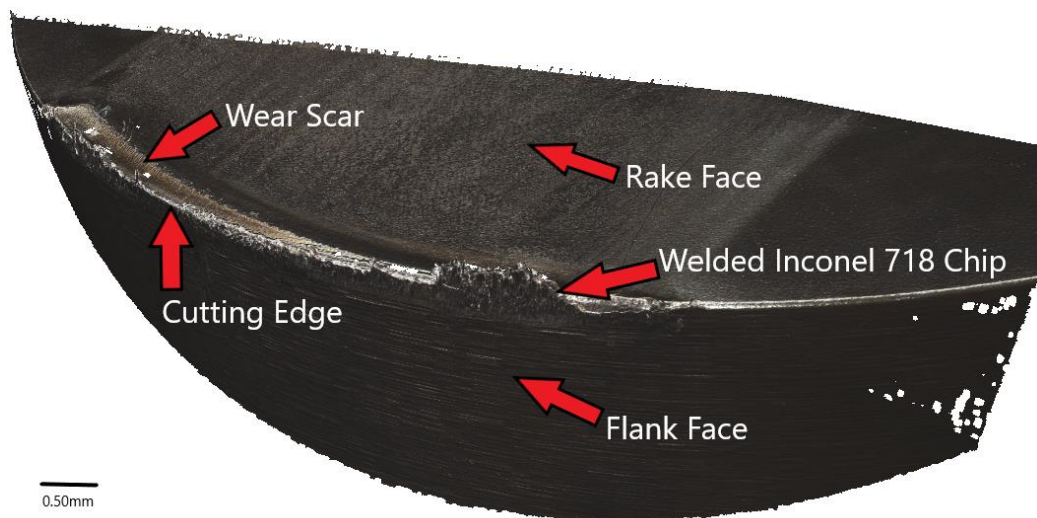
Figure 4.9. Wear scar on turning Insert C (SiAlON Grade 2) after Test Cut T7.2.

The seventh set of test cuts once again provided noticeable improvements in insert wear results when compared to six other sets of test cuts that had taken place beforehand. Insert C showed

no real signs of flank wear, crater wear or notch wear. There were slight signs of the abrasion on the rake face but that was to be expected and the lack of wear is visible in Figure 4.9. The same wear features that can be seen in Test Cut T5.1 and Test Cut T6.1, are also evident in Test Cut T7.1 but considerably less wear was visible. The increase in surface speed has certainly improved the wear resistance of the inserts throughout the second set of tests. It is hypothesised that the reason for the improved resistance to abrasion, flank wear and notching is that Tool 5 has a higher hot hardness, lower rates of thermal expansion and thermal conductivity and a tougher microstructure. It is clear that the tougher microstructure will come from the inclusion of more β-SiAlON grains, and the abrasion resistance and hot hardness will come from the α-SiAlON. The α-SiAlON and β- SiAlONs in Tool 5 look to have been hot-pressed to form an insert with superior hot hardness, toughness and abrasion resistance when compared to Insert A and Insert B.

The eighth set of test cuts utilised Insert D (whisker-reinforced alumina grade). The test consisted of two cuts at equal length and depth. Figure 4.10 shows a wear scar on turning Insert D (whisker-reinforced alumina grade) after Test Cut T8.2. During the eighth set of test cuts, very few vibrations were encountered.
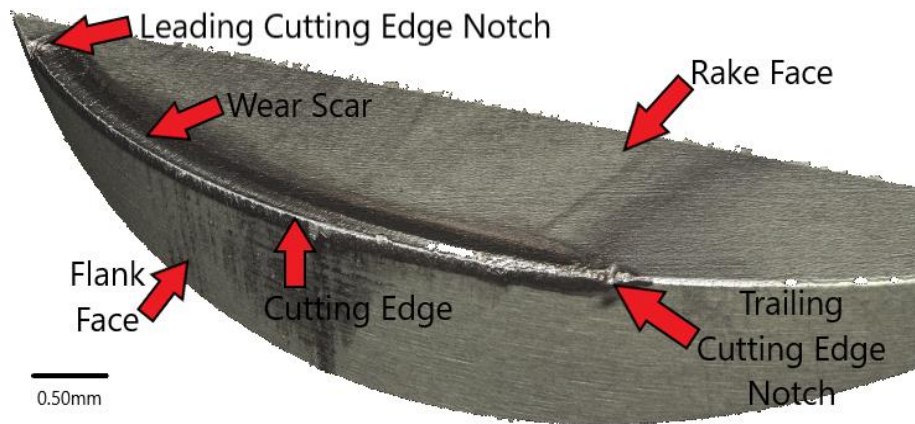
Figure 4.10. Wear scar on turning Insert D (whisker-reinforced alumina grade) after Test Cut T8.2.

The eighth set of test cuts provided noticeable results when compared to Test Cuts T5.1-T5.2 and T6.1-T6.2. Insert D showed no real signs of flank wear, crater wear or notch wear. The cutting edge was in very good shape after Test Cut T8.1. There were slight signs of the abrasion on the rake face, but that was to be expected considering the cutting conditions. The lack of wear is visible in Figure 4.10, likely due to the mechanical properties of whisker-reinforced alumina microstructure. The results indicate that Tool 6 has a higher modulus and fracture toughness when compared to Insert C (SiAlON grade 1, (Insert A and Insert B). Insert D

is also standard whisker-reinforced alumina grade for hard turning nickel-based alloys and has also delivered results as expected. Insert C (SiAlON Grade 2) has attained the least amount of flank wear and this is shown in Figure 4.9. Insert C and Insert D generated similar small wear scars when subjected to the same cutting conditions as the other test cuts. All of the cutting tools experienced considerably less vibration when the cutting speed was increased to 300 m/min. Figure 4.11. is raw data directly gathered from the machining trial, so no error bars have been included in the graph.
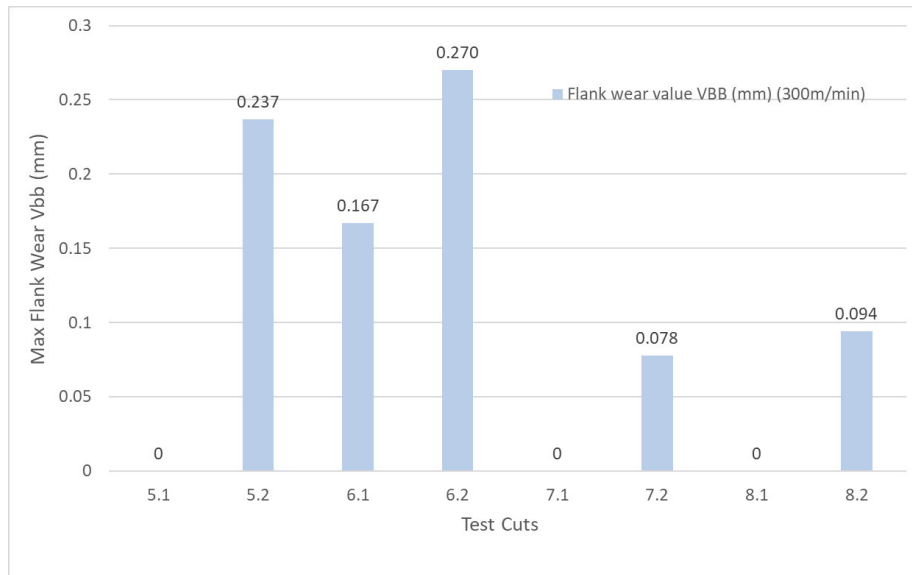
Figure 4.11. Measured flank wear (Vbb) experienced for each test cut at a cutting speed of 300m/min.

Test cuts T3.1-T3.2 (Insert C) and test cuts T7.1-T7.2 (Insert C) showed the lowest insert wear when compared to the other test cuts. Tool 5 ultimately outperformed Insert A, B and D in this regard. Each test cut was repeated twice so that correct amount of material was removed.

4.3 Chip analysis

The image analysis resulted in one image being captured for each of the four swarf chip samples. Digital images were taken at 200x resolution. The images captured on a Keyence VHX digital microscope highlighted the chip morphology and visually showed the level of deformation that the chip underwent as a result of the machining process. The images for each sample show in detail the brittle failure zones; the highly deformed microstructure of the chip visually highlighted the segmented chip morphology which was a result of fluctuation in specific shear forces during the machining process. The deformation characteristics of Inconel 718 chips followed slip lines and the Burgers vectors of dislocations that are apparent in a face centre

cubic crystal structure, these slip lines are shown in a Thompson tetrahedron which highlights the correlation between the slip lines [105].

4.3.1 Sample 1 – (Test No T4.2)

Sample 1 chips were produced with Insert D (whisker-reinforced alumina grade) at 250 m/min, 0.20 mm/rev, 2.0 mm Ap. Figure 4.12 shows an optical image demonstrating the common chip morphology characteristics of machining Inconel 718 at a cutting speed of 250 m/min. Figure 4.12 displays a serrated Inconel 718 swarf chip sample which has been produced during Test No T4.2. The maximum chip thickness (h_{c_max}) and minimum chip thickness (h_{c_min}) are displayed in Figure 4.12. The ratio of h_{c_max} and h_{c_max} provides the amount of segmentation (Ds), which is discussed earlier in Section 2.5. Segmentation analysis has been undertaken on swarf samples for T4.2, T.3.1, T.8.1 and T7.2. The variation in chip thickness and the amount of segmentation is captured in Figure 4.16 and Figure 4.17. During the machining process, the Inconel material deformed along localised shear planes and formed segments of different heights. The serrated chip morphology associated with Inconel 718 is highly influenced by cutting speed, as high cutting speed induce high levels of temperature in the chip/tool interface. The high temperatures in the chip/tool interface results in high level of thermoplastic deformation [106].
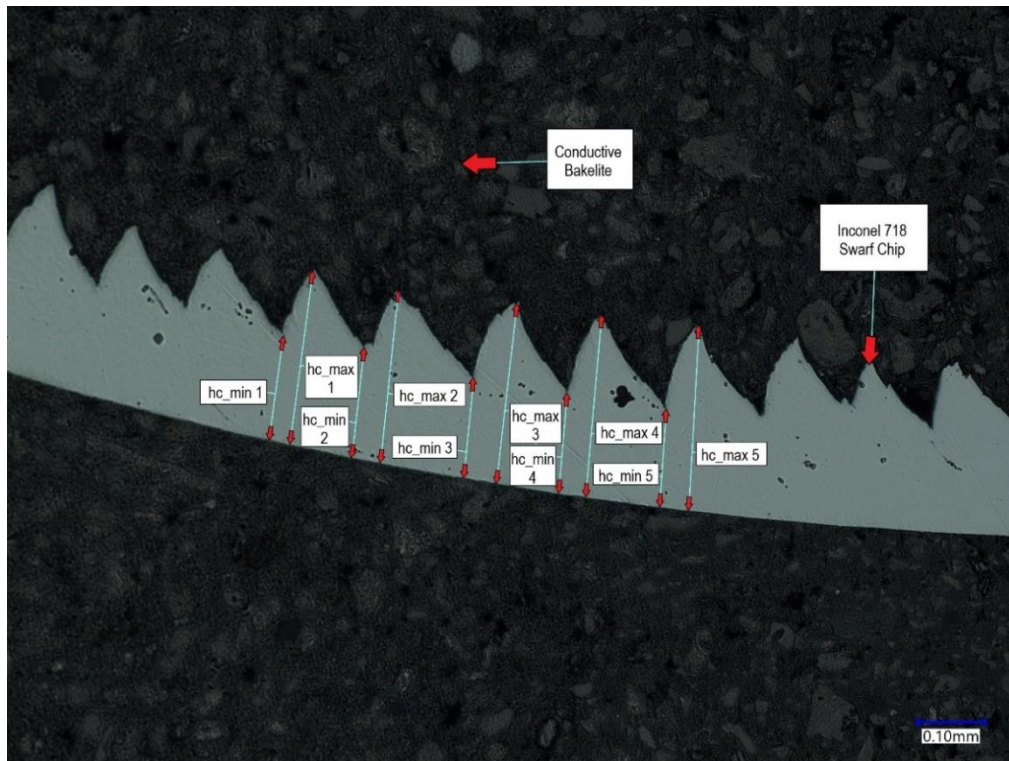
Figure 4.12. Test Cut T4.2 Image magnified 200x.

The face centre cubic structure and high strength of Inconel 718 encourage plastic deformation to take place along the (111) planes and in the direction of the (112) plane and this takes place when the material is subjected to a stress state, which is below the shear stress state that causes slip systems. If the stress state inverts, then it will follow the (110) plane direction instead of the (111) plane direction.

4.3.2 Sample 2 - (Test No T3.1)

Sample 2 chips were produced with an Insert C (SiAlON grade 2) at 250 m/min, 0.20 mm/rev, 2.0 mm Ap. Figure 4.13 shows a digital image, which visually display the common chip morphology characteristics of machining Inconel 718 at a cutting speed of 250 m/min. Figure 4.13 shows a serrated chip morphology which is visually similar to the chip morphology that is seen in Figure 4.12. The degree of variation in h_{c_max} and h_{c_min} for the five segments that is seen in Figure 4.13   is also seen in Figure 4.12. Although not visible in Figure 4.13, one of the reasons for the formation of this chip morphology is due to adiabatic shear as a result of instability in the chip/tool interface [107].
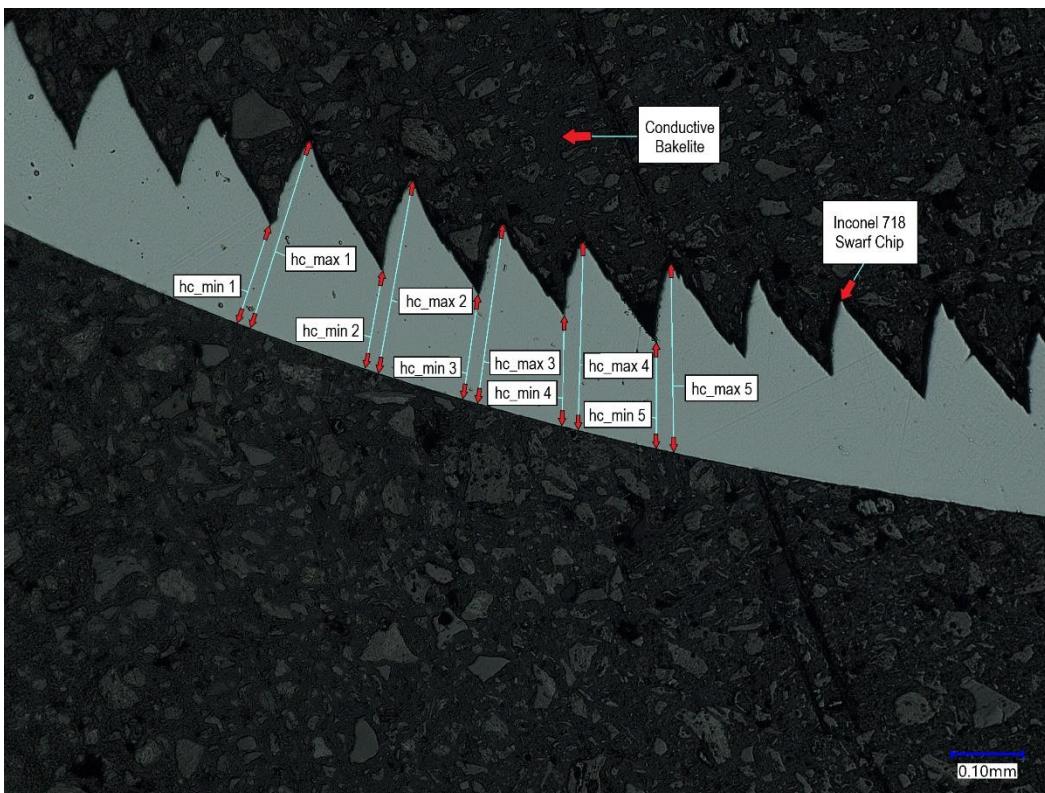
Figure 4.13. Test Cut T3.1 image magnified 200x.

The Inconel 718 chips are characterised to have relatively low deformation in the main section of the segments and evenly positioned localised intense, shear bands between each of the

segments. The chip morphology as in Figure 4.12 and Figure 4.13 is formed as a result of period thermoplastic shear instability in the shear plane, which is suggested in adiabatic shear theory [107].

4.3.3 Sample 3 – (Test No T8.1)

Sample 3 chips were produced with an Insert D (whisker-reinforced alumina grade) at 300 m/min, 0.20 mm/rev, and 2.0 mm Ap. Figure 4.14 show a digital image which demonstrate the common chip morphology characteristics of machining Inconel 718 at a cutting speed of 300 m/min. The increase in cutting speed from 250 m/min to 300 m/min intensified the localisation of the critical shear stress into localised bands which increases the segmentation rate. The increase in segmentation is seen more clearly in Figure 4.17, where the segmentation rate increases when the cutting speed is increased from 250 m/min to 300 m/min.
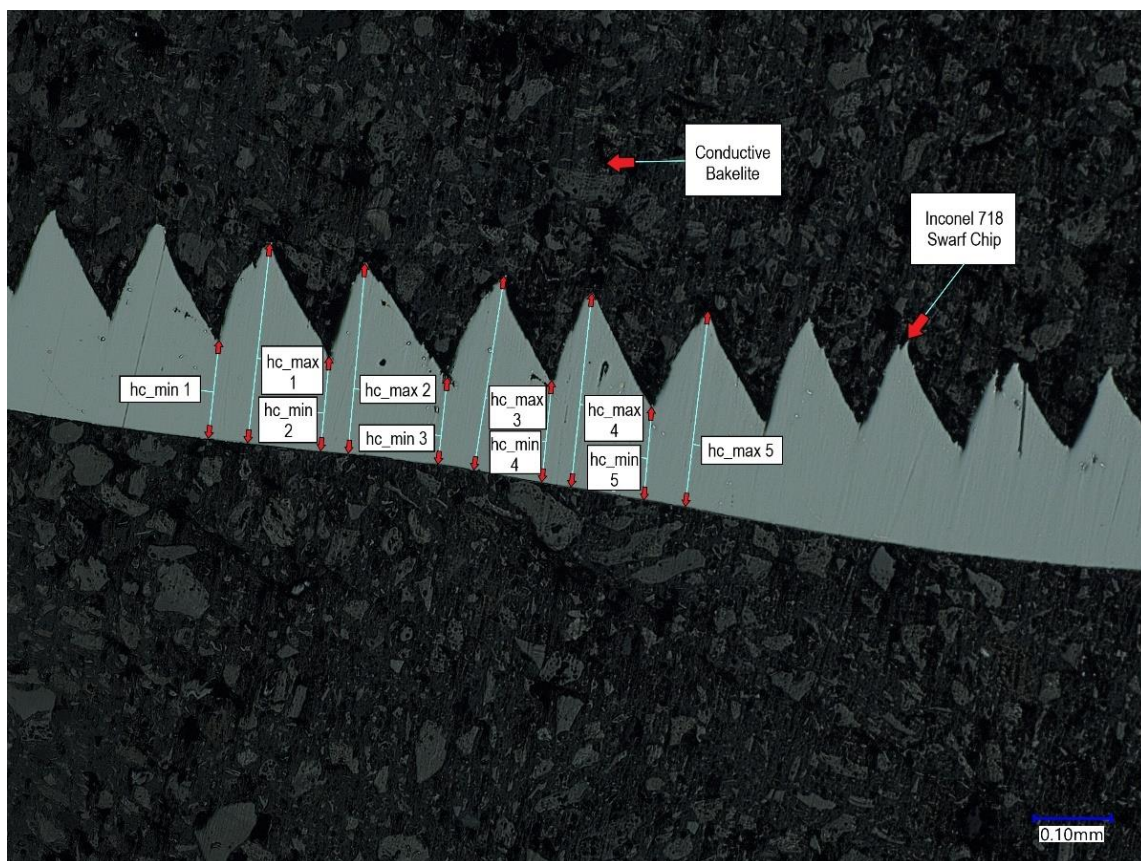
Figure 4.14. Test Cut T8.1 image magnified 200x.

The cutting temperatures of the primary shear zone also rose with an increase in the cutting speed. Similar results were gathered by Hao et al. [26]. In their study of characterising shear band localisation in Inconel 718 that had been machined at high cutting speeds.

Even though Test Cut T8.1 has been conducted at 300 m/min, the chip morphology is very different to the chip morphology that has been produced in Test Cut T7.2 which is displayed in Figure 4.15.

4.3.4 Sample 4 - (Test No T7.2)

Sample 2 chips were produced with an Insert C (SiAlON Grade 2) at 300 m/min, 0.20 mm/rev, 2.0 mm Ap. Figure 4.15 shows a digital image displaying the common chip morphology characteristics of machining Inconel 718 at a cutting speed of 300 m/min. The serrated chip morphology that is displayed in Figure 4.15, exhibits a much higher segmentation rate (Ds) and a higher difference between the h_{c_max} and h_{c_min} as displayed in Figure 4.16 and Figure 4.17. The segmentation rate has been calculated using Equation 2.1 in Section 2.5.1 The increase in speed from 250 m/min to 300 m/min for Test Cut T7.2 exhibits more severe plastic deformation as result of higher cutting temperatures in the chip/tool interface. The consequence of higher chip/tool interfacial temperatures concludes in higher strain rates and grain refinement and formation of adiabatic shear bands (ASBs). The adiabatic shear bands in Figure 4.15, are represented by faint angular bands.
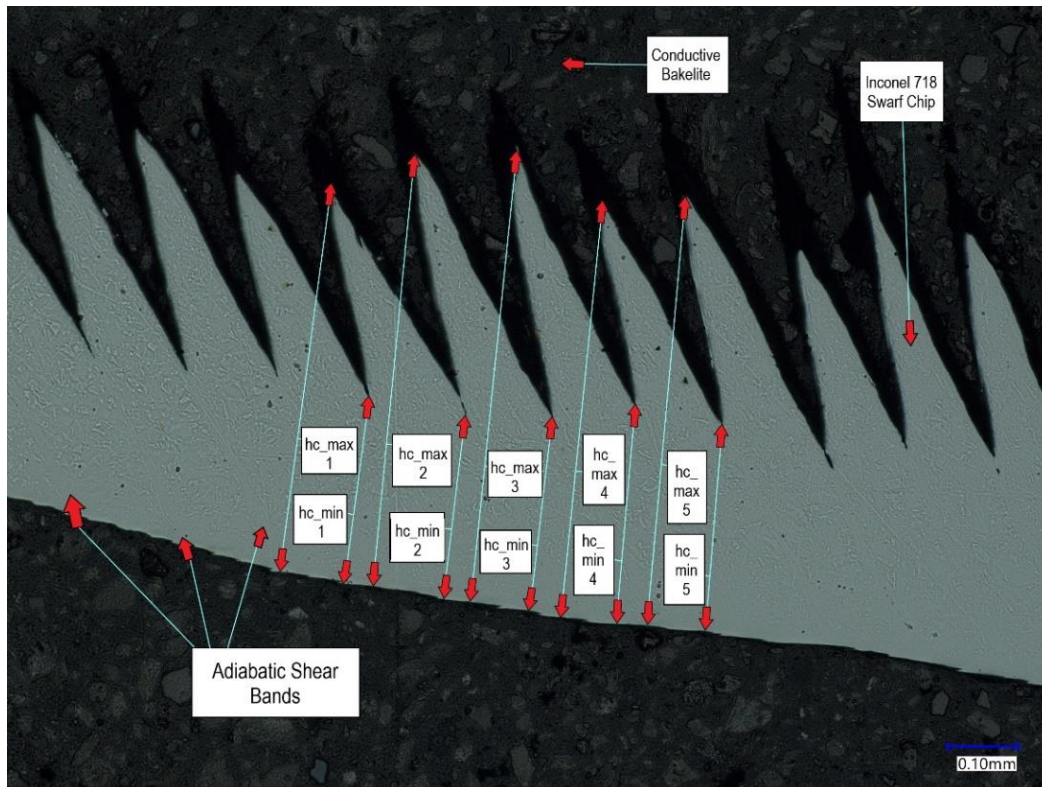
Figure 4.15. Test Cut T7.2 image magnified 200x.

The higher rates of grain refinement is due to higher rates of dislocation in the austenitic microstructure, which accumulates higher rates of segmentation [108]. In high speed turning operations that are evident in Test Cut 4.2, 3.1, 8.1 and 7.2, high strain rates are the principal reason for dislocations and grain deformation, which contributes to the formation of chip morphology [108].
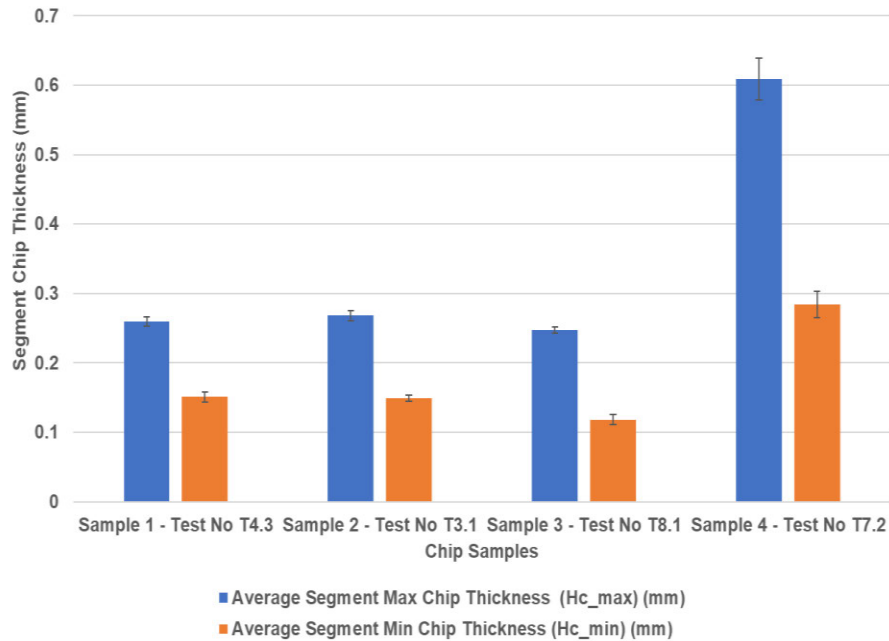
Figure 4.16. Variation in chip thickness for Sample 1-4
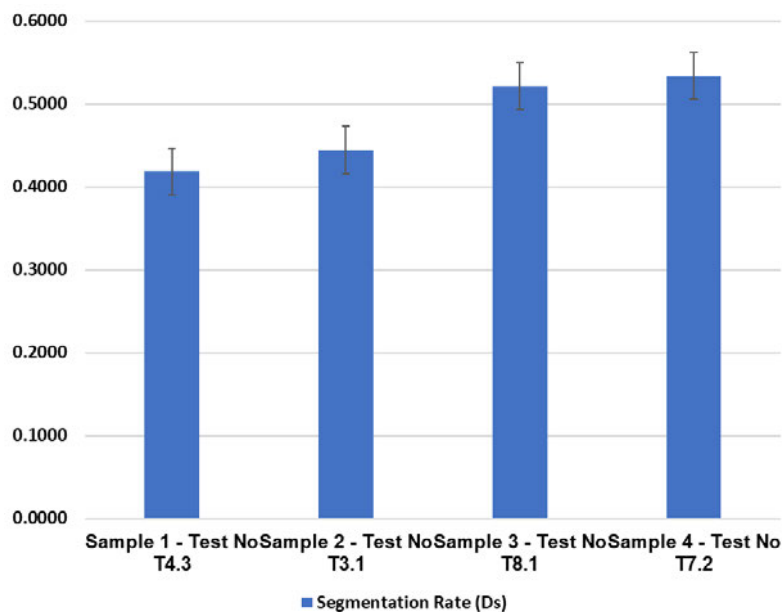
Figure 4.17. Segmentation rate for sample 1-4.

95

For Test Cut T7.2 looks to have sustained more instability in the chip/tool interface. The instability results in strain rates which higher degree of plastic deformation, which has resulted in a chip segmentation which is evident in Figure 4.15.

The type of serrated chip morphology which can be viewed in Figure 4.15 is also highly evident in the study which was conducted by Zhang et al. [109], that study was particularly focused on the evaluation of the fluctuation of cutting forces when turning Inconel 718.

4.4 Discussion
4.4.1 Insert Wear Analysis
During the machining trial, one of the prominent factors that was of interest was the amount of vibration which was encountered by each test cut. In Test Cut T1.1, large vibrations were experienced by the machine and the cutting tool. Figure 4.1 shows the result of these vibrations and Figure 4.2 shows how these large vibrations have had a catastrophic effect on the life of the tool. The reasons for the high vibrations could be due to the failure of the cutting tool edge for Test Cut T1.1 (Insert A). The roll in to cut will have generated an initial shock which caused a large crater to form on the cutting tool edge. This is interesting because the same roll in to cut approach was utilised throughout the machining trial. Notch wear is also visible, and the first cut generated a large amount of flank wear. The decision to fail the insert was taken due to it surpassing the default value of 1.0 mm for a wear scar.

Test Cut T2.1 also encountered some vibration over the first 25.0 mm of the cut and then stopped and cleaned up to provide a good surface finish. The flank wear in Test Cut T2.2 was still pretty high when compared to the other test cuts and the wear scars for Test Cut T2.2 were measured to be just under the default failure value. Test Cut T3.1 and T3.2 adopted the same 0.20 mm/rev feed rate and 2.0 mm Ap, but the surface finish was a lot better than the first two sets of test cuts when conducted at a 250 m/min surface speed. Test Cut T3.1 and Test Cut T3.2 delivered higher abrasion resistance results when compared to the first two test cuts.

Test Cut T4.1 also delivered notable abrasion resistance when subjected to the same cutting conditions. There was very little vibration encountered in Test Cut T4.1- T4.2 (Insert D), the reduction of vibration contributed to a subsequent reduction in overall wear that the insert sustained and this is visible in Figure 4.5 and Figure 4.10. Insert D showed high stability and high resistance to notching and resistance to flank wear. The novelty of this turning research focuses on attaining higher productivity that can be achieved when machining Inconel 718 at higher cutting speeds. The research study conducted by Altin et al. [110], concluded that high rates of insert wear were prominent above a cutting speed of 250 m/min. However, the study

conducted by Osmond et al. [46], concluded that rate of flank wear actually reduce when cutting speeds are increased above 250 m/min to 300 m/min.

In the second part of the turning trial the cutting speed was increased from 250 m/min to 300 m/min. The increase in cutting speed from 250 m/min to 300 m/min in the second part of the turning trial highlighted signified a marked improvement in the wear resistance capability of the inserts for Test Cuts T5.1-T5.2 (Tool 3), T6.1-T6.2 (Tool 4), T7.1-T7.2 (Insert C) and T8.1-T8.2 (Insert D). The improvement can be attributed to the higher cutting temperatures being created in the tool-chip interface as a result of the increase in cutting speed; this in turn reduced the perspective yield strength of the Inconel 718 material and the necessary cutting forces. The improvements in insert wear resistance followed the increase in cutting speeds which was clearly evident with T7.1-T7.2 (Insert C). The high wear and thermal shock resistance of Insert C (CTIS710 SiAlON substrate grade) is also apparent in Section 5.3 and Section 7.3.

The variation in chip morphology is a result of the fluctuations in cyclic specific shear forces being higher than that of continuous cutting forces, and it is this that causes the serrated chip morphology. The serrated chip effect is a result of shear bands forming between each of the serrated edges. The width of the shear band should decrease as the cutting speed is increased.

Throughout the machine trial, the finish cut diameter was measured to see what level of accuracy was achieved with each cut. Some work-piece spring-back was observed in the material in the F_y axis and some loss of rigidity in the machine. The required material removal was never exactly 273 cm^3, but apart from the failure Test Cut T1.1, all the test cuts were deemed to be a success.

4.4.2 Chip Morphology Analysis

During the study of the chip morphology and the stain hardening of the Inconel 718 chip, the focus was to gain an understanding of what happens to the swarf chip at different cutting speeds. The high cutting speeds that were used to create the Bakelite samples yielded shear localised chips. In each of the samples, a segmented and serrated edge chip profile typical of high-speed turning was evident. There were two stages involved in the chip formation process at these types of speeds. One stage comprised plastic instability and the other stage involved strain localisation in a narrow band in the primary shear zone.

The other stages which were involved in the formation of the Inconel 718 chip at high cutting speeds involved the formation of segments as the cutting tool advanced. Sample two seemed to show slightly higher shear localisation when compared to samples one - this was due to the

increase in cutting speed. During the latter stage, the chip experienced significant amounts of shear. The high cutting speed caused the chip to deform locally; the deformation in the localised shear bands ultimately causing the chip material to strain harden to the point of fracture. As the cutting speed increased, the length of contact between the segments decreased, which increased the shear strain, evident in Figure 4.15, which showed feathered chip segments were the result of reduced amounts of contact. The increase in periodic segmentation was due to the increase in cutting speed and this was evident in sample three, in Figure 4.15.

The discontinuous chips that were produced at cutting speeds of 250 m/min and 300 m/min all ultimately led to chip fracture due to strain localisation in the primary shear zone. The primary shear zone was exposed to higher cutting temperatures when the cutting speed increased from 250 m/min to 300 m/min. With the increase in cutting speeds, the cutting forces reduced because of the higher shear zone temperatures, reducing the yield strength of the Inconel 718 material.

The cutting conditions that were experienced at the two cutting speeds by the chip and the cutting tool were extreme. The poor thermal conductivity properties of Inconel 718 concentrated the heat into narrow deformation shear bands, which generate highly deformed localised chip segments. This created an extreme machining environment. The extreme cutting conditions caused the simultaneous fluctuation between the stress and strain in the Inconel 718 material. The extreme cutting environment ultimately yielded the shear localised chip in all four of the Bakelite samples used in this study. When machining hard to machine materials such as Inconel 718, it is important to utilise the correct machining parameters such as cutting speed, feed rate and depth of cut as these parameters have a noticeable effect on the amount tool wear that is generated, and ultimately, the tool life.

When using ceramic cutting tools, a compromise needs to be made so that the tool life is optimum with the serrated type of the swarf chip that is being produced. The surface finish of the Inconel 718 after the second cut with all four different ceramic turning inserts was very good indeed, which signifies that a cutting speed of 300 m/min and feed rate of 0.2 mm/rev can attain a good surface finish. This cutting speed will obviously result in an increase in intense shear band localization within the chip. The use of a 300 m/min cutting speed and 0.2 mm/rev feed rate will result in higher productivity and will allow for a good surface finish, which is ultimately what we have ascertained from this package of research.

These sort of cutting conditions have been advised by industrial cutting tool suppliers for a few years. Even though these cutting conditions are typical, the level of wear that has been ascertained during this machining trial is an improvement on what has been achieved in previous research studies Altin et al. [110] and Zeilman et al. [111].

4.5 Conclusions for (Test No T1.1-T8.2)

The conclusions which have been drawn for this wear of inserts study for turning tools are as follows:

1. Several wear mechanisms (flank, crater, notching, and plastic deformation) can occur and specifically when using round inserts, flank and notch wear are dominant. Notch wear was the most predominant wear mechanism that was captured during this machining trial.
2. The optimum cutting speed for machining Inconel 718 is 300 m/min. At cutting speeds above 250 m/min, intense shear band localisation in the primary shear zone of the chip/tool interface leads to increasing levels of chip segmentation and failure.
3. It is recommended that a SiAlON grade 2 (CTIS710 SiAlON grade) round cutting tool insert is used for rough machining of Inconel 718.

4.6 Summary

This chapter has attempted to establish a thorough understanding of some of wear characteristics that are exhibited by ceramic inserts when machining nickel-based superalloys such as Inconel 718. The two main objectives of this chapter were: (1) to ascertain the different wear mechanism which influence tool life and lead to tool failure, and (2) to ascertain how increasing the surface speed has a direct impact on the metallurgical morphology of the chip samples. What is established in this chapter is that high amounts of the thermal energy are generated in the chip tool interface and these high temperature result in high insert wear rates.

This chapter has also provided a crucial introduction regarding the wear characteristics of CTIS710 SiAlON grade when machining Inconel 718. The turning research that has been completed in this chapter provided the early evidence which influenced the decision to select CTIS710 SAlON grade for future machining trials. This grade of SiAlON was selected and used throughout all the later milling machining trials and tribological testing. Coating technologies have a been explored in previous machining trials. As discussed in Section 2.7.4, the benefits of depositing a protective wear resistance coating onto a SiAlON turning insert have been analysed in detail by Lui et al. [36]. The analysis conducted by Lui et al, and the subsequent reduction in wear which was attained in the study influenced my decision to look much deeper

into the literature concerning coated SiAlON tooling. As a result of an in-depth literature review, a gap in the knowledge was found concerning coated SiAlON ceramic milling tools for machining nickel based super alloys.

Chapter 5 Tool Wear Analysis Under Interrupted Cutting Conditions

Author's note: The work in this chapter has been published in the Proceedings of the Institution of Mechanical Engineers, Part B: Journal of Engineering Manufacture Osmond et al. [100].

5.1 Introduction

The machining environment that is created when machining aged Inconel 718 with SiAlON ceramic milling inserts suffers from very high attrition. Especially if this particular machining environments are compared to traditional machining environments that carbide tooling is exposed to. Therefore, one of the key motivations of this chapter, has been to understand and develop a thorough understanding of what coating elements and coating systems perform well in this extremely harsh machining environment.

The purpose of the research in this chapter is to gain further understanding and knowledge in regard to machining Inconel 718 with coated SiAlON ceramic cutting tools. In Chapter 4, a series of turning trials with different ceramic turning inserts were conducted. As a result of the flank wear results from those turning trials, the CTIS710 SiAlON grade (Insert C) was selected for the rest of the EngD machining trials and other tribological research.

Chapter 5 will look to explore what types of coating elements and coating systems are effective at protecting SiAlON ceramic milling inserts when machining aged Inconel 718. Chapter 5 will also analyse the effect the coating elements have on the microstructure of swarf chips, which are formed at different cutting speeds, as seen in Table 5.1.

In Sections 3.2.1-3.2.2 of Chapter 3, tool wear capturing techniques are discussed as well as the 3D profilometric, which have been used throughout this chapter. Section 3.9 provides the basis of the machining techniques, machining strategy and data capturing techniques that have been used throughout this chapter.

This chapter will look at the cutting force and insert wear analysis results that have been created during the completion of Tests M1-M13. Tests M1-M13 involved the interrupted, non-continuous milling insert wear machining trials, which were conducted at the AMRC knowledge transfer centre (KTC). The test number, machining parameters and test sequence, which have been used in the machining trials, are stipulated in Table 5.1.

Table 5.1. Test parameters machining trial. cutting conditions, used in this study. All inserts had an axial rake angle -7.1°, Radial rake angle -12.3° and 0.1 mm edge chamfer.

Test No	Tool Material	Bar Sections Machined	Cutting Speed (m/min)	Feed rate fz (mm/tooth)	Depth of Cut (Ap) mm	Radial Engagement (ae) (mm)
M1	CTIS710 SiAlON Uncoated	1-1 to 1-4	700	0.1	1.0	30
M2	CTIS710 SiAlON +Type A Coating	1-1 to 1-2	700	0.1	1.0	30
M3	CTIS710 SiAlON +Type B Coating	1-1 to 1-4	700	0.1	1.0	30
M4	CTIS710 SiAlON Uncoated	2-1 to 2-5	800	0.1	1.0	30
M5	CTIS710 SiAlON +Type A Coating	2-1 to 2-5	800	0.1	1.0	30
M6	CTIS710 SiAlON +Type B Coating	2-1 to 2-4	800	0.1	1.0	30
M7	CTIS710 SiAlON Uncoated	3-1 to 3-5	900	0.1	1.0	30
M8	CTIS710 SiAlON +Type A Coating	3-1 to 3-4	900	0.1	1.0	30
M9	CTIS710 SiAlON +Type B Coating	3-1 to 3-2	900	0.1	1.0	30
M10	CTIS710 SiAlON Uncoated	4-1 to 4-4	1000	0.1	1.0	30
M11	CTIS710 SiAlON +Type A Coating	4-1 to 4-4	1000	0.1	1.0	30
M12	CTIS710 SiAlON +Type B Coating	4-1 to 4-2	1000	0.1	1.0	30
M13	CTIS710 SiAlON +Type B Coating 'Retest'	2-1 to 2-3	800	0.1	1.0	30

Up-milling operations were conducted under dry conditions and no through-air cooling was applied to the cutting tool due to a limitation of the test platform, which might have caused fluctuation in cutting temperature. The thirteen samples were machined at cutting speeds ranging from 700-1000 m/min with a constant feed per tooth (fz) of 0.1 mm/tooth and constant axial depth of cut (Ap) of 1.0 mm in the F_z-direction and the radial engagement (ae) of 30.0 mm. The feed per tooth, depth of cut and the 30.0 mm radial engagement were selected to maintain chip thickness (H_{ex}) where possible.

For the removal of each bar section, the metal removal volume was 33.93 cm^3. A maximum of five bar sections were removed for each of the cutting speeds with the three different inserts. A new set of four inserts was used for each of the four cutting speeds. For each test to be deemed successful, 169.64 cm^3 of material had to be removed as this would have removed all five sections of the Inconel 718 sample. The 169.64 cm^3 of material was machined away in five 12.0 mm long sections, as seen in Figure 3.11.

Once the section had been successfully machined away, the tool was removed from the machine and the inserts kept in position so that insert flank and rake face wear data could be gathered using the optical microscope. Each of the five sections of material that were removed individually accounted for 33.93 cm^3 of the total volume of material removed. After each bar section of material had been removed, cutting force measurements and insert wear measurements were taken. The cutting distance which the inserts had achieved was also collated and plotted against insert wear.

5.2 Influence of Uncoated and Coated Inserts on Cutting Force

The primary aim of this chapter is focused on identifying if a protective coating can improve the machining performance, tool life and wear characteristics of SiAlON ceramic milling inserts. In order to identify if a protective coating would improve the wear characteristics of SiAlON ceramic milling inserts. The tool life and wear performance of two CVD coated SiAlONs milling inserts was compared to that of uncoated SiAlON milling inserts. From the data that was attained a series of wear patterns emerged. At the start of machining, Bar Sections 1-1, 2-1, 3-1 and 4-1, the stability of the Inconel 718 workpiece is at its lowest.

What counters this loss of stability is the amount of cutting force necessary to machine each bar section, which is also at its lowest as the inserts have not sustained any significant amounts of wear in the early stages of the test. Figure 5.1(a-b) shows the level of average cutting force in the F_x-axis, F_y-axis and F_z-axis throughout the machining trial.

(a)

Machined Bar Sections
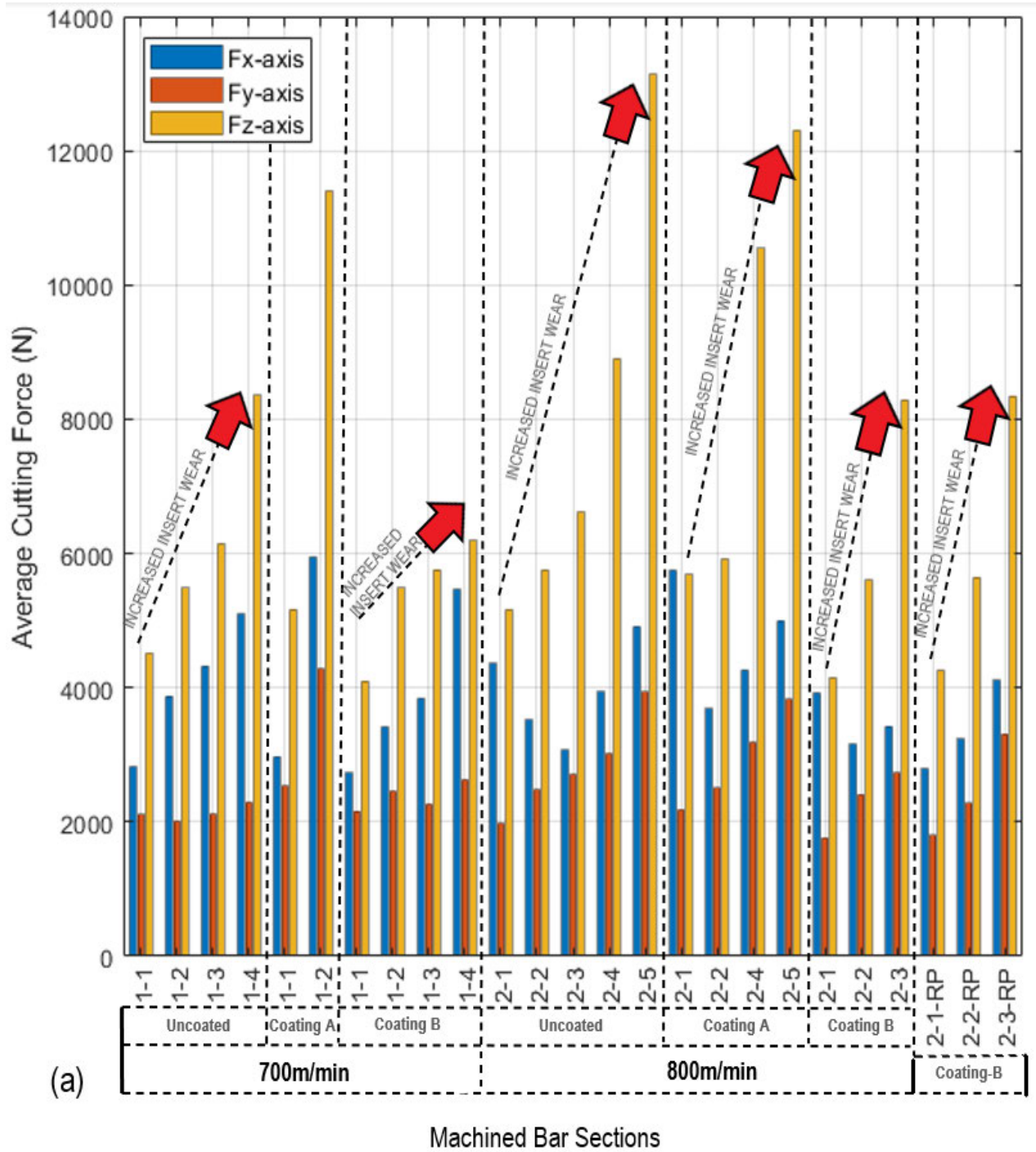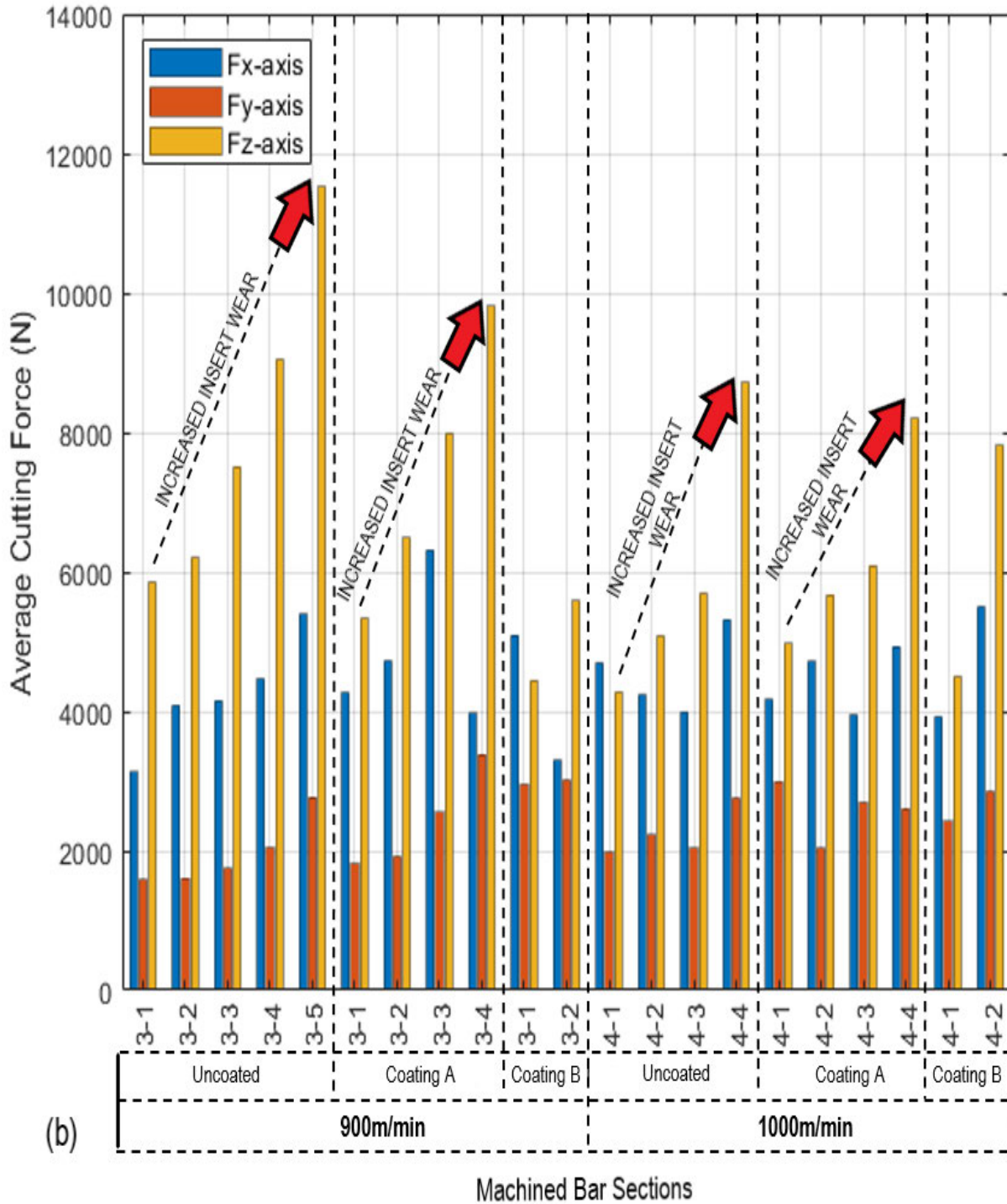
Figure 5.1. (a) Average Cutting Force versus Machined Bar Section at 700 m/min (Test No M1-M3) and 800 m/min (Test No M4-M6, M13), (b) Average Cutting Force versus Machined Bar Section at 900 m/min (Test No M7-M9) and 1000 m/min (Test No M10-M12).

The other reason for the high cutting forces in the F_x-axis, F_y-axis and especially the F_z-axis axis when compared to other research conducted by Molaiekiya et al. [38] and Tian et al. [31], is

down to the size of cut and radial engagement (ae). All the bar sections were machined with an initial full radial engagement (ae) of 30.0 mm, which stays constant for about two thirds of the cut and then the radial immersion reduces as each test cut travels through a full 360° and exits out of cut in the F_y-axis direction. The levels of resultant cutting force which the three types of SiAlON experienced, and the relationship between the average resultant cutting force and the change in cutting speed is also shown in Figure 5.2.
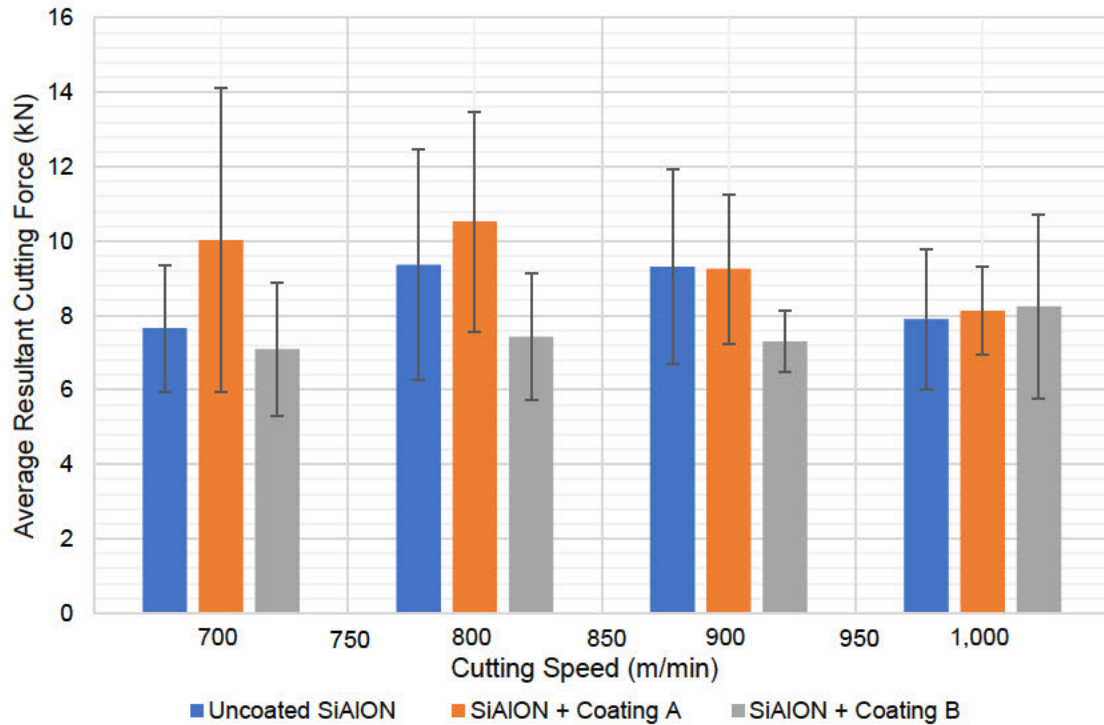
Figure 5.2. Resultant Cutting Force vs Cutting Speed (m/min) for Uncoated SiAlON milling inserts and for Coating A and Coating B.

Throughout the machining trial there has been a gradual increase in measured cutting force during the machining the bar sections which is presented in Figure 5.1(a-b). The gradual increase in cutting force correlates with the progressive level of wear which the inserts have sustained when machining each bar section. The gradual increase in insert flank face wear is represented in Figure 5.3(a-h), Figure 5.4(a-l), Figure 5.5(a-h) and Figure 5.6(a-h).

At the lower cutting speeds of 700 m/min and 800 m/min the workpiece material maintains higher hardness during the cutting process, as the workpiece has not undergone sufficient thermal softening in the chip/tool interface to reduce the yield strength of the workpiece material. The lack of thermal softening is shown in both Figure 5.1(a-b), where the uncoated and Coating A inserts required more cutting force to remove each cut and meant that the uncoated inserts

and the Coating A inserts experienced higher mechanical shock between the tool and the workpiece. The higher mechanical shock which is encountered between the outer Al_2O_3 of Coating A and the workpiece. This is likely due to the higher frictional characteristics of Al_2O_3 when compared to the outer layer of TiN for Coating B. The frictional coefficients and deformation characteristics of Coating A and Coating B are analysed in further detail in Chapter 6 with scratch and pin-on-disc testing. The Coating B inserts experienced lesser fluctuations in the average resultant cutting force at cutting speeds ranging from 700 to 900 m/min, which is likely due to the low friction characteristics of the titanium nitride outer coating.

However, this lower cutting force requirement changed when the cutting speed was increased from 900 m/min to 1000 m/min. Figure 5.1(a-b), highlights the impact of the thermal softening effect in the chip/tool interface, which led to a large reduction in the hardness and the shear stress which is necessary to remove each cut of workpiece material. This in turn also led to large reductions in the level of mechanical shock between the tool and workpiece which was evident by the sound of each cut.

5.3 Tool Failure Mechanisms

The types of tool failure patterns for the rake and flank faces are shown in Figure 5.3-Figure 5.6 and show that the wear mechanisms at high cutting speeds on the flank and rake face are flaking, chipping, notch wear and adhesive wear. These types of rake and flank face wear patterns has taken place at a cutting speed of 700, 800, 900 and 1000 m/min, when high-speed face-milling of Inconel 718 at fz=0.1 mm/tooth, Ap=1.0 mm, and ae=30.0 mm. It is clearly evident in (Region 1 and 2 in Figure 5.3) that Coating A has poor adhesion to the CTIS710 SiAlON substrate (insert).

The main reason for the poor adhesion is likely due to the bonding interlayer being titanium nitride (TiN) the metallic bonding structure of which has created a weak interfacial bond with the covalent SiAlON substrate microstructure. As a result, Coating A degrades and chips off the flank face a higher rate than that has been demonstrated by Coating B.

The thermal stability and adhesive properties of Coating B originate from the high strength ionic bonding characteristics of aluminium oxide Al_2O_3 interfacial layers with the covalent microstructure of SiAlON substrate, which is shown graphically in Figure 2.21 in Section 2.10.2. The creation of an adherent interfacial coating layer provides a stable foundation for the outer layer of titanium nitride to be deposited onto, which is shown graphically in Figure 2.24 in

Section 2.11.3. The higher stability and superior adhesive characteristics of Coating B can be seen in (Region 3 in Figure 5.3.) and in (Region 4 in Figure 5.3.).
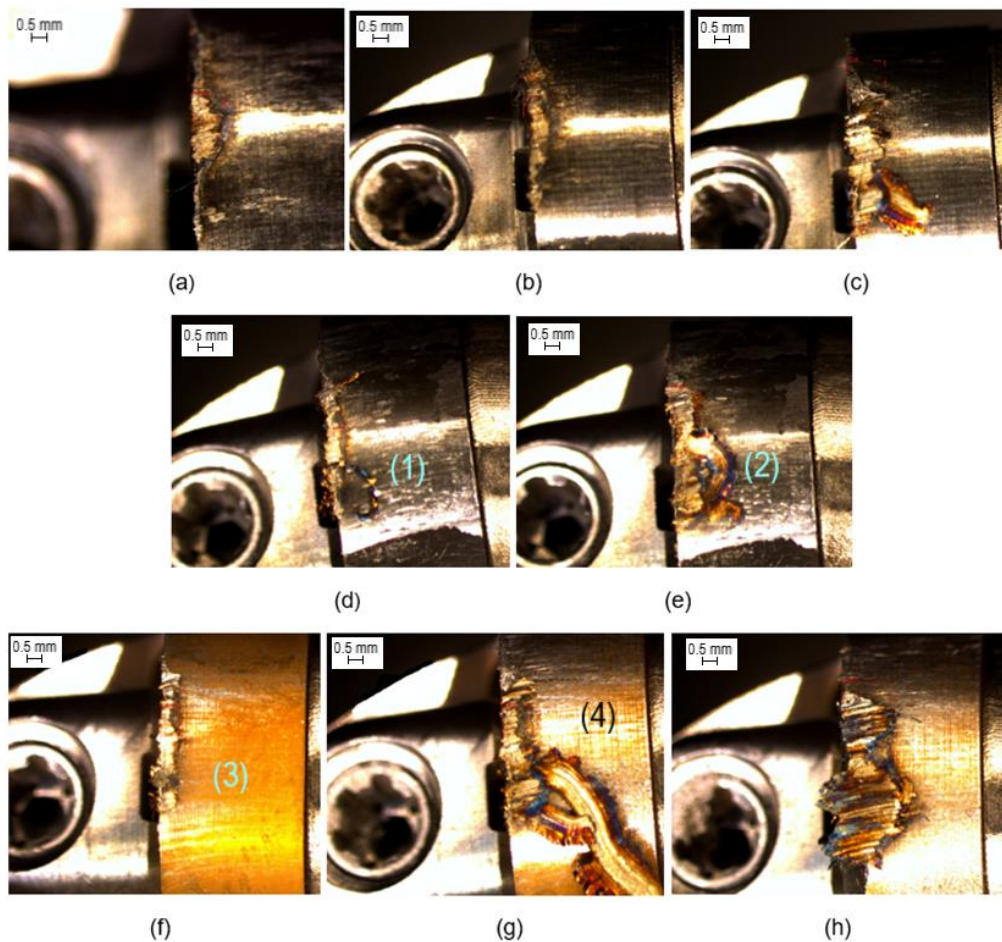
Figure 5.3. Flank wear visible (a-c) 700 m/min (Test No M1) and Flank wear visible (f-h) 700 m/min-(Test No M3), material removed is 101.80 cm³, flank wear visible (d-e) 700 m/min (Test No M2) material removed is 67.86 cm³.

In (Region 1 and 2 Figure 5.4) and in (Region 3 and 4 in Figure 5.4) begins to show the degradation of Coating B and the coating B retest, and after the completion of Bar Sections 2-2 and 2-3 test cuts it appears that Coating B certainly has better adhesive characteristics when compared to Coating A. The reflective shiny surface that is seen in (Region 1 and 2 in Figure 5.3, (Region 5 and 6 in Figure 5.4) represents freshly revealed SiAlON substrate, which indicates the Coating A has been removed. Conversely, (Region 3 and 4 in Figure 5.3) show the Coating B still adhered to the SiAlON substrate. However, once the TiN outer layer of Coating B is exposed to temperatures above 800°C it begins to oxidise, during which each cut leads to a rapid reduction during which each cut leads to a rapid reduction in its mechanical properties, significantly reducing its adhesive characteristics and causes further coating failure.
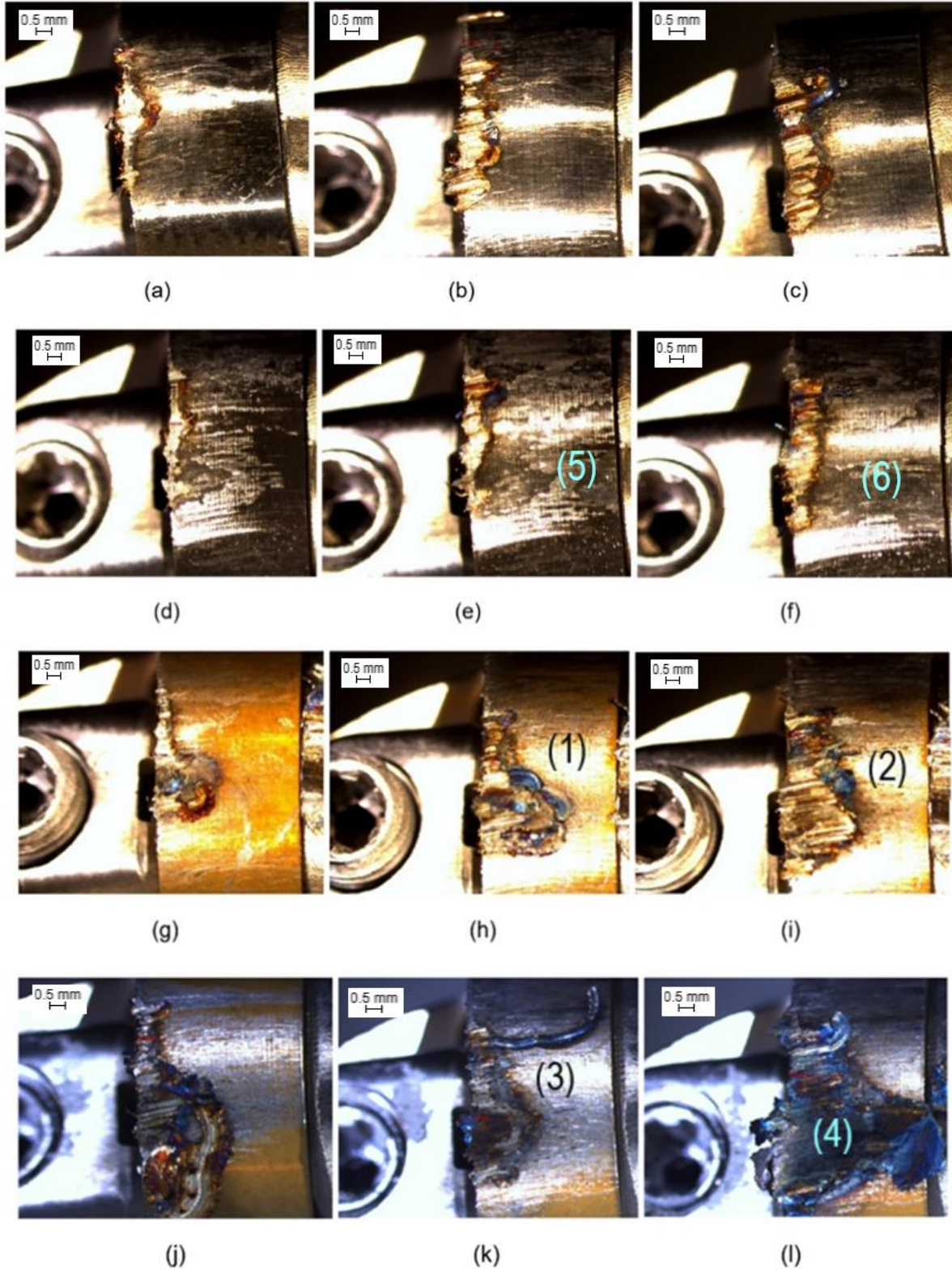
Figure 5.4. Flank wear visible (a-c) 800 m/min (Test No M4), Flank wear visible (d-f) 800 m/min (Test No M5), Flank wear visible (g-i) 800 m/min (Test No M6), Flank wear visible (j-l) 800 m/min (Test No M13). For all the material removed is 101.80 cm^3.

Zhu et al. [112] conclude that the ceramic ionic and covalent bonding phases do create strong interfacial bonds which contributes to the thermo-mechanical properties and their stability at high temperatures when compared to metallic phase bonds of titanium nitride. The weaker interfacial metallic phase bonds are the reason why the Coating A has flaked off the insert in the early stages of this set of test cuts (Region 3 and 4 Figure 5.5). Thouless et al. [113] proposed that once the stability between the substrate and the coating interfacial layer is weakened, microcracks begin to form due to the distribution of the cutting forces through brittle weak interfacial phases. As the three different types of inserts were used to machine Bar Sections 1-3-1-4, 2-3-2-5, the inserts ultimately succumbed to fracture as result of progressive tool damage on both the flank and rake face and with the increase in the volume of metal removal. The progressive wear of the three different types of inserts took place due to presents of high mechanical and thermal stresses taking place in the primary shear zone of the chip/tool interface and secondary wear zone on the flank face. The variation of high tensile and compressive stresses is generated by the heating and cooling of the cutting tool through each cutting cycle. The effects of the heat and cooling cycles were evident when the Coating B inserts could not complete Bar Sections (3-3-3-5) and (4-3-4-4) due to the quantity of wear that had been sustained by the Coating B inserts after machining Bar Sections (3-1-3-2) in Figure 5.5(g) and Figure 5.6(h) and Bar Sections (4-1-4-2) in Figure 5.6(g).

This was also apparent with the Coating B in (Regions 1 and 2 in Figure 5.5), because of isolated craters forming on the flank face. The isolated craters are likely as a result of the coating being removed via thermomechanical wear from the SiAlON substrate and diffusion wear taking place at temperatures in excess of 1000°C. At cutting temperatures over 1000°C the silicon nitride in the SiAlON milling inserts has a strong affinity for the iron in the workpiece material. This strong affinity between the silicon nitride and the iron initiates solid solution between the flank face of Coating B inserts and the workpiece, which causes rapid degradation of the flank face. The uncoated SiAlON ceramic inserts have less wear when compared to the coated SiAlON inserts.

The uncoated SiAlON inserts for the test cuts at 700, 800 and 900 m/min demonstrated the best wear resistance characteristics when compared to the coated SiAlON inserts. This lack of wear can be attributed to a chip/tool interface which created a superior sliding contact interaction between the Inconel 718 workpiece material and uncoated SiAlON inserts. The stable engagement into cut allowed for more consistent cutting forces, cutting temperatures and material removal, which contributed to extending the tool life of the uncoated SiAlON inserts.

Even though the uncoated inserts generated higher cutting forces than Coating B inserts as captured in Figure 5.1. The uncoated SiAlON inserts machined five bar sections when compared to four sections that were machined with Coating B inserts. Therefore, the wear resistance of the uncoated SiAlON inserts was higher than the Coating B inserts.
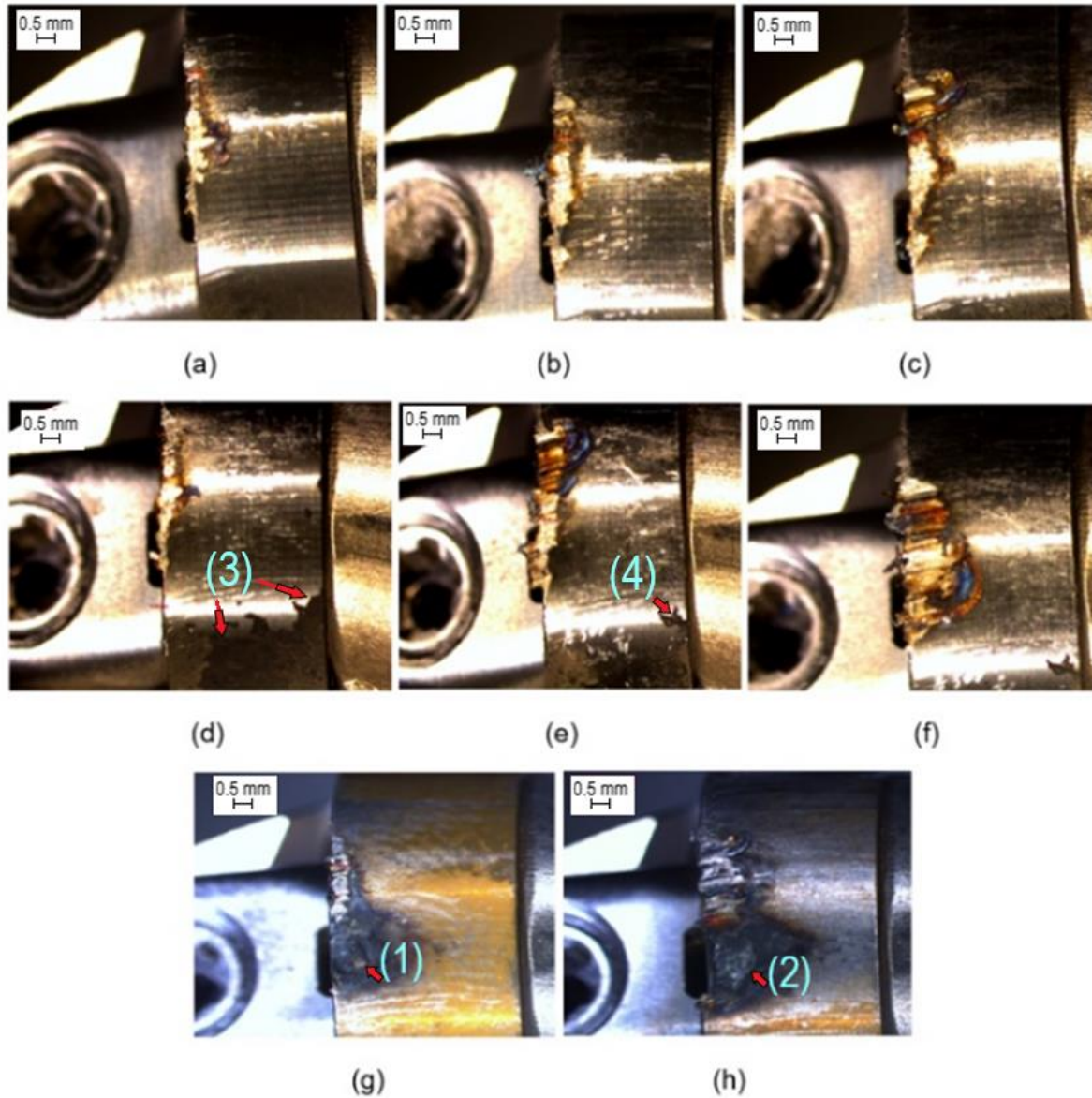
Figure 5.5. Flank wear visible (a-c) 900 m/min (Test No M7) and (d-f) 900 m/min (Test No M8) the material removed for both is 101.80 cm^3, Flank wear visible (g-h) 900 m/min (Test No M9) the material removed is 67.86 cm^3.

The chip/tool interface created by the coated SiAlON inserts has exhibited less stability. The lack of stability is a result of the less favourable sliding contact interaction between the Inconel 718 workpiece material and coated SiAlON inserts. The less stable engagement in cut resulted

in coating wear and degradation, which contributes to variation in the cutting forces, cutting temperatures and how the workpiece material is removed.
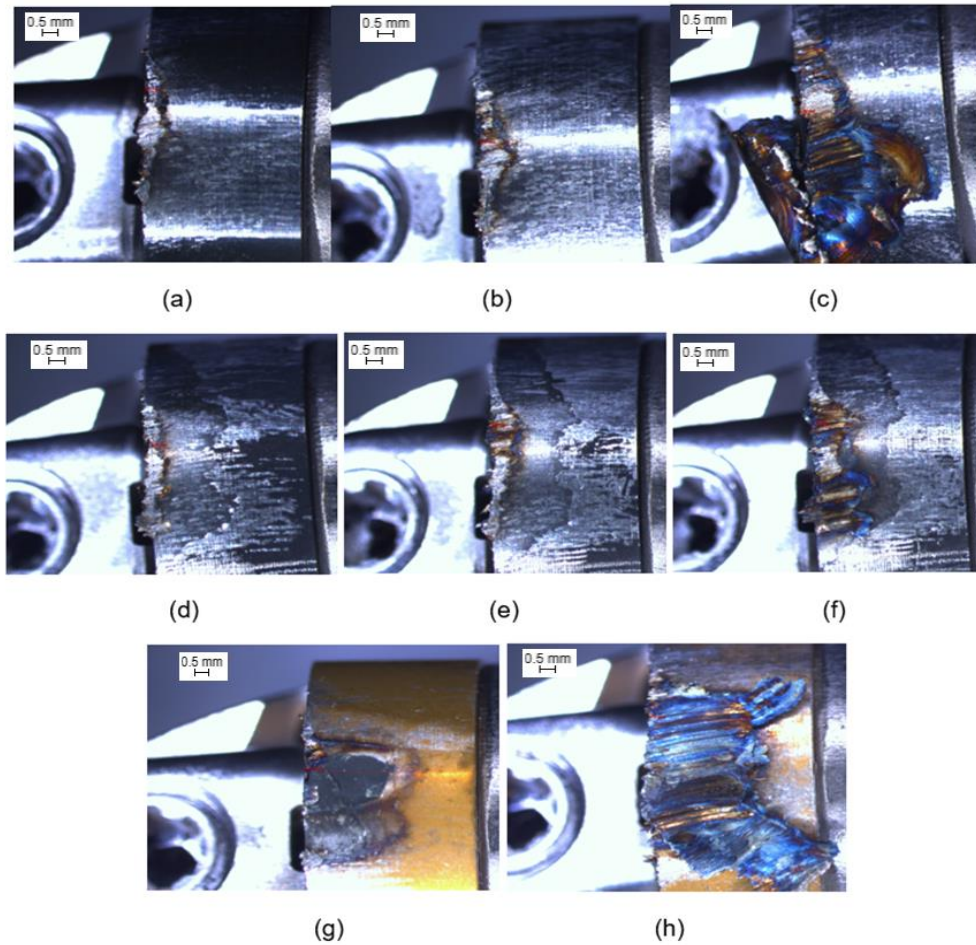
Figure 5.6. Flank wear visible (a-c) 1000 m/min (Test No M10) and (d-f) 1000 m/min (Test No M11) the material removed for both is 101.80 cm^3, Flank wear visible (g-h) 1000 m/min (Test No M12) the material removed is 67.86 cm^3.

A non-contact 3D profilometer (focus variation type), was used to scan the three different types of inserts are shown in Figure 5.7-Figure 5.10. Figure 5.7 highlights the types of primary and secondary wear mechanisms which the uncoated, Coating A and Coating B inserts sustained when facing milling Bar Sections (1-1-1-4) of Inconel 718 at a cutting speed of 700 m/min. Secondary wear mechanisms such as oxidative wear are visible on the rake face (Region 1 in Figure 5.7) and abrasive wear is visible on the cutting edge of the rake face for the uncoated and Coating A inserts (Regions 3 and 5 in Figure 5.7). As represented in Figure 5.7, non-contact 3D profilometer (focus variation type) scans were taken of Insert 1 and 3 for Test No M1 and Test No M2 and Insert 2 and 4 for Test No M3.

112

Flaking and chipping are evident on the rake face for the uncoated and Coating A inserts (Regions 2 and 4 in Figure 5.7). The flaking and chipping take place due to the change in cutting edge as result of abrasive wear, which causes the contact pressures in the chip/tool interface to increase to a point that it causes the SiAlON ceramic microstructure to shear along the grain boundaries. The shearing effect along the grain boundaries causes a wave like multilayer topography to form as can be seen on the rake face of the Coating B inserts (Regions 6 and 8 in Figure 5.8).

Primary wear mechanisms such as crater wear are visible on the flank face of the Coating B inserts (Regions 6 and 7 in Figure 5.8). During the machining process, as the three types of inserts sustain more wear on the flank and rake faces and remove more metal, the level of vibrations begin to increase. Once the coatings delaminate and flake off the inserts, a cutting surface with different coating thicknesses on both the rake and flank faces of the Coating A and Coating B inserts is created which contributed to the exacerbation of the insert wear mechanisms.

Figure 5.7. Non-contact 3D profilometer (focus variation type) scan: Test No M1(a-b) and Test No M1 (c-d) the material removed for both is 135.716 cm^3, Test No M1 (c-d) the material removed is 67.858 cm^3.

Figure 5.8 highlights the types of wear which the inserts sustained when facing milling Bar Sections (2-1-2-5) of Inconel 718 at a cutting speed of 800 m/min. Once again flaking and chipping are evident on the rake face for the uncoated and Coating A inserts (Regions 1, 2, 6, and 8 in Figure 5.8). The level of insert wear is reflected by the volume of metal that has been removed as Bar Sections (2-1-2-5) were machined by the uncoated and Coating A inserts. As represented in Figure 5.7, non-contact 3D profilometer (focus variation type) scans were taken of Insert 2 and 3 for Test No M4-M6 and Test No M13.

Figure 5.8. Non-contact 3D profilometer (focus - variation type) scan: Test No M4 (a-b) and Test No M5 (c-d) the material removed for both is 169.645 cm^3, Test No M6 (e-f) the material removed is 135.716 cm^3, Test No M13 (g-h) the material removed is 101.787 cm^3.

114

Isolated chipping and flaking were also evident on the rake face for the uncoated and Coating A inserts (Regions 3 and 4 in Figure 5.8). The isolated chipping and flaking are likely a result of fluctuating tensile and compressive stresses being distributed across the rake face. Oxidative wear is yet again visible on the rake face for all the inserts (Regions 5, 7, 9, 10 and 11 in Figure 5.8).

As the cutting speed was increase up to 900 m/min and 1000 m/min the type of insert wear mechanisms changed. Figure 5.9 highlights the types of wear mechanisms which the all the inserts sustained when facing milling Bar Sections (3-1-3-5) of Inconel 718 at a cutting speed of 900 m/min. Adhesive wear had been apparent throughout the machining tests, but adhesive wear was more prominent at cutting speeds of 900 m/min and 1000 m/min with the uncoated inserts (Region 1 in Figure 5.9). This increase in adhesive wear is due to an increase in temperature in the chip/tool interface and the localised welding and fusing of the chip onto the surface of the uncoated inserts. As represented in Figure 5.9, non-contact 3D profilometer (focus variation type) scans were taken of Insert 2 and 4 for Test No M7 and M8 and Insert 1 and 2 for Test No M13.
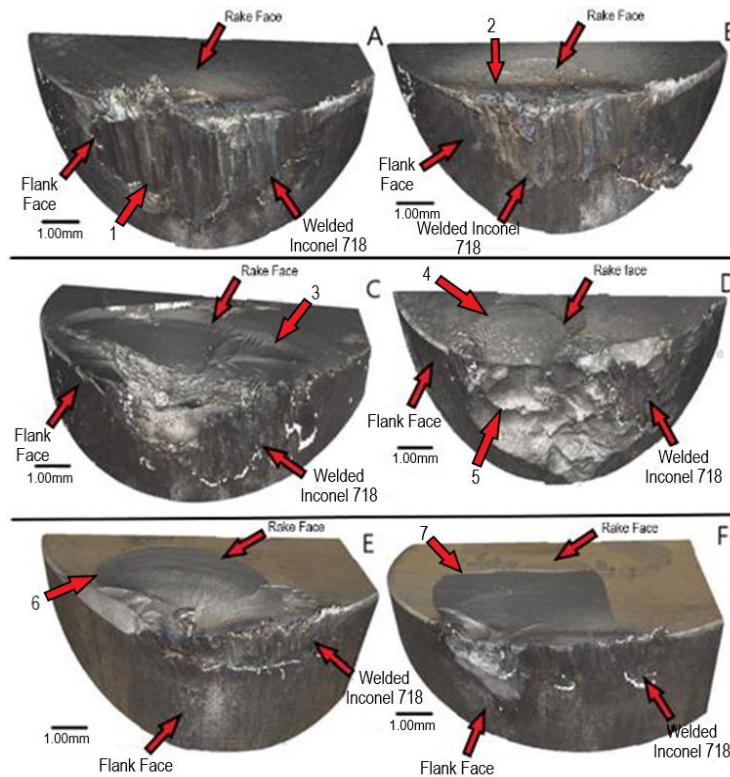
Figure 5.9. Non-contact 3D profilometer (focus - variation type) scan: Test No M7 (a-b) the material removed is 169.645 cm^3, Test No M8 (c-d) the material removed is 135.716 cm^3, Test No M9 (e-f) the material removed is 67.858 cm^3.

Coating A sustained significant amounts of chipping, flaking and crater wear (Regions 3, 4 and 5 in Figure 5.9) and Coating B inserts had chipping, flaking and crater wear (Regions 6 and 7 in Figure 5.9). However, the bilayer coating of Coating B failed after machining Bar Sections (3-1-3-2). This is likely due to titanium nitride (TiN) outer layer oxidising as a result of the increased cutting speed and cutting temperature.

The oxidised surface ablates off the surface of the insert causing the uneven sliding surface contact to exacerbate the flank and rake face wear. The uneven surface contact contributes to high fluctuations in the tensile and compressive stresses in the chip/tool interface and shortens the tool life of the Coating B inserts. As represented in Figure 5.10, non-contact 3D profilometer (focus variation type) scans were taken of Insert 1 and 2 for Test No M10 and Insert 2 and 4 for Test No M11 and Test No M12.
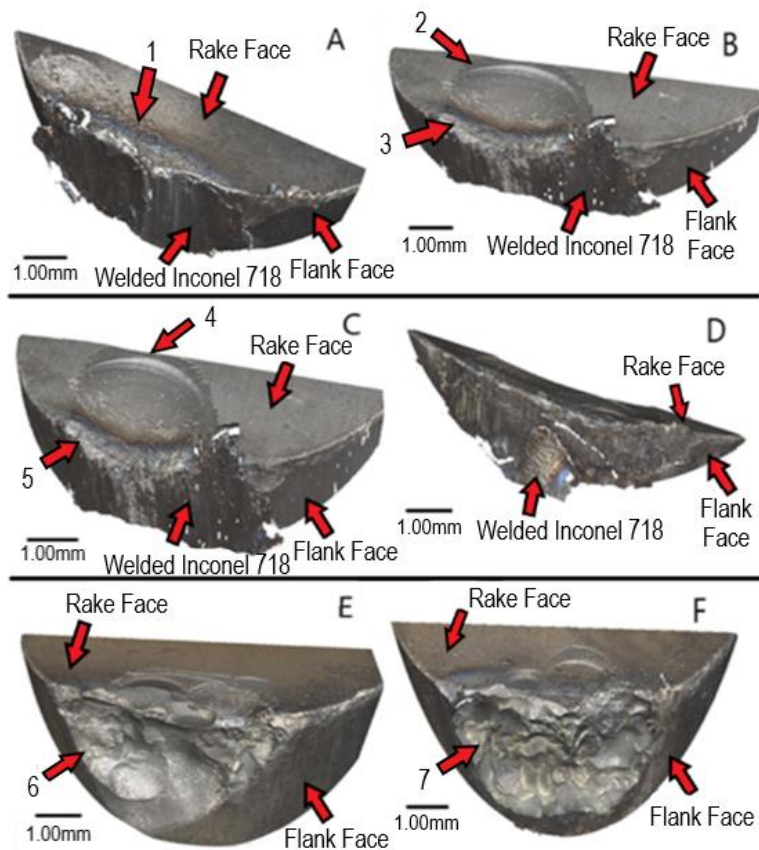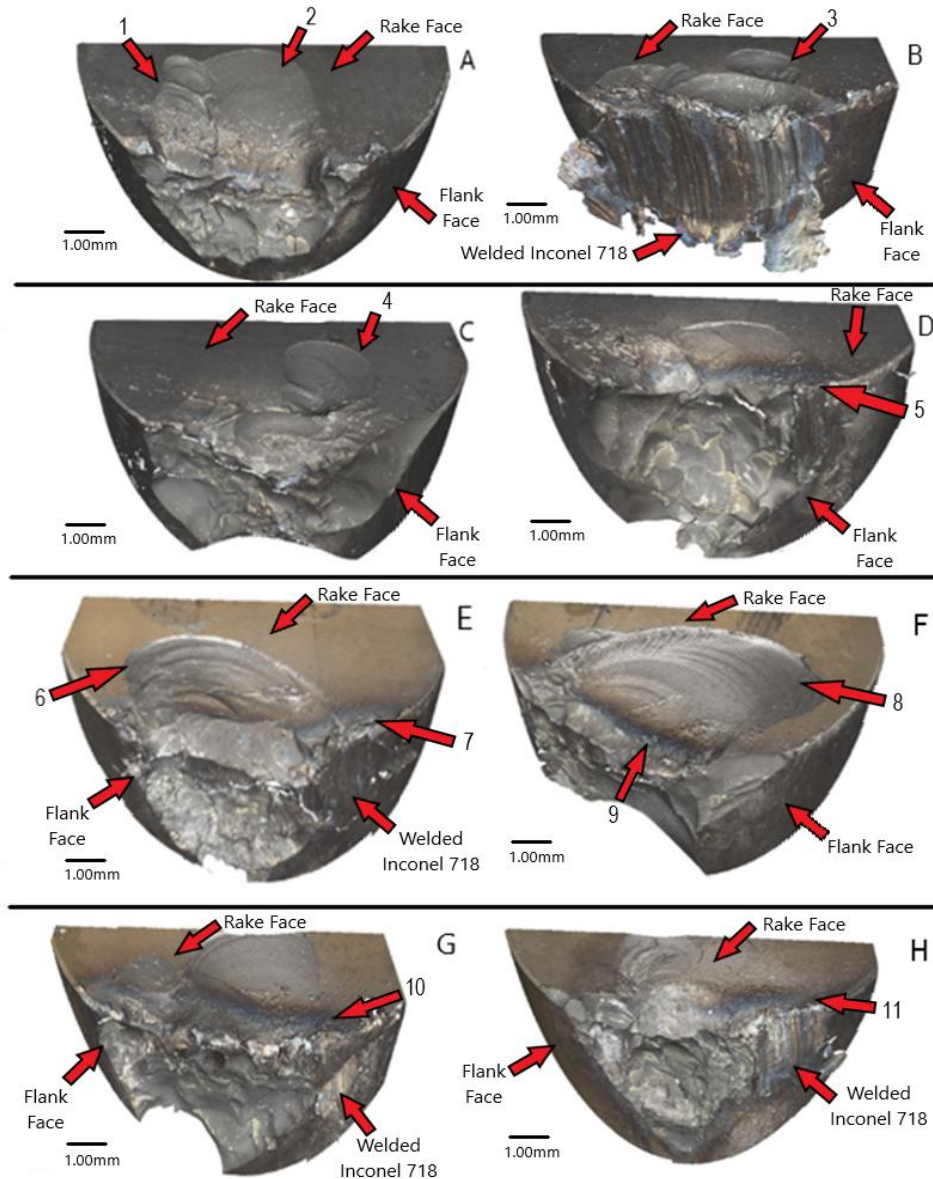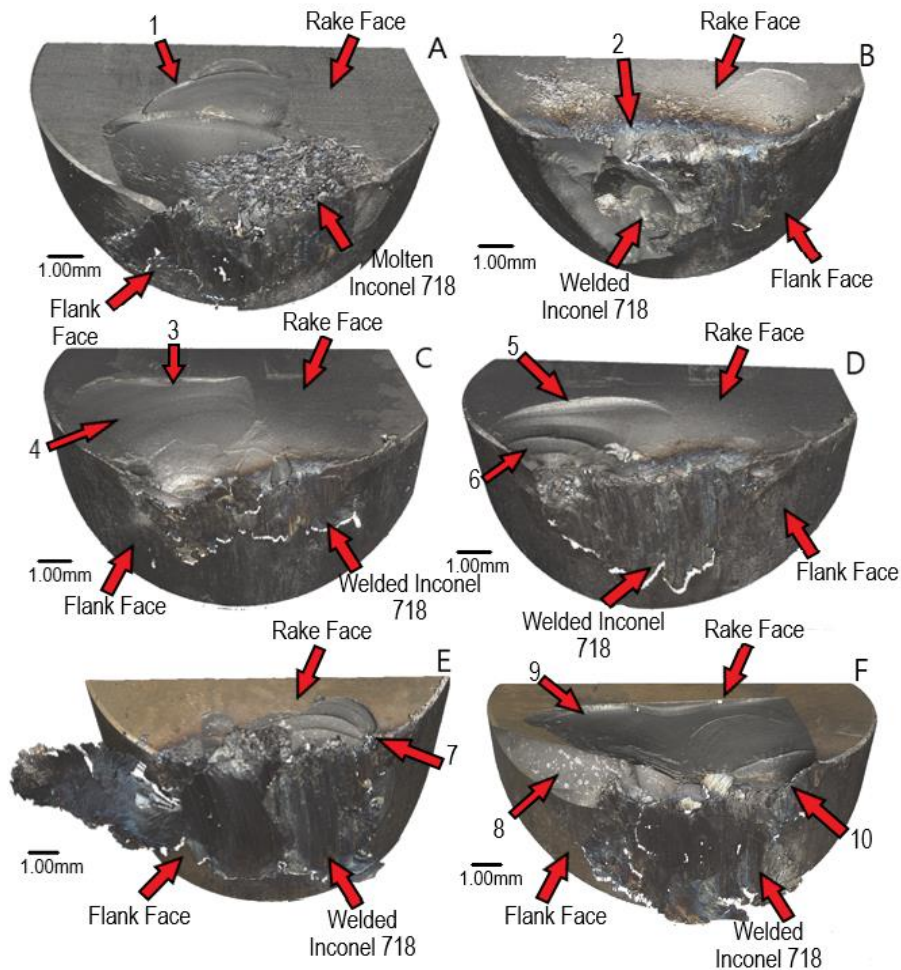

Figure 5.10. Non-contact 3D profilometer (focus - variation type) scan: Test No M10 (Images a-b) and Test No M11 (c-d) the material removed for both is 135.716 cm^3, Test No M12 (e-f) the material removed is 67.858 cm^3.

Figure 5.10 highlights the types of wear which all the inserts sustained when facing milling Bar Sections (4-1-4-4) at a cutting speed of 1000 m/min. The failures that had been evident for Coating B at a cutting speed of 900 m/min were also evident when the inserts were tested at 1000 m/min. Coating B failed after machining Bar Sections (4-1-4-2), with the TiN outer coating degrading in the same way that had been experiences in the previous test that were completed at 900 m/min. Flaking, chipping Figure 5.10 shows that all three types of insert suffer from flaking and chipping (Regions 1, 3, 5, 6, 7 and 9 in Figure 5.10) with tool fracture happening with Coating B (Regions 8 and 10 in Figure 5.10). What must also be noted is how the Coating A inserts improved in wear resistance, in comparison to the uncoated inserts as the cutting speed was increase in cutting speed up to 1000 m/min.

5.4 Tool life curves

The tool life curve which is shown in Figure 5.11 describes the magnitude of flank wear which each of the three different CTIS710 SiAlON ceramic milling inserts experienced when operated at a cutting speed of 700, 800, 900 and 1000 m/min.
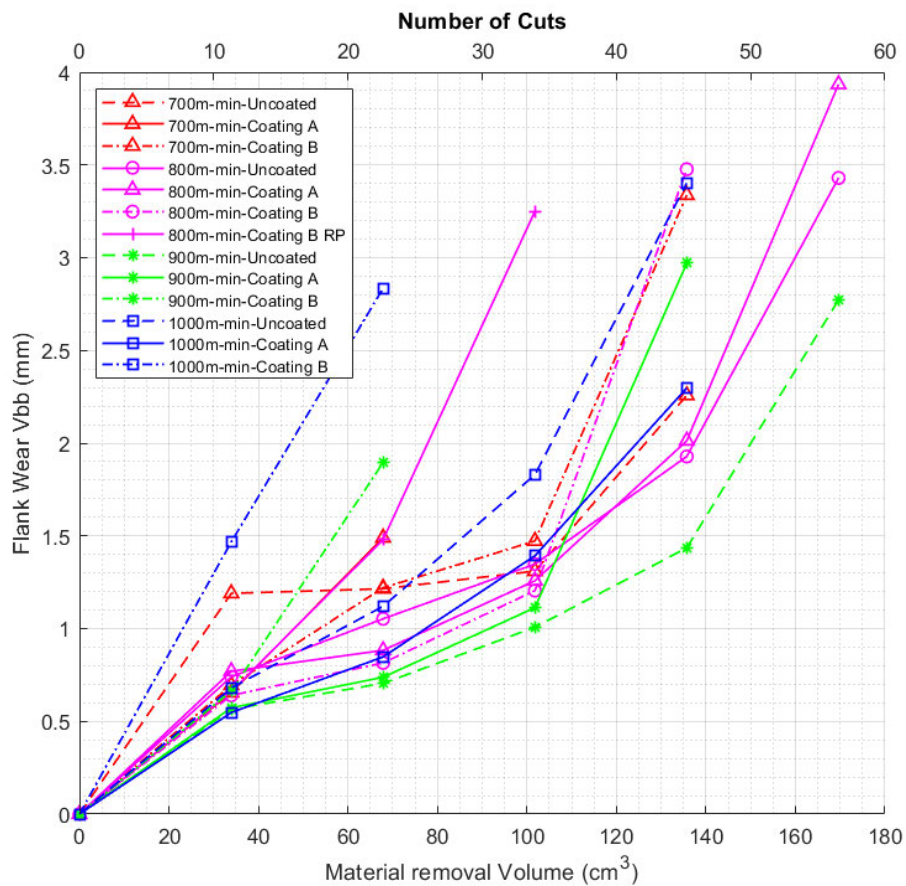
Figure 5.11. 700 m/min (Test No M1-M3), 800 m/min (Test No M4-M6 & M13), 900 m/min (Test No M7-M9), 1000 m/min (Test No M10-M12).

The 1.0 mm depth of cut and feed per tooth of 0.1 mm/tooth remained constant throughout the entire machining trial. Over the four sets of cutting speeds, the uncoated CTIS710 milling inserts achieved the best overall wear resistance and resistance to sudden failure. The CVD coated SiAlON ceramic milling inserts have performed well at cutting speeds of 700 m/min and 800 m/min regarding flank wear measurements that were captured from in the earlier sets of test cuts.

When the cutting speed was increased to 900 m/min and 1000 m/min, however, Coating B seemed to suffer from a series of exacerbated wear mechanisms ranging from thermomechanical wear, oxidation, abrasive wear, crater, and notch wear, which ultimately led to poor tool life and high tool wear rates.

Coating A appeared to perform better when the cutting speed was increased. The increase in cutting performance is likely due to Coating A being removed from the surface of the SiAlON substrate rather easy during the machining of the sections one and two. Once Coating A has subsequently been removed from the surface of the SiAlON, it leaves a clean fresh cutting surface which can be used in the machining of the latter sections.

5.5 Conclusions for (Test No M1-M13)
The following conclusions can be drawn from this study:

1. The uncoated SiAlON inserts achieved more consistent cutting performance in terms of material removed from the workpiece for a given magnitude of insert flank wear.
2. Coating B generated less cutting force when machining initial sections when compared to A and the uncoated inserts.
3. The degradation of Coating B is due to the presence of oxidised titanium nitride, exacerbating flank and rake face wear.
4. Titanium nitride in CVD coatings should not be used for protecting SiAlON ceramic milling inserts due to their poor thermal performance.

5.6 Summary
The present chapter looks to develop further understanding and explore the main research hypothesis. Therefore, Test No M1-M13 has focused on clarifying what coating elements and coating system would increase the tool life of CTIS710 SiAlON milling inserts. The use of CVD coatings is well established in literature, as this coating technique has proven to deposit abrasion resistant elements on to the surface of ceramic substrates that attain high adhesion and greatest resistance to delamination. This chapter has attempted to establish a thorough

understanding of some of the wear characteristics, cutting forces and metallurgical aspects of chip morphology, when using coated and uncoated ceramic inserts to machine Inconel 718.

The main output from of completing Test No M1-M13, has identified that amorphous grade Al_2O_3 has exhibited high thermo-mechanical stability and high adhesion to the CTIS710 milling insert substrate, throughout the two-part machining trial. The amorphous grade Al_2O_3 bonded very well on an interatomic level with the CTIS710 milling insert substrate. Although the Al_2O_3 was utilised in the Coating A outer layer, it is the Al_2O_3 interfacial layer that is represented in Coating B that was of real interest for later chapters in this thesis. However, the machining performance of Coating B inserts was impeded by the poor wear performance and oxidation resistance of the titanium nitride outer coating for Coating B. Coating A also suffered with the inclusion of titanium nitride in the interfacial layer, as the adhesion characteristics that were exhibited by Coating A were poor.

Another key output from Experiment Two has focused on the simplifying the coating systems and how this will improve the tribological contact at the chip/tool interface. The multilayer coating system for Coating A failed rapidly and the bilayer coating system for Coating B adhered so well to the CTIS710 SiAlON; that the bilayer coating of Coating B actually exacerbated the primary and secondary wear mechanisms and reduced the tool life.

Therefore, it was determined that improvements in tool life and wear characteristics could be attained by depositing a single layer of amorphous Al_2O_3 on to the CTIS710 SiAlON substrate. The single layer coating system would exploit the high thermo-mechanical stability of amorphous Al_2O_3 and the high adhesion characteristics. The novelty of this 3-axis high speed milling trial has provided different layers of information about the different types of wear mechanisms, which effect SiAlON ceramic milling inserts when machining Inconel 718. The layers of novel information focus on wear resistance, resistance to oxidation, adhesion to the SiAlON substrate and thermochemical resistance of the coated and uncoated inserts. The coating wear mechanisms that have been witnessed in the work completed by Osmond et al. [100] are also evident in Section 7.2 and Section 7.4.

To further develop the understanding of what coating elements should be utilised in Coating C, the next chapter will look to gain further knowledge and develop a greater understanding of the tribological and mechanical characteristics of the two CVD coatings. This will be accomplished with a series of tribological tests in the form of scratch testing, pin-on-disc testing and nano-indentation testing. Experiment Three will look to compare the results and conclusions of

tribological tests and compare them with the results and conclusions that have been drafted in this chapter. The cross comparison is hoped to provide useful information which can be extracted to influence the development of Coating C.

Chapter 6 Coating Characterization of Coating A and B

Author's note: The work in this chapter has been published in the Journal of Materials and Manufacturing Processes Osmond et al. [96].

6.1 Introduction

This chapter will include the published research, which focused at the tribological tests that were conducted on two CVD coated SiAlON milling inserts. The wear resistance testing of the two coatings was attained via the pin-on-disc method. The tests were conducted to ascertain a thorough understanding of the wear characteristics of the two coatings, which were deposited onto the silicon aluminium oxynitride SiAlON ceramic inserts. Understanding of the adhesion characteristics of the two CVD coatings was attained via scratch testing. As a result of fractographic examination of the two CVD coatings via scanning electron microscope images, it was established that the adhesion and wear characteristics of coating A and coating B varied extensively.

6.2 Results - Scratch Testing Analysis

The purpose of the research in this section of Chapter 6 is to gain further knowledge in regard to the adhesion properties of the two CVD coatings that have been deposited onto the CTIS710 SiAlON substrate. In Sections 3.5.1 and 3.5.3 and Section 3.6 of Chapter 3, the 3D profilometric, scanning electron microscopy techniques and scratch testing techniques are discussed; these techniques have been utilised throughout Sections 6.2 and 6.3 of this chapter. Section 3.6 provides the foundation of the scratch techniques that were utilised to perform the two scratches.

The analysis from the scratch testing has confirmed that Coating A had suffered from substantial amounts of wear, sudden fracture of the coating, which resulted in delamination, as seen in Figure 6.1(a) and Figure 6.1(c), as the level of scratch force was increased.

Figure 6.1(b) and Figure 6.1(d) indicate that Coating B had endured very little wear and no coating delamination. A scanning electron microscope (SEM) was used to perform an examination of the two CVD-coated SiAlON ceramic milling inserts, and this visual SEM analysis is captured in Figure 6.3-Figure 6.11.

From observations it was noted that the amount of adhesion to the SiAlON ceramic substrate of CVD Coating A, ($TiN+TiCN+Al_2O_3$), varied quite considerably when compared to the adhesion attained by Coating B, (Al_2O_3+TiN). The highly adherent properties that were exhibited by Coating B are due to the high strength interfacial bonds that are created between the SiAlON

ceramic substrate and the interfacial layer of amorphous α-Al_2O_3 during the CVD coating process.
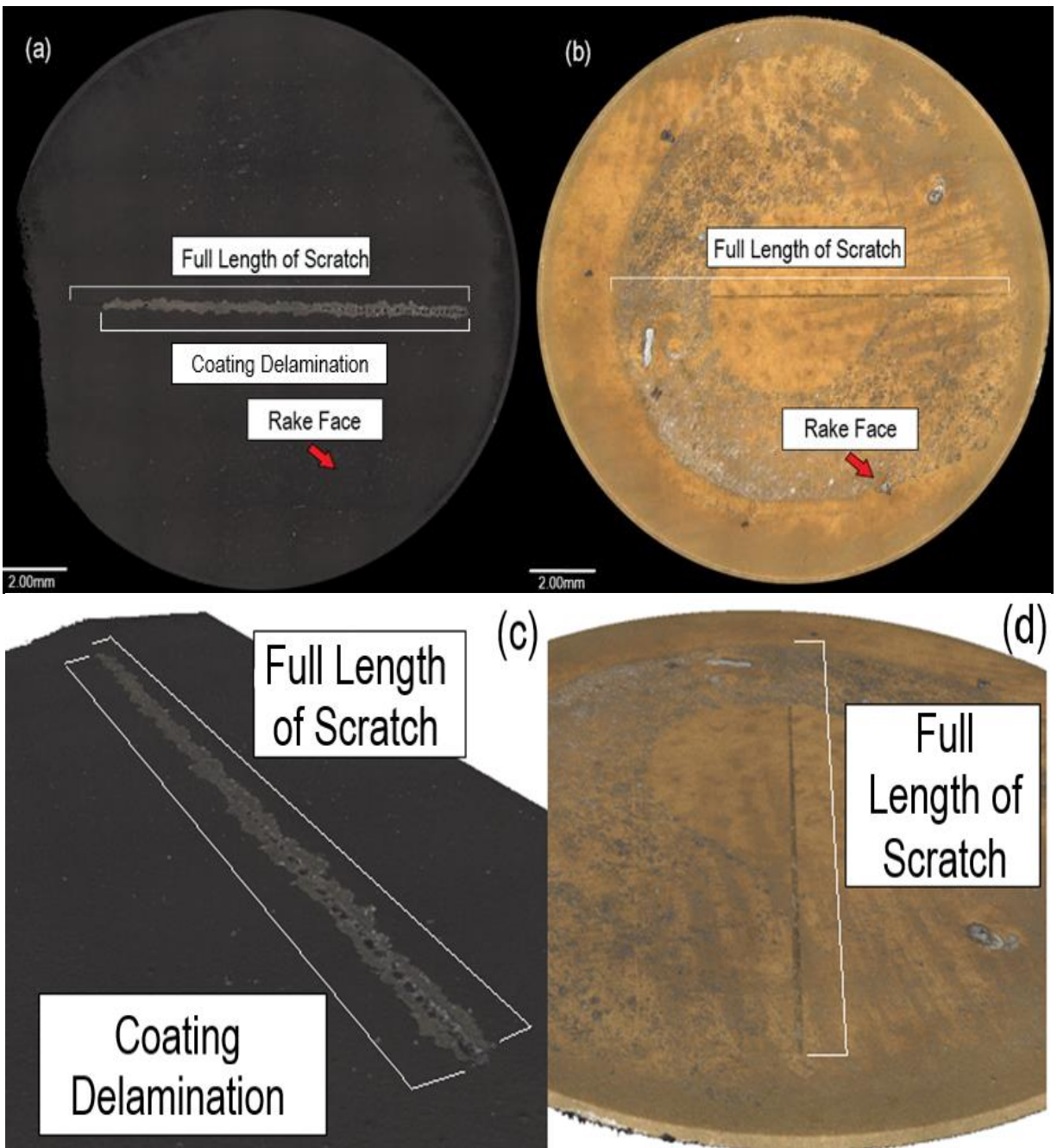
Figure 6.1.(Non-contact 3D profilometer (focus—variation type) scan of (a,c) the Coating A scratch and (b,d) the Coating B scratch.

The high temperature chemical vapor deposition process takes place in the region of 1050°C, which is an ideal temperature for chemical reactions to take place to create the amorphous α-Al_2O_3 polymorphs. The high temperatures establish high thermal interfacial bonding energies to

122

be created between the SiAlON ceramic substrate and the gaseous $AlCl_3/H_2/CO_2$ vapor gas mixture of atoms. Previous work conducted by Vuorinen et al. [114] and Fredriksson et al. [115] concluded that as vapor decomposes and begins to nucleate and bond with the SiAlON ceramic substrate, the amorphous α-Al_2O_3 polymorphs will begin to grow, layer by layer, to create an amorphous aluminium oxide coating.

However, the work conducted by Ruppi et al. [90], which focused on controlling the orientation of α-Al_2O_3 crystals, proposes that when α-Al_2O_3 polymorph layers grow perpendicularly on the basal 0001 plane to substrate, as a result of layer growth, a highly textured, hexagonal, closed packed microstructure is formed, which in turn creates a highly thermodynamically stable coating.

The textured aluminium oxide α-Al_2O_3 microstructure provides high stability and resistance to the fluctuating shear and tensile stresses, which prevents the creation of fracture cracks between the interfacial bonding layer and the SiAlON ceramic substrate.

It is the stability of the α-Al_2O_3 interfacial layer, which provides the resistance to deformation, that is evident in Figure 6.8 and Figure 6.11. During the Coating A and Coating B scratch tests, a diamond stylus was subjected to a linearly increasing load of 100 N/min whilst being drawn at a rate of 10 mm/min across the coated surface up until the point of adhesion failure, and a critical load was reached.

Typically, before a hard coating begins to fail, it will suffer from the formation of microcracks at the surface of the scratch. Therefore, determining the "lower critical load" (L_{C1}) is important for clarifying the minimum load value at which the cracks first begin to develop. Another important value to determine is the "higher critical load" (L_{C2}), which determines when complete delamination of the coating begins.

One of the key tasks of the research in this chapter, was determining the critical load strength of the two coatings, which was important in defining the difference in mechanical properties between Coatings A and B. The critical scratch loads for two stages of coating deformation are captured in Figure 6.2.

Equation (6.1) was used to calculate the critical load L_{CN} value for both Coating A and Coating B. L_{C1} – the critical scratch load in N, L_{rate} – the rate of force application (N/min) in specific test, l_N – the distance in mm between the start of the scratch track, X_{rate} – the rate of horizontal

displacement (mm/min) in the specific scratch test and L_{start} – the preload stylus force in newtons established at the start of the scratch test.
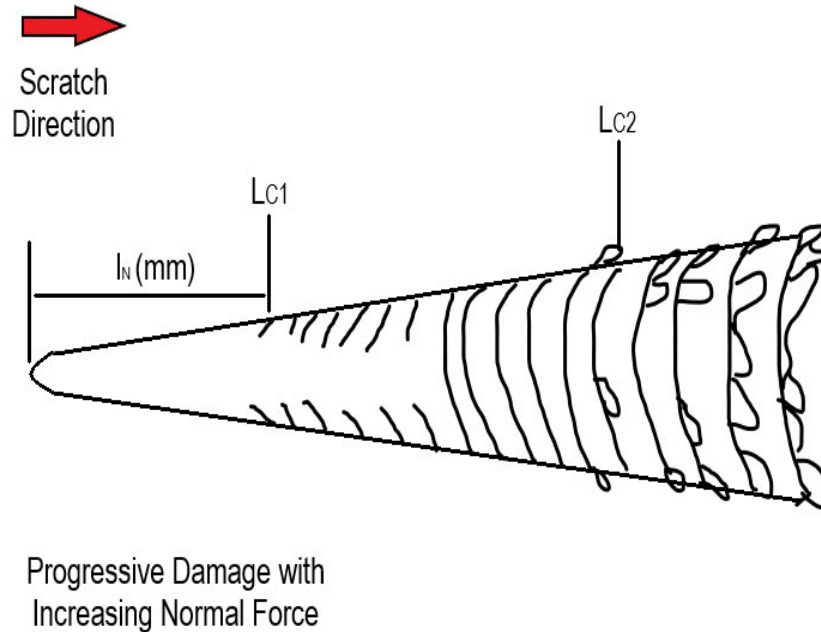
Figure 6.2. Critical Scratch Load Damage Features in Progressive Load Test. [96]

For both coatings, the L_{C2} = L_{C1}. This is due to Coating A catastrophically failing in the coating/substrate interface after a linear distance of 1.057mm. The coating/substrate interface failure of Coating A resulted in complete delamination of the coating for the rest of the scratch. Coating B deformed but did not fail at any point along the entire scratch, therefore L_{C2} = L_{C1}.

$$L_{C1} = \left[L_{rate} - \left\{\frac{l_N}{X_{rate}}\right\}\right] + L_{start} \qquad \text{Equation 6.1}$$

$$Coating\ A\ L_{C1} = \left[100(\text{N/min}) - \left\{\frac{1.057(\text{mm})}{10(\text{mm/min})}\right\}\right] + 0 = 10.57\text{N} \pm 0.001\text{N}$$

$$Coating\ B\ L_{C1} = \left[100(\text{N/min}) - \left\{\frac{9.89(\text{mm})}{10(\text{mm/min})}\right\}\right] + 0 = 99.01\text{N} \pm 0.001\text{N}$$

For both coatings, the L_{C2} = L_{C1}. This is due to Coating A catastrophically failing in the coating/substrate interface after a linear distance of 1.057mm. The coating/substrate interface

124

failure of Coating A resulted in complete delamination of the coating for the rest of the scratch. Coating B deformed but did not fail at any point along the entire scratch, therefore $L_{C2} = L_{C1.}$
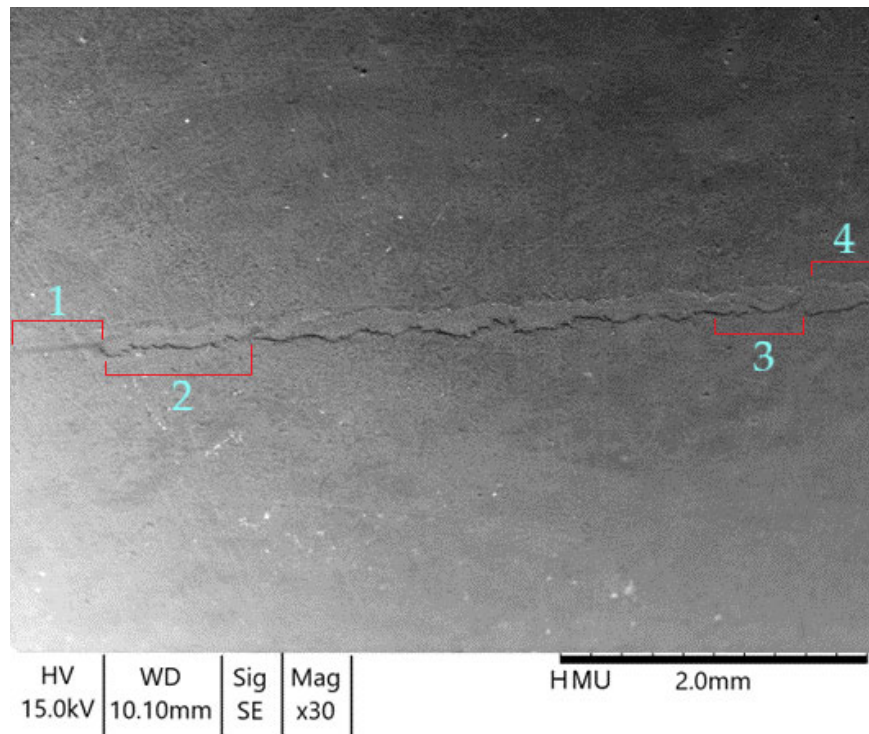
Figure 6.3. Coating A scratch Position 1, 2, 3, 4 at x30 Mag.

The image that is shown in Figure 6.3 highlight the deformation of the scratch at different stages. The weak adhesive properties of Coating A are demonstrated in Figure 6.4(a-b), Figure 6.5(a-b), Figure 6.6(a-b) and Figure 6.7(a-b).
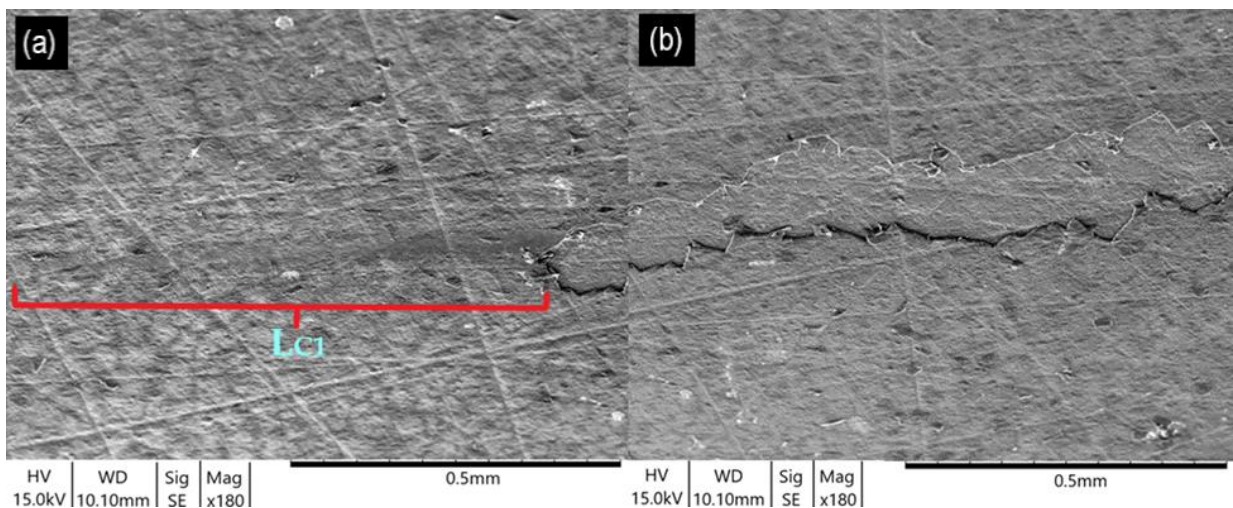
Figure 6.4. (a) Coating A Scratch Position 1, Initial scratch L_{C1}, (b) Coating A scratch Position 2 Coating fracture and delamination position, at x180 magnification.

The inadequate adhesion being to the SiAlON ceramic substrate, demonstrated by Coating A, was due to the low strength interfacial bonds that had been formed between the titanium nitride (TiN) interfacial bond layer and SiAlON ceramic substrate.
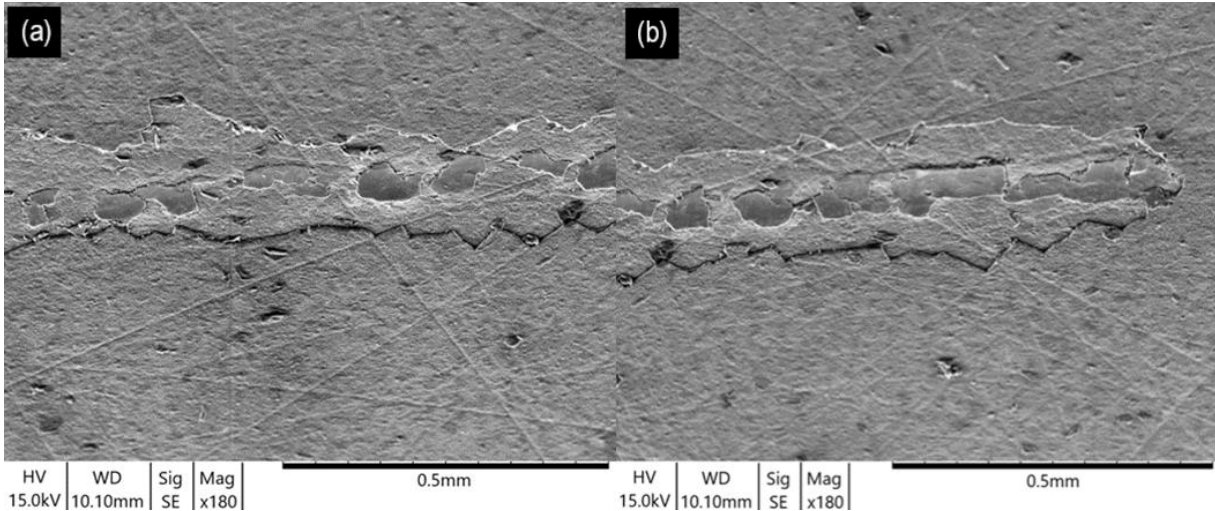
Figure 6.5.(a) Coating A scratch position 3 (continued delamination and spalling) and (b) Coating A scratch position 4 (end of the scratch SEM) at ×180 magnification.

After 1.0 mm of linear travel at a load of 10.57 N $\pm$ 0.001 N, tensile and shear stresses culminated in a sudden total fracture of the coating. Therefore, $L_{C1} = L_{C2}$ for Coating A, which was 10.57 N $\pm$ 0.001 N.
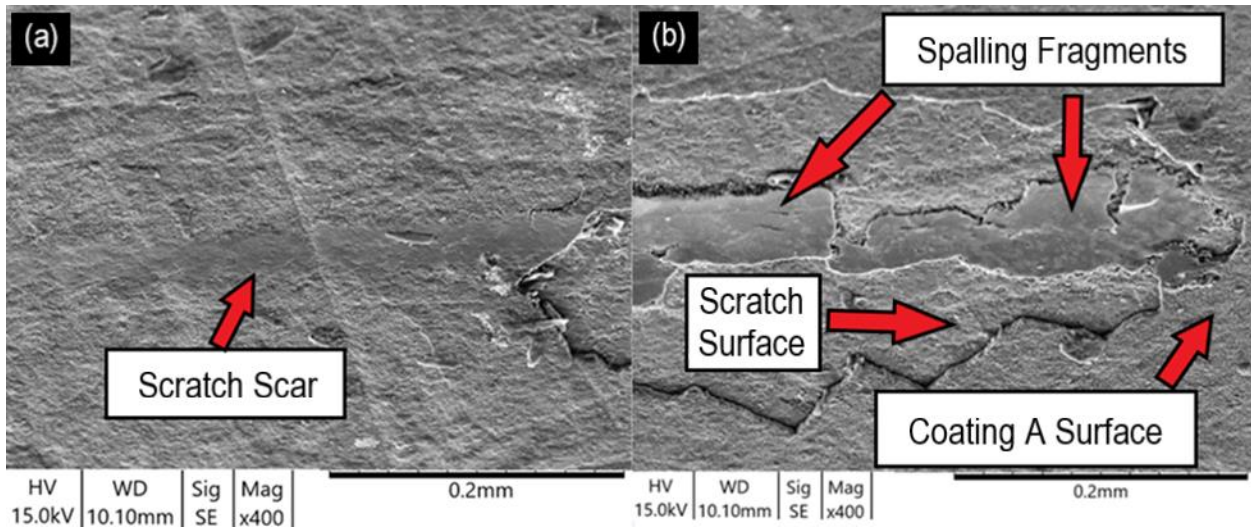
Figure 6.6. (a) Coating A Scratch Position 1, Initial scratch L_{C1}, (b) Coating A scratch Position 4, End of Scratch SEM, at x400 magnification.

The inability of Coating A to adequately distribute the linearly increasing tensile and shear stresses throughout the coating microstructure resulted in the delamination of Coating A from

126

the SiAlON ceramic substrate. Characteristically, hard coatings deteriorate from small cracks prior to failure, though here, Coating A failed catastrophically as result of brittle and weak interfacial layers, which in turn initiated the delamination of the rest of the coating as load was increased.
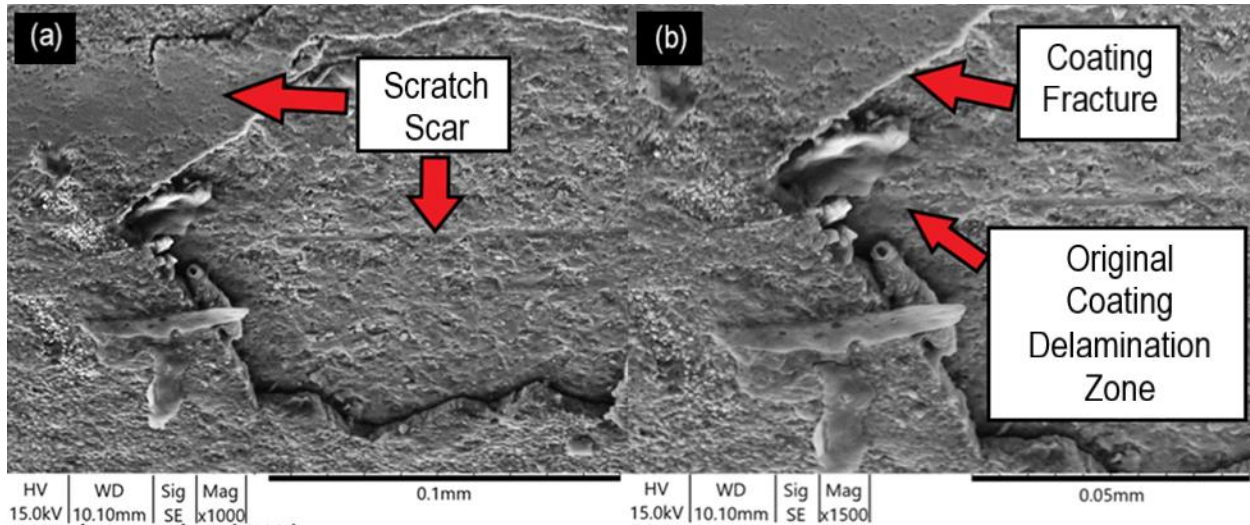
Figure 6.7. (a) Coating A Scratch Position 1, Initial scratch L_{C1}, at x1000 magnification (b) Coating A Scratch Position 1, Initial scratch L_{C1}, at x1500 magnification.

As the coating load increased, the spalling effects increased, and this is evident in Figure 6.6(b). The principal cause for the abrupt failure of Coating A can be credited to the low strength interatomic bonds being initiated between the isomorphic phases of titanium nitride (TiN) (lattice structure) in which metallic bonds occur.

These metallic bonds do not have the same capability to share valence electrons with the SiAlON covalent microstructure on an interatomic level as ionic bonds of Al_2O_3 have. The metallic covalent interactions between TiN and SiAlON ceramic atoms resulted in the creation of low-strength energy sites for nucleation, which in turn initiated the creation of low-strength interatomic bonds between the covalent microstructure of the silicon aluminium oxynitride (SiAlON) ceramic. Hence, once the TiN and the SiAlON ceramic interfacial bonds were exposed to adequate fluctuating shear and tensile stresses, interfacial cracks started to propagate and were thus the root cause of Coating A catastrophically failing after travelling 1.0 mm.

The image in Figure 6.8 highlights the deformation of the scratch at different stages. Figure 6.9 and Figure 6.10 illustrate the lack of coating deformation and subsequent delamination. There is no noticeable cracking when compared to the level of wear that can be viewed in Figure 6.3 and Figure 6.7 with Coating A.
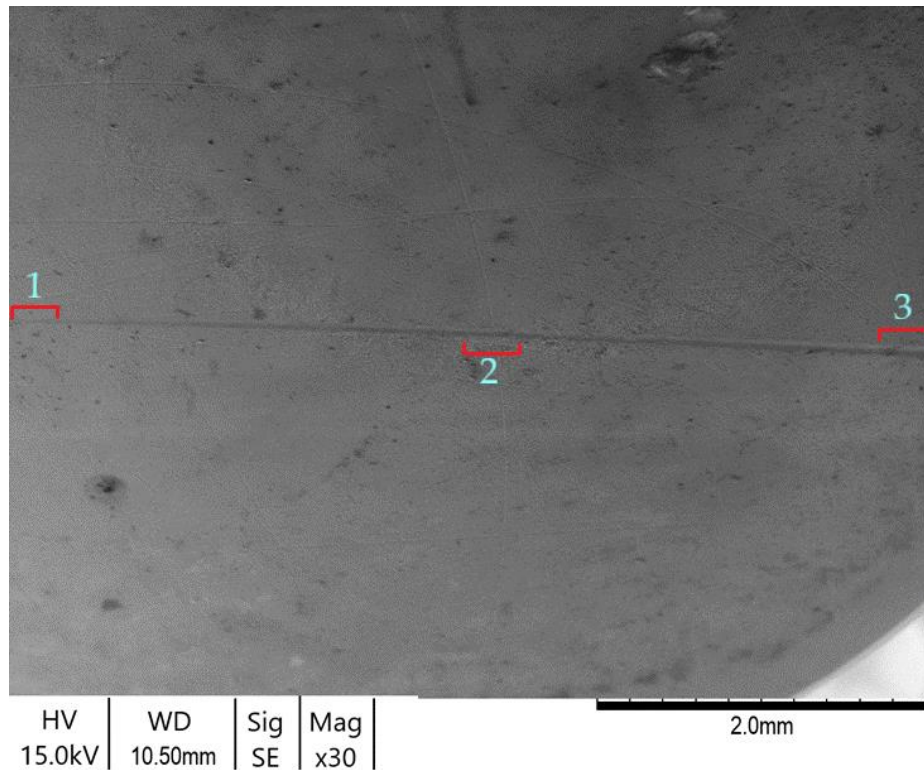
Figure 6.8. Coating B scratch Position 1, 2, 3, at x30 magnification.

Figure 6.9(a-c), Figure 6.10(a-b) and Figure 6.11(a-b) highlight the lack of physical degradation of the coating, which suggests that the interface that was created between the α-Al$_2$O$_3$ and the SiAlON ceramic substrate formed high strength interatomic bonds.
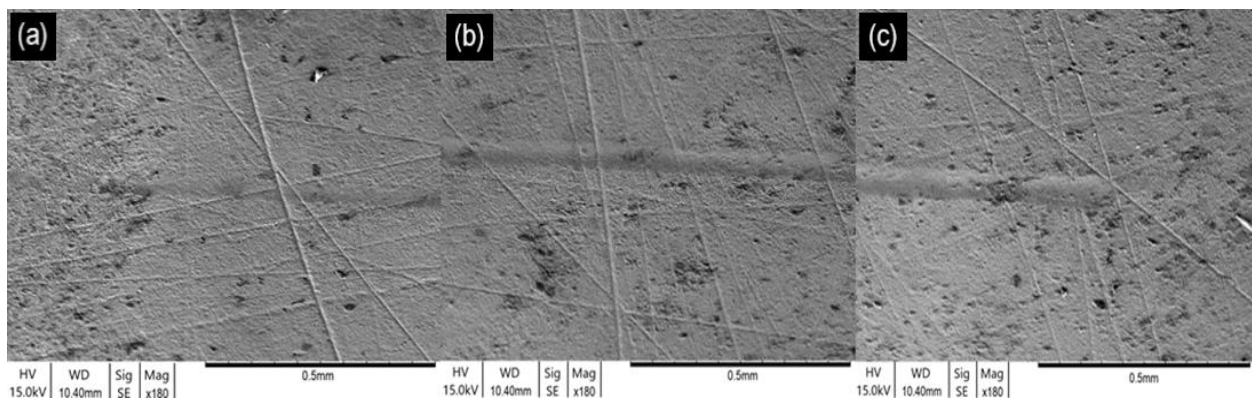
Figure 6.9. (a) Coating B scratch Position 1, (b) Coating B scratch Position 2, (c) Coating B scratch Position 3, at x180 magnification.

Aluminium oxide (α-Al$_2$O$_3$) ionic bonds have the capability to share valence electrons with the SiAlON ceramic covalent microstructure. This resulted in the electronegativity interactions between Al$_2$O$_3$, and SiAlON ceramic atoms, which initiated high energy sites for the nucleation

of the α-Al$_2$O$_3$ interfacial layer atoms onto the surface of the SiAlON ceramic substrate. High interatomic bonds were then formed with the covalent microstructure of the silicon aluminium oxynitride (SiAlON) ceramic.
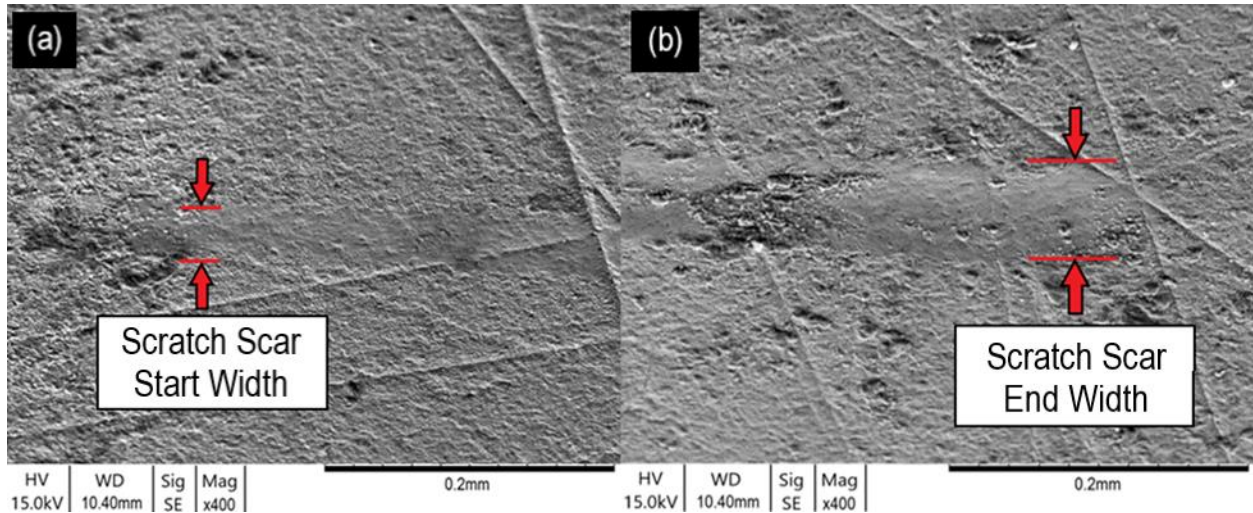
Figure 6.10. (a) Coating B scratch Position 1, (b) Coating B scratch Position 3, at x400 magnification.

Furthermore, the tribological interaction of the diamond stylus between Coating A and B was different as the friction coefficient between the aluminium oxide (α-Al$_2$O$_3$) outer layer of Coating A was slightly higher than the titanium nitride (TiN) outer layer of Coating B, but not significantly so. However, this particular characteristic would have had an effect on the sliding contact stresses, which were transmitted through the stylus tip into the surface of the coating.
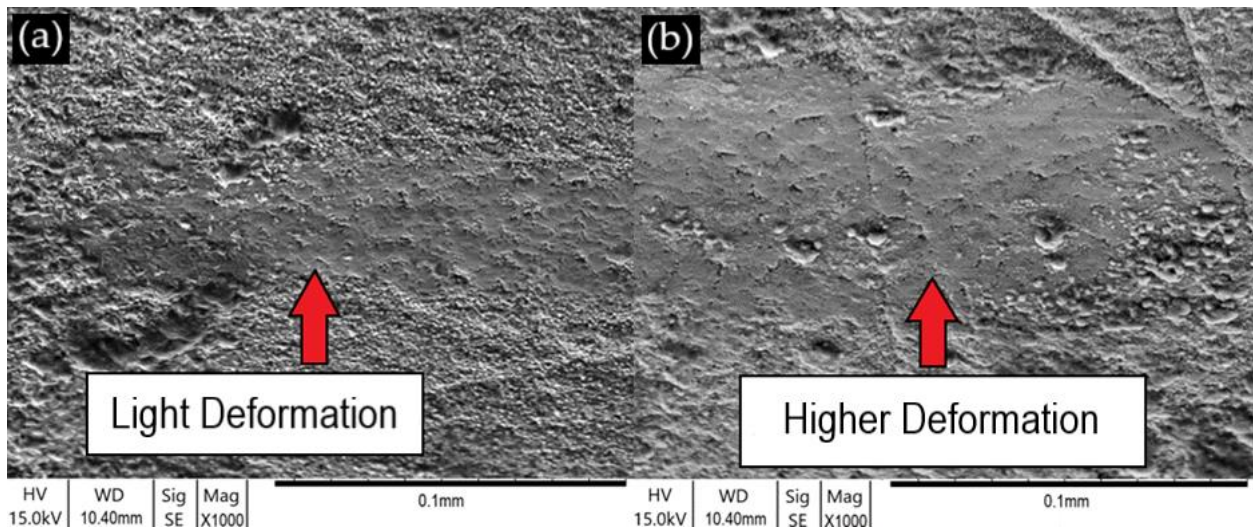
Figure 6.11. (a) Coating B scratch Position 1, (b) Coating B scratch Position 3, at x1000 magnification.

129

Nonetheless, Coating B succeeded in withstanding the fluctuating shear and tensile stresses, which were transmitted through the stylus up to a maximum load of 100 N.

Therefore, the L_{C1} value for Coating B was >100 N, and, since there had not been any deformation or complete failure in Coating B, L_{C1} = L_{C2}; thus, the higher critical load, L_{C2}, is >100 N. The lack of deformation for Coating B is represented by the width of the wear scar in Figure 6.10(a) and Figure 6.10(b). As a result of Coating B exhibiting superior resistance to deformation, and due to the complete lack of delamination, it is suggested that amorphous α-Al_2O_3 should be utilized in this type of coating and for future coating applications.

6.3 Results – Pin-on-disc Test Analysis

In Section 3.1.2 and 3.3.3 and Section 3.3.2 of Chapter 3, the 3D profilometric, scanning electron microscopy techniques and pin-on-disc techniques are discussed, these techniques have been utilised throughout Section 6.3 and 6.5 of this chapter. Section 3.3.2 and 3.3.5 provides the basis of the pin-on-disc techniques that were utilised to perform the pin-on-disc testing on the two coated SiAlON inserts.

The results of pin-on-disc testing for Coating A and B for Tests 1a and 2a are shown in in Figure 6.12 and Test 1b and 2b are shown in Figure 6.13, respectively. From the Hertzian analysis, the applied loads that Coating B was subjected to were higher than the applied loads that Coating A were subjected to. This is because of the better resistance to deformation of the coating microstructure that is exhibited by Coating B when compared to the stability of Coating A.

(a)
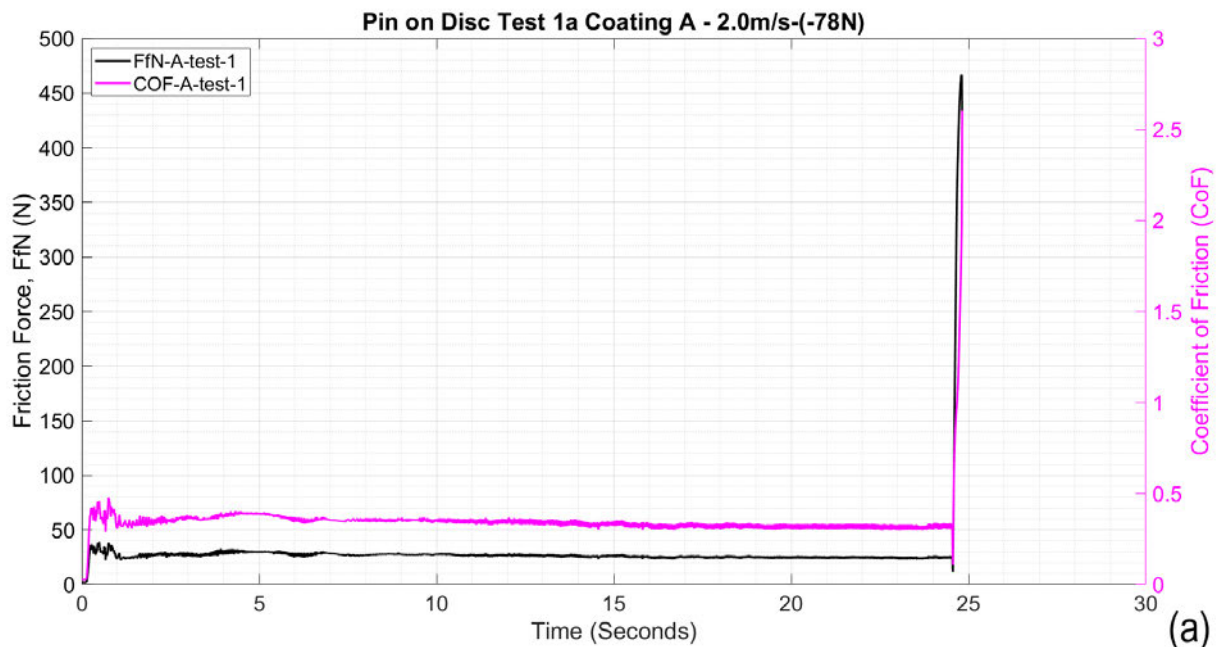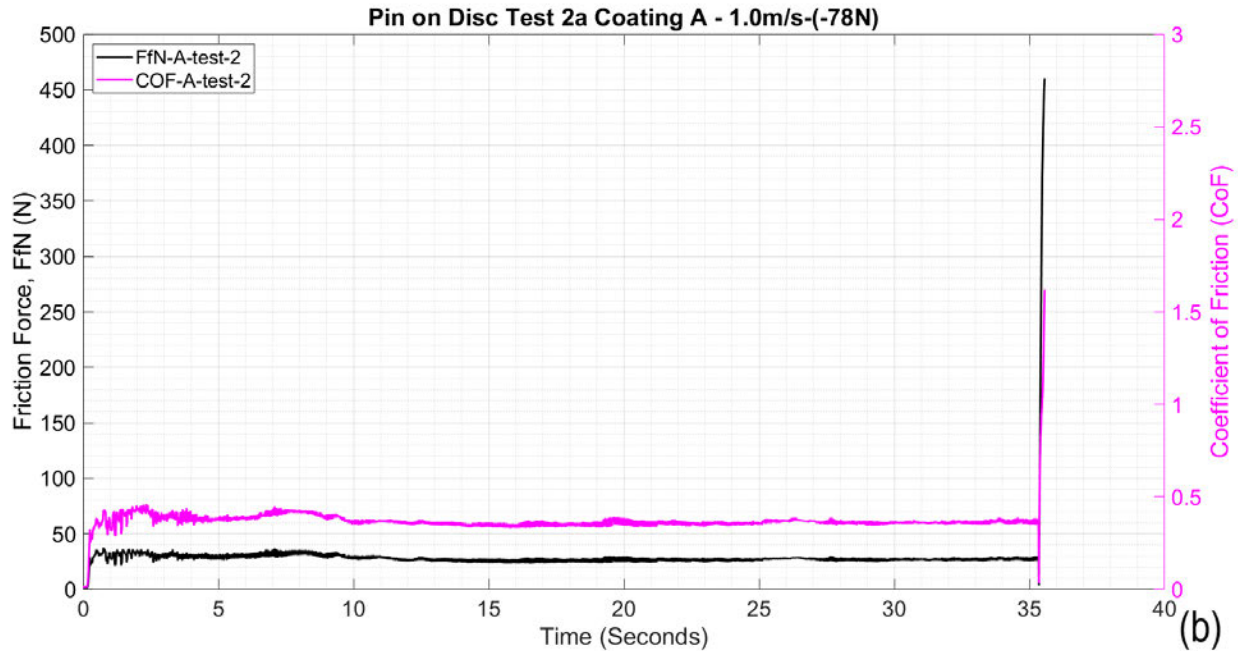
Figure 6.12. Friction coefficient plot vs. time (seconds) vs. friction force (N): (a) Test 1a and (b) Test 2a for Coating A.

To reach the required 1000 m sliding distance stipulated in ASTM Standard Test Method G-99-17 [99], the tests would each need to last 496 seconds. As a result of the contact conditions the two CVD coatings quickly degraded after about 22 seconds at linear velocity 2.0 m/s in Test 1a and Test 1b.
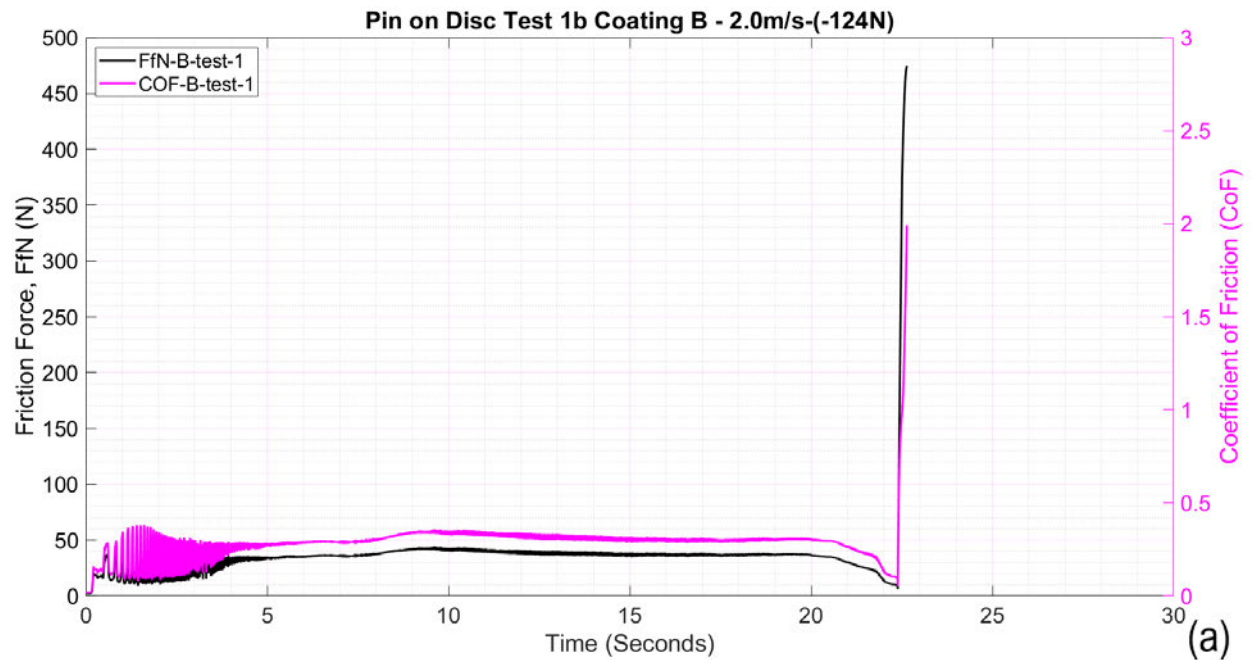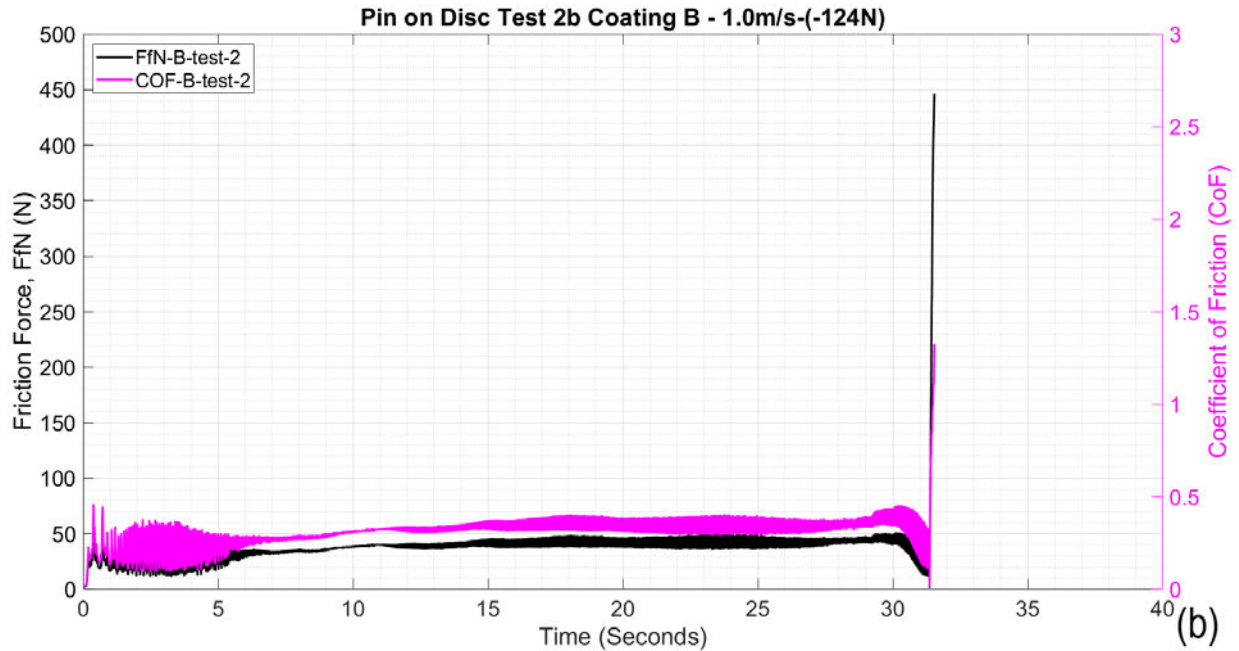
Figure 6.13. Friction coefficient plot vs. time (seconds) vs. friction force (N): (a) Test 1b and (b) Test 2b for Coating B.

For the first three seconds for the Tests 1a and 1b, the applied loads of 78 N and 124 N were applied to the surface of the CVD coated inserts. The insert support fixture was spun up to a linear velocity of 2.0 m/s for the first test. Then the test fixture was spun up to a linear velocity of 2.0 m/s for the second test. The applied loads were applied by the actuator and measured by the load cell transducer, together with a sliding velocity of 2.0 m/s for Test 1a and Test 1b, which culminated in Coating A failing after 24.81 seconds Figure 6.12(a). The calculated sliding distance and the times are shown in Table 6.1.

Table 6.1. Pin-on-disc test Sliding Distance Results.

Test No	Tool Material	Linear Velocity (m/s)	Load (N)	Time (s)	Sliding Distance (m)
1a	CTIS710 SiAlON +Type A Coating	2.0	78	24.81	29.78
1b	CTIS710 SiAlON +Type B Coating	2.0	124	22.64	27.16
2a	CTIS710 SiAlON +Type A Coating	1.0	78	35.56	42.67
2b	CTIS710 SiAlON +Type B Coating	1.0	124	31.54	37.84

Once the fixture had reached a linear velocity of 2.0 m/s, the 4.0 mm diameter 52100-steel ball counter specimen quickly succumbed to high frictional forces in the contact region and began to degrade and wear quickly. The friction coefficient for Coating A, as seen in Figure 6.12(a), remained constant until the adhesion between the now heavily worn steel ball counter specimen, as seen in Figure 6.14 and Coating A (Region 4 in Figure 6.16a) resulted in

delamination of Coating A (Regions 1 and 2 in Figure 6.15) and (Regions 5 in Figure 6.16b). Once Coating A began to delaminate and the coefficient of friction increased sharply, Test 1a was stopped.

The primary reason for the failure of Coating A is likely due to the weak interfacial bonds being created between interfacial layer of titanium nitride (TiN) and the SiAlON ceramic substrate. Although Test 1b for Coating B lasted a slightly shorter period of time at 22.64 seconds, and Coating B was exposed to a higher applied load, the improved wear characteristics of Coating B when compared to Coating A are evident in Figure 6.17. The red boxes seen in Figure 6.15, Figure 6.16, Figure 6.17, Figure 6.18, Figure 6.19, Figure 6.20, Figure 6.21 and Figure 6.22 signify areas of interest for further magnification.
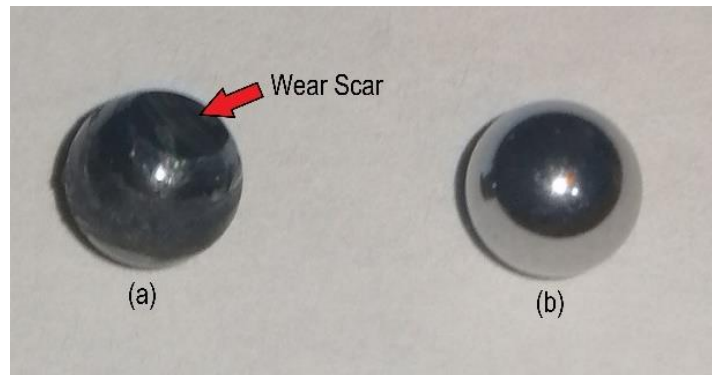
Figure 6.14. (a) Worn 4mm diameter 52100 steel ball pin-on-disc Test 1a- Coating-A, (b) Unused 4.0 mm diameter 52100 steel ball.
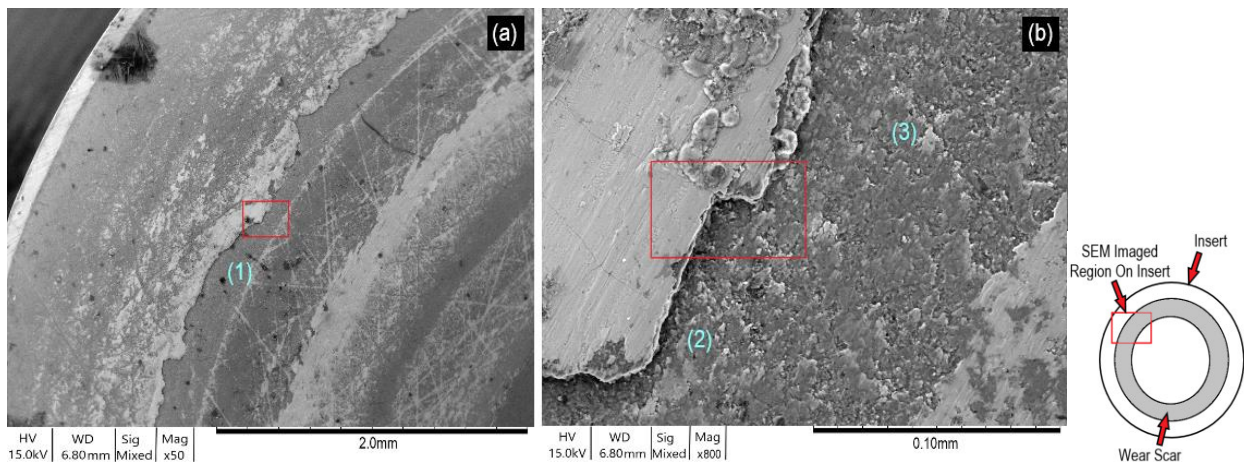
Figure 6.15. SEM images of Coating A after pin-on-disc Test 1a: (a) ×50 magnification, (b) ×800 magnification.

The high hardness contributes to low friction between the steel ball counter specimen, when compared to the frictional characteristics of the aluminium oxide Al_2O_3 outer layer of Coating A.

Figure 6.16. SEM images of Coating A after pin-on-disc Test 1a, (a) x1500 magnification, (b) x3000 magnification.

The high resistance to delamination of Coating B (Regions 1, 2, in Figure 6.17) and (Regions 4, 5, in Figure 6.18), compared to the delamination of Coating A (seen in Regions 1, 2 in Figure 6.15) and (Region 5 in Figure 6.16b). The friction coefficient for Coating B fluctuated slightly, as seen in Figure 6.13(a). The fluctuating friction forces levelled out until the adhesion between the now heavily worn steel ball counter specimen and Coating B became excessive, as represented in Figure 6.14.
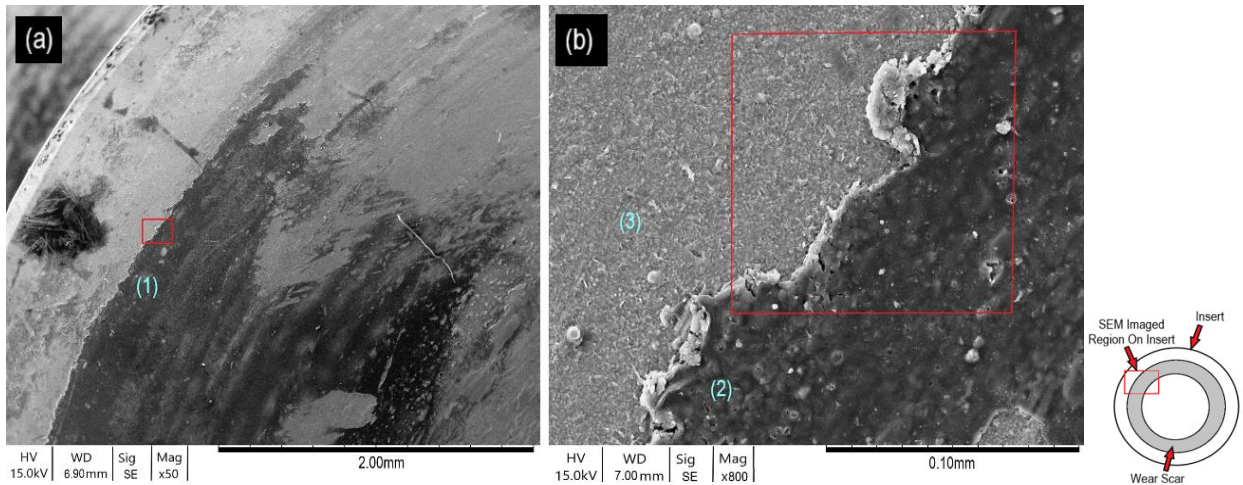
Figure 6.17. SEM images of Coating B after pin-on-disc Test 1b, (a) x50 magnification, (b) x800 magnification.

The higher adhesion characteristics, greater resistance to deformation and delamination of Coating B were likely attained due to high interfacial ionic/covalent bonds being created between the interfacial layer of amorphous α-Al_2O_3 and the SiAlON ceramic substrate.

134

Figure 6.18. SEM images of Coating B after pin-on-disc Test 1b, (a) x1500 magnification, (b) x3000 magnification.

The lower friction characteristics of titanium nitride (TiN) micro-structure can be attributed to the higher stability characteristics. Shoja et al. [116], concluded that α-Al_2O_3 coatings plastically deform on the rake face at different locations with different slip systems. The basal slip system is mostly activated during deformation, which is followed by the first and second prismatic slip systems.

This type of deformation correlates into a controlled and effective dispersion of the applied loads between the steel ball counter specimen and Coating B. The high stability characteristics and low coefficient of friction of the TiN outer layer, together with the higher stability and robustness of the amorphous α-Al_2O_3 interfacial layer of Coating B compared to Coating A, created a coating microstructure that was equipped to resist and distribute the high loads being applied. M'Saoubi et al. [117], conclude in their research that that a textured α-Al_2O_3 microstructure that has a controlled crystal orientation. M'Saoubi et al also conclude that subsurface α-Al_2O_3 layers was the result of the activation of basal slip mechanism, which is attributed to a combination of shear stress at high cutting temperatures on the rake face. The high resistance to deformation as can be seen in Figure 6.17 and Figure 6.18. The textured microstructure exhibits very high stability when subjected to high load forces at ambient temperatures have been applied.

For Tests 2a and 2b (Figure 6.19, Figure 6.20, Figure 6.21, and Figure 6.22) the test fixture linear velocity was reduced to 1.0 m/s when compared to the linear velocity of 2.0 m/s that was utilised in Tests 1a and 1b for Coating A and B. The reduction in linear velocity was undertaken to investigate if this would have an impact on the sliding distance that could be attained before failure and the wear characteristics that had been evident in Test 1a and 1b for both Coating A

135

and Coating B. The friction coefficient for Coating A, as seen in Figure 6.12(b), remained near-constant until the adhesion between the now heavily worn steel ball counter specimen as represented in Figure 6.14.
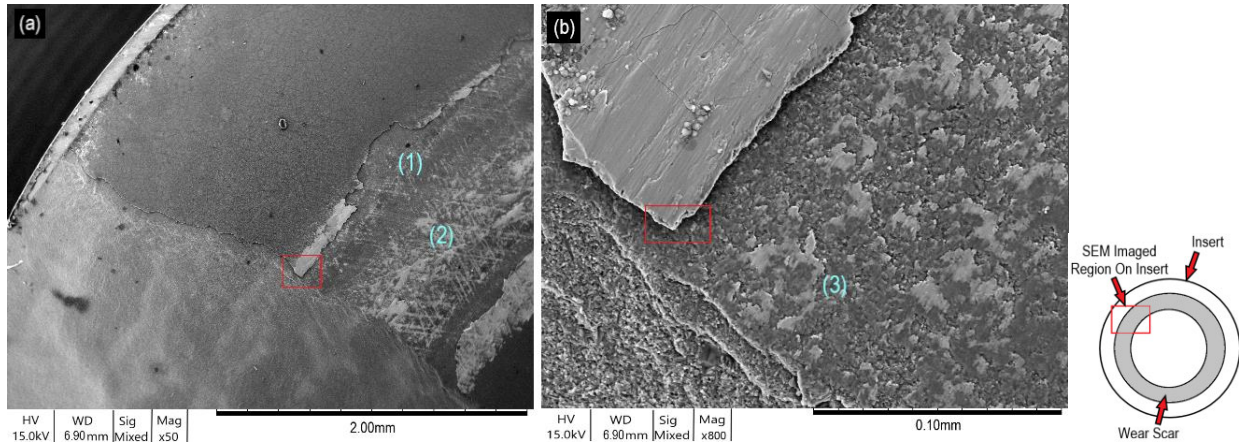
Figure 6.19. SEM images of Coating A after pin-on-disc Test 2a, (a) x50 magnification, (b) x800 magnification.
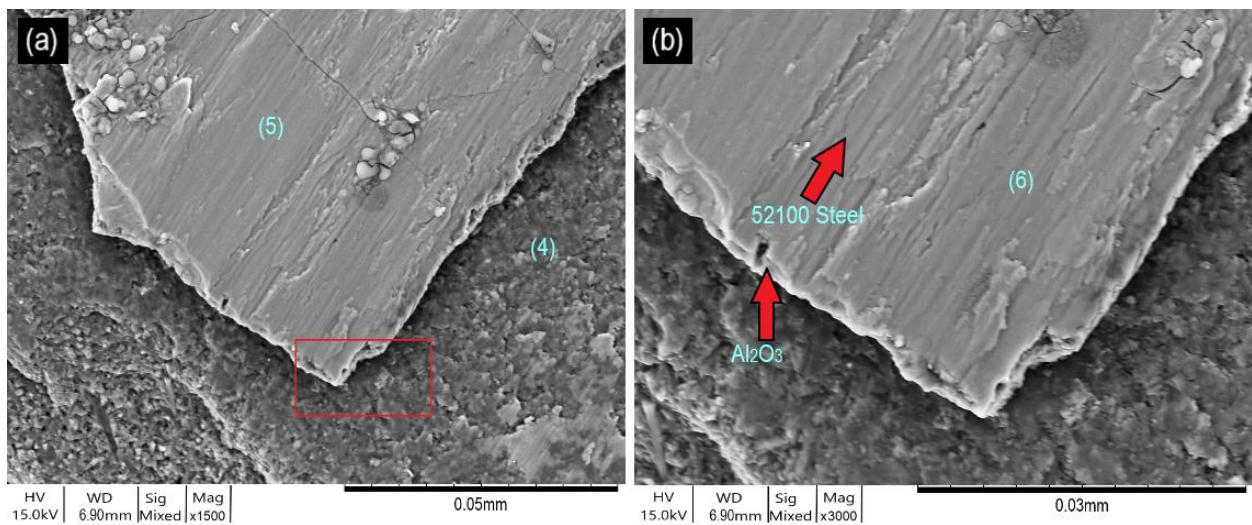
Figure 6.20. SEM images of Coating A after pin-on-disc Test 2a, (a) x1500 magnification, (b) x3000 magnification.

However, when the insert support fixture had reached a linear velocity of 1.0 m/s, the 4.0 mm diameter steel ball counter specimen began to degrade and wear as result of the high forces in the contact region. The degradation of the Coating A and the steel ball was slightly slower and resulted in the Test 2a being stopped after a time of T=35.56 seconds. The friction coefficient as seen in Figure 6.12(b) remained near constant, until the adhesion between the heavily worn steel ball counter specimen and Coating A (Regions 5 and 6 in Figure 6.20) resulted in delamination. Once Coating A began to delaminate and the coefficient of friction increased

quickly, from 0.43 up to 2.7 as seen in Figure 6.12(b), Test 2a was stopped. Coating A failed as result of weak interfacial bonds being created between the titanium nitride (TiN) interface layer and SiAlON ceramic substrate. What was apparent in both Tests 1a and 2a for Coating A and Tests 1a and 2a for Coating B, was that the steel ball degraded quickly, which is represented in Figure 6.14. The degradation was due to thermomechanical wear of steel ball counter specimen, which is evident by the formation of circular metallic wear tracks being left on the insert rake face (Region 1 and 2 in Figure 6.21a).
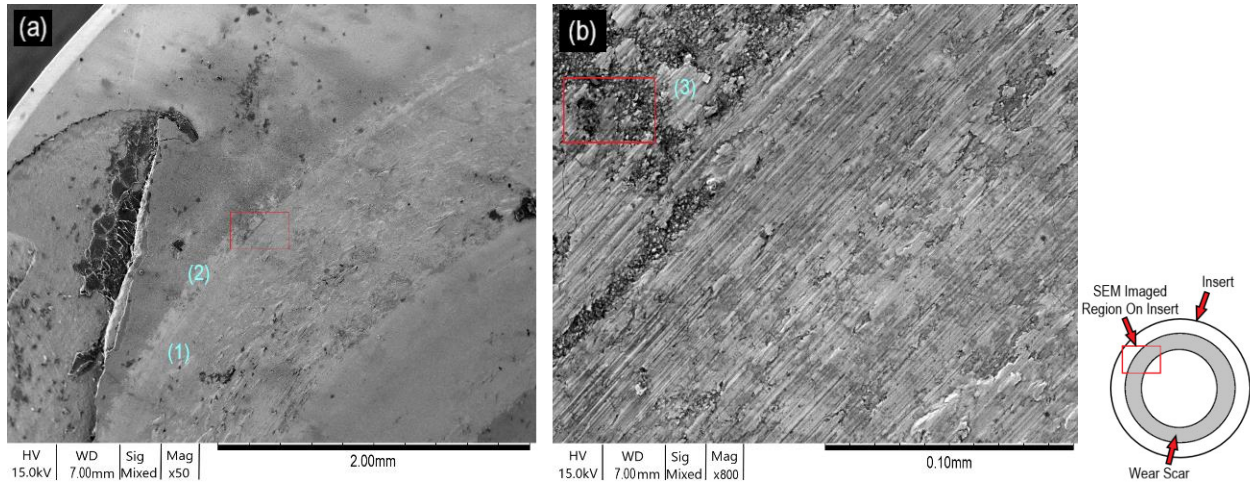
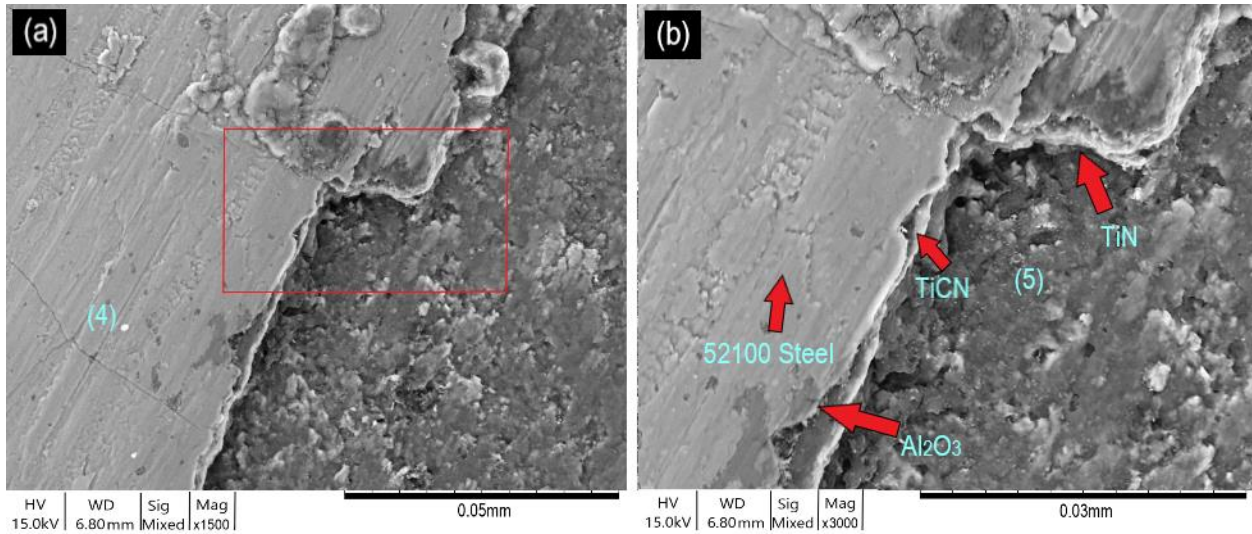Figure 6.21. SEM images of Coating B after pin-on-disc Test 2b, (a) x50 magnification, (b) x800 magnification.

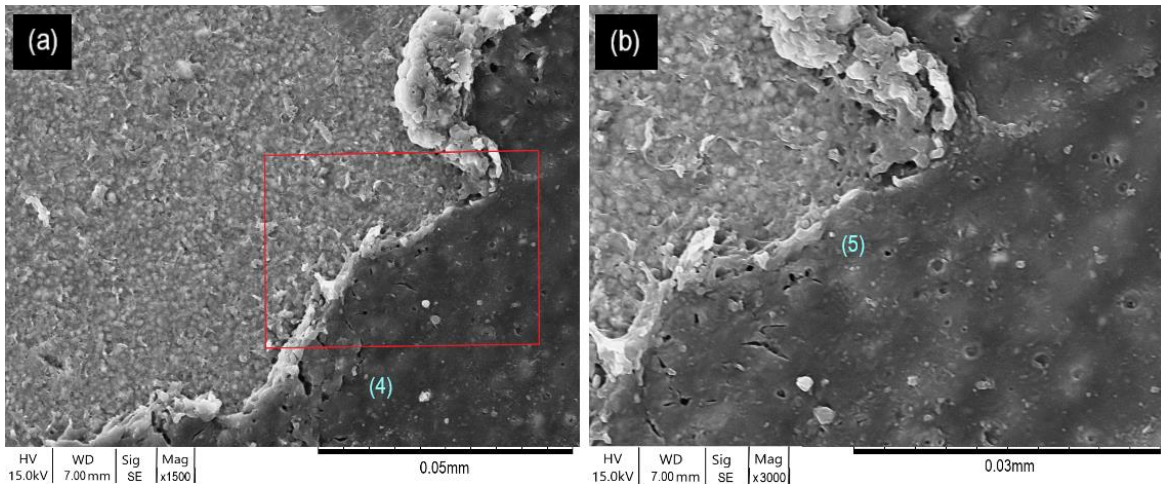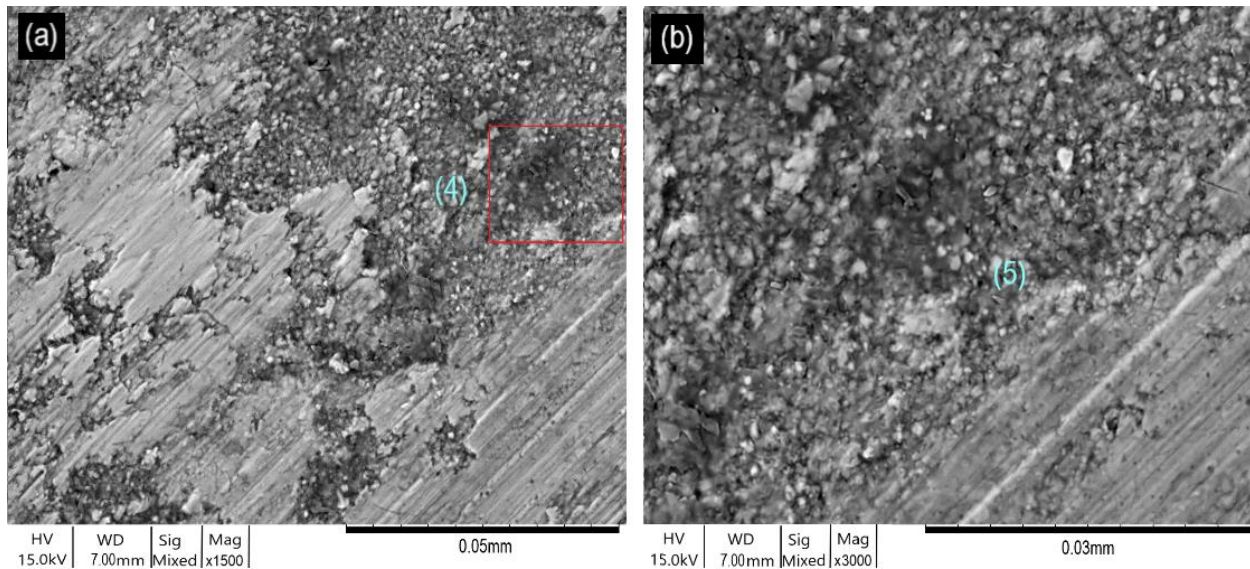Figure 6.22. SEM images of Coating B after pin-on-disc Test 2b, (a) x1500 magnification, (b) x3000 magnification.

The metallic wear track was a result of degradation and wear of the steel ball counter specimen (Figure 6.14), which in turn increases the contact area. Once the adhesion between the worn

137

steel ball counter specimen and the outer layer of the Al_2O_3 was sufficient, the tensile stresses being induced into the coating microstructure in the contact region, prompted the titanium nitride (TiN) interfacial layer to shear, which quickly resulted in coating delamination. For Test 2b with Coating B, the high stability of Coating B is evident in Figure 6.21 and Figure 6.22.

The lack of deformation of the Coating B can be in seen in (Regions 1 and 2 in Figure 6.21). What was clear from Tests 1b and 2b, was that the bilayer (Al_2O_3+TiN) micro-structure of Coating B resisted the compressive stress being induced into the coating microstructure. The resistance to the fluctuating compressive stresses originated from high interfacial bonds being created in the Al_2O_3 coating/SiAlON ceramic substrate interface, which reduced the rate of deformation of the interface. The high wear resistance, and low coefficient of friction of titanium nitride (TiN), created a contact which suffered from less adhesion and, in turn, the level of fluctuating stresses, which led to coating failure. Test 2b for Coating B was stopped as result of the steel ball failing due to significant thermomechanical wear.

6.4. Comparing Tribological Analysis with Machining Trial Analysis

For comparison, the images seen in Figure 6.23 show SiAlON milling inserts that have been CVD coated with Coating A and Coating B. These inserts came from the same batch that have been used in the experimental tests for the pin-on-disc and scratch testing.
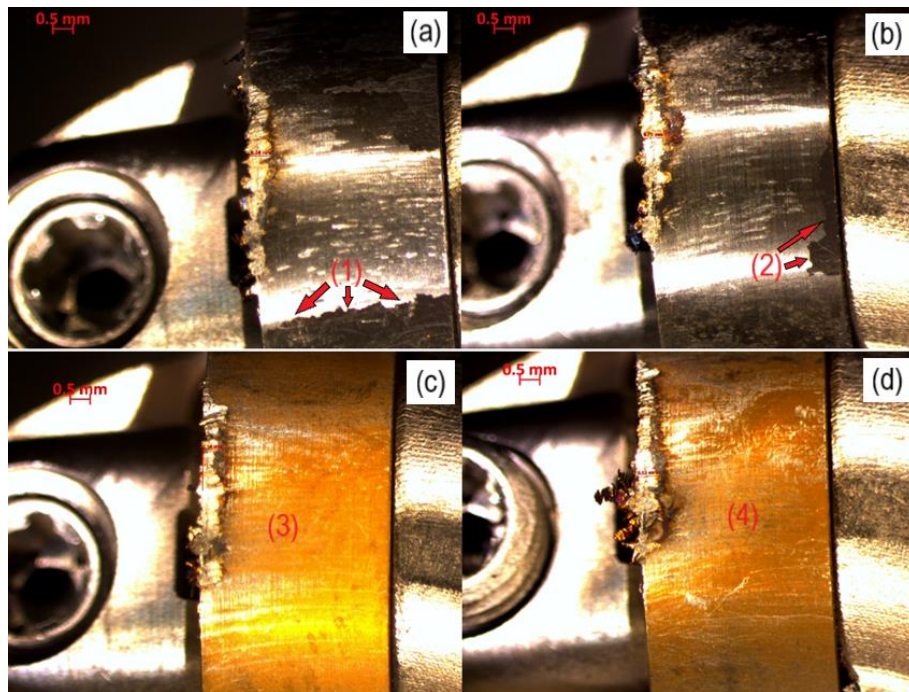
Figure 6.23. Coating A RNGN Insert Test (a) 700 m/min (b) 800 m/min, Coating B RNGN Insert Test (c) 700 m/min (d) 800 m/min.

These inserts were used in a previously completed machining trial, that utilized face milling operations. The Coating A and Coating B RNGN SiAlON milling inserts were used to machine precipitation hardened Inconel 718 specimens, with 1.0 mm Ap and 3-axis machining toolpaths. The typical cutting speed for machining Inconel 718 with SiAlON milling inserts varies from 500–1000 m/min, as stated in previous studies [38],[23],[103].

Comparing the images of Coating A in Figure 6.23(a-b) to Figure 6.15, Figure 6.16(a-b), Figure 6.1(c), Figure 6.3 and Figure 6.4(a-b), there is good correlation between coating failure, coating removal and delamination similarities and the results of pin-on-disc and scratch testing for Coating A. If the images (Region 1 in Figure 6.15(a)), (Region 2 in Figure 6.15(b)) and (Region 5 in Figure 6.16(b)) are compared with (Region 1 and 2 in Figure 6.23(a-b)), there is a coating failure and fracture and delamination. The shiny light greyish surface that is evident above coating (Region 1 in Figure 6.15(a)), (Region 2 in Figure 6.15(b)) is a freshly revealed surface of SiAlON substrate.

The same similarities and correlations are also evident for Coating B when comparing Figure 6.23(c-d) to Figure 6.17(a-b), Figure 6.1(d), Figure 6.9(a-c), Figure 6.10(a-b) and Figure 6.11(a-b) in terms of coating removal, with Coating B exhibiting high resistance to deformation and delamination. If (Region 2 in Figure 6.17(b)) and (Region 5 in Figure 6.18(b)) are compared with (Region 3 and 4 in Figure 6.23(a-b)), there is very little degradation or delamination of the Coating B coating. Which shows consistent correlation between the resistance to deformation, coating delamination and the results of pin-on-disc and scratch testing for Coating B.

6.5 Conclusions for Pin-on-disc Testing
The following conclusions can be drawn from this study:

1. Amorphous α-Al_2O_3 has very high stability as an interfacial layer coating and demonstrated very high resistance to deformation when subjected to high tensile and shear stresses. When amorphous α-Al_2O_3 is deposited onto coating materials such as TiN and TiCN, the high stability is effectively lost due dependence on metallic coating microstructures, which lacks sufficient structural stability when subjected alternating shear and tensile stresses. Therefore, multi-layered coating system such as TiN+TiCN+Al_2O_3 should be avoided for this type of cutting tool application.

2. TiN as a coating material has demonstrated a series of mechanical and tribological characteristics. Other favourable characteristics are the low frictional interactions between the

52100 steel balls in the pin on disc tests and the diamond stylus in the scratch tests. TiN has also demonstrated very high resistance to wear and abrasion. However, TiN has also exhibited low stability in the interfacial layer of Coating A. This has created a coating microstructure that is not able to resist and distribute the high compressive forces being applied in applications such as this.

6.6 Conclusions Scratch Testing

1. Coating A (TiN+TiCN+Al_2O_3) has exhibited significantly less adhesion to the SiAlON ceramic substrate than Coating B. This is due to low interfacial metallic /covalent bonds being created between the interfacial layer of amorphous TiN and the SiAlON ceramic substrate.

2. Coating B (Al_2O_3+TiN) was effectively bonded with the SiAlON ceramic substrate compared Coating A. This is due to high interfacial ionic/covalent bonds being established between the interfacial layer of amorphous α-Al_2O_3 and the SiAlON ceramic substrate.

6.7 Summary

The present chapter has endeavoured to develop further understanding and explore the main research hypothesis which has been laid out by this project.

Therefore, one of the key motivations of this chapter, has been to develop a thorough understanding of what failure mechanisms are exhibited by the coating elements and coating systems.

Experiment Three has focused on characterising the structure and tribological properties of Coating A and Coating B with two well established tribological tests, which is scratch testing and pin-on-disc testing. This chapter has attempted to establish a thorough understanding of how the two coatings fail and what useful information can be used to influence the development of Coating C.

As discussed before in Chapter 5.6, Experiment Two identified that amorphous grade Al_2O_3 had performed really well throughout the two-part machining trial. Experiment Two also identified that amorphous grade Al_2O_3 had bonded very well on an interatomic level with the CTIS710 milling insert substrate.

The impressive bonding characteristics of amorphous grade Al_2O_3 that had been displayed in the two-part machining, were also exhibited in the scratch and the pin-on-disc tests. The highly

positive scratch testing results provided great early evidence, that amorphous grade Al_2O_3 should be utilised in the future coating applications. The novelty of the scratch and the pin-on-disc results has provided further understanding of how well amorphous grade Al_2O_3 has bonded with the CTIS710 SiAlON milling substrate. The pin-on-disc results further clarified the importance of utilising amorphous grade Al_2O_3 in future coating systems.

The results of Experiment Four will look to extract useful information that has been collated in this chapter and Chapter 5 to develop Coating C. From the results and conclusions that have been established in Chapter 5 and Chapter 6, Coating C will come in the form of a single CVD layer of amorphous grade Al_2O_3. Coating C will be thicker than Coating A and Coating B as it is hoped the thicker coating structure will have higher microstructural stability at high temperatures. A series of three and five axis machining trials will be undertaken, to clarify if Coating C will improve the tool life and wear characteristics when compared to uncoated CTIS710 SiAlON milling inserts.

Chapter 7 Coating C Tool Wear Analysis and Development Machining Trial Results

All of the previous experimental chapters have included different objectives, which have contributed to and influenced the decisions for this final chapter.

Chapter 4 helped to develop some experience with using ceramic cutting tools to machine Inconel 718. It also helped determine what grade of ceramic was best suited to this research, in terms of thermomechanical wear resistance.

Chapter 5 helped to develop knowledge and experience with milling Inconel 718 at high cutting speeds. It also contributed to the selection of certain coating materials that are thought to have the capability to endure this intense machining environment.

Chapter 6 has provided further important information regarding the tribological properties of certain coating materials. The important adhesion information that was collated from the tribological testing proved to be invaluable and influenced my decision to select just a single thicker layer of amorphous α-Al_2O_3 for use in Coating C. The utilisation of a single layer of α-Al_2O_3 would simplify the chip/tool interface, which was hoped would deliver an improvement in the wear characteristics of the coating and improve the tool life.

7.1 Introduction

This chapter will determine whether Coating C, is effective at protecting SiAlON ceramic milling inserts when machining aged Inconel 718. Chapter 7 will also analyse the effect that continuous to near-continuous toolpaths have on the wear characteristics and tool life when compared to interrupted non-continuous toolpaths. In Section 3.2, tool wear capturing techniques are discussed and Section 3.11 provides the basis of the machining techniques, machining strategy (5-axis mill turning) and data capturing techniques that have been used throughout this chapter.

This chapter will look at the insert wear analysis results that were generated with the completion of Tests M14 and M15 and that of Tests M16 and M17. The results for Test M14 and M15 were generated at Ceratizit's facility based at the Advanced Manufacturing Park (AMP) in Rotherham. Tests M14 and M15 involved interrupted, non-continuous milling insert wear machining trials. Tests M16 and M17 have been conducted at the AMRC Factory of the Future (FoF) and continuous to near continuous machining trials. which continuous to near continuous machining trials. The test number, machining parameters and test sequence, which have been used in the machining trials, are stipulated in

Table 3.2 and Table 3.3 and Table 7.1. The flank wear, tool life, time in cut and material removal volume are all directly compared between Tests M1-M17 in Table 7.3.

7.2 Results (Test No M14-M15)

In this section, the machining trial described in Section 3.11.1 will be discussed. Two age hardened Inconel 718 test samples were machined with CTIS710 SiAlON ceramic milling inserts CVD coated with Coating C.

Tests M14 and M15 involved machining aged Inconel 718 specimens at cutting speeds of 800 m/min and 900 m/min with a constant feed per tooth of 0.1 mm and constant depth of cut (Ap) of 1.0 mm. The two cutting speeds of 800 m/min and 900 m/min had been selected from Tests M1-M13. The two cutting speeds were selected due to the higher tool life that had been exhibited by the Coating A and B and uncoated SiAlON inserts. The aim of Tests M14 and M15, was to understand the benefits of applying a CVD coating (Coating C) to SiAlON milling inserts. The insert wear data was captured using a USB microscope.

The results in Section 7.2 will look at the insert flank and rake face wear results, which have been collated during Tests M14 and M15. For a test to be successful, five sections are required to be machined away with x12-off 1.0 mm Ap whilst using the same cutting edge. Individually each section of material accounted for 33.929 cm^3. A successful test would mean that 169.64 cm^3 of material would have been removed as shown in Figure 3.11.

All of the bar sections were machined with an initial full radial engagement (ae) of 30.0 mm, which stays constant for about two thirds of cut and then the radial immersion reduces as each test cut travels through a full 360° and exits tangentially out of cut in the F_y-axis direction. The test number, machining parameters and test sequence which have been used in the machining trials are stipulated in Table 7.1.

Table 7.1. Test parameters machining trial. cutting conditions, used for Test No M14 and M15. All inserts had an axial rake angle -7.1°, Radial rake angle -12.3° and 0.1mm edge chamfer.

Test No	Tool Material	Bar Sections Machined	Cutting Speed (m/min)	Feed rate fz (mm/tooth)	Depth of Cut (Ap) mm	Radial Engagement (ae) (mm)
M14	CTIS710 SiAlON + Type C Coating	2-1 to 2-3	800	0.1	1.0	30.0
M15	CTIS710 SiAlON + Type C Coating	3-1	900	0.1	1.0	30.0

7.2.1 800m-min Coating C (Test No M14) Results

The first machining operation for Test M14 involved the of machining Bar Section 2-1. The cutting tool began with a tangential engagement into cut in the F_y-axis. As each cut engaged tangentially into the workpiece, the cutting tool travelled through 360°, which resulted in a gradual increase in radial immersion up to 30.0 mm ae, and then a decrease in radial immersion that ended in a tangential exit out of cut in the F_y-axis direction.

The main failure types of tool wear are highlighted in Figure 7.1(a-h), Figure 7.2(a-h) and Figure 7.3(a-h). Adhesive wear and built-up edge (BUE) are evident in (Regions 1, 2, 3 in Figure 7.1). Notch wear, adhesion wear and BUE are apparent in (Regions 1, 2, 3, 4, and 5 in Figure 7.2) and thermochemical wear, oxidation is apparent in (Regions 6, 7, 8, 9 and 10 in Figure 7.2). In (Regions 1, 2, 3, 4, 5, 6, 7, 8, 9 and 10 in Figure 7.3) a mixture of thermochemical wear, oxidation, flaking, chipping, notch wear, BUE and adhesive wear are evident. Figure 7.3 gives a good representation of the main types of tool wear which has taken place at high cutting speeds on the flank and rake face.

These types of rake and flank face wear patterns have taken place at a cutting speed of 800 m/min, when high-speed face-milling of Inconel 718 at fz=0.1 mm/tooth, Ap=1.0 mm, and ae=30.0 mm. The wear characteristics that have been demonstrated by Coating B inserts in Test 14 as seen in Figure 7.1, Figure 7.2 and Figure 7.3, have also been apparent in Figure 5.3. for Test M3 and Figure 5.4. for Tests M6 and M13.

Figure 7.1. Test No M14-Bar Section-2.1-insert-Coating-C-insert-1-4 (a-d) flank face & Insert-1-4 (e-h) rake face.

The thermal stability and adhesive properties of Coating B throughout Test M3, Test M6 and M13, have also been demonstrated by Coating C in Test M14. These properties originate from the high strength ionic bonding properties of aluminium oxide Al_2O_3 interfacial layers with the covalent microstructure of SiAlON substrate, which create a stable foundation for the outer layer of titanium nitride to be deposited onto. The high stability and superior adhesive attributes are evident in Figure 7.1(a-h). The adhesion properties that were exhibited by the Coating C inserts were very similar to the wear characteristics that has been demonstrated by Coating B.

Figure 7.2 (e-h) begins to show the degradation of Coating C flank face after the completion of Bar Section 2-2. Once the TiN outer layer of Coating C is exposed to temperatures above 800°C it begins to oxidise, which leads to a rapid reduction in the coating's mechanical properties, significantly reducing its adhesion properties and causes further coating failure.

Figure 7.2. Test No M14-Bar Section-2.2-insert-Coating-C-insert-1-4 (a-d) flank face & Insert-1-4 (e-h) rake face.

Upon the completion of Bar Section 2-3, it was evident in Figure 7.3(a-h) that the Coating C inserts exhibited progressive tool damage, which ultimately resulted in fracture on both the flank and rake face. The flaking and chipping take place due to the change in cutting edge as result of abrasive wear, which causes the contact pressures in the chip/tool interface to increase to a point that it causes the SiAlON ceramic microstructure to shear along the grain boundaries.

During the machining process, as the Coating C inserts sustain more wear on the flank and rake faces and remove more metal, the level of vibrations begin to increase. Once Coating C delaminates and flake off the inserts, a multi-layered insert contact area is created. The increase in contact area results in more of the cutting forces being transmitted through the insert

microstructure, which contributed to the exacerbation of the insert wear. The high stability and wear resistance of the α-Al$_2$O$_3$ coating is visible in Figure 7.1(e-h), Figure 7.2(e-h). The large chip that has formed on the rake face of insert 1 as seen in Figure 7.2e is likely down to a few variables.

The first main variable focuses on the alternating compressive and tensile stresses that the rake face was subjected to during the machining process. The alternating stresses have caused a build-up of residual stress in the Al$_2$O$_3$ coating. Therefore, the Al$_2$O$_3$ coating has sheared along polymorphic grain boundaries due to high contact pressures and friction on the rake face.

Figure 7.3. Test No M14-Bar Section-2.3-insert-Coating-C-insert-1-4 (a-d) flank face & Insert-1-4 (e-h) rake face.

A few variables were added because of a 0.5 μm thick TiN coating being wrongly deposited onto the surface of the α-amorphous Al$_2$O$_3$ 6.5 μm thick coating.

The first variable is associated with thermal cooling stresses, which have been induced into the α-amorphous Al$_2$O$_3$ coating microstructure during the deposition of the TiN outer layer.

The second variable is the removal of the TiN outer coating during post processing. The removal of the TiN coating via post processing will have introduced further residual stresses into the SiAlON substrate and the Al$_2$O$_3$ microstructure.

The third variable is the introduction of compressive stresses which have been induced in the coating microstructure because of polishing. The fourth variable is a result of a stress release. The stress release is a result of the coating microstructure being exposed to high cutting

temperatures in the chip/tool interface, the cutting temperature in the chip/tool interface increase as the insert begin to degrade and wear.

7.2.2 900m-min Coating C (Test No M15) Results

The first machining operation for Test M15 involved the of machining Bar Section 3-1. The cutting tool began with a tangential engagement into cut in the F_y-axis. As each cut engaged tangentially into the workpiece, the cutting tool went through a full 360°, which resulted in a gradual increase in radial immersion up to 30.0 mm ae, and then a decrease in radial immersion that ended in a tangential exit out of cut in the F_y-axis direction. Figure 7.4(a-h) highlights that the main failure types of tool wear which takes place at high cutting speeds on the flank and rake face. Built-up edge (BUE) is evident in (Regions 1 and 5 in Figure 7.4).

Flaking, chipping, notch wear and adhesive wear are apparent in (Regions 2, 3, 4 and 7 in Figure 7.4) and thermochemical wear, oxidation is apparent in (Regions 6, 8, and 9 in Figure 7.4). These types of rake and flank face wear patterns has taken place at a cutting speed of 900 m/min, when high-speed face-milling of Inconel 718 at fz=0.1 mm/tooth, Ap=1.0 mm, and ae=30.0 mm. Once again, the wear characteristics that were exhibited by the Coating C inserts were very similar to the wear characteristics that have been demonstrated by Coating B inserts in previous machining trials. Upon the completion of Bar Section 3-1, that the Coating C inserts exhibited substantial amounts of wear on both the flank and rake face for all four of the inserts, this it is evident in Figure 7.4(a-h). The Coating C inserts displayed thermomechanical wear characteristics that were very similar to the wear characteristics that had been demonstrated previously by the Coating B inserts.
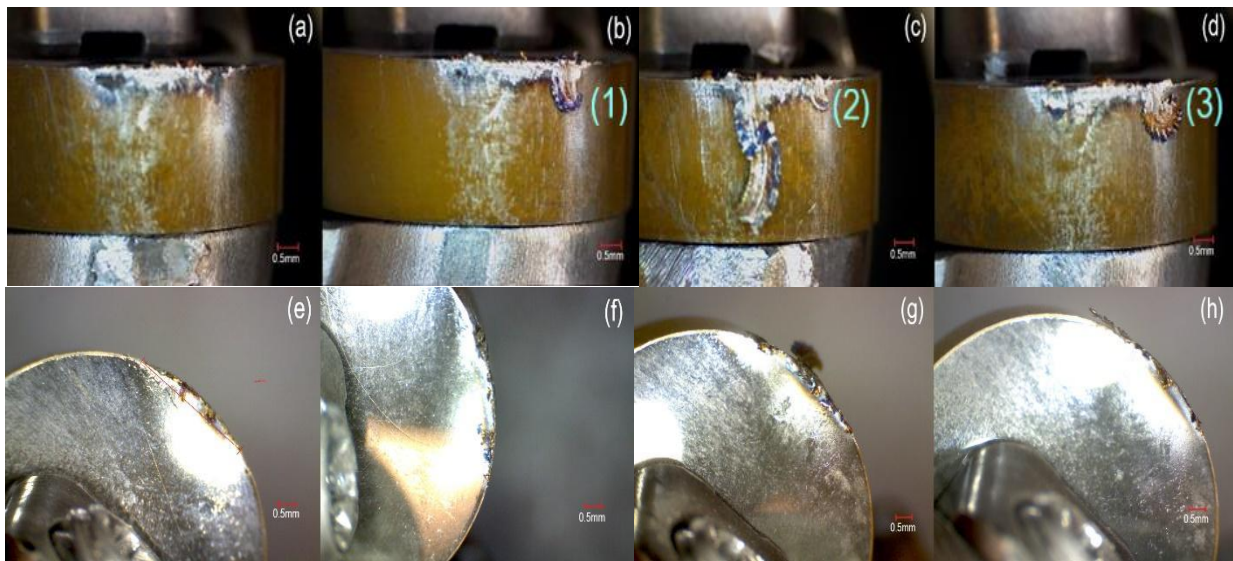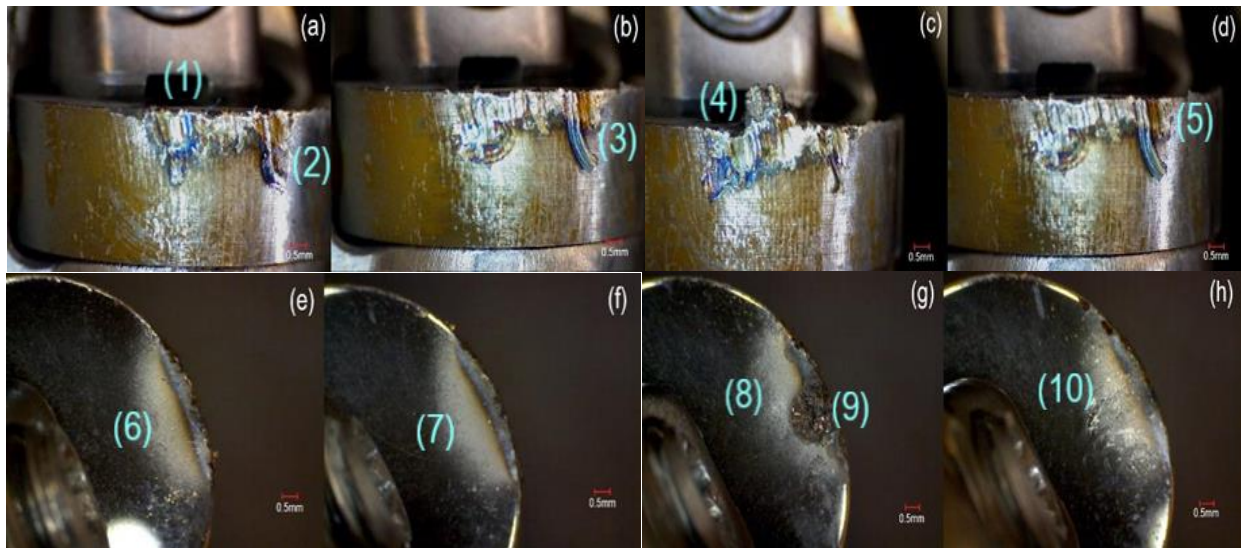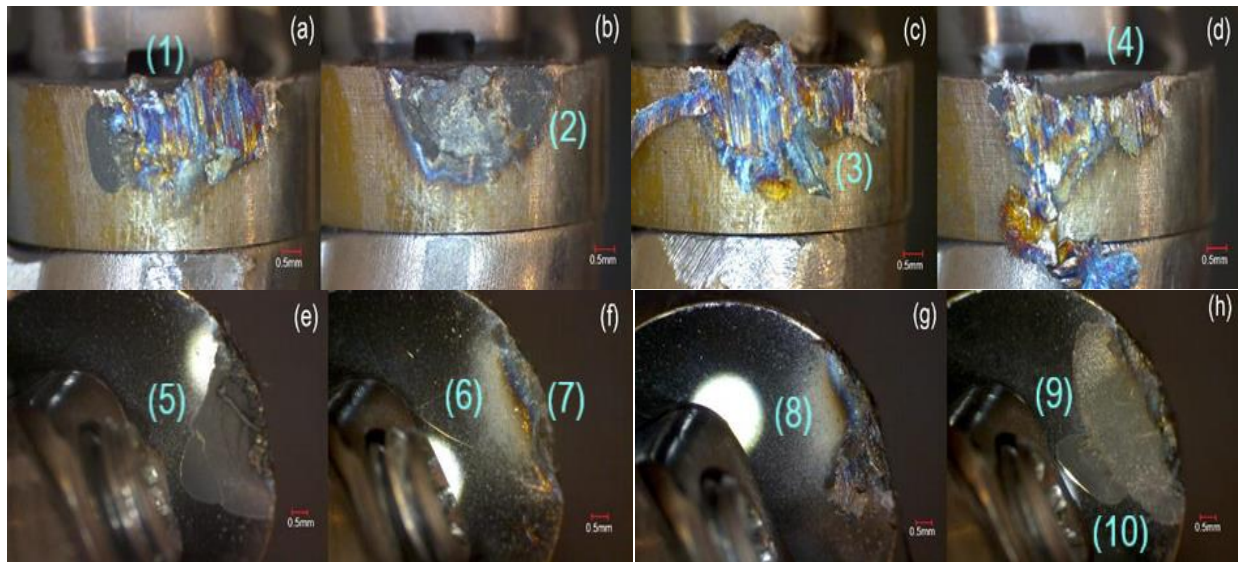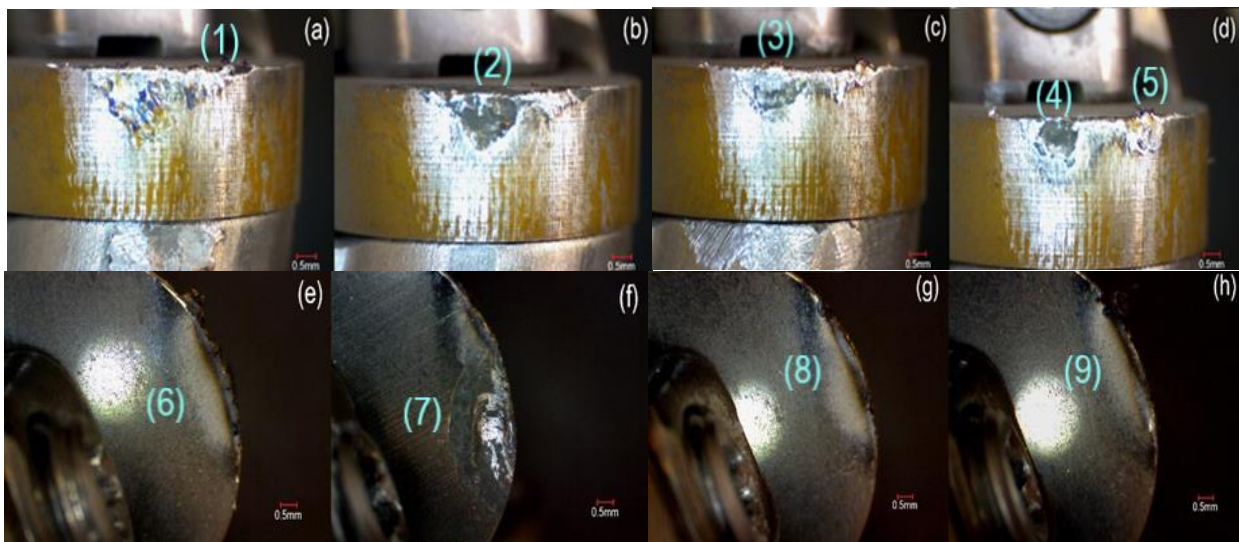

Figure 7.4.Test No M15-Bar Section-3.1-insert-Coating-C-insert-1-4 (a-d) flank face & Insert-1-4 (e-h) rake face.

As mentioned earlier in Section 7.3.1, a few variables have been added which have certainly had an effect on the SiAlON ceramic substrate microstructure and also the microstructure of the α-amorphous Al_2O_3 coating. The increase in cutting speed from 800 m/min to 900 m/min brings about an increase in cutting temperature in the chip/tool interface. The increase in cutting temperature accelerates the rate at which the titanium nitride (TiN) outer coating begins to oxidise and degrade. The accelerated rate of coating degradation then exacerbates the primary wear mechanisms such as notching, abrasive wear. The accelerated wear of ever-changing insert cutting edge and changing insert topology contributes to fluctuations in compressive and tensile stresses that results in localised craters. The craters form due to flaking and chipping, from an increase in cutting edge area as result of abrasive wear.

The increase in cutting edge area causes the contact pressures in the chip/tool interface to increase and also increases the load on the spindle as a result of increased frictional resistance. Once the contact pressures have a reached a certain point it causes the SiAlON ceramic microstructure to shear along the grain boundaries. When sufficiently high enough fluctuating stresses are applied to the covalent SiAlON microstructure, the covalent microstructure slip systems do not plastically deform, they shear along grain boundaries. Therefore, reducing the rate at which the coating degrades is very important and TiN should not be used in protective coating systems for this type of application in the future.

7.3 Results – Uncoated SiAlON Insert Wear Results (Test No M16A-B)

This section will the insert flank and rake face wear results, which have been collated during the latest set of milling insert wear machining trials. The machining trials were conducted at the AMRC Factory of the Future. The objective of this section of Chapter 7 is to establish the hypothesis, which is to ascertain whether uncoated and coated SiAlON inserts will attain a longer tool life and achieve higher material removal volumes when operated in a continuous/near continuous machining environment.

The results in Section 7.2 will look at the insert flank and rake face wear results, which have been collated during Tests M14 and M15. For a test to be successful, a elliptical geometry needs to be machined in to the Inconel 718 bar stock.

To machine an elliptical geometry from the round bar stock, a series of continuous cylindrical toolpaths (Test No M16A and M17A) and near continuous toothpaths (Test No M16B and M17B) were utilised. The machining conditions that were utilised in Test cut M16A-B and M17A-B are captured in Table 7.2.

Table 7.2. All completed 5-axis milling EngD machining trial experiments.

Experiment No	Test No	Machining Operation	Tool Material	Bar Sections Machined	Cutting Speed (m/min)	Feed rate fz (mm/tooth)	Depth of Cut (Ap) mm	Radial Engagement (ae) (mm)
Four	M16A	5-axis Milling	CTIS710 SiAlON Uncoated	1-4, 5-8	840	0.06	1.5	35.5-10.0
Four	M16B	5-axis Profile Milling	CTIS710 SiAlON Uncoated	9-11, 12	880	0.07	1.0	26.14-7.0
Four	M17A	5-axis Milling	CTIS710 SiAlON +Type C Coating	1-3, 4-6, 7-8	840	0.06	1.5	35.5-10.0
Four	M17B	5-axis Profile Milling	CTIS710 SiAlON +Type C Coating	9-10, 11-12	880	0.07	1.0	26.14-7.0

The machining trials were conducted at the AMRC Factory of the Future. The objective of this section of Chapter 7 is to establish the hypothesis, which is to ascertain whether uncoated and coated SiAlON inserts will attain a longer tool life and achieve higher material removal volumes when operated in a continuous/near continuous machining environment.

7.3.1 Uncoated RNGN SiAlON Milling Insert (Test No M16 Part A) Results (Stages 1–4)

For Test M16 Part A Stages 1-4, 4-off uncoated RNGN SiAlON milling inserts were utilised. To avoid wraparound of the cutting tool with the machining workpiece the machining stages were staggered. The uncoated inserts exhibited substantially less amounts of wear on both the flank and rake face, which is represented by Insert 1.3, this it is evident in Figure 7.5(a-h).

Upon the completion of Stage 1, the uncoated inserts exhibited substantially less amounts of wear on both the flank and rake face, which is represented by Insert 1.3, this it is evident in Figure 7.5(a) and Figure 7.5e). Figure 7.5(a) and Figure 7.5(e) shows the tool condition of the flank and rake face after removing Stage 1, which corresponds to completing 2 minutes and 46 seconds of in cut time and removing 64161.1 mm^3 of material. In (Regions 1, 2, 3, and 4 in Figure 7.5), the uncoated inserts displayed thermomechanical wear characteristics that were similar to the wear characteristics that had been demonstrated previously by the uncoated inserts from the previous non-continuous machining trials.

Figure 7.5. 840 m/min-test 16A-Stage-1-4-insert-uncoated-insert-1.3-edge-1.1 (a-d) flank face & Insert-1.3-edge-1.1 (e-h) rake face. Total material removed after four cuts 218857.3 mm^3.

Figure 7.5(b) and Figure 7.5(f) begins to show very small amounts of wear on the flank faces at Stage 2. Figure 7.5(b) and Figure 7.5(f) show the tool condition of the flank and rake face after removing Stage 2, which equates to completing another 2 minutes and 23 seconds of in cut time and removing another 58021.7 mm^3 of material. The main wear mechanisms which are exhibited at this stage are adhesive wear, notch wear, oxidative wear, thermochemical wear, and built-up edge (BUE). However, this small amount of tool wear was encouraging to see considering the quantity of material that had been removed and the time in cut that's had been attained.

Figure 7.5(c) Figure 7.5(g) shows the tool condition of the flank and rake face after removing Stage 3, and yet again the level of insert wear is progressive but minimal compared to the volume of material that has been removed. Figure 7.5(c) Figure 7.5(g) show the tool condition of the flank and rake face after removing Stage 3, which equates to completing another 2 minutes and 14 seconds of in cut time and removing a further 51448.1 mm^3 of material. The main wear mechanisms which are exhibited at this stage are adhesive wear, notch wear, oxidative wear, thermochemical wear. The main wear mechanisms which are exhibited at this stage are adhesive wear, notch wear, oxidative wear, thermochemical wear.

Figure 7.5(d) and Figure 7.5(h) continues to show progressively higher levels of flank and rake face wear. Figure 7.5(d) and Figure 7.5(h) shows the tool condition of the flank and rake face after removing Stage 4, which equates to completing another 2 minutes of in cut time and removing a further 45226.3 mm^3 of material.

At this stage the main wear mechanisms which are exhibited are adhesive wear, notch wear, oxidative wear, thermochemical wear. The quantity of insert wear at this stage of machining trial is impressive, when compared to levels of wear which were exhibited in the non-continuous machining trials. During the machining trial, a series of sensors for the machine protection control (MPC) on the main spindle of the DMG Mori NTX2500 machine were monitoring the levels of vibration that the main spindle was experiencing. At the end of machining Stage 4, it was decided to completely replace the four inserts to prevent excessive vibration in the machine. The main wear mechanisms which are exhibited at this stage are adhesive wear, notch wear, oxidative wear, thermochemical wear.

7.3.2 Uncoated RNGN SiAlON Milling Insert (Test No M16 Part A) Results (Stages 5-8)

For Test M16 Part A Stages 5-8, a new set of 4-off uncoated RNGN SiAlON milling inserts were utilised. Once again, to avoid wraparound of the cutting tool with the machining the stages were staggered. Upon the completion of Stage 5, the uncoated inserts exhibited substantially less amounts of wear on both the flank and rake face for all four of the inserts, this it is evident in Figure 7.6(a-h). Once again, the uncoated inserts displayed thermomechanical wear characteristics that were similar to the wear characteristics that had been demonstrated previously by the uncoated inserts from the previous non-continuous machining trials.

Upon the completion of Stage 5, the uncoated inserts exhibited substantially less amounts of wear on both the flank and rake face, which is represented by Insert 2.4, this it is evident in Figure 7.6(a) and Figure 7.6(e).
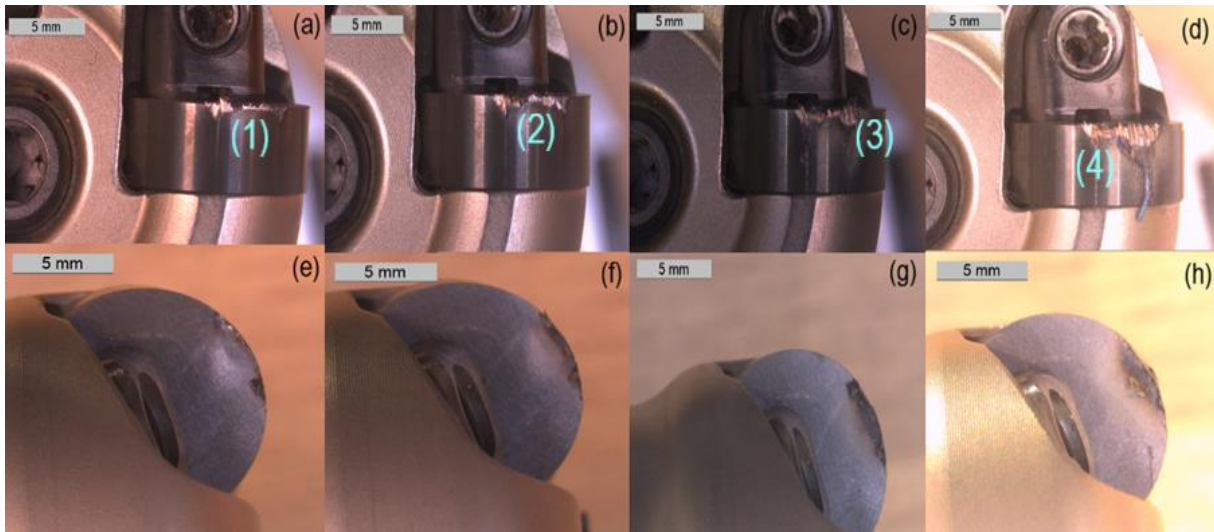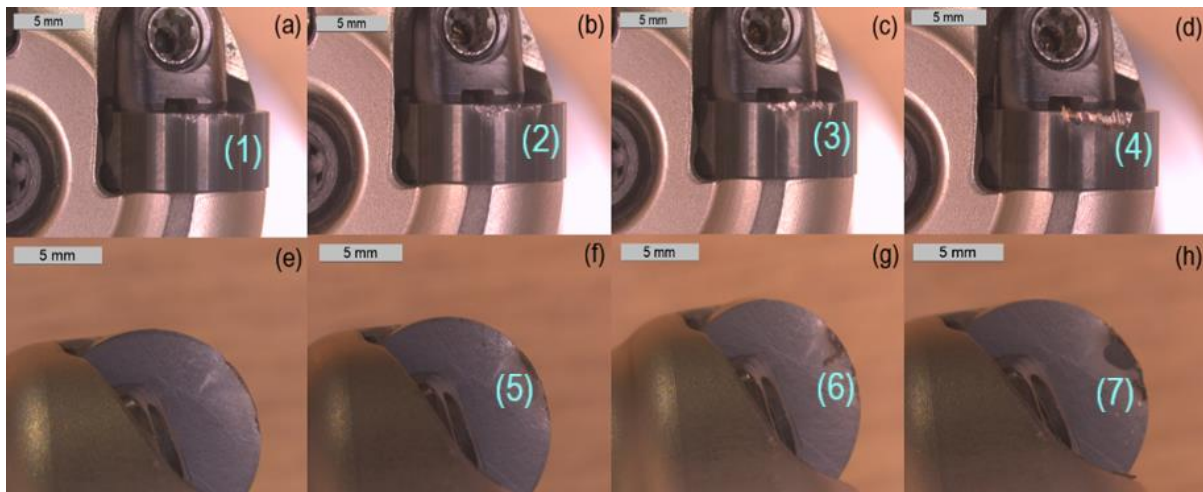

Figure 7.6. 840 m/min-test 16A-Stage-5-8-insert-uncoated-insert-2.4-edge-2.1 (a-d) flank face & Insert-1.4-edge-2.1 (e-h) rake face. Total material removed after eight cuts 347244.6 mm³.

Figure 7.6(a) and Figure 7.6(e) show the tool condition of the flank and rake face after removing Stage 5, which equates to completing another 1 minute and 43 seconds of in cut time and removing a further 39599.5 mm^3 of material.

At this stage the main wear mechanisms are notch wear, which is evident in (Regions 1, 2, 3, and 4, in Figure 7.6). The other main wear mechanisms which are exhibited at this stage are oxidative wear, thermochemical wear as seen in (Regions 5, 6, and 7 in Figure 7.6).

Figure 7.6(b) and Figure 7.6(f) begins to replicate the level of wear that was exhibited in the early cuts as the inserts show very small amounts of wear on the flank faces after machining Stage 6. The small amount of tool wear was once again encouraging to see, considering the quantity of material that had been removed and the time in cut that's had been attained.

The time in cut is gradually getting shorter and shorter throughout machining trial as the cuts were staggered to avoid damaging the inserts and cutting too deeply into the workpiece material. Figure 7.6(b) and Figure 7.6(f) shows the tool condition of the flank and rake face after removing Stage 6, which equates to completing another 1 minute and 33 seconds of in cut time and removing a further 34361 mm^3 of material. The main wear mechanisms which are exhibited at this stage are high adhesive wear, notch wear, oxidative wear, thermochemical wear, flaking, chipping.

Figure 7.6(c) and Figure 7.6(g) shows the tool condition of the flank and rake face after removing Stage 7, which display very low levels of insert wear. What is apparent with the uncoated inserts up to this point, is the stability of the chip/tool interface, the machining environment and sheer quantity of material that has been removed versus the level of insert wear. The main wear mechanisms which are exhibited at this stage are mainly progressive low levels of thermomechanical wear on the rake and flank faces.

Figure 7.6(d) and Figure 7.6(g) shows the tool condition of the flank and rake face after removing Stage 8. Figure 7.6(d) and Figure 7.6(g) shows the tool condition of the flank and rake face after removing Stage 8, which equates to completing another 1 minute and 10 seconds of in cut time and removing a further 25004.7 mm^3 of material. At this stage the main wear mechanisms which are exhibited are high adhesive wear, notch wear, oxidative wear, thermochemical wear, flaking, chipping.

The levels of wear are once again very low compared to that have been captured in previous non-continuous machining trials.

The levels of wear can be attributed to the stability of the chip/tool interface and how the workpiece material is being removed.

These types of rake and flank face wear patterns have taken place at a cutting speed of 840 m/min, when high-speed face-milling of Inconel 718 with continuous spiral tools at fz=0.06 mm/tooth, Ap=1.5 mm, and ae=35.5-10.0 mm. The insert wear versus the material removal volume have greatly surpassed that of the non-continuous rates of insert wear versus material removal volume.

7.3.3 Uncoated RPGN SiAlON Milling Insert (Test No M16 Part B) Results (Stages 9-11)

For Test M16 Part B Stages 9-11, a new set of 3-off uncoated RPGN SiAlON milling inserts were utilised. Once again, to avoid wraparound of the cutting tool with the workpiece during machining the stages were staggered. Images of the types of tool failure patterns for the flank and rake faces on the RPGN inserts are presented in Figure 7.7(a-h), respectively.

The main wear mechanisms which are exhibited by the uncoated RPGN inserts at this stage are notch wear, oxidative wear, thermochemical wear. At this stage the main wear mechanisms which are exhibited are adhesive wear in (Regions 1 and 2 in Figure 7.7) and notch wear, chipping and oxidative wear, as seen in (Regions 3, 4, and 5 in Figure 7.7). These types of rake and flank face wear patterns have taken place at a cutting speed of 880 m/min, when high-speed face-milling of Inconel 718 with near-continuous elliptical spiral tool paths at fz=0.07 mm/tooth, Ap=1.0 mm, and ae=26.14-7.0 mm.

Figure 7.7(a) and Figure 7.7(d) shows the tool condition of the flank and rake face after removing Stage 9, which equates to completing another 2 minutes and 01 seconds of in cut time and removing a further 12141.6 mm^3 of material.

The main wear mechanisms which are exhibited at this stage are notch wear, oxidative wear, thermochemical wear. The axial increase and decrease in immersion for each of the elliptical cuts allowed for a gradual increase in cutting forces. The gradual increase in cutting forces culminated in minimising the fluctuation in tensile and compressive stresses, which assists in the tribological interaction at the chip/tool interface between the workpiece material and the uncoated inserts.

Figure 7.7. 880 m/min-test 16B-Stage-9-11-insert-uncoated-insert-1.1-edge-1.1 (a-d) flank face & Insert-1.1-edge-1.1 (e-h) rake face. Total material removed after Three cuts 31610.2 mm³.

Figure 7.7(b) and Figure 7.7(e) shows the tool condition of the flank and rake face after removing Stage 10, which equates to completing another 1 minute and 42 seconds of in cut time and removing a further 12141 mm³ of material. The main wear mechanisms which are exhibited at this stage are notch wear, oxidative wear, thermochemical wear.

Figure 7.7(c) and Figure 7.7(f) shows the tool condition of the flank and rake face after removing Stage 11, which equates to completing another 1 minute and 38 seconds of in cut time and removing a further 9163.5 mm³ of material. During the machining trial, a series of sensors on the main spindle of the DMG Mori NTX2500 machine were monitoring the levels of vibration that the main spindle was experiencing. The vibrational sensors in the DMG Mori NTX2500 indicated a sharp increase in vibrational velocity on the main spindle which increased from 13.0 mm/s to 27.0 mm/s (See Appendix A).

At the end of machining Stage 11, it was decided to completely replace the three inserts. Upon visual inspection, the inserts were observed to have suffered multiple insert failure. The main wear mechanisms which are exhibited at this stage are high adhesive wear, notch wear, oxidative wear, thermochemical wear, flaking, chipping.

Upon the completion of Stage 11, it was evident in Figure 7.7(a-f) the uncoated inserts exhibited progressive tool damage, which ultimately resulted in fracture on both the flank and rake face. The flaking and chipping take place due to the change in cutting edge as result of abrasive

154

wear, which causes the contact pressures in the chip/tool interface to increase to a point that it causes the SiAlON ceramic microstructure to shear along the grain boundaries.

7.3.4 Uncoated RPGN SiAlON Milling Insert (Test No M16 Part B) Results (Stage 12)

The last stage of the Test M16B utilised a new set of 3-off uncoated RPGN SiAlON milling inserts. Figure 7.8(a-f) shows the tool condition of the flank and rake face after removing Stage 12, which equates to completing another 1 minute and 16 seconds of in cut time and removing a further 6936.2 mm^3 of material. The main wear mechanisms which are exhibited at this stage are notch wear, which is seen in (Regions 1, 2, and 3 in Figure 7.8) and oxidative wear, thermochemical wear is seen in (Regions 4, 5, and 6 in Figure 7.8).

These types of rake and flank face wear trends for Stage 12 have taken place at a cutting speed of 880 m/min, when high-speed face-milling of Inconel 718 with near-continuous elliptical spiral tool paths at fz=0.07 mm/tooth, Ap=1.0 mm, and ae=26.14-7.0 mm.

As no positive geometry (RPGN) inserts were used in the previously completed non-continuous machining trials, there is no direct comparative data to compare to for insert wear versus materials removal. The machining of the elliptical spiral tool paths required the utilisation of a smaller radial engagement, this helped with maintaining stability during the machining of the 2D elliptical geometry.
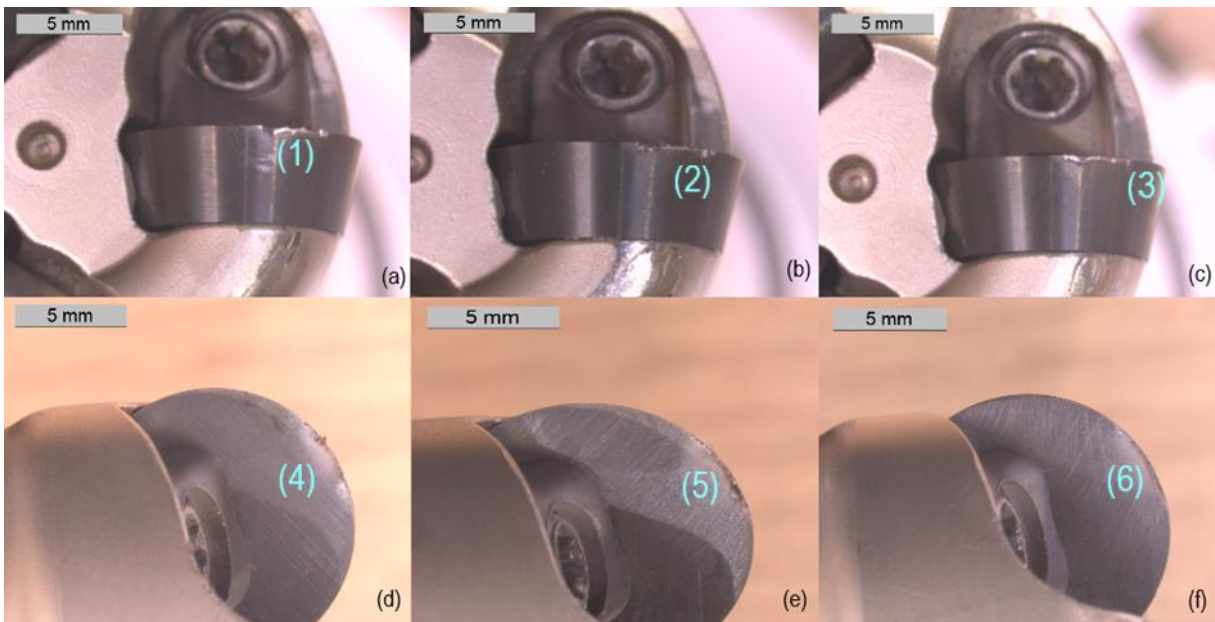
Figure 7.8. 880 m/min-test 16B-Stage-12-insert-uncoated-insert-2.1-2.3-edge-2.1 (a-c) flank face & Insert-2.1-2.3-edge-2.1 (d-f) rake face. Material removed for this cut 6936.2 mm^3. Total material removed in after four cuts 38546.5 mm^3.

However, when the inserts approach the centre of the bar material the main spindle vibration sensors from the (MPC) on the NTX2500 would initiate. This level of vibration was anticipated as the middle of the bar material is subjected to highest degree of deflection.

7.4 Results – CVD Coated SiAlON Insert Wear Results (Test No M17A-B)

7.4.1 Coating C RNGN SiAlON Milling Insert (Test No M17 Part A) Results (Stages 1-3)

The results in Section 7.4 will look at the insert flank and rake face wear results of the Coating C RNGN and RPGN SiAlON inserts, which have been collated during the latest set of milling insert wear machining trials. For Test M17 Part B Stages 1-3, 4-off coated RNGN SiAlON milling inserts have utilised. Once again, to avoid wraparound of the cutting tool with the machining workpiece the machining stages are staggered.

The results in Section 7.4 will look at the insert flank and rake face wear results, which have been collated during the latest set of milling insert wear machining trials. The machining trials were conducted at the AMRC Factory of the Future, which is situated on the advanced manufacturing park in Rotherham, South Yorkshire.

Upon the completion of Stage 1, the Coating C inserts exhibited substantially less amounts of wear on both the flank and rake face for all four of the inserts, this it is evident in Figure 7.9(a) and Figure 7.9(d) shows the tool condition of the flank and rake face after removing Stage 1, which equates to completing 2 minutes and 46 seconds of in cut time and removing 64161.1 mm^3 of material.
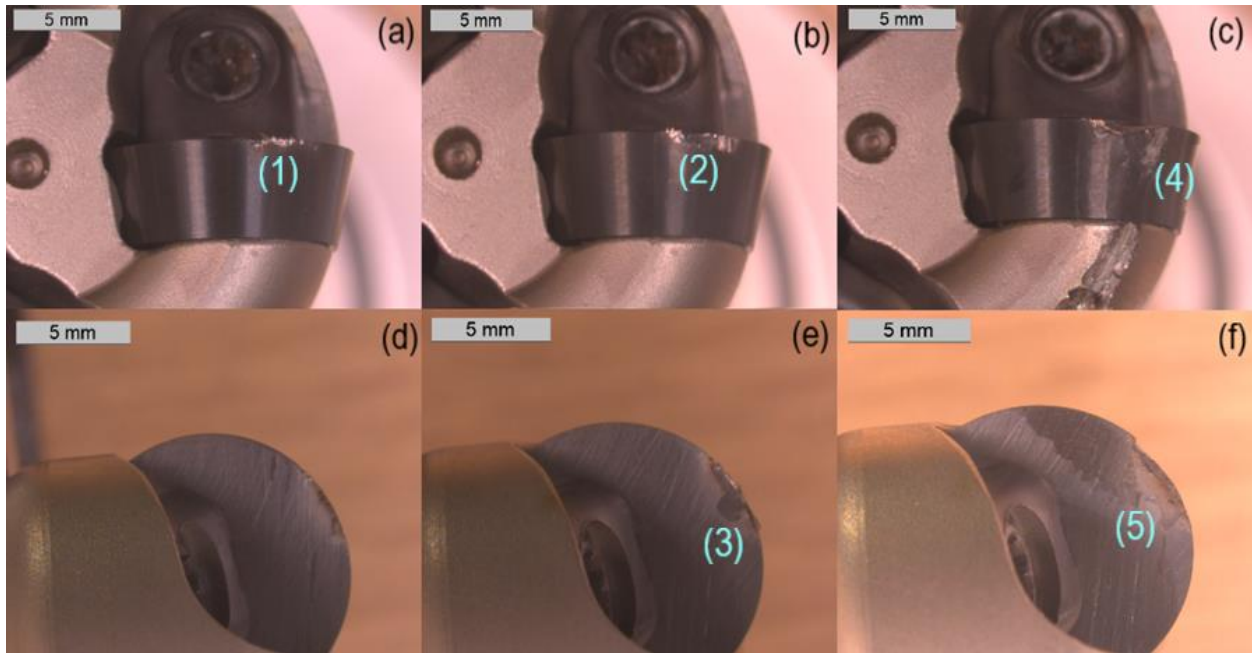

Figure 7.9. 840 m/min-test 17A-Stage-1-3-insert-uncoated-insert-1.1-edge-1.1 (a-c) flank face & Insert-1.1-edge-1.1 (d-f) rake face. Total material removed after three cuts 173631 mm^3.

The main wear mechanisms which are exhibited at this very early stage are adhesive wear, notch wear and oxidative wear. After stages 1-3 had been completed, the Coating C inserts displayed less adhesive wear, oxidation, BUE and notch wear as in (Regions 1, 2, 3, 4, 5, and 6 in Figure 7.9), when compared to the Coating C inserts from the previous non-continuous tests, as seen in Figure 7.1, Figure 7.2 and Figure 7.3.

Figure 7.9(b) and Figure 7.9(e) begins to show very small amounts of wear on the flank and rake faces after machining Stage 2. Figure 7.9(b) and Figure 7.9(e) shows the tool condition of the flank and rake face after removing Stage 2, which equates to completing another 2 minutes and 23 seconds of in cut time and removing another 58021.7 mm^3 of material.

The main wear mechanisms which are exhibited at this stage are adhesive wear, notch wear, oxidative wear, thermochemical wear and BUE. The lack of degradation that has been exhibited by Coating C RNGN inserts can be attributed to improved wear mechanics between the aluminium oxide coating and the workpiece material. This is encouraging considering the quantity of material that had been removed and the time in cut that's had been attained.

Figure 7.9(c) and Figure 7.9(f) shows the tool condition of the flank and rake face after removing Stage 3, and yet again the level of insert wear is progressive but minimal compared to the volume of material that has been removed. Which equates to completing another 2 minutes and 14 seconds of in cut time and removing a further 51448.1 mm^3 of material.

At this stage the main wear mechanisms which are exhibited are adhesive wear, notch wear, oxidative wear, thermochemical wear. Figure 7.9(c) and Figure 7.9(f) continues to show progressively higher levels of flank and rake face wear. The quantity of insert wear that is being displayed at this stage of machining trial is significantly less, when compared to levels of wear which were exhibited in the non-continuous machining trials. During the machining trial, a series of sensors on the main spindle of the DMG Mori NTX2500 machine were monitoring the levels of vibration that the main spindle was experiencing. At the end of machining Stage 3, it was decided to completely replace the four inserts.

The main wear mechanisms which are exhibited at this stage are adhesive wear, notch wear, oxidative wear, thermochemical wear.

7.4.2 Coating RNGN SiAlON Milling Insert (Test No M17 Part A) Results (Stages 4-6)

For Test M17 Part A Stages 4-6, a new set of 4-off coated RNGN SiAlON milling inserts have utilised. To avoid wraparound of the cutting tool with the machining workpiece during the machining stages were staggered. Upon the completion of Stage 4, the Coating C inserts have

yet again exhibited substantially less amounts of wear on both the flank and rake face for all four of the inserts, this it is evident in Figure 7.10(a-f).

The Coating C inserts displayed in Figure 7.10(a) and Figure 7.10(d) show thermomechanical wear characteristics that were comparable to the earlier test cut Stage 1 as seen in Figure 7.10(a) and Figure 7.10(d). Figure 7.10(a) and Figure 7.10(d) show the tool condition of the flank and rake face after removing Stage 4, which equates to completing another 2 minutes of in cut time and removing a further 45226.3 mm^3 of material.

After completing Stages 4-6, the main wear mechanisms which are evident in (Regions 1, 2, 3, 4, 5, and 6 in Figure 7.10) are adhesive wear, notch wear, oxidative wear, thermochemical wear. The level of wear of the RNGN inserts is comparable to the level of insert wear that has been attained Stages 1-3, as viewed in Figure 7.9.
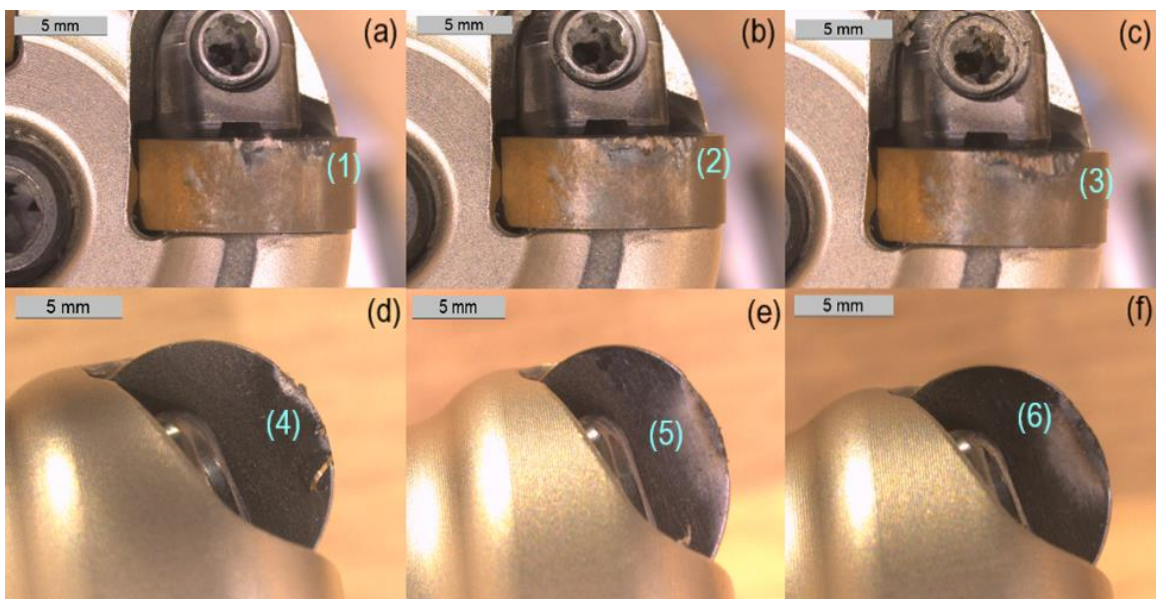

Figure 7.10. 840 m/min-test 17A-Stage-4-6-insert-uncoated-insert-2.1-edge-1.1 (a-c) flank face & Insert-2.1-edge-1.1 (d-f) rake face. Total material removed after six cuts 258456.8 mm^3.

Figure 7.10(b) and Figure 7.10(e) begins to replicate the level of wear that was exhibited in the early cuts as the inserts show very small amounts of wear on the flank faces after machining Stage 5. Although the Coating C inserts are exhibiting higher amounts of flank and rake face wear that the uncoated inserts, the level of insert wear is notably less than the non-continuous wear result. The small amount of tool wear was once again encouraging to see, considering the quantity of material that had been removed and the time in cut that's had been attained.

As mentioned before in Section 7.3, the time in cut is gradually getting shorter and shorter throughout machining trial as the cuts are staggered to avoid damaging the inserts and cutting too deeply into the workpiece material. Figure 7.10(b) and Figure 7.10(e) show the tool condition of the flank and rake face after removing a Stage 5, which equates to completing another 1 minute and 43 seconds of in cut time and removing a further 39599.5 mm^3 of material. The main wear mechanisms which are exhibited at this stage for the Coating C RNGN inserts are notch wear, oxidative wear, thermochemical wear.

Figure 7.10(c) and Figure 7.10(f) shows the tool condition of the flank and rake face after removing Stage 6, which display very low levels of insert wear. What is still very apparent with the Coating C inserts up to this point, is the stability of the chip/tool interface and the chip removal process. The quantity of material that has been removed versus the level of insert wear is impressive.

The main wear mechanisms which are exhibited at this stage are mainly progressive low levels of thermomechanical wear on the rake and flank faces. Figure 7.10(c) and Figure 7.10(f) shows the tool condition of the flank and rake face after removing Stage 6, which equates to completing another 1 minute and 33 seconds of in cut time and removing a further 34361 mm^3 of material. The main wear mechanisms which are exhibited at this stage are high adhesive wear, notch wear, oxidative wear. The level of adhesive and notch wear is comparable to the level of insert wear that has been attained Stages 1-3, as viewed in Figure 7.9.

7.4.3 Coating C RNGN SiAlON Milling Insert (Test No M17 Part A) Results (Stages 7-8)

For Test M17 Part A Stages 7-8, a new set of 4-off coated RNGN SiAlON milling inserts have utilised. Once again, to avoid wraparound of the cutting tool with the machining workpiece during the machining stages the stages were staggered.

Upon the completion of Stage 7, the Coating C inserts have again exhibited substantially better wear characteristics less amounts of wear on both the flank and rake face for all four of the inserts, this it is evident in Figure 7.11. (a) and Figure 7.11. (c). The Coating C inserts displayed thermomechanical wear characteristics that were comparable to the earlier test cut Stage 4 as seen in Figure 7.11. (a-d). Figure 7.11. (a) and Figure 7.11. (c) show the tool condition of the flank and rake face after removing Stage 7, which equates to completing another 1 minute and 24 seconds of in cut time and removing a further 29422.1 mm^3 of material.

The main wear mechanisms which are exhibited by the Coating C RNGN inserts at this stage are notch wear, oxidative wear, thermochemical wear.
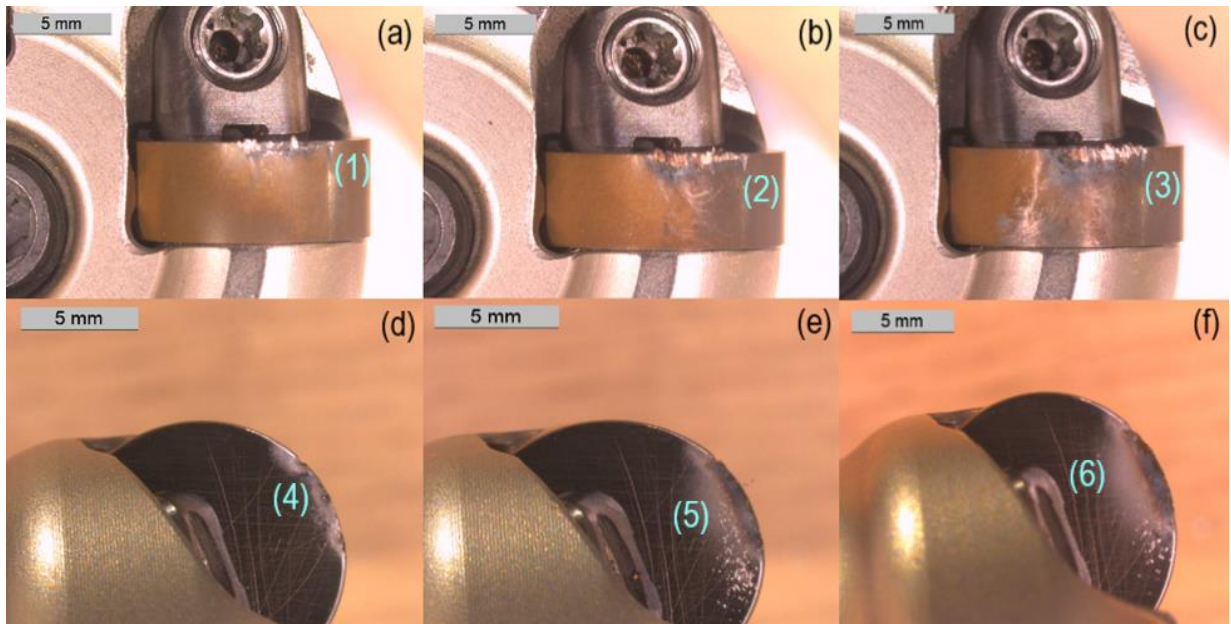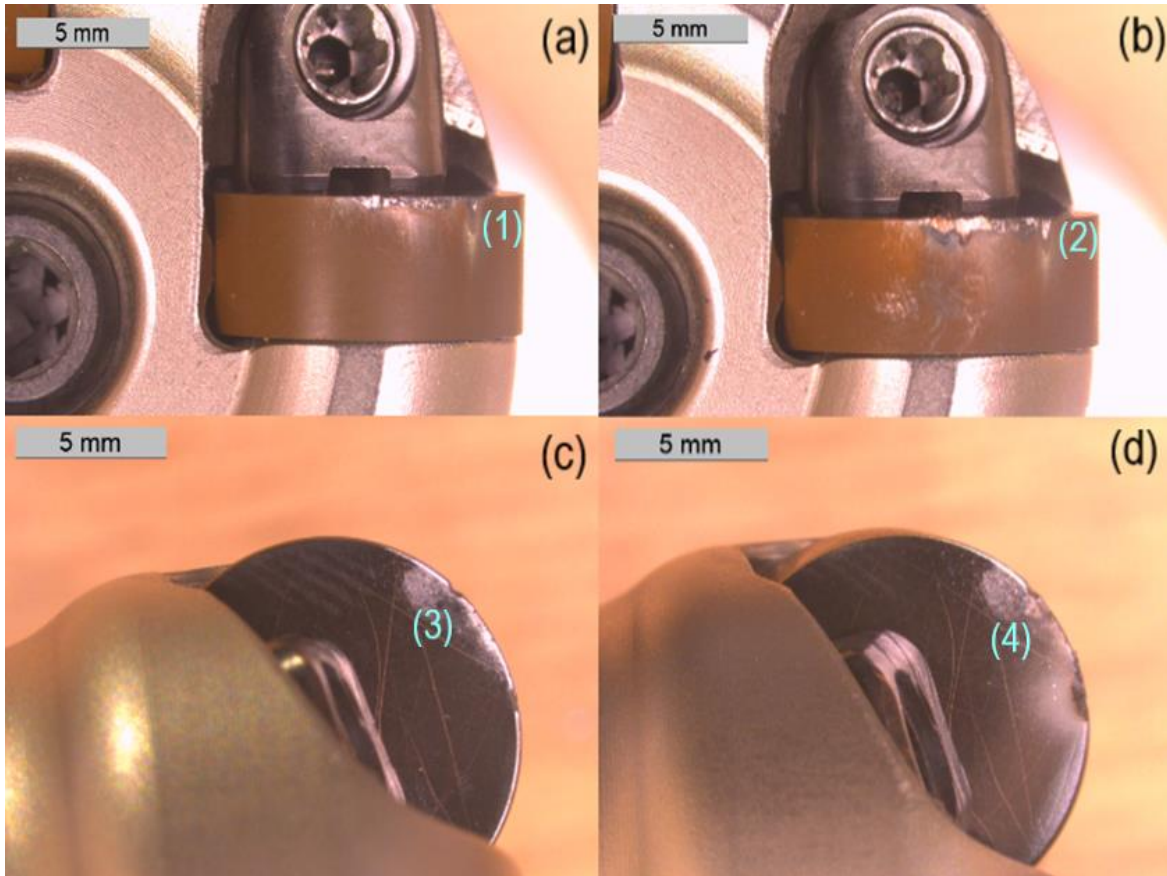
Figure 7.11. 840 m/min-test 17A-Stage-7-8-insert-uncoated-insert-1.4-edge-3.1 (a-d) flank face & Insert-1.4-edge-3.1 (e-h) rake face. Total material removed after eight cuts 347244.6 mm^3.

The level of wear that is displayed in (Regions 1, 2, 3, and 4 in Figure 7.11.) by the Coating C RNGN inserts at this stage, is comparable to the levels of insert wear that has been displayed earlier in Stages 1-6, which is captured in Figure 7.9 and Figure 7.10.

Figure 7.11. (b) and Figure 7.11. (d) shows the tool condition of the flank and rake face after removing Stage 8, which display very low levels of insert wear. What was still very apparent with the Coating C inserts up to this point, is the stability of the chip/tool interface and the chip removal process. The main wear mechanisms which are exhibited at this stage are progressive thermomechanical wear on the rake and flank faces.

Figure 7.11. (b) and Figure 7.11. (d) shows the tool condition of the flank and rake face after removing Stage 8, which equates to completing another 1 minute and 10 seconds of in cut time and removing a further 25014.7 mm^3 of material.

These types of rake and flank face wear trends have taken place at a cutting speed of 840 m/min, when high-speed face-milling of Inconel 718 with continuous spiral tools at fz=0.06

mm/tooth, Ap=1.5 mm, and ae=35.5-10.0 mm. The insert wear versus the material removal volume have greatly surpassed that of the non-continuous rates of insert wear versus material removal volume.

7.4.4 Coating C RPGN SiAlON Milling Insert (Test No M17 Part B) Results (Stages 9-10)

For Test M17 Part B Stages 9-10, a new set of 3-off coated RPGN SiAlON milling inserts were utilised. To avoid wraparound of the cutting tool with the workpiece material during machining the stages were staggered. Images of the types of tool failure patterns for the flank and rake faces on the RPGN inserts are presented in Figure 7.12(a-d) and Figure 7.13(a-d), respectively.

Figure 7.12. 880 m/min-test 17B-Stage-9-10-insert-uncoated-insert-2.1-edge-1.1 (a-b) flank face & Insert-1.1-1.3-edge-1.1 (c-d) rake face. Total material removed after two cuts 22446.7 mm^3.

The main wear mechanisms which are exhibited at this stage are higher adhesive wear, notch wear, oxidative wear, thermochemical wear. At this stage the main wear mechanisms which are

exhibited are adhesive wear, notch wear, oxidative wear, thermochemical wear. These types of rake and flank face wear trends have taken place for Stages 9-12 at a cutting speed of 880 m/min, when high-speed face-milling of Inconel 718 with near-continuous elliptical spiral tool paths at fz=0.07 mm/tooth, Ap=1.0 mm, and ae=26.14-7.0 mm.

Figure 7.12(a) and Figure 7.12(c) shows the tool condition of the flank and rake face after removing Stage 9, which equates to completing another 2 minutes and 01 seconds of in cut time and removing a further 12141.6 mm^3 of material. The main wear mechanisms which are exhibited at Stages 9-10 in (Regions 1, 2, and 4 in Figure 7.12) are notch wear, flaking and chipping.

The radial increase and decrease in immersion for each of the elliptical cuts allowed for a gradual increase in cutting forces. The gradual increase in cutting forces culminated in minimising the fluctuation in tensile and compressive stresses, which assists in the tribological interaction at the chip/tool interface between the workpiece material and the uncoated inserts.

Figure 7.12(b) and Figure 7.12(d) shows the tool condition of the flank and rake face after removing Stage 10, which equates to completing another 1 minute and 38 seconds of in cut time and removing a further 9163.5 mm^3 of material. During the machining trial, a series of sensors on the main spindle of the DMG Mori NTX2500 machine were monitoring the levels of vibration that the main spindle was experiencing. The sensors indicated a sharp increase in vibration on the main spindle.

At the end of machining Stage 10, it was decided to completely replace the three inserts. Upon visual inspection, the inserts were observed to have suffered multiple insert failure. The main wear mechanisms which are exhibited at this stage are high adhesive wear, notch wear, oxidative wear, thermochemical wear, flaking, chipping.

7.4.5 Coating C RNGN SiAlON Milling Insert (Test No M17 Part B) Results (Stages 11-12)

For Test M17 Part B Stages 11-12, a new set of 3-off coated RPGN SiAlON milling inserts were utilised. Once again, to avoid wraparound of the cutting tool with the workpiece during machining the stages were staggered. Figure 7.13 (a-d) shows the tool condition of the flank and rake face after removing Stage 11, which equates to completing another 1 minute and 38 seconds of in cut time and removing a further 9163.5 mm^3 of material. During the machining trial, a series of sensors on the main spindle of the DMG Mori NTX2500 machine were monitoring the levels of vibration that the main spindle was experiencing.
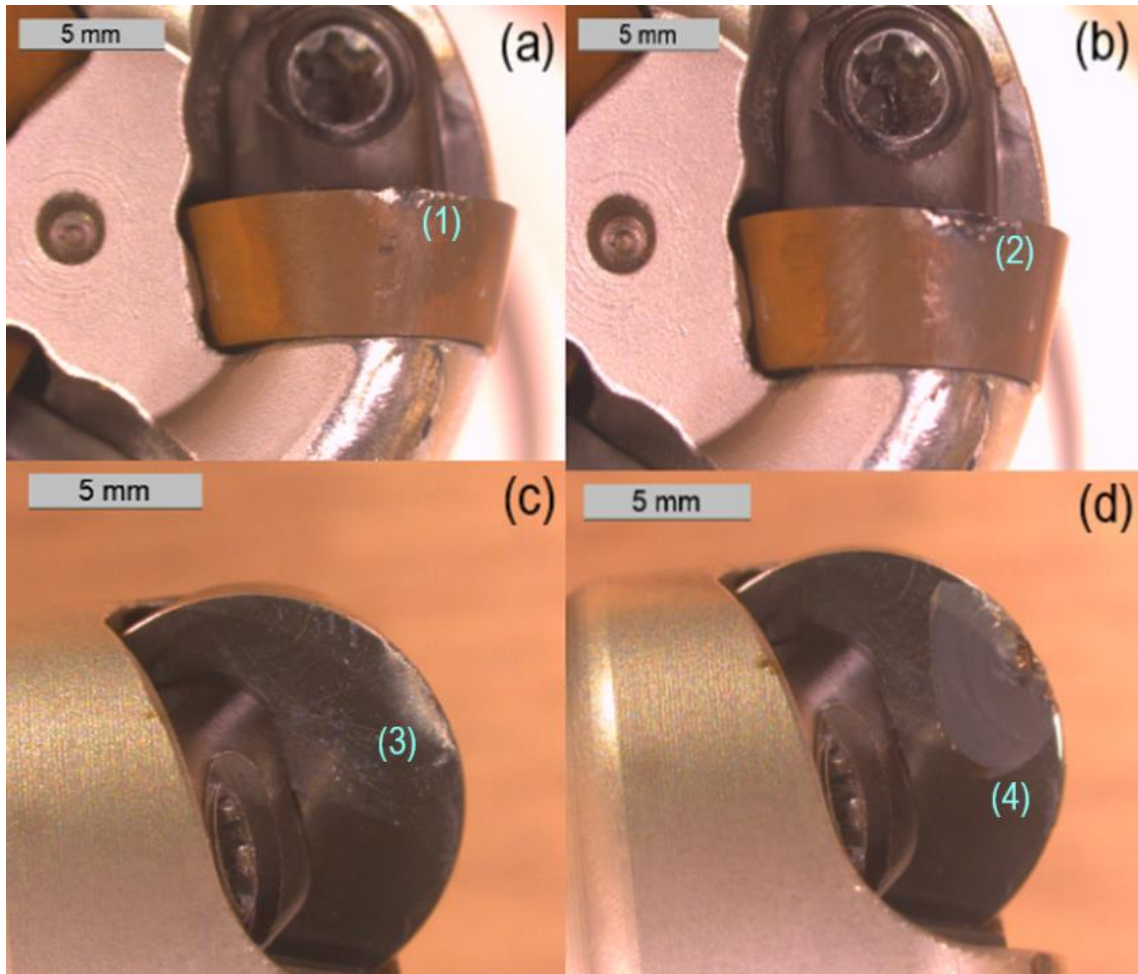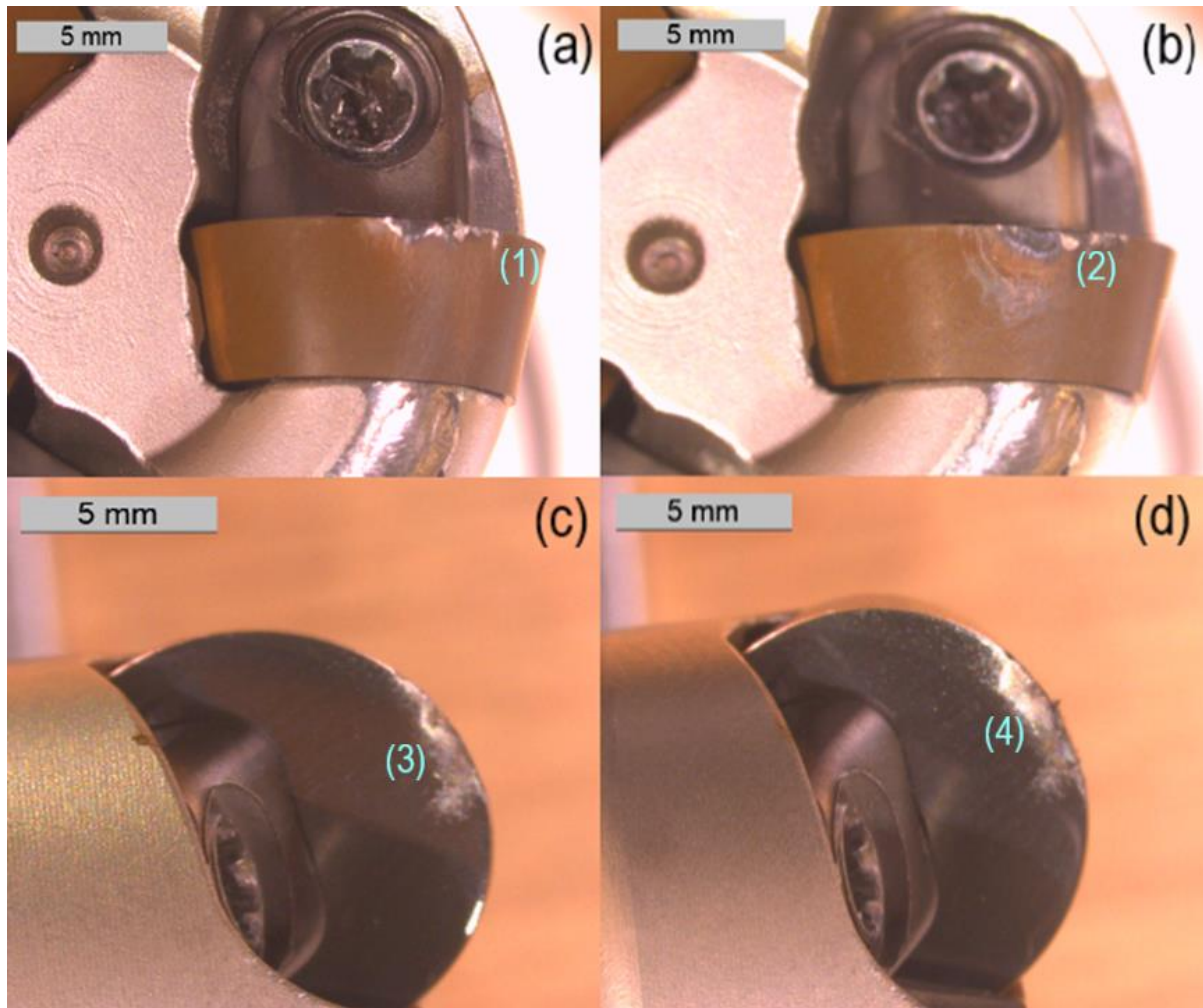
Figure 7.13. 880 m/min-test 17B-Stage-11-12-insert-uncoated-insert-2.1-edge-1.1 (a-b) flank face & Insert-1.1-1.3-edge-1.1 (c-d) rake face. Material removed for this cut 12141 mm^3. Total material removed after two cuts 38546.5mm^3.

Figure 7.13(a-d) shows the tool condition of the flank and rake face after removing Stage 12, which equates to completing another 1 minute and 16 seconds of in cut time and removing a further 6936.2 mm^3 of material. The main wear mechanisms which are exhibited at Stage 11 in (Regions 1 and 4 in Figure 7.13) are notch wear, oxidative wear. Figure 7.13(b) and Figure 7.13(d) shows the tool condition of the flank and rake face after removing Stage 12, which equates to completing another 1 minute and 16 seconds of in cut time and removing a further 6936.2 mm^3 of material. The main wear mechanisms which are exhibited at Stage 12 in (Regions 2 and 4 in Figure 7.13) are notch wear, oxidative wear, thermochemical wear.

As mentioned earlier in Section 7.2.1, a few variables have been added which have certainly had an effect on the SiAlON ceramic substrate microstructure and the microstructure of the α-amorphous Al$_2$O$_3$ Coating. The thorough refinement of the NC programme machining strategies,

163

together with tap testing of both the workpiece material and the two cutting tools, has led to a detailed understanding of dynamic machining environments that are present during part tests 16A and 17A and test 16B and 17B.

In Test M14 and M15, cutting speeds of 800 m/min and 900 m/min with non-continuous tool paths were utilised. For Tests M16A-B and M17A-B, the toolpaths underwent a six to eight months refinement process, which involved the use of Vericut simulation and tap testing modal analysis in Cutpro (See Appendix C). What is apparent from the completion of Tests M16A-B and M17A-B, is that tap testing has provided valuable dynamic information, which has helped determined what cutting speeds, depths of cut and feed rates deliver optimum cutting conditions for material removal. The selection of the two cutting speeds (840 m/min and 880 m/min) and their respective feed rates and depths of cut, have delivered outstanding levels of material removal versus insert wear, when compared to previous non-continuous machining trials.

7.5 Tool Life Data (Test No M1-M17)

In order to get a better understanding of improvements that have been attained from utilising continuous tool paths, the flank wear and total time in cut data for the non-continuous tool paths have been included in a Table 7.3 for comparison. Due to the variability of the data that is captured in Table 7.3 a combined bar has not been utilised. However, the data is later presented in Section 7.5 with plots in Figure 7.14, Figure 7.15, Figure 7.18 and bar charts in Figure 7.16, Figure 7.17 and Figure 7.19.

The improvement in the wear rates for both the uncoated and Coating C inserts are related to improvements in the chip/tool interface. The adoption of continuous spiral and near-continuous elliptical spiral tool paths has allowed for minimal fluctuations in cutting temperature.

The lack of fluctuation in cutting temperature has meant that the chip/tool interface for both the uncoated and coated inserts have not had to endure high rates of heating and cooling, which has exacerbated the primary wear mechanisms in earlier machining trials which have utilised interrupted non-continuous tool paths, particularly the CVD coated SiAlON inserts.

Throughout the machining trial there has been a distinct lack of coating degradation on both flank face and rake face. The TiN outer coating on the flank face of both the RNGN and RPGN show significantly less oxidation and degradation. The Al_2O_3 coating on the rake faces of RNGN inserts displayed very high stability and a lack of oxidative wear, coating degradation or thermomechanical wear. This lack of coating degradation is even more evident when compared to wear data that was collated in non-continuous machining trials.

Table 7.3. Flank wear versus total time in cut for comparison between non-continuous and continuous tool paths.

Test No	Cutting Speed (m/min)	Tool Material	Stage No	Flank Wear Vbb (mm)	Total time in cut (Mins) Non-con	Total time in Cut (Secs)	Removed Material Volume (mm^3)
1	700 m/min	RNGN CTIS710 Uncoated Non-con		2.26	5.03	301.6	135716.0
2	700 m/min	RNGN CTIS710 Coating A Non-con		1.49	2.51	150.8	67858.0
3	700 m/min	RNGN CTIS710 Coating B Non-con		3.34	5.03	301.6	135716.0
4	800 m/min	RNGN CTIS710 Uncoated Non-con		3.43	5.85	350.9	169640.0
5	800 m/min	RNGN CTIS710 Coating A Non-con		3.94	5.85	350.9	169640.0
6	800 m/min	RNGN CTIS710 Coating B Non-con		3.48	4.68	280.7	135716.0
13	800 m/min	RNGN CTIS710 Coating B Retest Non-con		3.25	3.51	210.5	101787.0
14	800 m/min	RNGN CTIS710 Coating C Non-con		2.41	3.51	210.5	101787.0
7	900 m/min	RNGN CTIS710 Uncoated Non-con		2.77	5.51	330.6	169640.0
8	900 m/min	RNGN CTIS710 Coating A Non-con		2.97	4.41	264.5	33929.0
9	900 m/min	RNGN CTIS710 Coating B Non-con		1.90	2.20	132.2	67858.0
15	900 m/min	RNGN CTIS710 Coating C Non-con		1.36	1.1	66	101787.0
10	1000 m/min	RNGN CTIS710 Uncoated Non-con		3.40	4.18	250.6	135716.0
11	1000 m/min	RNGN CTIS710 Coating A Non-con		2.30	4.18	250.6	135716.0
12	1000 m/min	RNGN CTIS710 Coating B Non-con		2.84	2.09	125.3	67858.0
16A	840 m/min	RNGN CTIS710 Uncoated continuous NC2076-010-040	1-4	1.104	9.33	559.7	218857.3
16A	840 m/min	RNGN CTIS710 Uncoated continuous NC2076-050-080	5-8	0.928	5.85	351.0	173631.0
17A	840 m/min	RNGN CTIS710 Coating C continuous NC2076-010-030	1-3	0.968	7.34	440.5	173631.0
17A	840 m/min	RNGN CTIS710 Coating C continuous NC2076-040-060	4-6	0.865	5.27	316.2	119186.8
17A	840 m/min	RNGN CTIS710 Coating C continuous NC2076-070-080	7-8	0.773	2.57	154	54426.8

Figure 7.14 features the tool life curves for all seventeen milling tests that have been completed during this EngD. Figure 7.15 and Figure 7.16 highlight the level of flank wear versus material removal volume (MRV) and the increase in time in cut. The tool life curves for uncoated and coated RNGN inserts are shown in Figure 7.14.

Figure 7.15 represents the magnitude of insert flank wear versus MRV for continuous tool paths (Stage 1 to Stage 8), which were conducted at a cutting speed of 840 m/min, and the previous non-continuous machining trials that utilised cutting speeds of 700, 800, 900 and 1000 m/min.

Figure 7.16 clearly indicates a rapid improvement in tool life has been attained and concludes that adopting continuous to near continuous tool paths should be implemented where possible in future machining strategies, that utilise SiAlON milling inserts.

Over the course of the machining trial, the uncoated CTIS710 milling inserts achieved the best overall wear. However, the Coating C SiAlON milling inserts have demonstrated the best improvement in machining performance. The Coating C inserts exhibited very low insert wear on both flank and rake face when compared to the earlier tests that were conducted with interrupted non-continuous tool paths. As the temperature has been maintained in the chip/tool interface, the sliding contact between the workpiece and the rake faces is at an optimum as the Inconel 718 microstructure is thermally softened.

This has resulted in minimal fluctuation in tensile and compressive stresses, which helps to simplify the tribo-mechanics and improve the evacuation of the swarf chip.

For the latest machining trial, 2D bar blade geometries have been machined using uncoated and CVD coated RNGN and RPGN CTIS710 SiAlON inserts. Figure 7.17 represents the level of in cut time in minutes that the uncoated and Coating C RNGN inserts have attained and the level of flank wear.
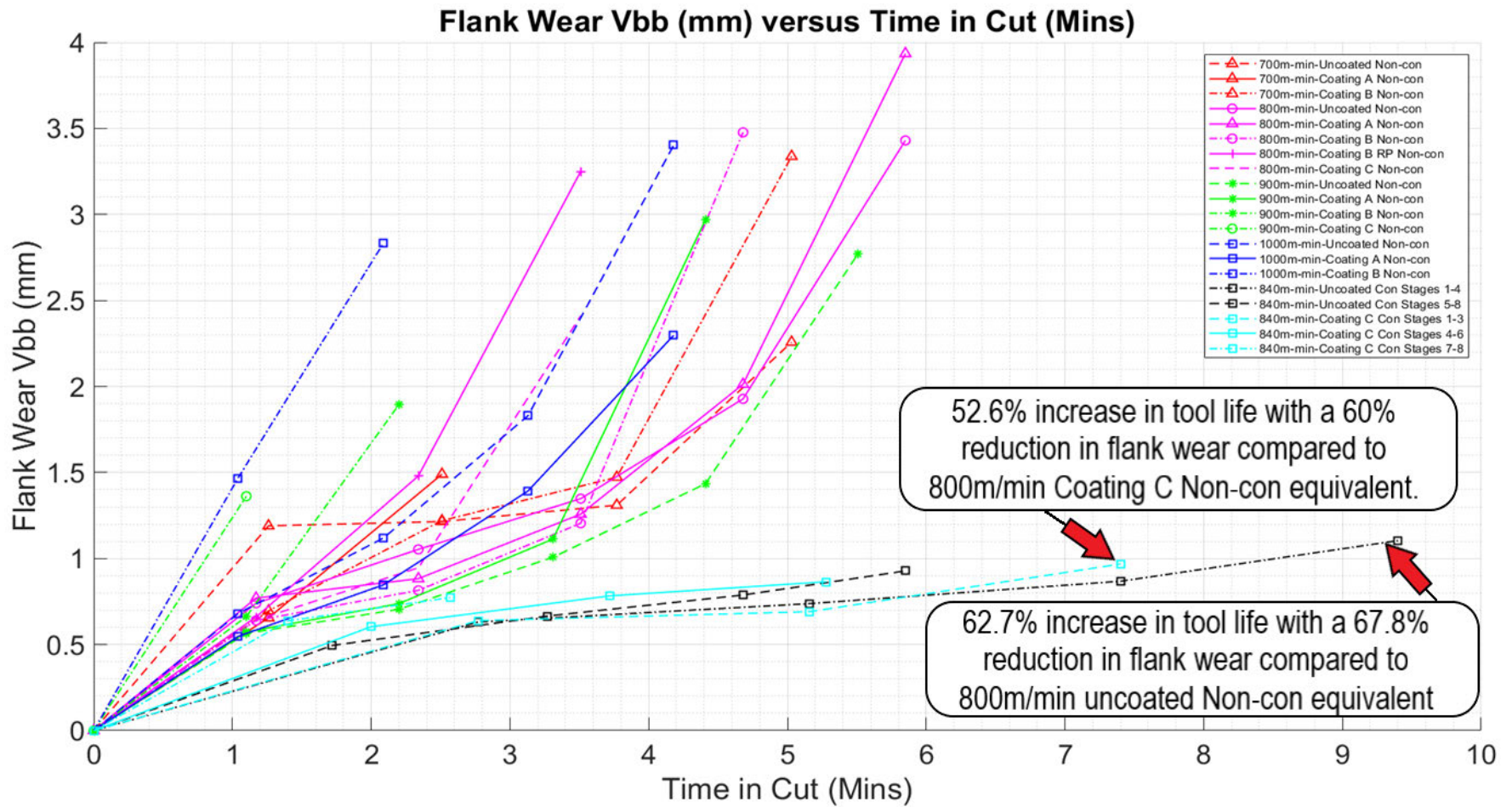
Figure 7.14. 700, 800, 900, 1000 m/min facing ops 1.1-4.5 Uncoated / Coating A / Coating B / Coating B RP / Coating C, 840 m/min continuous spiral ops Stages 1-8 Uncoated / Coating C.
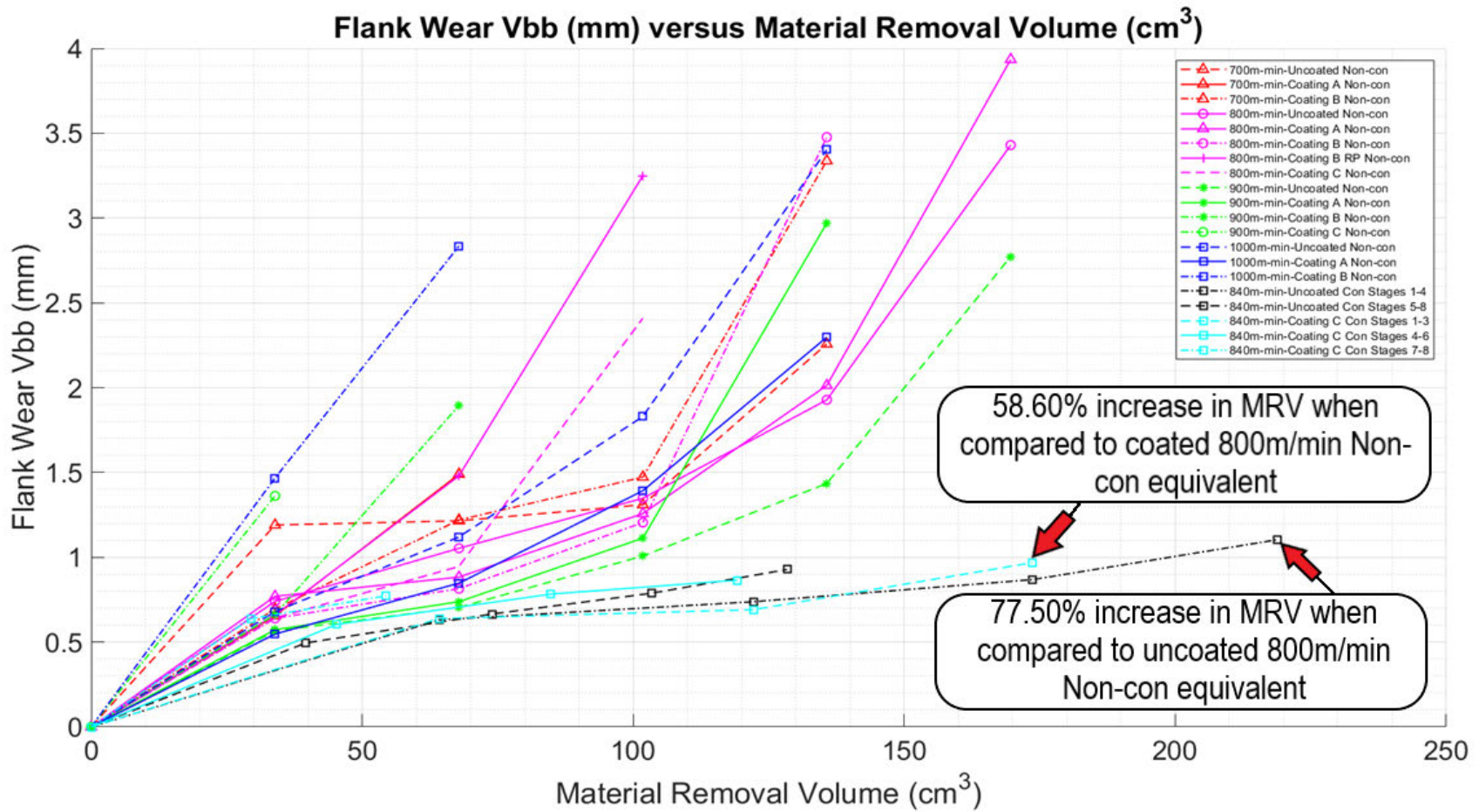
Figure 7.15. 700, 800, 900, 1000 m/min facing ops 1.1-4.5 Uncoated / Coating A / Coating B / Coating B RP / Coating C, 840 m/min continuous spiral op Stage 1-8 Uncoated / Coating.
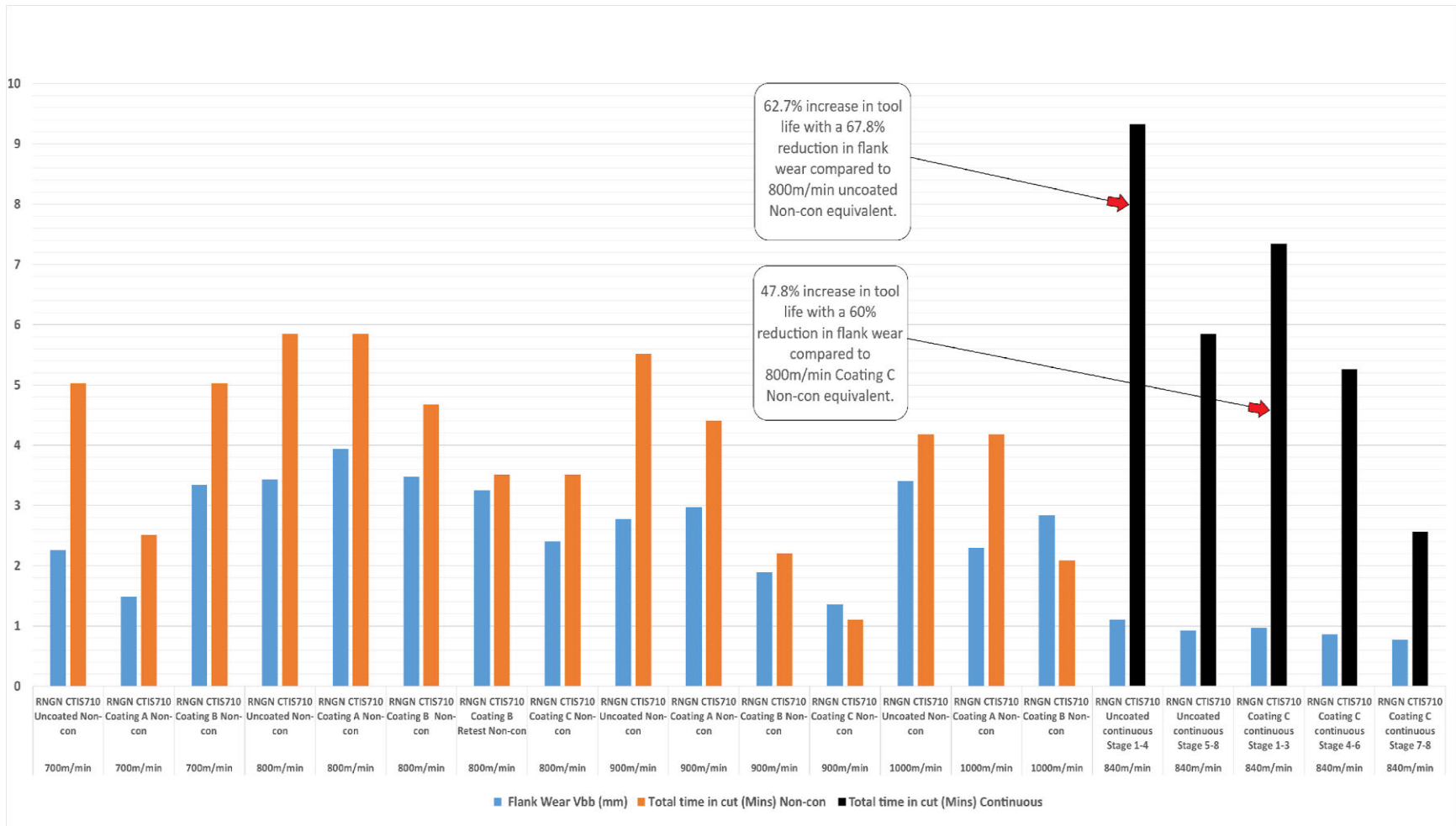
Figure 7.16. Tool life versus flank wear comparison between non-continuous and continuous tool paths.

Once again, the uncoated RPGN SiAlON inserts have removed the most of material but have displayed the highest level of flank wear as shown in Figure 7.17.
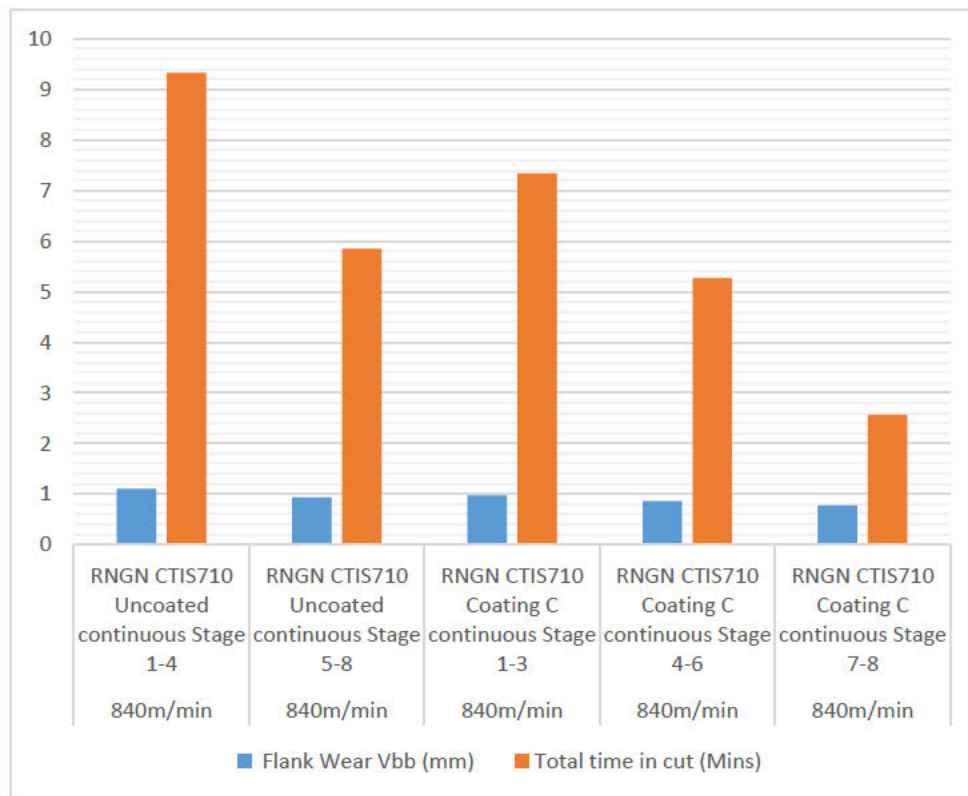
Figure 7.17. Average RNGN insert flank wear (mm) versus time in cut (minutes).

The uncoated RPGN SiAlON inserts displayed low levels of flank and rake face wear after completing Stage 9 and Stage 10 in Figure 7.7(a,d) and Figure 7.7(b,e), respectively. What was evident in Figure 7.7(c,f) after completing Stage 11 with uncoated RPGN SiAlON inserts, multiple insert failure looks to have taken place. This was due to flaking and chipping taking place due to an increase in cutting edge area as result of abrasive wear and cyclic variation in contact pressures on the rake faces. The increase in cutting edge area causes the contact pressures in the chip/tool interface to increase and also increases the load on the spindle as a result of increased frictional resistance.

Once the contact pressures have a reached a certain point it causes the SiAlON ceramic microstructure to shear along the grain boundaries. When sufficiently high enough fluctuating stresses are applied to the covalent SiAlON microstructure, the covalent microstructure slip systems do not plastically deform; they shear along grain boundaries. Therefore, reducing the rate at which the coating degrades is very important and TiN should not be used in protective

181

coating systems for this type of application in the future. Figure 7.18 highlight the level of flank wear versus material removal volume (MRV).
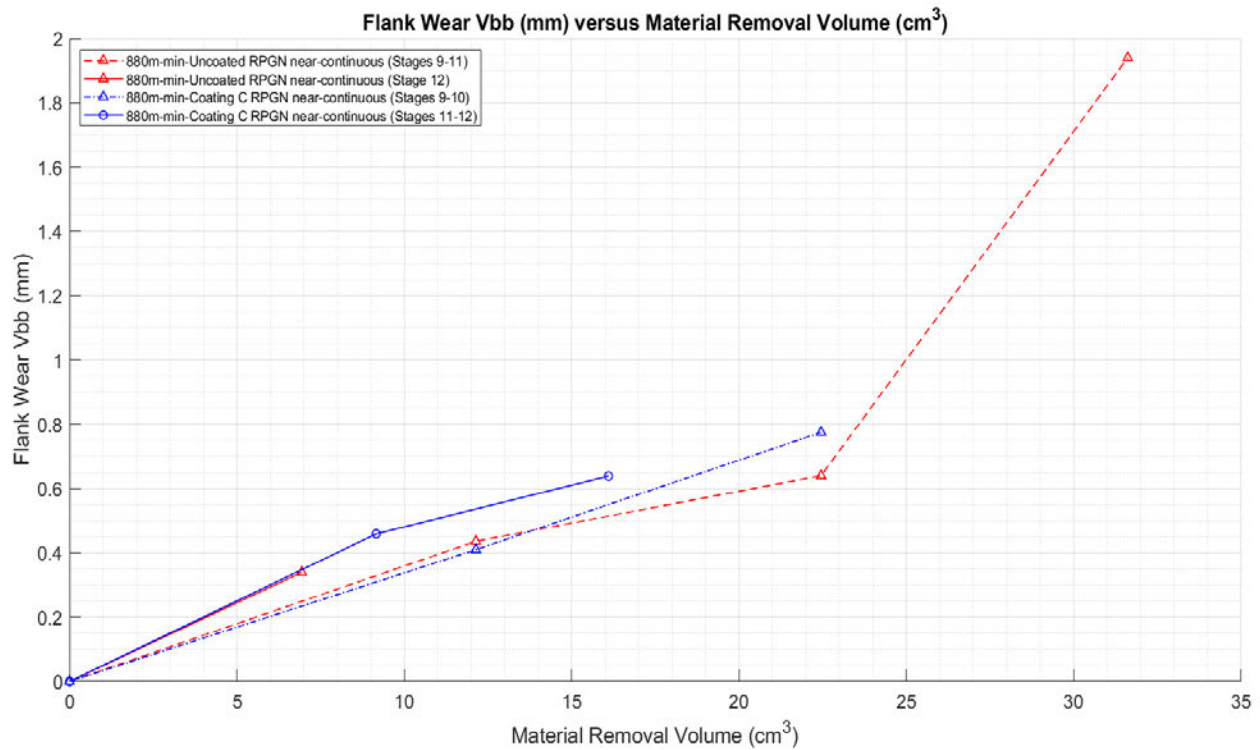
Figure 7.18. 880 m/min near-continuous elliptical spiral ops Stage 9-12 Uncoated / Coating C.

Figure 7.19 represents the level of in cut time in minutes that the uncoated and Coating C RPGN inserts have attained and the level of flank wear.

Upon the completion of Stage 9 with Coating C RPGN SiAlON inserts, the levels of flank and rake face wear was modest. Once Stage 10 had been completed, one of the Coating C RPGN inserts had chipped and flaked. During the machining of Stage 10 the level of vibration increased as the cutting tool reached the centre of the bar blade, which was indicated by an on-machine spindle vibration alarm sensor on the DMG Mori NTX2500. Once this vibration reached a certain level, the rake faces of the RPGN inserts are exposed to variation in tensile and compressive stresses, which culminated in the concentration of contact pressures at certain points on rake face.

This leads to shear along the grain boundaries and flaking of Coating C and the SiAlON microstructure. Once again, the uncoated RPGN SiAlON inserts have performed the best in terms of removing the most of material volume but have exhibited the highest level of flank wear

182

as shown in Figure 7.18. As mentioned before, the high level of flank wear for the uncoated RPGN SiAlON inserts is due to multiple insert failure.
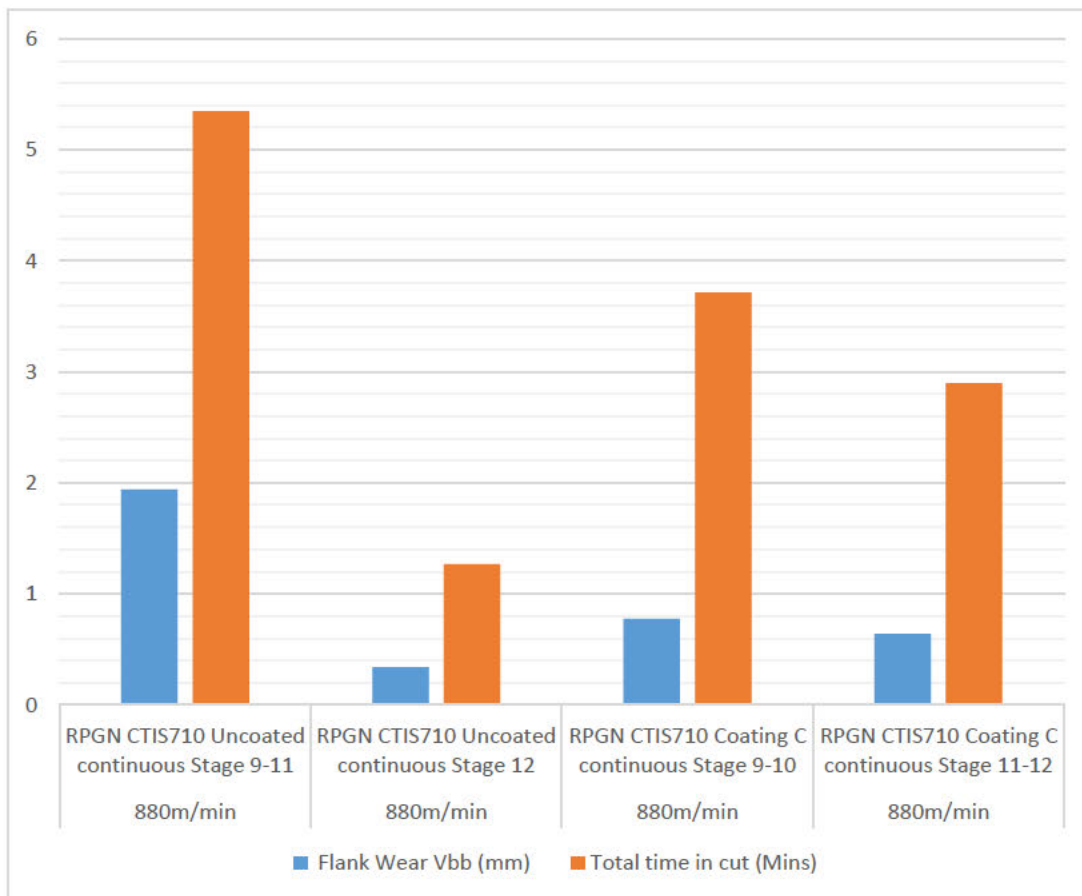
Figure 7.19. Average RPGN insert flank wear (mm) versus time in cut (minutes).

What is evident in Figure 7.12(a,c) is the Coating C inserts exhibited progressive tool wear after completing Stage 9, but not enough wear to warrant an insert change. However, in Figure 7.13(b,d) one of the inserts suffered an insert failure. From what is evident in Figure 7.12(b,d) the rake face that has failed has been subjected to a fluctuation in peak tensile and compressive stresses, which causes the contact pressures in the chip/tool interface to increase to a point that it causes the SiAlON ceramic microstructure to shear along the grain boundaries. The fluctuation in tensile and compressive stresses are likely down to the deflection and incurrent vibration that has stemmed from the cutting tool reaching the middle of the bar, where the deflection is at its highest.

As seen earlier in Section 7.2 in the interrupted non-continuous machining trial that were conducted at Ceratizit's AMG facility, the Coating C inserts have been subjected to further post treatment operations which create a series of variables that have potential deleterious effects on

183

the insert microstructure and the interface between the CVD coating and the SiAlON substrate. These variables come in the form of a thermal and mechanical stresses. A few variables were added as a result of a 0.5-µm thick TiN coating being wrongly deposited onto the surface of the α-amorphous Al_2O_3 6.5-µm thick coating.

The first variable is associated with thermal cooling stresses, which have been induced into the α-amorphous Al_2O_3 coating microstructure during the deposition of the TiN outer layer. The second variable is the removal of the TiN outer coating during post processing. The removal of the TiN coating via post processing will have introduced further residual stresses into the SiAlON substrate and the Al_2O_3 microstructure. The third variable is the introduction of compressive stresses which have been induced into the coating microstructure as a result of polishing. The fourth variable is a result of a stress release.

The stress release is a result of the coating microstructure being exposed to high cutting temperatures in the chip/tool interface, the cutting temperature in the chip/tool interface increase as the insert begin to degrade and wear. With regards to the level of insert flank wear versus MRV that has been captured in Figure 7.15 and Figure 7.18.

The level of insert wear indicates that the uncoated RNGN and RPGN inserts have displayed a superior tribological interaction at the chip/tool interface with the workpiece material, when compared to Coating C RNGN and RPGN Inserts. The uncoated SiAlON RNGN and RPGN inserts are likely going to have experiences a smaller coefficient of friction than the Coating C inserts. The lower coefficient of friction is created at high cutting temperature, with the interaction of SiAlON ceramic ions mixing with the Inconel 718 workpiece ions, which form lubricious oxide films. These lubricious oxide films create a more favourable shearing/chip removal machining process and reduce fluctuation in cutting force, which prolongs the longevity of the flank and rake faces and increases the tool life.

The Coating C RNGN and RPGN inserts seem to create a lubricious oxide with a coefficient of friction that is slightly higher that the uncoated inserts. The high temperatures that are created in the chip tool interface between the Coating C RNGN and RPGN inserts, and Inconel 718 workpiece are above >1000°C. At temperatures above 1000°C, the hot hardness of amorphous α-Al_2O_3 degrades from 18 GPa to 8 GPa [118]. The degradation in hot hardness of the α-Al_2O_3 coating leads to microstructural deformation of the polymorphic phases of the α-Al_2O_3 CVD coating and an increase in the coefficient of friction. Which creates shearing/chip removal machining process that is subjected to high fluctuation in cutting forces that reduces the

184

longevity of the Coating C flank and rake races and overall tool life.

The uncoated RNGN and RPGN inserts maintained higher stability at temperatures above >1000°C. The uncoated SiAlON rake faces for the both the RNGN and RPGN inserts displayed high resistance to thermal deformation. The high resistance to thermal deformation is due to the preservation of the hot hardness above >1000°C. The hot hardness of SiAlON is typically 13 GPa at above temperatures of >1000°C [118], [119]. The inclusion of yttrium oxides during the sintering process promotes the formation of glassy phases. The high hardness of the glass phases along with the high toughness of β-SiAlON's and high hardness of α-SiAlON, creates a composite microstructure with high thermal shock resistance, high hot hardness, and oxidation resistance.

It was therefore established in Tests M14 and M15 that Coating C had not improved the wear characteristics of CTIS710 SiAlON RNGN milling inserts. The lack of improvement in wear resistance and tool life, was evident when compared to the uncoated CTIS710 SiAlON RNGN milling inserts. However, in the latest bar blade machining trial the wear characteristics of the RNGN SiAlON inserts that have been CVD coated with Coating C have greatly improved. The levels of flank and rake face wear which have been exhibited by the Coating C coated RNGN inserts, show a great reduction in the level of flank wear versus the quantity of material that has been removed. The Coating C RNGN insert shows a significant reduction in the level of flank and rake face wear, when compared to RNGN insert wear which was collected from the previous non-continuous machining trials.

Principally, the main reason for the improvement and reduction in tool wear was down to a few factors.

1. The first factor involved improving the tool engagement in to cut by fine tuning the NC programme in Siemens NX and via Vericut NC programme reviews.
2. The second factor focused on optimising the depth of cut (Ap) and radial engagement to maintain the chip thickness (H_{ex}) value.
3. The third main factor was focused on reducing the fluctuation in cutting temperature in the chip/tool interface to a minimum, this near continuous cutting temperature contributed significantly to efficient material removal.
4. Another factor for improving the wear characteristics focused on tap testing the tool and the workpiece material. The tap testing modal analysis in Cutpro software, helped to establish suitable cutting speeds and feed rates to reduce overall vibration in the

machining process to a minimum. Although oxidation and thermomechanical wear on the Coating C inserts was evident, the levels of wear were significantly less when compared to previous interrupted non-continuous RNGN SiAlON milling insert wear data.

7.6 Conclusions for Test No M14-M15
The following conclusions can be drawn from the interrupted non-continuous tests:

1. Due to the poor thermal resistance properties of titanium nitride, it is advised not to use titanium nitride in CVD coatings used for protecting SiAlON ceramic milling inserts. Throughout this two-part machining trial, amorphous α-Al_2O_3 has proven to be very effective at providing protection for SiAlON ceramic milling inserts and in intense machining environments. It is recommended that amorphous α-Al_2O_3 be used utilised in future protective CVD coatings for SiAlON ceramic milling inserts.

2. The thermal cooling stresses have been induced into Al_2O_3 coating microstructure as result of a thin TiN coating being deposited onto the surface of the Al_2O_3 coating layer.

3. The removal of the TiN coating via post processing induces further residual stresses into the coating microstructure and SiAlON substrate.

4. Polishing the post processed Al_2O_3 coating introduces further compressive stresses into the coating microstructure, which has had a potentially deleterious effects on the Coating C interfacial layer.

5. The high temperature chip/tool interface created during the machining process, causes the induced stresses to be released. The heating and cooling cycles which were incurred during the interrupted cuts has also had an effect on the mechanical structure of the coatings due to the thermal expansion and contraction differences and hence exacerbated the wear mechanisms encountered by the coated inserts.

7.7 Conclusions for Test No M16-M17
The following conclusions can be drawn from the continuous/near continuous test cuts:

1. The flank wear values that have been captured for the test conducted at 840 m/min with uncoated & CVD coated SiAlON ceramic milling inserts (Coating C), indicates that continuous toolpaths should be featured extensively in all NC programme strategies, which utilise SiAlON ceramic milling inserts. Optimisation of the toolpaths has led to significant increase in tool life, material removal rates and material removal volumes.

2. The first and second objective have successfully met with this study. The NC programme have delivered significant improvement in tool life and demonstrated high stability. The hypothesis stated for the second objective has been proven to be correct. Substantial reductions in flank and rake face wear were demonstrated by the Coating C RNGN inserts, especially the uncoated RNGN and RPGN SiAlON ceramic milling inserts.

3. Due to the poor thermal resistance properties of titanium nitride, it is advised not to use titanium nitride in CVD coatings used for protecting SiAlON ceramic milling inserts. Throughout this machining trial, amorphous α-Al_2O_3 has proven to be very effective at providing protection for SiAlON ceramic milling inserts in intense machining environments. It is recommended that amorphous α-Al_2O_3 be used utilised in future protective CVD coatings for SiAlON ceramic milling inserts.

4. The thermal cooling stresses have been induced into the α-Al_2O_3 coating microstructure as result of a thin TiN coating being deposited onto the surface of the Al_2O_3 coating layer.

5. The removal of the TiN coating was undertaken via a honing post processing route. The process was selected as it can gently remove the TiN coating. However, the removal of the coating induced further residual stresses into the coating microstructure and SiAlON substrate.

6. Polishing the post processed Al_2O_3 coating introduces further compressive stresses into the coating microstructure, which has had a potentially deleterious effects on the Coating C interfacial layer.

7. The high temperature chip/tool interface created during the machining process, causes the induced stresses to be released. The heating and cooling cycles which were incurred during the interrupted cuts, had an effect on the mechanical structure of the coatings due to the thermal expansion and contraction differences, and hence exacerbated the wear mechanisms encountered by the coated inserts. One of the main recommendations for future work would be to reduce interrupted cuts to a minimum, as this aids the longevity of CVD coated SiAlON milling inserts.

7.8 Summary

The present chapter has endeavoured to develop further understanding and explore the main research hypothesis. Chapter 7 has attempted to establish a thorough understanding of the wear characteristics of the newly developed Coating C. The wear characteristics of Coating C

were then compared with uncoated SiAlON ceramic inserts when machining precipitation hardened Inconel 718.

Experiment Four has looked to explore the wear characteristics with a series of machining tests with Tests M14-M15 and Tests M16A-B and M17A-B. Tests M14 and M15 utilised interrupted non-continuous 3-axis toolpaths with cutting speeds of 800 m/min and 900 m/min. As discussed before in Section 7.2, these two cutting speeds were selected based on the levels of tool wear from the two-part machining trial that was conducted in Experiment Two. From the results of Test M14 and Test M15, the Coating C inserts displayed high levels of flank wear and coating degradation. Especially, when the levels of flank wear were compared to the other coated and uncoated inserts which were used in Tests M1-M13. The interrupted machining environment utilised in Tests M14-M15 has created a challenging environment for Coating C at the two cutting speeds.

As discussed earlier in Section 7.2.1, due to a coating error and the addition of a thin 0.5µm thick layer of TiN on top of the 6.5µm thick α-amorphous Al_2O_3 layer has created a series of problematic variables. The four variables concluded in Section 7.2.1 that the Coating C inserts were exposed to 1. thermal cooling stresses, 2. induced residual stresses from coating removal, 3. compressive stresses and finally a stress release due to the high temperatures at the chip/tool interface.

The main output that was established from Test M14 and Test M15 was centred around maintaining the temperature in the chip/tool interface. The objectives of the Test M16A-B and Test M17A-B was to establish if the maintaining the chip/tool interfacial temperatures would increase tool life and increase the benefit of applying a protective coating to SiAlON ceramic substrate.

Tests M16A-B and M17A-B utilised continuous 5-axis toolpaths and utilised a combination of CTIS710 RNGN and RPGN SiAlON milling inserts. The uncoated RNGN SiAlON inserts which were utilised for Test M16A displayed significant improvements in material removal versus insert flank and rake face wear.

The improvement in material removal versus insert wear is clearly displayed very clearly in Figure 7.15. An improvement has also been clearly exhibited by Test M17A. The Coating C inserts that were utilised in Test M17A also displayed significant improvements in material removal versus tool wear with the adoption of continuous toolpaths.

If the results in Figure 7.14 and Figure 7.16 are compared, the improvements in tool life and material removal are greater for the Coating C inserts when compared to the uncoated inserts. The novelty of the 5-axis machining trial has clarified that keeping the cutting tool in a continuous/near continuous machining environment, leads to reductions in tool wear and improvements in MRV. Refinement of the continuous toolpaths has delivered a real increase in cutting tool performance. Which emphasises the importance of creating NC programmes that are thoroughly thought through and refined.

Chapter 8 Conclusions

Although there has been some discussion and a summary included in each chapter of this thesis, this chapter will gather all these and provide some insights into the author's views on the different findings.

8.1 Conclusions

The research in this thesis was centred around five main objectives that have been presented in Section 1.1. Therefore, this section will comprise the conclusions which have been drawn against each one of the objectives.

8.1.1 Objective One

1. The first objective focused on reviewing the literature available on cutting processes and chip formation 1(a), ceramic cutting insert materials 1(c), and workpiece material and machining characteristics of nickel-based superalloys 1(f).

The critical analysis and summary have highlighted the importance of protective coating in the machining industry and there is a lot of literature that is focused on coated carbide and even coated SiAlON turning inserts. It was concluded that adding a suitable protective coating to SiAlON milling inserts would constitute a relevant area of research. There is very little utilisation and development of coated SiAlON milling inserts when compared to SiAlON turning inserts and other ceramic inserts. However, the main conclusion that can be drawn from these sections, is that the selection of the correct coating techniques (i.e., CVD) and coating materials (i.e., α-Al_2O_3), has a strong influence on the final wear characteristics and capabilities of the protective coating for a cutting tool application. This is especially relevant for coating ceramic cutting inserts.

8.1.2 Objective Two

The second objective was to plan and undertake a series of experimental tests to collect cutting force signal data via a dynamometer orientated machine setup and machining insert wear data. The second experiment attempted to clarify the wear characteristics of Coating A and Coating B SiAlON milling inserts when compared to uncoated CTIS710 SiAlON milling inserts. The first main finding from Test M1-M13 established that uncoated inserts suffered the least amount of flank wear when compared to Coating A and Coating B under non-continuous machining conditions. Coating A demonstrated poor adhesion to the CTIS710 SiAlON milling insert substrate, due to poor interfacial bonds as a result of the inclusion of titanium nitride in the interfacial layer. The poor adhesion characteristics culminated in the rapid removal of Coating A, which resulted in Coating A inserts displaying very similar wear characteristics to the uncoated

inserts. Coating B demonstrated high adhesion to the CTIS710 SiAlON milling insert substrate. However, the high adhesion characteristics of Coating B was overshadowed by the poor machining performance and overall tool life. The poor machining of Coating B was highly influenced by poor wear performance and oxidation resistance of titanium nitride outer coating.

The second main finding of Experiment Two suggests that amorphous grade Al_2O_3 was highlighted as suitable coating material to use in Coating C. The amorphous grade Al_2O_3 bonded very well on an interatomic level with the CTIS710 milling insert substrate. Although the Al_2O_3 was utilised in the Coating A outer layer, it was the Al_2O_3 interfacial layer that had proven to attain high adhesion to CTIS710 milling insert substrate.

8.1.3 Objective Three

The third objective of the research was to attain greater understanding of the tribological properties of the Coating A and Coating B that had been utilised in Test M1-M13. The first main finding from Experiment Three established quite a few similarities between the results of Experiment Two and Experiment Three. The notable bonding characteristics of amorphous grade Al_2O_3 that had been displayed in the two-part machining, were also exhibited in the scratch tests. The scratch testing results provided the first evidence for the inclusion of amorphous grade Al_2O_3 in Coating C. The second main finding from Experiment Three were established in the pin-on-disc tests. The amorphous grade Al_2O_3 in Coating B once again demonstrated very high resistance to deformation and high adhesion to the CTIS710 milling insert substrate. However, Coating A exhibited low adhesion to the CTIS710 milling insert substrate. The pin-on-disc helped to refine the decision to include amorphous grade Al_2O_3 in Coating C. The third main finding from Experiment Three concluded that a thicker single CVD layer of amorphous grade Al_2O_3 should be utilised for Coating C. Coating C was designed to be thicker than Coating A and Coating B as it was hoped that the thicker coating structure will have higher microstructural stability at high temperatures.

8.1.4 Objective Four

The fourth objective of the research focused on optimising the cutting parameters and machining environment. From the results of Test M14 and Test M15, the Coating C inserts displayed high levels of flank wear and coating degradation. Unfortunately, as discussed in Section 3.11.4 there was a coating error, which resulted in a thin layer of the titanium nitride level being deposited onto the 6.5µm thick α-amorphous Al_2O_3 coating. A post processing operation was utilised to remove the 0.5µm thick TiN coating on the rake face of the round button (RNGN) SiAlON milling inserts. The post processing involved polishing the 0.5µm thick

TiN coating off the rake face post, which revealed the amorphous Al_2O_3 coating. The polishing introduced compressive stresses into the Coating C microstructure. The high temperature chip/tool interface created during Tests M14 and M15, causes the induced stresses to be released. The heating and cooling cycles that were encountered during the non-continuous cuts had an effect on the mechanical structure of Coating C, due to the thermal expansion and contraction differences and hence exacerbated the wear mechanisms encountered by the coated inserts. The first main finding of Experiment Four was the effects of the heat and cooling cycle of the interrupted non-continuous cuts, which caused rapid degradation of the Coating C microstructure that culminated into high levels of wear on the flank and rake faces. The second main finding of Experiment Four concluded that eliminating or heavily reducing the non-continuous cut and maintaining the temperature in the chip/tool interface would help to improve the wear characteristics of the Coating C Inserts.

Part two of Experiment Four consisted of testing the Coating C (RNGN and RPGN) inserts with machining parameter information, which utilised continuous machining conditions in a five-axis machining environment. As discussed in Section 7.7, the uncoated RNGN SiAlON inserts (Test No M16A) displayed significant improvements in material removal versus insert flank and rake face wear as shown in Figure 7.15. The tool wear curves in Figure 7.14 showed a rapid improvement in flank wear for the Coating C RNGN SiAlON inserts (Test No M17A). The flank wear versus material removal rate (MRR) shown in Figure 7.15, concluded and proved the hypothesis that including continuous tool paths could improve the wear characteristics and tool life of uncoated and coated SiAlON milling inserts.

8.1.5 Objective Five
The fifth Objective is based on the results from Experiment Four, the three coating systems which have been utilised in this research have not outperformed the uncoated (RNGN and RPGN) inserts in terms of flank wear and tool life. Machining nickel-based superalloys such Inconel 718 result in an extreme machining environment which results in rapid tool wear. The high temperatures in the chip/tool interface caused Coatings A, B and C to degrade via a series of failure mechanism, which resulted in exacerbated wear mechanisms and reduced the overall tool life when compared to the uncoated inserts. The sliding contact between the chip and tool proved to be very important in the end. As the frictional sliding interaction between the chip and tool proved to the main differentiator between the uncoated inserts and the Coating C SiAlON inserts in Test M16A and M17A. The sliding contact between the chip/tool ultimately controls the level of cutting force, which are transmitted though the tool and into the spindle. The sliding

contact at the chip/tool between the uncoated SiAlON insert and Inconel 718 workpiece was more favourable than the sliding contact for Coating C SiAlON inserts. The main finding from this research is that uncoated SiAlON has a mixture of microstructural and tribological characteristics, which allow the SiAlON microstructure to attain a required tool life in the extreme machining environments associated with the high-speed milling of Inconel 718.

8.2 Contribution to Knowledge and Novelty

The main novel contribution which this research has attempted to provide, has focused on trying to improve the wear characteristics and attainable tool life of silicon aluminium oxynitride (SiAlON) milling inserts. Little or no research has been conducted with CVD coated SiAlON milling inserts for machining Inconel 718. In the previous chapters, the hypothesis was presented with the aim of improving the thermochemical wear characteristics of SiAlON milling inserts, by depositing a protective wear resistant coating via chemical vapour deposition techniques. The published research in this thesis and the links between the experimental wear data and the application of wear resistant coatings to SiAlON ceramic milling inserts is novel.

8.3 Recommendations for Future Work

The flank wear characteristics of Coating C were significantly improved during part two of Experiment Four (Test No 17A). However, the application of a 6.5 µm thick α-amorphous Al_2O_3 coating for Coating C, was not enough to outperform flank wear characteristics of the uncoated SiAlON milling inserts. The following section will discuss some of the potential topics of further work.

In regard to the primary contributions, there are features of this research project which were established for potential further work.

8.3.1 Methodology Development

1. The rapid improvements in flank wear that were attained for the uncoated inserts and Coating C inserts provided confidence in the five-axis toolpath. The α-amorphous Al_2O_3 coating for Coating C, still suffered from increased amounts of flank wear when compared to the uncoated inserts.

Future work could involve further analysis of the continuous 5-axis toolpaths to improve the dynamics between the workpiece and the cutting tool. Additional future work could also focus on refining the coating deposition process and the microstructure of the coating interface and the texture of the coating.

As discussed in Section 7.1, the frictional interaction between the Inconel 718 workpiece and the rake face of Coating C developed more vibration, which was monitored on the NTX2500 spindle sensor. The sound during the machining process for Test No M17A in Chapter 7 was emitting a slightly higher noise level for the Coating C than for the uncoated inserts of Test No M16A. The slightly higher noise sound was an indicator of higher potential frictional interaction between the Inconel 718 chip and the rake face of the Coating C inserts during the sliding contact.

The sliding contact between the Inconel 718 workpiece and insert rake face has a direct impact on the transmission of the cutting forces through the SiAlON microstructure, especially the coating microstructure. The other problem with the utilisation of an α-amorphous Al_2O_3 coating is the capability of the Al_2O_3 microstructure to cope with thermal shock. Especially if the Al_2O_3 microstructure has been honed and polished, which was the post processing route for removing the 0.5μm thick TiN coating, which had been deposited due to a coating error.

As discussed in Section 2.11, the selection of materials for protective coatings is paramount for attaining the desired level of protection and longevity for the underlying SiAlON substrate. Attaining the correct mechanical properties and microstructure of the coating is also paramount. Achieving an α-amorphous Al_2O_3 coating microstructure requires CVD coating temperatures over 1000°C. These high temperatures are necessary to encourage the phase transformation behaviour, where κ-Al_2O_3 polymorphs transform into α-Al_2O_3 polymorphs, which are the most thermodynamically stable form of polymorph. Controlling the growth direction of the textured α-Al_2O_3 microstructure is also paramount. As a highly texture α-Al_2O_3 microstructure in the 0001 basal plane has a controlled rates of deformation and greater wear resistance.

However, the phase transformations which have been utilised to produce a textured α-Al_2O_3 polymorphic coating structure also limits what coatings can be deposited on to the surface afterwards.

The microstructure of a SiAlON has an excellent combination of high oxidation resistance, high hot hardness, chemical inertness, and high thermal shock resistance. The SiAlON microstructure attains its high temperature hardness and thermal shock resistance from a combination of tough β-SiAlONs and α-SiAlONs with intermixed glasses, glass-ceramic phases, which are created due to the introduction of yttrium oxide, which aids densification. The β-SiAlONs provide the microstructural toughness and the intermix of α-SiAlONs and glass-ceramic phases provide the high wear resistance and hot hardness [120], [121].

Another key mechanical property of SiAlONs is the noticeable change to the friction co-efficient at high temperatures. As discussed in Section 8.1, there was a noted difference between the frictional characteristics of SiAlON and α-Al$_2$O$_3$ of Coating C, which resulted in a different sliding contact condition and actively contributed to reducing wear resistance and tool life. Previous studies have focused on establishing the friction co-efficient between sliding contact between Inconel 718 discs and SiAlON ceramic inserts. The research studies have found that the friction co-efficient for SiAlON reduces with temperature, which would explains the change in sound in Test M16A and Test M17B [122], [12].

8.3.2 Future Coating Development

For future coating development a number of mechanical characteristics would need to be attained for further progress to be made in this field of coating and cutting tool development. The first coating mechanical characteristic that would need to achieve, is suitable coating microstructure. Attaining an amorphous Al$_2$O$_3$ coating microstructure that is highly textured in the 0001 basal plane is paramount for thermodynamic stability i.e., high oxidation resistance and be chemically inert to diffusion wear but also for high adhesion to a SiAlON substrate. The adhesion characteristics that have been demonstrated by α-amorphous Al$_2$O$_3$ coating in this research are evident of how important it is to attain this coating microstructure. The coating microstructure would also need to have high resistance to thermal shock, high oxidation resistance. Typically, a SiAlON microstructure but without the silicon addition.

The second coating characteristics that needs to be attained would be focused on controlling the surface roughness profile of the coating with post processing techniques such as honing and polishing. The surface roughness profile has been shown to have a direct link with how much of the cutting force is transmitted through the CVD coating and SiAlON microstructure. Therefore, for future coating research differing polishing sequences could be utilised to create different roughness profiles. The different polished coated SiAlON inserts could then be subjected to tribological testing such as pin-on-disc and scratch testing, to ascertain which roughness profile has the best wear characteristics [123].

The third coating characteristic that could be assessed is with the incorporation of a hybrid coating structure. The achieve this type of coating strategy the hybrid coating approach would be broken down into series of tasks. The first task would focus on depositing a single layer of highly textured α-amorphous Al$_2$O$_3$ onto the surface of a SiAlON milling insert substrate via Chemical vapour deposition. The layer of α-Al$_2$O$_3$ would have a thickness of 6.5 µm. The 6.5 µm thick layer of α-Al$_2$O$_3$ would provide high adhesion to the SiAlON substrate, high wear

resistance and high thermodynamic stable foundation for the second task. The second task would then focus on depositing a 2.0 μm thick layer of chromium oxide Cr_2O_3 on to the surface of the α-Al_2O_3 CVD coating layer. The process of depositing the Cr_2O_3 on to the surface of α-Al_2O_3 would be completed via atmospheric-pressure plasma enhanced chemical vapor deposition (AP-PECVD) or via radio frequency magnetron sputtering. The AP-PECVD coating technique has been successfully utilised in a previous study to deposit chromium oxide onto alumina samples [124]. The first reason for the selection of Cr_2O_3, is due to Cr_2O_3 having the highest hardness of all the metallic oxides, which is in the region of 30 GPa and has very low co-efficient of friction [125]. The second reason for selecting Cr_2O_3 is that the oxide has very high wear resistance and very high thermodynamic stability and exhibits a hardness of 16 GPa at 700°C [126], which is comparable to hot hardness of SiAlON that has been stated in the study conducted by Brooke et al. [118]. The third reason for selecting Cr_2O_3 is focused on the crystal structure of Al_2O_3 and Cr_2O_3. Both α-Al_2O_3 and Cr_2O_3 have the same corundum crystalline microstructure with a space group of $\overline{R}3c$, which means the lattice parameter mismatch is less than 5% [127]. Both oxides exhibit a hexagonal closed packed microstructure, with α-Al_2O_3 having cations of (Al^{3+}) and Cr_2O_3 (Cr^{3+}). The hexagonal closed packed microstructural properties of α-Al_2O_3 and Cr_2O_3 allows for substitutional solid solutioning to occur between the two oxides. The substitution solid solutioning characteristics enables the epitaxial growth of a Cr_2O_3 crystalline structure on the nucleation layer on the α-Al_2O_3 substrates [128]. It is hoped that the interactions between the two oxides at interatomic level will equate to a stable bilayer coating. The third task would be to polish and hone the crystalline Cr_2O_3 layer to attain a surface roughness profile of 0.5 μm or less. The high temperature capability of highly polished Cr_2O_3 layer would lessen the effects of the cutting forces being transmitted through the cutting tool due to having a low coefficient of friction. This hybrid coating approach is hoped to improve the wear resistance and tool life of SiAlON milling inserts.

Chapter 9 REFERENCES

[1]   I. Ali and O. M. L. Alharbi, 'COVID-19: Disease, management, treatment, and social impact', *Sci. Total Environ.*, vol. 728, p. 138861, Aug. 2020, doi: 10.1016/j.scitotenv.2020.138861.

[2]   Airbus, 'Flying by nature Global Market Forecast 2007-2026 Airbus Report', AIRBUS S.A.S. 31707 BLAGNAC CEDEX, FRANCE, Global Forecast Report, 2007.

[3]   Boeing, 'COMMERCIAL MARKET OUTLOOK 2018–2037', Boeing, 10 W Washington St, 100 North Riverside Building, Chicago, IL 60606-1550, Global Forecast Report, 2018.

[4]   E. O. Ezugwu, J. Bonney, and Y. Yamane, 'An overview of the machinability of aeroengine alloys', *J. Mater. Process. Technol.*, vol. 134, no. 2, pp. 233–253, Mar. 2003, doi: 10.1016/S0924-0136(02)01042-7.

[5]   J. J. deBarbadillo and S. K. Mannan, 'Alloy 718 for Oilfield Applications', *JOM*, vol. 64, no. 2, pp. 265–270, Feb. 2012, doi: 10.1007/s11837-012-0238-z.

[6]   W. Akhtar, J. Sun, P. Sun, W. Chen, and Z. Saleem, 'Tool wear mechanisms in the machining of Nickel based super-alloys: A review', *Front. Mech. Eng.*, vol. 9, no. 2, pp. 106–119, Jun. 2014, doi: 10.1007/s11465-014-0301-2.

[7]   G. Zheng, J. Zhao, A. Li, X. Cui, and Y. Zhou, 'Failure mechanisms of graded ceramic tool in ultra high speed dry milling of Inconel 718', *Int. J. Precis. Eng. Manuf.*, vol. 14, no. 6, pp. 943–949, Jun. 2013, doi: 10.1007/s12541-013-0124-9.

[8]   V. Ramaswamy, P. R. Swann, and D. R. F. West, 'Observations on intermetallic compound and carbide precipitation in two commercial nickel-base superalloys', *J. Common Met.*, vol. 27, no. 1, pp. 17–26, Apr. 1972, doi: 10.1016/0022-5088(72)90100-2.

[9]   R. Y. Zhang *et al.*, 'Evolution of Lattice Spacing of Gamma Double Prime Precipitates During Aging of Polycrystalline Ni-Base Superalloys: An In Situ Investigation', *Metall. Mater. Trans. A*, vol. 51, no. 2, pp. 574–585, Feb. 2020, doi: 10.1007/s11661-019-05536-y.

[10]   B. Wang and Z. Liu, 'Influences of tool structure, tool material and tool wear on machined surface integrity during turning and milling of titanium and nickel alloys: a review', *Int. J. Adv. Manuf. Technol.*, vol. 98, no. 5–8, pp. 1925–1975, Sep. 2018, doi: 10.1007/s00170-018-2314-1.

[11]   A. Renz, I. Khader, and A. Kailer, 'Tribochemical wear of cutting-tool ceramics in sliding contact against a nickel-base alloy', *J. Eur. Ceram. Soc.*, vol. 36, no. 3, pp. 705–717, Dec. 2016, doi: 10.1016/j.jeurceramsoc.2015.10.032.

[12]   I. Khader, A. Renz, and A. Kailer, 'A wear model for silicon nitride in dry sliding contact against a nickel-base alloy', *Wear*, vol. 376–377, pp. 352–362, Apr. 2017, doi: 10.1016/j.wear.2016.12.019.

[13]   B. Mills, 'Recent developments in cutting tool materials', *J. Mater. Process. Technol.*, vol. 56, no. 1–4, pp. 16–23, Jan. 1996, doi: 10.1016/0924-0136(95)01816-6.

[14]   G. E. Spriggs, 'A history of fine grained hardmetal', *Int. J. Refract. Met. Hard Mater.*, vol. 13, no. 5, pp. 241–255, Jan. 1995, doi: 10.1016/0263-4368(95)92671-6.

[15]   R. C. Reed, *The Superalloys: Fundamentals and Applications*, 1st Edition. Cambridge University Press, 2006. [Online]. Available: www.cambridge.org/9780521859042

[16]   I. A. Choudhury and M. A. El-Baradie, 'Machinability of nickel-base super alloys: a general review', *J. Mater. Process. Technol.*, vol. 77, no. 1–3, pp. 278–284, May 1998, doi: 10.1016/S0924-0136(97)00429-9.

[17]   K. Zhuang, D. Zhu, X. Zhang, and H. Ding, 'Notch wear prediction model in turning of Inconel 718 with ceramic tools considering the influence of work hardened layer', *Wear*, vol. 313, no. 1–2, pp. 63–74, May 2014, doi: 10.1016/j.wear.2014.02.007.

[18]   A. Kruk, A. M. Wusatowska-Sarnek, M. Ziętara, K. Jemielniak, Z. Siemiątkowski, and A. Czyrska-Filemonowicz, 'Characterization on White Etching Layer Formed During Ceramic Milling of Inconel 718', *Met. Mater. Int.*, vol. 24, no. 5, pp. 1036–1045, Sep. 2018, doi: 10.1007/s12540-018-0056-0.

[19]   M. Brown, P. Crawforth, and D. Curtis, 'Rapid non-destructive sizing of microstructural surface integrity features using x-ray diffraction', *NDT E Int.*, vol. 131, p. 102682, Oct. 2022, doi: 10.1016/j.ndteint.2022.102682.

[20]   D. Dudzinski, A. Devillez, A. Moufki, D. Larrouquère, V. Zerrouki, and J. Vigneau, 'A review of developments towards dry and high speed machining of Inconel 718 alloy', *Int. J. Mach. Tools Manuf.*, vol. 44, no. 4, pp. 439–456, Mar. 2004, doi: 10.1016/S0890-6955(03)00159-7.

[21]   J. Ma, Z. Jia, G. He, Z. Liu, X. Zhao, and F. Qin, 'Influence of cutting tool geometrical parameters on tool wear in high-speed milling of Inconel 718 curved surface', *Proc. Inst. Mech. Eng. Part B J. Eng. Manuf.*, vol. 233, no. 1, pp. 18–30, Jan. 2019, doi: 10.1177/0954405417716495.

[22]   J. Ma, Y. Gao, Z. Jia, D. Song, and L. Si, 'Influence of spindle speed on tool wear in high-speed milling of Inconel 718 curved surface parts', *Proc. Inst. Mech. Eng. Part B J. Eng. Manuf.*, vol. 232, no. 8, pp. 1331–1341, Jun. 2018, doi: 10.1177/0954405416668925.

[23]   W. Ming, X. Huang, M. Ji, J. Xu, F. Zou, and M. Chen, 'Analysis of cutting responses of Sialon ceramic tools in high-speed milling of FGH96 superalloys', *Ceram. Int.*, vol. 47, no. 1, pp. 149–156, Jan. 2021, doi: 10.1016/j.ceramint.2020.08.118.

[24]   G. Zheng, J. Zhao, X. Cheng, R. Xu, and G. Zhao, 'Experimental Investigation on Sialon Ceramic Inserts for Ultra-high-speed Milling of Inconel 718', *Mater. Manuf. Process.*, vol. 31, no. 5, pp. 633–640, Apr. 2016, doi: 10.1080/10426914.2015.1019090.

[25]   F. Molaiekiya, M. Aramesh, and S. C. Veldhuis, 'Chip formation and tribological behavior in high-speed milling of IN718 with ceramic tools', *Wear*, vol. 446–447, p. 203191, Apr. 2020, doi: 10.1016/j.wear.2020.203191.

[26]   Z. Hao, R. Cui, and Y. Fan, 'Formation mechanism and characterization of shear band in high-speed cutting Inconel718', *Int. J. Adv. Manuf. Technol.*, vol. 98, no. 9–12, pp. 2791–2799, Oct. 2018, doi: 10.1007/s00170-018-2435-6.

[27]   T. Özel and D. Ulutan, 'Effects of machining parameters and tool geometry on serrated chip formation, specific forces and energies in orthogonal cutting of nickel-based super alloy Inconel 100', *Proc. Inst. Mech. Eng. Part B J. Eng. Manuf.*, vol. 228, no. 7, pp. 673–686, Jul. 2014, doi: 10.1177/0954405413510291.

[28]   T. I. El-Wardany, E. Mohammed, and M. A. Elbestawi, 'Cutting temperature of ceramic tools in high speed machining of difficult-to-cut materials', *Int. J. Mach. Tools Manuf.*, vol. 36, no. 5, pp. 611–634, May 1996, doi: 10.1016/0890-6955(95)00043-7.

[29]   K. Mahesh, J. T. Philip, S. N. Joshi, and B. Kuriachen, 'Machinability of Inconel 718: A critical review on the impact of cutting temperatures', *Mater. Manuf. Process.*, vol. 36, no. 7, pp. 753–791, May 2021, doi: 10.1080/10426914.2020.1843671.

[30]   Z. Hao, Y. Fan, J. Lin, F. Ji, and X. Liu, 'New observations on wear mechanism of self-reinforced SiAlON ceramic tool in milling of Inconel 718', *Arch. Civ. Mech. Eng.*, vol. 17, no. 3, pp. 467–474, May 2017, doi: 10.1016/j.acme.2016.12.011.

[31]   X. Tian, J. Zhao, J. Zhao, Z. Gong, and Y. Dong, 'Effect of cutting speed on cutting forces and wear mechanisms in high-speed face milling of Inconel 718 with Sialon ceramic tools', *Int. J. Adv. Manuf. Technol.*, vol. 69, no. 9–12, pp. 2669–2678, Dec. 2013, doi: 10.1007/s00170-013-5206-4.

[32]   X. Tian, J. Zhao, Y. Dong, N. Zhu, J. Zhao, and A. Li, 'A comparison between whisker-reinforced alumina and SiAlON ceramic tools in high-speed face milling of Inconel 718', *Proc. Inst. Mech. Eng. Part B J. Eng. Manuf.*, vol. 228, no. 8, pp. 845–857, Aug. 2014, doi: 10.1177/0954405413512814.

[33]   Y. Li *et al.*, 'Wear patterns and mechanisms of sialon ceramic end-milling tool during high speed machining of nickel-based superalloy', *Ceram. Int.*, vol. 47, no. 4, pp. 5690–5698, Feb. 2021, doi: 10.1016/j.ceramint.2020.10.155.

[34]   M. Xiao, N. He, and L. Li, 'Modeling notch wear of ceramic tool in high speed machining of Nickel-based superalloy', *J. Wuhan Univ. Technol.-Mater Sci Ed*, vol. 25, no. 1, pp. 78–83, Feb. 2010, doi: 10.1007/s11595-010-1078-8.

[35]   M. A. Shalaby and S. C. Veldhuis, 'Wear and Tribological Performance of Different Ceramic Tools in Dry High Speed Machining of Ni-Co-Cr Precipitation Hardenable Aerospace Superalloy', *Tribol. Trans.*, vol. 62, no. 1, pp. 62–77, Jan. 2019, doi: 10.1080/10402004.2018.1486494.

[36]   J. Liu, C. Ma, G. Tu, and Y. Long, 'Cutting performance and wear mechanism of Sialon ceramic cutting inserts with TiCN coating', *Surf. Coat. Technol.*, vol. 307, pp. 146–150, Dec. 2016, doi: 10.1016/j.surfcoat.2016.08.069.

[37]   A. Çelik, M. Sert Alağaç, S. Turan, A. Kara, and F. Kara, 'Wear behavior of solid SiAlON milling tools during high speed milling of Inconel 718', *Wear*, vol. 378–379, pp. 58–67, May 2017, doi: 10.1016/j.wear.2017.02.025.

[38]   F. Molaiekiya *et al.*, 'Influence of process parameters on the cutting performance of SiAlON ceramic tools during high-speed dry face milling of hardened Inconel 718', *Int. J. Adv. Manuf. Technol.*, vol. 105, no. 1–4, pp. 1083–1098, Nov. 2019, doi: 10.1007/s00170-019-04210-2.

[39]   M. A. Shalaby and S. C. Veldhuis, 'Effect of Cutting Speed on Chipping and Wear of the SiAlON Ceramic Tool in Dry Finish Turning of the Precipitation Hardenable IN100 Aerospace Superalloy', *J. Tribol.*, vol. 141, no. 2, p. 021604, Feb. 2019, doi: 10.1115/1.4041072.

[40]   A. E. Diniz and J. A. G. Ferrer, 'A comparison between silicon nitride-based ceramic and coated carbide tools in the face milling of irregular surfaces', *J. Mater. Process. Technol.*, vol. 206, no. 1–3, pp. 294–304, Sep. 2008, doi: 10.1016/j.jmatprotec.2007.12.035.

[41]   J. Sun, S. Huang, H. Ding, and W. Chen, 'Cutting performance and wear mechanism of Sialon ceramic tools in high speed face milling GH4099', *Ceram. Int.*, vol. 46, no. 2, pp. 1621–1630, Feb. 2020, doi: 10.1016/j.ceramint.2019.09.134.

[42]   H. Addhoum and D. Broussaud, 'Interaction of ceramic cutting tools with nickel-based alloys', *Mater. Sci. Eng. A*, vol. 109, pp. 379–387, Mar. 1989, doi: 10.1016/0921-5093(89)90618-7.

[43]   A. Çelik, 'Dopant-dependent diffusion behavior of SiAlON ceramics against Inconel 718 superalloy', *Ceram. Int.*, vol. 44, no. 14, pp. 17440–17446, Oct. 2018, doi: 10.1016/j.ceramint.2018.06.211.

[44]   David A Stephenson, *Metal Cutting Theory and Practice*, Third Edition. 6000 Broken Sound Parkway NW, Suite 300 Boca Raton, FL 33487-2742: CRC Press Taylor & Francis Group, 2016.

[45]   J. Vleugels, P. Jacobs, J. P. Kruth, P. Vanherck, W. Du Mong, and O. Van Der Biest, 'Machining of steel with sialon ceramics: influence of ceramic and workpiece composition on tool wear', *Wear*, vol. 189, no. 1–2, pp. 32–44, Oct. 1995, doi: 10.1016/0043-1648(95)06620-9.

[46]   L. Osmond, D. Curtis, and T. Slatter, 'Chip formation and wear mechanisms of SiAlON and whisker-reinforced ceramics when turning Inconel 718', *Wear*, vol. 486–487, p. 204128, Dec. 2021, doi: 10.1016/j.wear.2021.204128.

[47]   A. Rizzo *et al.*, 'The Critical Raw Materials in Cutting Tools for Machining Applications: A Review', *Materials*, vol. 13, no. 6, p. 1377, Mar. 2020, doi: 10.3390/ma13061377.

[48]   M. M. Noor, K. Kadirgama, H. H. Habeeb, M. M. Rahman, and B. Mohammad, 'Performance of carbide cutting tools when machining of nickel based alloy', *Int. J. Mater. Form.*, vol. 3, no. S1, pp. 475–478, Apr. 2010, doi: 10.1007/s12289-010-0810-4.

[49]   N. Anand Krishnan and J. Mathew, 'Studies on wear behavior of AlTiN-coated WC tool and machined surface quality in micro endmilling of Inconel 718', *Int. J. Adv. Manuf. Technol.*, vol. 110, no. 1–2, pp. 291–307, Sep. 2020, doi: 10.1007/s00170-020-05875-w.

[50]   M. A. Khan and K. Gupta, 'A study on machinability of nickel based superalloy using micro-textured tungsten carbide cutting tools', *Mater. Res. Express*, vol. 7, no. 1, p. 016537, Jan. 2020, doi: 10.1088/2053-1591/ab61bf.

[51]   Hargovind Soni and P. M. Mashinini, 'An Analysis on Tool-Chip Interaction During Dry Machining of SS316 Using Textured Carbide Tools', *1-11*, vol. 46, pp. 7611–7621, Feb. 2021, doi: 10.1007/s13369-021-05499-6.

[52]   L. Vel, G. Demazeau, and J. Etourneau, 'Cubic boron nitride: synthesis, physicochemical properties and applications', *Mater. Sci. Eng. B*, vol. 10, no. 2, pp. 149–164, Oct. 1991, doi: 10.1016/0921-5107(91)90121-B.

[53]   E. D. Whitney, *Ceramic Cutting Tools - Materials, Development, and Performance*, 1st Edition. Park Ridge, New Jersey, U.S.A.: Noyes Publications, 1994.

[54]   J. Vigneau, J. J. Boulanger, and F. Le Maître, 'Behaviour of Ceramic Tools During the Machining of Nickel Base Alloys', *CIRP Ann.*, vol. 31, no. 1, pp. 35–39, 1982, doi: 10.1016/S0007-8506(07)63264-8.

[55]   J. Aucote and S. R. Foster, 'Performance of sialon cutting tools when machining nickel-base aerospace alloys', *Mater. Sci. Technol.*, vol. 2, no. 7, pp. 700–708, Jul. 1986, doi: 10.1179/mst.1986.2.7.700.

[56]   G. Brandt, A. Gerendas, and M. Mikus, 'Wear mechanisms of ceramic cutting tools when machining ferrous and non-ferrous alloys', *J. Eur. Ceram. Soc.*, vol. 6, no. 5, pp. 273–290, Jan. 1990, doi: 10.1016/0955-2219(90)90019-C.

[57]   N. Richards and D. Aspinwall, 'USE OF CERAMIC TOOLS FOR MACHINING BASED ALLOYS', *Int. J. Mach. Tools Manuf.*, vol. 29, no. 4, pp. 575–588, 1989.

[58]   S. N. Grigoriev, S. V. Fedorov, and K. Hamdy, 'Materials, properties, manufacturing methods and cutting performance of innovative ceramic cutting tools – a review', *Manuf. Rev.*, vol. 6, p. 19, 2019, doi: 10.1051/mfreview/2019016.

[59]   K. H. Jack, 'Sialon tool materials', *Met. Technol.*, vol. 9, no. 1, pp. 297–301, Jan. 1982, doi: 10.1179/030716982803285639.

[60]   A. Rosenflanz, 'Silicon nitride and sialon ceramics', *Curr. Opin. Solid State Mater. Sci.*, vol. 4, no. 5, pp. 453–459, Oct. 1999, doi: 10.1016/S1359-0286(00)00004-8.

[61]   A. Gatto and L. Iuliano, 'Advanced coated ceramic tools for machining superalloys', *Int. J. Mach. Tools Manuf.*, vol. 37, no. 5, pp. 591–605, May 1997, doi: 10.1016/S0890-6955(96)00075-2.

[62]   E. Heikinheimo, I. Isomäki, A. A. Kodentsov, and F. J. J. van Loo, 'Chemical interaction between Fe and silicon nitride ceramic', *J. Eur. Ceram. Soc.*, vol. 17, no. 1, pp. 25–31, Jan. 1997, doi: 10.1016/S0955-2219(96)00082-9.

[63]   D. Hofmann, B. Hensel, M. Yasuoka, and N. Kato, 'New multilayer PVD-coating technique for cutting tools', *Surf. Coat. Technol.*, vol. 61, no. 1–3, pp. 326–330, Dec. 1993, doi: 10.1016/0257-8972(93)90247-L.

[64]   Z. Peng, H. Miao, W. Wang, S. Yang, C. Liu, and L. Qi, 'Hard and wear-resistant titanium nitride films for ceramic cutting tools by pulsed high energy density plasma', *Surf. Coat. Technol.*, vol. 166, no. 2–3, pp. 183–188, Mar. 2003, doi: 10.1016/S0257-8972(02)00776-4.

[65]   L. A. Dobrzański, D. Pakuła, and E. Hajduczek, 'Structure and properties of the multi-component TiAlSiN coatings obtained in the PVD process in the nitride tool ceramics', *J. Mater. Process. Technol.*, vol. 157–158, pp. 331–340, Dec. 2004, doi: 10.1016/j.jmatprotec.2004.09.052.

[66]   M. Soković *et al.*, 'Cutting properties of the Al2O3+SiC(w) based tool ceramic reinforced with the PVD and CVD wear resistant coatings', *J. Mater. Process. Technol.*, vol. 164–165, pp. 924–929, May 2005, doi: 10.1016/j.jmatprotec.2005.02.071.

[67]   L. A. Dobrzański, D. Pakuła, A. Křiž, M. Soković, and J. Kopač, 'Tribological properties of the PVD and CVD coatings deposited onto the nitride tool ceramics', *J. Mater. Process. Technol.*, vol. 175, no. 1–3, pp. 179–185, Jun. 2006, doi: 10.1016/j.jmatprotec.2005.04.032.

[68]   M. Staszuk, D. Pakuła, M. Pancielejko, T. Tański, and L. A. Dobrzański, 'Investigations on Wear Mechanisms of PVD Coatings on Carbides and Sialons', *Arch. Metall. Mater.*, vol. 62, no. 4, pp. 2095–2100, Dec. 2017, doi: 10.1515/amm-2017-0310.

[69]   M. Volosova, S. Grigoriev, A. Metel, and A. Shein, 'The Role of Thin-Film Vacuum-Plasma Coatings and Their Influence on the Efficiency of Ceramic Cutting Inserts', *Coatings*, vol. 8, no. 8, p. 287, Aug. 2018, doi: 10.3390/coatings8080287.

[70]   A. Baptista, F. Silva, J. Porteiro, J. Míguez, and G. Pinto, 'Sputtering Physical Vapour Deposition (PVD) Coatings: A Critical Review on Process Improvement and Market Trend Demands', *Coatings*, vol. 8, no. 11, p. 402, Nov. 2018, doi: 10.3390/coatings8110402.

[71]   S. N. Grigoriev and A. A. Krapostin, 'Multilayer composite nanoscale coatings as a method to increase reliability and tool life of cutting tools made of mixed ceramic Al $_2$ O $_3$ -TiC', *Mech. Ind.*, vol. 17, no. 7, p. 704, 2016, doi: 10.1051/meca/2016070.

[72]   H. Fukui, 'Evolutional History of Coating Technologies for Cemented Carbide Inserts — Chemical Vapor Deposition and Physical Vapor Deposition', p. 7.

[73]   Vinod K. Sarin and Sergej-Tomislav Buljan, 'NITRIDE COATED SILICON NITRIDE CUTTING TOOLS', 4,406,668, Sep. 27, 1983

[74]   Vinod K. Sarin and Sergej-Tomislav Buljan, 'CARBONITRIDE COATED COMPOSITE MODIFIED SILICON ALUMENUM OXYNTRDE CUTTING TOOLS', 4,406,669, Sep. 27, 1983

[75]   L. A. Dobrza, 'PVD and CVD gradient coatings on sintered carbides and sialon tool ceramics', vol. 1, p. 54, 2011.

[76]   M. Staszuk, L. A. Dobrzanski, T. Tanski, W. Kwasny, and M. Musztyfaga-Staszuk, 'The Effect of PVD and CVD Coating Structures on the Durability of Sintered Cutting Edges', *Arch. Metall. Mater.*, vol. 59, no. 1, pp. 269–274, Mar. 2014, doi: 10.2478/amm-2014-0044.

[77]   H. O. Pierson and H. O. Pierson, *Handbook of chemical vapor deposition*, 2nd ed. Norwich, NY: Noyes Publications, 1999.

[78]   I. Yu. Konyashin, 'Chemical vapor deposition of thin coatings onto A1203 indexable cutting inserts', *Surf. CoatingsTechnology*, vol. 85, no. 1996, pp. 131–137, Jul. 1995.

[79]   J. Qin, Y. Long, J. Zeng, and S. Wu, 'Continuous and varied depth-of-cut turning of gray cast iron by using uncoated and TiN/Al2O3 coated silicon nitride-based ceramic tools', *Ceram. Int.*, vol. 40, no. 8, pp. 12245–12251, Sep. 2014, doi: 10.1016/j.ceramint.2014.04.068.

[80]   N. Chen, B. Shen, G. Yang, and F. Sun, 'Tribological and cutting behavior of silicon nitride tools coated with monolayer- and multilayer-microcrystalline HFCVD diamond films', *Appl. Surf. Sci.*, vol. 265, pp. 850–859, Jan. 2013, doi: 10.1016/j.apsusc.2012.11.133.

[81]   K. Bobzin, 'High-performance coatings for cutting tools', *CIRP J. Manuf. Sci. Technol.*, vol. 18, pp. 1–9, Aug. 2017, doi: 10.1016/j.cirpj.2016.11.004.

[82]   H. Holleck, 'Material selection for hard coatings', *J. Vac. Sci. Technol. Vac. Surf. Films*, vol. 4, no. 6, pp. 2661–2669, Nov. 1986, doi: 10.1116/1.573700.

[83]   S. Saketi, J. Östby, and M. Olsson, 'Influence of tool surface topography on the material transfer tendency and tool wear in the turning of 316L stainless steel', *Wear*, vol. 368–369, pp. 239–252, Dec. 2016, doi: 10.1016/j.wear.2016.09.023.

[84]   L. A. Dobrzański, K. Gołombek, J. Mikuła, and D. Pakuła, 'Cutting ability improvement of coated tool materials', *J. Achiev. Mater. Manuf. Eng.*, vol. 17, no. 1, p. 5, 2006.

[85]   S. Zhang and X. Zhang, 'Toughness evaluation of hard coatings and thin films', *Thin Solid Films*, vol. 520, no. 7, pp. 2375–2389, Jan. 2012, doi: 10.1016/j.tsf.2011.09.036.

[86]   D. G. Bhat, H. E. Rebenne, and C. Strandberg, 'Analysis of coating interlayer between silicon nitride cutting tools and titanium carbide and titanium nitride coatings', *J. Mater. Sci.*, vol. 26, no. 17, pp. 4567–4580, Sep. 1991, doi: 10.1007/BF00612391.

[87]   G. L. Doll, B. A. Mensah, H. Mohseni, and T. W. Scharf, 'Chemical Vapor Deposition and Atomic Layer Deposition of Coatings for Mechanical Applications', *J. Therm. Spray Technol.*, vol. 19, no. 1–2, pp. 510–516, Jan. 2010, doi: 10.1007/s11666-009-9364-8.

[88]   M. Staszuk, D. Pakuła, G. Chladek, M. Pawlyta, M. Pancielejko, and P. Czaja, 'Investigation of the structure and properties of PVD coatings and ALD + PVD hybrid coatings deposited on sialon tool ceramics', *Vacuum*, vol. 154, pp. 272–284, Aug. 2018, doi: 10.1016/j.vacuum.2018.04.032.

[89]   M. Fallqvist a,∗, M. Olsson a, and S. Ruppi b, 'Abrasive wear of texture-controlled CVD α-Al2O3 coatings', *Surf. Coat. Technol.*, vol. 202, no. 837–843, p. 7, 2007, doi: doi:10.1016/j.surfcoat.2007.06.063.

[90]   S. Ruppi, 'Enhanced performance of α-Al2O3 coatings by control of crystal orientation', *Surf. Coat. Technol.*, vol. 202, no. 17, pp. 4257–4269, May 2008, doi: 10.1016/j.surfcoat.2008.03.021.

[91]   S. Shoja, N. Mortazavi, E. Lindahl, S. Norgren, O. Bäcke, and M. Halvarsson, 'Microstructure investigation of textured CVD alumina coatings', *Int. J. Refract. Met. Hard Mater.*, vol. 87, p. 105125, Feb. 2020, doi: 10.1016/j.ijrmhm.2019.105125.

[92]   T. Jadam, S. Datta, and M. Masanta, 'Influence of cutting tool material on machinability of Inconel 718 superalloy', *Mach. Sci. Technol.*, vol. 25, no. 3, pp. 349–397, May 2021, doi: 10.1080/10910344.2020.1815047.

[93]   F. Guo, Z. Yin, D. Hong, K. Yu, and J. Yuan, 'Cutting performance of a new spark plasma sintered SiAlON ceramic tool for high-speed milling of Inconel 718', *Int. J. Adv. Manuf. Technol.*, vol. 119, no. 11–12, pp. 7327–7338, Apr. 2022, doi: 10.1007/s00170-022-08702-6.

[94]   Y. Chen, J. L. Milner, C. Bunget, L. Mears, and T. R. Kurfess, 'Investigations on Performance of Various Ceramic Tooling While Milling Nickel-Based Superalloy', in *Volume 1: Processing*, Madison, Wisconsin, USA: American Society of Mechanical Engineers, Jun. 2013, p. V001T01A035. doi: 10.1115/MSEC2013-1220.

[95]   L. A. Dobrzański and D. Pakuła, 'Comparison of the structure and properties of the PVD and CVD coatings deposited on nitride tool ceramics', *J. Mater. Process. Technol.*, vol. 164–165, pp. 832–842, May 2005, doi: 10.1016/j.jmatprotec.2005.02.094.

[96]   L. Osmond, I. Cook, and T. Slatter, 'Tribological Properties of Multilayer CVD Coatings Deposited on SiAlON Ceramic Milling Inserts', *J. Manuf. Mater. Process.*, vol. 7, no. 2, p. 67, Mar. 2023, doi: 10.3390/jmmp7020067.

[97]   G. F. V. Voort and B. Ltd, 'Metallography Of Superalloys'. Industrial Heating, 2003.

[98]   'ASTM C1624 – 05 Standard test for Adhesion strength and Mechanical Failure Modes of Ceramic Coatings by Quantitative Single Point Scratch Testing'. ASTM, 2015.

[99]   'ASTM G99-17 - Standard Test Method for Wear Testing with a Pin-on-disk Apparatus'. ASTM, 2017. doi: 10.1520/G0099-17.

[100]   L. Osmond, I. Cook, D. Curtis, and T. Slatter, 'Tool life and wear mechanisms of CVD coated and uncoated SiAlON ceramic milling inserts when machining aged Inconel 718', *Proc. Inst. Mech. Eng. Part B J. Eng. Manuf.*, p. 09544054231180653, Jun. 2023, doi: 10.1177/09544054231180653.

[101]   AB Sandvik Coromant, 'Sandvik Coromant Application Guide for Heat Resistant Super Alloys'. AB Sandvikens Tryckeri, Sweden, Aug. 2010. [Online]. Available: https://www.manualsdir.com/manuals/407504/sandvik-coromant-heat-resistant-super-alloys.html

[102]   AB Sandvik Coromant, 'Ceramics - For smart and productive machining of super alloys - Sandvik Coromant'. AB Sandvik Coromant, Dec. 2010.

[103]   Ç. V. Yıldırım, T. Kıvak, and F. Erzincanlı, 'Tool wear and surface roughness analysis in milling with ceramic tools of Waspaloy: a comparison of machining performance with different cooling methods', *J. Braz. Soc. Mech. Sci. Eng.*, vol. 41, no. 2, p. 83, Feb. 2019, doi: 10.1007/s40430-019-1582-5.

[104]   Gwidon W. Stachowiak and Andrew W. Batchelor, *ENGINEERING TRIBOLOGY*, Third. 30 Corporate Drive, Suite 400, Burlington, MA 01803, USA Linacre House, Jordan Hill, Oxford OX2 8DP, UK: Elsevier Butterworth-Heinemann, 2005.

[105]   R. Komanduri and T. A. Schroeder, 'On Shear Instability in Machining a Nickel-Iron Base Superalloy', *J. Eng. Ind.*, vol. 108, no. 2, pp. 93–100, May 1986, doi: 10.1115/1.3187056.

[106]   R. S. Pawade and S. S. Joshi, 'MECHANISM OF CHIP FORMATION IN HIGH-SPEED TURNING OF INCONEL 718', *Mach. Sci. Technol.*, vol. 15, no. 1, pp. 132–152, Apr. 2011, doi: 10.1080/10910344.2011.557974.

[107]   M. A. Shalaby and S. C. Veldhuis, 'Tool wear and chip formation during dry high speed turning of direct aged Inconel 718 aerospace superalloy using different ceramic tools', *Proc. Inst. Mech. Eng. Part J J. Eng. Tribol.*, vol. 233, no. 7, pp. 1127–1136, Jul. 2019, doi: 10.1177/1350650118822388.

[108]   A. Shu, J. Ren, J. Zhou, and Z. Wang, 'Grain refinement mechanism in chip and the machined subsurface during high-speed machining of Inconel 718 alloy', *Mater. Charact.*, vol. 207, p. 113559, Jan. 2024, doi: 10.1016/j.matchar.2023.113559.

[109]   S. Zhang, J. Li, X. Zhu, and H. Lv, 'Saw-tooth chip formation and its effect on cutting force fluctuation in turning of Inconel 718', *Int. J. Precis. Eng. Manuf.*, vol. 14, no. 6, pp. 957–963, Jun. 2013, doi: 10.1007/s12541-013-0126-7.

[110]   A. Altin, M. Nalbant, and A. Taskesen, 'The effects of cutting speed on tool wear and tool life when machining Inconel 718 with ceramic tools', *Mater. Des.*, vol. 28, no. 9, pp. 2518–2522, Jan. 2007, doi: 10.1016/j.matdes.2006.09.004.

[111]   R. P. Zeilmann, F. Fontanive, and R. M. Soares, 'Wear mechanisms during dry and wet turning of Inconel 718 with ceramic tools', *Int. J. Adv. Manuf. Technol.*, vol. 92, no. 5–8, pp. 2705–2714, Sep. 2017, doi: 10.1007/s00170-017-0329-7.

[112]   B. Zhu, Y. Zhu, X. Li, and F. Zhao, 'Effect of ceramic bonding phases on the thermo-mechanical properties of Al2O3-C refractories', *Ceram. Int.*, vol. 39, no. 6, pp. 6069–6076, 2013, doi: 10.1016/j.ceramint.2013.01.024.

[113]   M. D. Thouless, 'Some mechanics for the adhesion of thin films', *Thin Solid Films*, vol. 181, no. 1–2, pp. 397–406, Dec. 1989, doi: 10.1016/0040-6090(89)90508-7.

[114]   S. Vuorinen and L. Karlsson, 'Phase transformation in chemically vapour-deposited κ-alumina', *Thin Solid Films*, vol. 214, no. 2, pp. 132–143, Jul. 1992, doi: 10.1016/0040-6090(92)90761-Y.

[115]   E. Fredriksson and J.-O. Carlsson, 'PHASE TRANSFORMATION DURING CVD OF ALUMINIUM OXIDE', *J. Phys. Colloq.*, vol. 50, no. C5, pp. C5-391-C5-399, May 1989, doi: 10.1051/jphyscol:1989547.

[116]   S. Shoja, O. Alm, S. Norgren, H.-O. Andrén, and M. Halvarsson, 'Calculated and experimental Schmid factors for chip flow deformation of textured CVD α-alumina coatings', *Surf. Coat. Technol.*, vol. 412, p. 126991, Apr. 2021, doi: 10.1016/j.surfcoat.2021.126991.

[117]   R. M'Saoubi *et al.*, 'Microstructure and wear mechanisms of texture-controlled CVD α-Al2O3 coatings', *Wear*, vol. 376–377, pp. 1766–1778, Apr. 2017, doi: 10.1016/j.wear.2017.01.071.

[118]   K. Brookes, 'There's more to hard materials than tungsten carbide alone', *Met. Powder Rep.*, vol. 66, no. 2, pp. 36–45, Mar. 2011, doi: 10.1016/S0026-0657(11)70062-5.

[119]   T. Ekstrom and J. Persson, 'Hot Hardness Behavior of Yttrium Sialon Ceramics', *J. Am. Ceram. Soc.*, vol. 73, no. 10, pp. 2834–2838, Oct. 1990, doi: 10.1111/j.1151-2916.1990.tb06683.x.

[120]   P. Pettersson, Z. Shen, M. Johnsson, and M. Nygren, 'Thermal shock resistance of a/b-sialon ceramic composites', *J. Eur. Ceram. Soc.*, p. 7, 2001.

[121]   Nurcan Calis Acikbasa, Sermet Tegmena, Selcuk Ozcanb, and Gokhan Acikbasc, 'Thermal shock behaviour of α:β-SiAlON–TiN composites', *Ceram. Int.*, vol. 40, pp. 3611–3618, 2014, doi: doi.org/10.1016/j.ceramint.2013.09.064.

[122] B. Zhao, I. Khader, R. Raga, U. Degenhardt, and A. Kailer, 'Tribological behavior of three silicon nitride ceramics in dry sliding contact against Inconel 718 over a wide range of velocities', *Wear*, vol. 448–449, p. 203206, May 2020, doi: 10.1016/j.wear.2020.203206.

[123] A. Riedl, N. Schalk, C. Czettl, B. Sartory, and C. Mitterer, 'Tribological properties of Al2O3 hard coatings modified by mechanical blasting and polishing post-treatment', *Wear*, vol. 289, pp. 9–16, Jun. 2012, doi: 10.1016/j.wear.2012.04.022.

[124] W. Yu *et al.*, 'Depositing chromium oxide film on alumina ceramics enhances the surface flashover performance in vacuum via PECVD', *Surf. Coat. Technol.*, vol. 405, p. 126509, Jan. 2021, doi: 10.1016/j.surfcoat.2020.126509.

[125] X. Pang, K. Gao, and A. A. Volinsky, 'Microstructure and mechanical properties of chromium oxide coatings', *J. Mater. Res.*, vol. 22, no. 12, pp. 3531–3537, Dec. 2007, doi: 10.1557/JMR.2007.0445.

[126] M. Mohammadtaheri, Q. Yang, Y. Li, and J. Corona-Gomez, 'The Effect of Deposition Parameters on the Structure and Mechanical Properties of Chromium Oxide Coatings Deposited by Reactive Magnetron Sputtering', *Coatings*, vol. 8, no. 3, p. 111, Mar. 2018, doi: 10.3390/coatings8030111.

[127] Yin Gao, Harald Leiste, Michael Stueber, and Sven Ulrich, 'The process of growing Cr2O3 thin films on α-Al2O3 substrates at low temperature by r.f. magnetron sputtering', *J. Cryst. Growth*, vol. 457, pp. 158–163, 2017, doi: doi.org/10.1016/j.jcrysgro.2016.08.009.

[128] P. Zhao, H. Zhao, J. Yu, H. Zhang, H. Gao, and Q. Chen, 'Crystal structure and properties of Al2O3-Cr2O3 solid solutions with different Cr2O3 contents', *Ceram. Int.*, vol. 44, no. 2, pp. 1356–1361, Feb. 2018, doi: 10.1016/j.ceramint.2017.08.195.

Appendix A
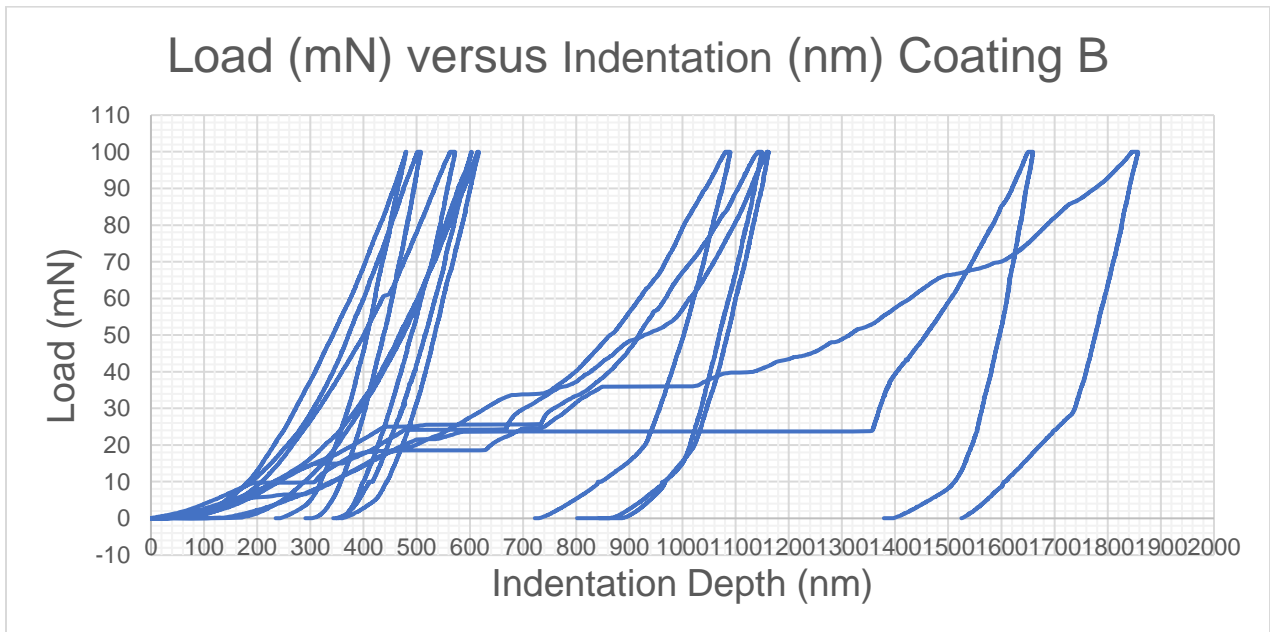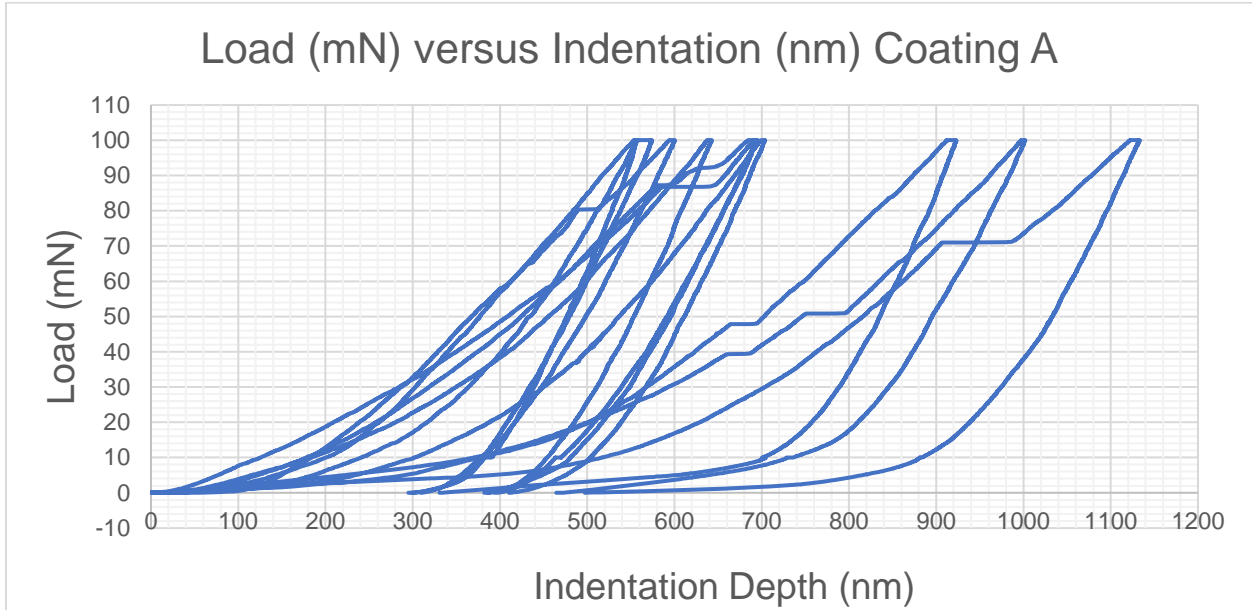
Concern : Vibration of tool
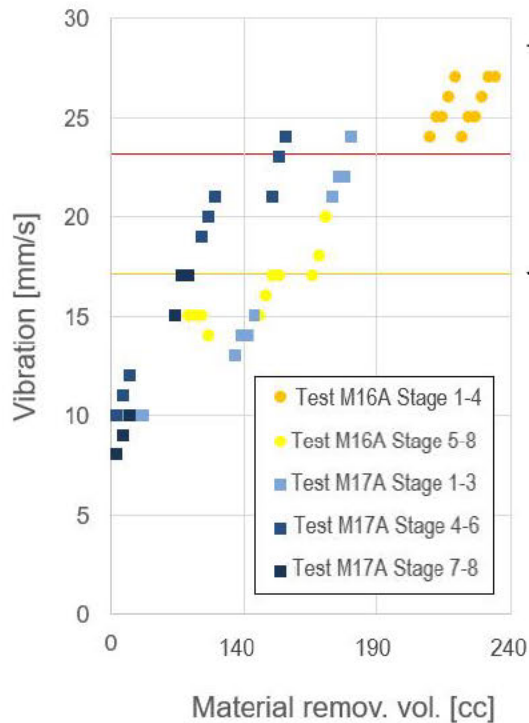
- Vibration reached 27 mm/s finally
- No or little difference between with/without coating
- Load : Low (under 20% except for X-axis)

Appendix B

Load (mN) versus Indentation (nm) Coating A
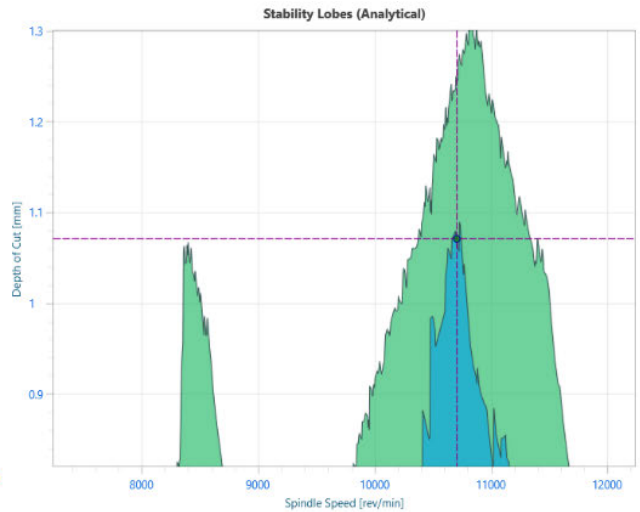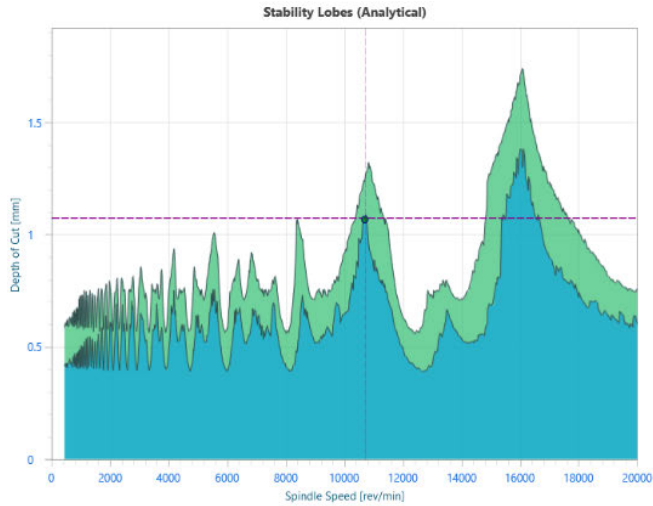

Load (mN) versus Indentation (nm) Coating B

Appendix C
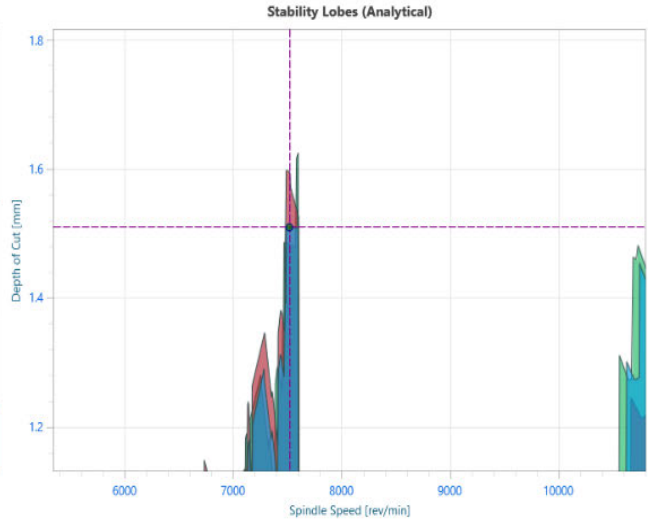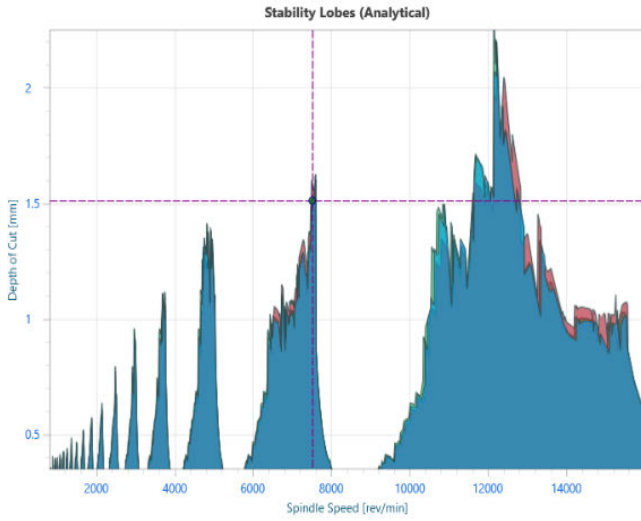
C1. RNGN Insert Modal Overlap Analysis for depth of cut, cutting speed and feed rate selection.

C2. RPGN Insert Modal Overlap Analysis for depth of cut, cutting speed and feed rate selection.

The modal analysis that has been used to determine the final cutting speed, depth of cut and feed rate has been included in Appendix C1 and C2. In the blue colour represent the modal analysis data for tool 1. The turquoise colour represents the modal analysis for the end of the bar tap test. The red colour in Appendix C1 represents the modal analysis data for the middle of the bar tap test. The modal overlap that is evident in Appendix C1 and Appendix C2, has highlighted what speed, feed rate and depth of cut to use in order to attain high stability in the machining environment.